Fault tolerant control and path planning for quasi-LPV systems : application to quadrotor

Eslam Abouselima

université PARIS-SACLAY

Fault Tolerant Control and Path Planning for Quasi-LPV Systems : Application to Quadrotor

Planification et Contrôle Tolérants aux Défauts de Systèmes Quasi-LPV : Application sur un Quadrotor

Thèse de doctorat de l'université Paris-Saclay

École doctorale n°580 : sciences et technologies de l'information et de la communication (STIC)
Spécialité de doctorat : automatique
Graduate School : Sciences de l'ingénierie et des systèmes, Référent : Université d'Évry Val d'Essonne

Thèse préparée dans la unité de recherche IBISC (Université Paris-Saclay, Univ Evry), sous la direction de Saïd Mammar, Professeur des Universités, UEVE-Université Paris-Saclay, la co-direction de Dalil Ichalal, Professeur des Universités, UEVE-Université Paris-Saclay

Thèse soutenue à Paris-Saclay, le 10 Juin 2022, par

Eslam ABOUSELIMA

Composition du jury

Sihem TEBBANI Professeur des Universités, CentraleSupélec - Université Paris-Saclay	Présidente
Mohamed DJEMAI Professeur des Universités, INSA Hauts-de-France	Rapporteur
Rodolfo ORJUELA Professeur des Universités, Université de Haute-Alsace	Rapporteur
Alessandro VICTORINO Maître de Conferences-HDR, Université de Technologie de Compiègne	Examinateur
Saïd MAMMAR Professeur des Universités, UEVE-Université Paris-Saclay	Directeur de thèse
Dalil ICHALAL Professeur des Universités, UEVE-Université Paris-Saclay	Co-directeur de thèse

THESE DE DOCTORAT
NNT : 2022UPAST085

To my wife, my mother, and my whole family I wasn't to achieve this work without your faith.

Acknowledgements

Throughout my PhD thesis, I had the opportunity to meet a lot of people for whom I am and I will always be really grateful for their help, support, and faith. First of all, my PhD advisor Saïd MAMMAR, apart from the scientific ideas and research directions he had always guided me through, he has a wonderful personality. It is hard to remember a specific time, but what I remember clearly is that after each meeting with him I had been always motivated and encouraged to advance in my work. Nevertheless, I would like to thank my co-supervisor Dalil ICHALAL for his continuous support, precious technical advice, and insightful reviews.

My deepest thanks go the dissertation committee members including Mohamed DJEMAI, Professor at university INSA Hauts-de-France and Rodolfo ORJUELA Professor at university Haute-Alsace it is an honor to have them as reporters of my thesis. In addition to Sihem TEBBANI professor at CentraleSupélec - Université Paris-Saclay and Alessandro VICTORINO assistant professor at university of Compiègne for accepting to be the thesis examiners of the thesis. It was a real pleasure for me to have such a discussion of the thesis through the defense.

I am really grateful to my current and past team mates in the IBISC Laboratory: Hicham TOUZANI, Yassine KIBBATI, Akram ELTARABELY, Majda FOUKA, Rayane BENYOUCEF, Sara IFQIR, and Sushil SHARMA for the ideas, the information, and the fun we have shared. Also, special thanks are dedicated for Mahmoud KHAIRALLAH for the journey we started together and to be continued, he has been always a real asset for me. I need to mention also my professors and my old friends from aerospace department at Cairo university who have shaped my background and still pushing me forward for further scientific contribution. Furthermore, my childhood friends for their continuous support and unconditional trust in a way that encourages me to move forward even during the hard time.

I want also to thank all my family members they have been always a tremendous emotional and psychological support. Although the words won't be enough to express my gratitude to my mother, I wish to thank her for everything, she has shaped the person I am on now with lots sacrifices, encouragement, and inspiration. Last but not least, I would like to express my sincere feelings for my wife, the piece who completes me and the person who would always be swinging with my resonant frequency. This work wasn't to be achieved without her understanding and patience, she hasn't spare any effort to support me and push me forward all the time.

Contents

List of Notations and Acronyms

Notations

$\|\|G\|\|_-$	$\mathcal{H}_-$ index of G
$\|\|G\|\|_\infty$	$\mathcal{H}_\infty$ norm of G
A^{-1}	inverse of a matrix A
A^T	transpose of a matrix A
$A^\dagger$	pseudo inverse of a matrix A
Φ	set containing the varying parameters
Φ_j	set containing the derivatives of the varying parameters
$P > 0$	matrix P is symmetric positive definite or semi-definite matrix $(P \geq 0)$
$P < 0$	matrix P is symmetric negative definite or semi-definite matrix $(P \leq 0)$
I_n	$n \times n$ identity matrix
0_n	$n \times n$ zero matrix

Acronyms

FTC	Fault-Tolerant Control
AFTCS	Active Fault-Tolerant Control Systems
PFTCS	Passive Fault-Tolerant Control Systems
FDD	Fault Detection and Diagnosis
UAV	Unmanned Aerial Vehicle
VTOL	Vertical Take-Off and Landing
LTI	Linear Time Invariant
LTV	Linear Time Varying
LPV	Linear Parameter Varying
CG	Center of Gravity
LQG	Linear Quadratic Gaussian
LQR	Linear Quadratic Regulator
LQE	Linear Quadratic Estimator
PID	Proportional Integral Derivative
LMI	Linear Matrix Inequality
BMI	Bilinear Matrix Inequality
ARE	Algebraic Riccati Equation

List of Figures

List of Tables

List of Publications

[1] Eslam Abouselima, Dalil Ichalal, and Saïd Mammar. Quadrotor control and actuator fault detection: Lqg versus robust $\mathcal{H}_-/\mathcal{H}_\infty$ observer. In *2019 4th Conference on Control and Fault Tolerant Systems (SysTol)*, pages 86–91. IEEE, 2019.

[2] Eslam Abouselima, Dalil Ichalal, and Said Mammar. Robust actuator fault diagnosis for lpv systems: Application to quadrotor. In *2021 American Control Conference (ACC)*, pages 4938–4945. IEEE, 2021.

[3] Eslam Abouselima, Dalil Ichalal, and Said Mammar. Robust sensor fault estimation for lpv systems: Application to quadrotor uav. In *2021 9th International Conference on Systems and Control (ICSC)*, pages 373–379. IEEE, 2021.

Chapter 1

General Introduction

Chapter abstract

Recently, autonomous systems are getting more and more popular and are widely deployed in several applications in our daily life. That's why a great concern has been dedicated to the problem of autonomous systems Fault Detection and Diagnosis (FDD) and further Fault-Tolerant Control (FTC). As if the system is provided with FDD and FTC units, it will be able to create an alert in case of system malfunction while preserving an acceptable performance to complete the required task. Evidently, the UAVs are among the systems that are in need of such FTC algorithms because any system malfunction can cause severe damage not just for the vehicle itself but for the surrounding environment as well. So this work is investigating the problem of designing an FTC algorithm for a quadrotor aiming to be a worthy contribution to the evolution of UAVs safety and reliability.

1.1 Context

In the recent few years, the word automation has been getting more popular as most of the processes executed by machines in our daily life are being automated from cleaning the clothes in a washing machine to landing an airplane. Although there is remarkable progress in the field of machines' automation and control, autonomous systems are still vulnerable to sudden malfunction of sensors, actuators, or the plant itself (cables, structure, etc.). In such cases, the feedback controller can hide the initial deficiency from being detected leading to further amplification of the fault which may result in a complete system failure as stated in [1].

Hence, to increase the reliability, maintainability, and robustness of the autonomous systems they must be provided with Fault-Tolerant Control (FTC) algorithms. The resulting fault-tolerant control systems (FTCS) are defined in [2] as the control systems which possess the ability to accommodate component failures automatically such that

they are capable of maintaining overall system stability and acceptable performance in the event of such failures.

According to [3] two types of FTC systems can be investigated: passive fault-tolerant control systems (PFTCS) and active fault tolerant control systems (AFTCS). In PFTCS the controller is designed to be robust against faults and uncertainties such that it preserves system stability in case of degraded performance, while in AFTCS the controller is reconfigured upon the information extracted from the FDD unit.

Thus an active FTC scheme contains two main units: FDD unit for identifying, evaluating, and isolating the fault that's why it can be referred to as the Fault Detection and Isolation (FDI) unit. On the other hand, the controller reconfiguration unit's role is to reshape the control law such that it can overcome the malfunction and stabilize the system in the presence of the fault. Prior to switching to an AFTC mode, the system must generate an adequate alert indicating that it is experiencing some kind of breakdown, that's why a great concern has been dedicated to the problem of FDD unit design.

Before discussing the principles of fault diagnosis, the concept of system redundancy should be stated. In [4] one can specify two types of system redundancy: hardware (direct) redundancy and software (analytical) redundancy. Hardware redundancy is due to the existence of multiple components for the same process so fault diagnosis can be accomplished by comparing their performance. Despite the reliable results of the hardware redundancy, it is not likely to be available because of the cost and weight. Nevertheless, the software redundancy can be more cost-efficient with no extra weight required but more challenging owing to model uncertainty, measurement noise, and exogenous disturbances.

Generally, the fault diagnosis process depends on generating robust residuals defined [5] as fault indicators based on the deviation between measurements and model-based computations that should remain small in fault-free cases, and become sufficiently noticeable whenever faults occur. The resulting residuals are analyzed through three stages: fault detection, determining the existence and timing of the fault; fault isolation, locating the fault; and fault estimation, deciding type, shape, and intensity of the fault. According to the observer type and formulation, it can perform only fault detection with multiple observers for fault isolation or it can provide fault detection and isolation simultaneously.

Indeed, the FTC techniques are very essential for several applications of autonomous systems among which the Unmanned Aerial Vehicles (UAVs) exist. This fact is demonstrated through discussing the gap between the market need for such vehicles in different operations and the stage of security and sustainability they have achieved. According to the survey performed in [6], for the sake of integrating the UAVs in civil airspace, they must ensure the same level of safety as manned aircraft. Let's first enumerate some of the fields in which the UAVs play a vital role:

- relatively classical drones are able to carry up to $2.5\ kg$ and travel with a velocity of $55\ mph$ which make them perfectly suitable for lightweight home delivery like the DHL deliver drone[1].

[1] https://www.electrive.com/2019/05/20/china-dhl-launches-drone-delivery-service/

- they can be very beneficial for risk management by providing vital information during search and rescue operations including damage assessment such as Anafi Ai[2] drone shown in figure 1.1 and further disasters counteracting such as firefighting.
- in agriculture, they are used for monitoring the health of the field crops in a way that can highly improve the land production.
- for urban transportation they provide an astonishing solution for traffic jams, for example, the CityAirbus[3] is an under-construction aircraft to be employed as an autonomous taxi drone.
- nevertheless, UAVs are used in leisure activities like filming, photography, and racing games.

Figure 1.1: Drone performing Inspection task

Actually, there are plenty of other areas of interest where UAVs are used, after listing some of them there is no doubt that there exists a large market demand for deploying such vehicles on a large scale thanks to their practicality and availability. However, many constraints slow down their integration in civil airspace particularly the poor reliability level as a consequence of their increasing accidents record. It is clear that in case of a drone malfunction, besides the probable complete loss of the vehicle itself, the whole surrounding environment is subjected to a significant menace. That's why several recent investigations conducted by the BEA (Bureau d'Enquêtes et d'Analyses pour la securite de l'aviation civile) are concerned with the drones and UAVs incidents. Among them, there exists a serious *DJI - Inspire 2* drone incident[4] during filming a music festival gathering several thousand people at Barcarès, France.

[2] https://www.parrot.com/fr/drones/anafi-ai

[3] https://www.airbus.com/innovation/zero-emission/urban-air-mobility/cityairbus.html

[4] https://bea.aero/en/investigation-reports/notified-events/detail/serious-incident-with-a-dji-inspire-2-drone-on-14-07-19-at-le-barcares/

The accident happened due to the drastic loss of one battery charge that lead to a complete loss of control which resulted in crashing the drone into a vertical structure on the stage.

Another dangerous UAV incident[5] took place when a Belgian large drone having a wingspan of $3\ m$ went out of control and crossed the French border. The drone has scrambled two Rafale aircraft to follow for two hours until it crashed in the Aisne department, France. These are a few examples of UAVs accidents that prove that great attention has to be paid to their safety and security due to the social and ecological effects that may arise because of unwise use in daily life. Or in other words, for the sake of empowering large-scale deployment of these vehicles, they must be provided with additional FTC schemes that can handle unexpected malfunction.

In order to be able to provide a solution for aircraft failures, the sources of the faults and the consequent damage have to be identified precisely. Certainly, there doesn't exist a unified method for handling all system problems, however, the proposed solution based on the FTC technique is appealing as it is dedicated to the system parts that are more likely to fail than others. According to [7], about 40% of UAVs failures are due to power plants faults and around 15% are resulting from the navigation system malfunction, which urges this work to investigate the problem of UAVs sensors and actuators faults aiming to propose an effective solution in a form of an active FTC algorithm that increases UAVs security and sustainability.

One special type of UAVs is the quadrotor which possesses the ability of Vertical Take-Off and Landing (VTOL) besides being able to hover at a certain spatial position, so it is very practical for surveillance and inspection tasks. Also, the quadrotor is more advantageous than other multi-rotor aerial vehicles such as hexacopters and octocopters that perform the same required missions but with higher power consumption due to the existence of more brushless motors. However, a quadrotor is an underactuated system depending on 4 motors to perform 6 degrees of freedom motion in space, thus actuator faults are fatal and cause serious losses (some of them will not only harm the system itself but also the environment).

In addition, a quadrotor is usually equipped with lightweight, low-cost sensors like IMU for orientation, ultrasonic for altitude, and GPS for the position, and despite their acceptable performance in nominal conditions, they are vulnerable to sensor faults see [8]. Such malfunction may induce the inability of the vehicle to perform its mission, therefore it is beneficial to supply a quadrotor with an additive sensor FTC unit. Concerning this topic, the methodology followed in [9] shows how important an FDD unit is for establishing an effective sensor FTC algorithm where the controller reconfiguration is based on the residual signal obtained after system diagnosis.

That's why a great concern has been dedicated in academic research for the problem of quadrotors fault-tolerant control in a general manner regarding sensors and actuator faults see [10]. Consequently, the work presented in this thesis consists of a continuation of the recent approaches aiming to be a worthy contribution to the evolution of UAVs safety and reliability particularly quadrotors.

[5] https://www.vrt.be/vrtnws/en/2016/03/01/french_jets_scrambledtofollowout-of-controlflemishdrone-1-2587685/

1.2 Problem statement

The problem addressed in this work is to investigate the design of an AFTC algorithm for a quasi-LPV system. The developed methods are validated on a quadrotor helicopter such that it can keep stable and complete the required task in case of system malfunction. Such a problem can be tackled through some fundamental steps beginning with creating an adequate model for the system that is able to represent the physical dynamics accurately to guarantee the effectiveness of the algorithms established after. Then, the challenging task is to design a robust controller that stabilizes the system and makes it able to follow the desired trajectory. Later, to ensure that the system generates a correct alarm in case of malfunction an effective FDD unit has to be introduced to locate the fault precisely and estimate its magnitude. Afterward, the results are evaluated to decide whether the controller can accommodate the damage or it needs to be reconfigured to contain the fault and maintain the whole system stability.

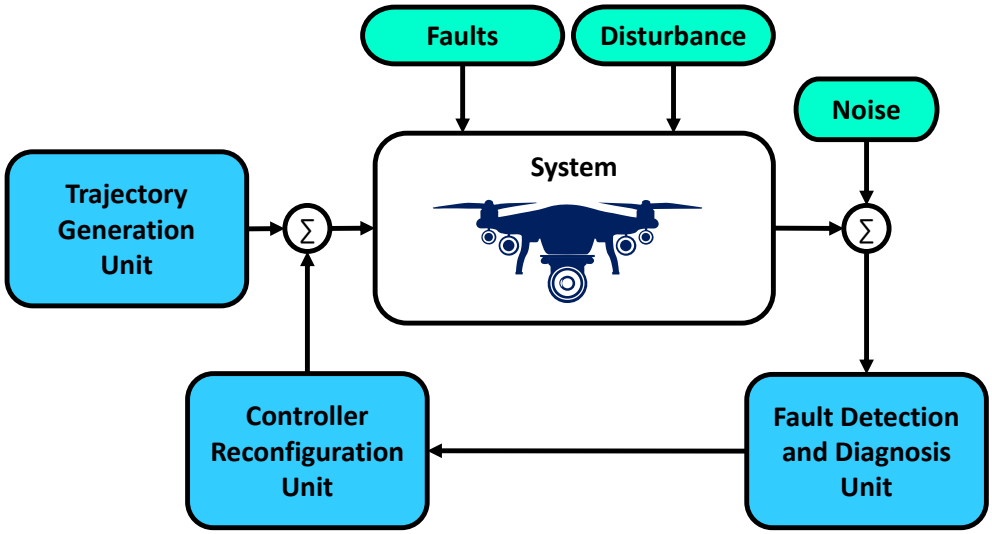

Figure 1.2: Problem schematic

As shown in figure 1.2 the AFTC scheme consists of an FDD unit to identify and evaluate the fault then transfer this information to a controller reconfiguration unit to modify the required control action needed for stabilizing the system while it is subjected to exogenous disturbances and measurement noise. In the next chapters, we will give a detailed mathematical description for each block diagram and the accompanying design methodology to ensure optimal performance.

1.3 State of the art

So as to achieve an innovative optimal design methodology for each of the mentioned tasks, one has to investigate the recent algorithms introduced in the literature properly. An overview of the main approaches that are currently developed and have directly contributed to the accomplishment of this work is presented in this section. Concerning

the quadrotor modeling, the Newton-Euler formulation presents an efficient solution for describing the vehicle kinematics and dynamics followed by a linearization using small disturbance theory to produce a model that can facilitate the controller design as illustrated in [11]. Another powerful methodology for representing the system dynamics is the Linear Parameter Varying (LPV) which approximates the model's nonlinear terms by linearly varying functions. In that manner, the resulting system ensures a simpler dynamical analysis and control law design besides accurate modeling of the system dynamics as can be found in [12] and [13].

Based on the deduced model of the quadrotor, a suitable control law can be designed and since the controller is applied in real-time on the actual nonlinear system, great attention has to be paid to the model derivation. For the linear system model, a PID classical control law can be introduced as in [14], nevertheless, the controller robustness is achieved by loop shaping technique in [15]. Another solution for the controller design of an LTI system is to use an LQR control law which is able to count for the control input limitation and state variation rate through finding an optimal solution of the given cost function as presented in [16]. On the other hand, while seeking a robust controller design methodology against exogenous signals for LPV system, a powerful solution is to consider minimizing the $\mathcal{H}_\infty$ norm value of the closed-loop system which is presented in [17] and further deployed in controlling a quadrotor modeled in an LPV framework in [18] and [19].

Concerning the fault detection and diagnosis problem, several methods have been introduced in the literature among them there exists the model-based approach in a form of a state observer to check the matching between the model output and the actual system output. Aiming at precise fault detection, a deterministic system model can be handled using Luenberger type observer as in [20] while for a stochastic model affected by Gaussian noise for measurement and uncertainty a convenient solution is to use Kalman filter as proposed by [21]. In order to ensure the robustness of the observer in a way that minimizes the effect of the unknown disturbance while being sensitive to the actual system fault, the $\mathcal{H}_-/\mathcal{H}_\infty$ technique used in [22] presents a reliable solution.

Nevertheless, such $\mathcal{H}_-/\mathcal{H}_\infty$ approach could be transformed into a simple minimization form in the work of [23] and further deployed by [24] with the aid of a perturbation output effect to satisfy the regularity condition [25] needed for ensuring the feasibility of the quadratic $\mathcal{H}_\infty$ norm minimization problem. In addition, the solution presented in [26] is appealing since the introduced virtual residual term enables the observer to perform fault estimation. The observer design in such work considers an auxiliary output of the system derived using the output signal derivatives [27] according to its relative degree with the fault [28]. After ensuring adequate fault estimation performed by the FDD unit, the results can be integrated with a controller reconfiguration unit to complete the active FTC scheme as in [29] and [30]. In the next few chapters, it will be illustrated how these works have encouraged and influenced the developed algorithms throughout this thesis besides its main contributions that are summarized in the next section.

1.4 Work contributions

In this section, the main contributions of the thesis are highlighted to give a clear track for the reader of the most important achievements which can be summarized as follows:

1. while modeling the quadrotor position states dynamics, it is found that the heading angle plays a vital role in the position loop as it enables to generate smoother trajectories where the drone can move freely in $x-y$ plane. Such a degree of freedom is lost while the classical linearization of the system around the hovering point is performed assuming small variations of ψ angle to simplify the trigonometric functions existent in the position dynamics. This simplification imposes a constraint on motion in the $x-y$ plane where the system is obliged to perform a decoupled motion along both axes x and y. In this work, a solution for such a problem is proposed benefiting the LPV system properties where the heading angle is considered as a macro varying parameter and then the trigonometric functions are approximated by linear representation according to the value of the heading angle $\psi \in [-\frac{\pi}{2}, \frac{\pi}{2}]\ rad$.

2. the proposed LPV controller takes the form of a self-scheduled state feedback control law aiming to minimize the quadratic $\mathcal{H}_\infty$ performance level with respect to the exogenous disturbance by solving the Bounded Real Lemma (BRL). Furthermore, an additional degree of freedom is provided to the controller design algorithm by introducing the Lyapunov inequality in an LMI form to achieve the required closed-loop system time response characteristics.

3. through investigating the literature of the problem of fault detection numerous model-based approaches are found to be efficient and produce reliable results. So in this work, a comparison is held between two well-known observers namely, continuous-time Kalman filter, and $\mathcal{H}_-/\mathcal{H}_\infty$ technique. The performance of both algorithms is evaluated through simulation of the quadrotor model subjected to measurement noise and exogenous disturbances. By executing a precise analysis of the simulation results, the observer designed using $\mathcal{H}_-/\mathcal{H}_\infty$ technique is found to be more indicative for fault detection thus it represents a promising solution for further fault diagnosis.

4. during formulating the $\mathcal{H}_-/\mathcal{H}_\infty$ optimization problem into a set of LMIs to solve, the regularity condition has to be satisfied by introducing a term modeling the effect of actuators faults on the measured output directly. Such an issue is solved by exploiting the recent development of robust algorithms for output signal differentiation in a way that ensures realistic modeling of actuators' faults on extended system output. To guarantee the extended (auxiliary) output includes the faults effect, the output relative degree to faults is introduced and analyzed for the quadrotor model.

5. by introducing a virtual residual term, a generalized residual generator design methodology is proposed alternative to the $\mathcal{H}_-/\mathcal{H}_\infty$ technique. This proposed algorithm investigates two decoupling conditions based on the

system model that can lead to either exact or asymptotic residual to fault convergence. If the system doesn't convey with any of the discussed conditions, an enhanced $\mathcal{H}_-/\mathcal{H}_\infty$ algorithm benefiting an additional degree of freedom for gains assignment is deployed for simultaneous fault detection and estimation.

6. the results obtained using the developed residual generator design methodology encouraged to apply the same technique for the case of sensor faults. So by means of adding an integral action to the system, an augmented system is attained where the sensor faults are masked to be affecting directly the system states. Such an approach empowers the residual generator to count for the effect of the exogenous disturbance on the measured output while performing fault estimation and isolation.

1.5 Thesis plan

***Chapter* 1** indicates the motive behind this work through discussing the basic concepts of fault-tolerant control and showing how important it is for autonomous systems especially aerial ones. In addition, it explains why a quadrotor is an aerial vehicle chosen for applying the developed algorithms by reviewing its characteristics and fields of deployment. Afterward, an overview of the problem formulation is provided followed by the main work contributions such that the thesis organization becomes more comprehensible.

***Chapter* 2** provides a methodology for deriving the quadrotor mathematical model based on Newton-Euler formulation for describing the vehicle's linear and angular motions. Then some linearization techniques have been introduced aiming to achieve a simplified, yet accurate linear model such that the algorithms built on this model comply with the real-time implementation constraints. After that, a piecewise affine modeling technique has been investigated to enhance the obtained linear model. Finally, the quadrotor has been represented in an LPV framework which covers all the system nonlinearities and expresses them as linearly time-varying parameters.

***Chapter* 3** investigates the control techniques compatible with the derived quadrotor models, beginning with a classical PID control law to stabilize the linear model described by transfer functions. The control algorithm is then enhanced based on loop shaping of the sensitivity and complementary sensitivity transfer functions to satisfy the required $\mathcal{H}_\infty$ norm characteristics. Afterward, an LQG control scheme consisting of an LQR controller besides an LQE state observer is proposed for the piecewise affine model in state-space form. Thereafter a self-scheduled robust feedback LPV controller is introduced for each subsystem of the quadrotor quasi-LPV model such that the system is maintaining a quadratic $\mathcal{H}_\infty$ performance index against undesired inputs. For each of the aforementioned techniques, the design methodology is provided in addition to the simulations executed using Matlab Simulink to test their efficiency and applicability. Finally, for generating a 3D trajectory between initial and final spatial points, an

approach is presented based on cartesian polynomial curves and validated by simulation with the quadrotor LPV model.

***Chapter* 4** is dedicated to handling the problem of system fault detection and diagnosis based on model-based observer design which serves as a residual generator then applies the obtained results on the quadrotor model. So, some design methodologies are introduced like Lunberger type observer for the deterministic model, continuous-time Kalman filter for the stochastic system, and $\mathcal{H}_-/\mathcal{H}_\infty$ technique as a robust observer. A comparison between the latter two approaches in fault detection of quadrotor experiencing actuators malfunction is conducted using Matlab-Simulink. Afterward, the comparison conclusions urged us to investigate further enhancements of the $\mathcal{H}_-/\mathcal{H}_\infty$ approach which is achieved by introducing a virtual residual signal in the observer scheme. In that way, some structural properties of the system are studied to improve the residual generator design such that it becomes able to provide fault detection, estimation, and isolation. Also, the proposed method benefits from the differentiated output signal which preserves the feasibility of the algorithm by satisfying the regularity condition. Finally, to demonstrate the applicability and effectiveness of the proposed algorithm it is first applied for sensors and actuators fault diagnosis considering some LTI and LPV examples. Nevertheless, the obtained residual generator is used for fault estimation of the quadrotor LPV model subjected to sensors and actuators faults and operating in environmental conditions imposing exogenous disturbances and measurement noise.

***Chapter* 5** introduces a design methodology of an actuator FTC law based on the estimated fault provided by the residual generator which enables the quadrotor to follow the desired trajectory during fault existence. The proposed FTC law is then analyzed to ensure a smooth convergence of the faulty states to their corresponding healthy model values. Afterward, the eigenvalues of the controllability gramian and the closed-loop faulty system are computed with respect to the magnitude of the actuators' loss of efficiency justifying the degraded system performance in the absence of the FTC law. The limitations of the proposed FTC law are then found to lie behind the fact that the quadrotor is an underactuated system that doesn't possess physical actuator redundancy. Finally by means of simulation of the quadrotor LPV model in different actuators fault scenarios, the potential of the introduced FTC scheme is proven by the adequate trajectory following the system exhibits despite the existence of the fault.

***Chapter* 6** provides a general conclusion that gathers the results of the work presented in the thesis in an integrated form after discussing each problem separately, in addition to the perspectives and future work that can complete and enhance the presented techniques in a way that guarantees a wide use in real-time applicatio

Chapter 2

System Modelling

Chapter abstract

The Newton-Euler formulation is used for modeling the quadrotor dynamics resulting in a mathematical model that describes the relation between the applied forces and the system states. In order to guarantee that the developed algorithms comply with real-time implementation constraints, the obtained model is linearized around the hovering point using the small disturbance theory. But as the resulting model is excessively simplified some other propositions are investigated. One suggestion is to assume a constant value for the nonlinear terms in the attitude loop instead of neglecting them leading to an affine system representation. However, the second method adopted is appealing as the system is modeled in an LPV framework where the nonlinear terms are considered as linearly time-varying within the given parameter limits.

2.1 Introduction

The process of system modeling is the way to describe the physical properties of the system and its surrounding environment by mathematical equations. The resulting mathematical model varies according to the designer's perspective, however, it has to be representing the dynamics of the system precisely. It is a very crucial task because the model is the milestone for designing the suitable control law which is further used in real-time reference tracking or system regulation.

Despite the necessity of an adequate model, there is always a compromise between the model accuracy and its simplicity as mentioned in [31]. Besides representing the physical dynamics well, the derived mathematical model should be reasonably simple to facilitate the process of the controller design. According to the type of the system, the model may include highly nonlinear differential equations and the challenge is to choose the nonlinear terms that can be neglected without affecting the model accuracy.

Thus, mathematical model linearization is a common procedure while considering control systems analysis to obtain a simplified yet accurate system model. Several approaches have been introduced for linearization like the small disturbance theory detailed in [32] for aircraft modeling and control, and Jacobian linearization [33] based on Taylor's series expansion.

The nutshell of linearization varies according to the application and the dynamic behavior of the system. According to the resulting mathematical model it can be classified as Linear Time-Invariant (LTI) and Linear Time-Varying (LTV) systems. Briefly, an LTI system can be represented in state space form with constant matrices, while for an LTV case the system matrices are varying with time, more illustration can be found in [31].

In this work, we are concerned with Linear Parameter Varying (LPV) systems which were first introduced in [34]. An LPV system is defined by [35] as a type of linear time-varying systems whose state space matrices are functions of time-varying parameters. The difference between LPV and LTI systems is evident as LPV system varies with respect to time, however, it is not the same case when they are compared with LTV systems. The behavior of an LPV system for a specific trajectory of the varying parameter is similar to a LTV system, but the main distinction is on the level of analysis and synthesis as stated in [36].

The LPV models are classified according to the source of the varying parameters into two main categories, one where the varying parameters are exogenous signals referred to as pure or standard LPV model, while the other having the system states themselves as varying parameters called quasi-LPV system. Generally, The LPV framework is very promising as it offers to embed the model nonlinearities as time-varying parameters instead of neglecting them. That's why such modeling methodology is being widely used in several domains like observer design for lateral vehicle dynamics estimation [37], aircraft control [38], and quadrotor fault-tolerant control [35].

Concerning quadrotor modeling, as mentioned earlier these vehicles are very popular and interesting for the research community, so several vehicle models have been proposed in the literature. The most popular method is to use Newton-Euler formulation to describe the system kinematics and dynamics then linearize the resulting model around the hovering point. Besides that, such a method assumes a small variation of the attitude angles to generate 2D motion. This technique can be found in several works like [39] in which the relation between attitude angles and control inputs is described by a double pole transfer function, besides [40] which gives a state space linearized model for a quadrotor. In [41] one can find a piecewise affine modeling of attitude dynamics giving a more realistic representation which can allow for larger flight envelop by assuming constant values for the nonlinear terms instead of neglecting them.

Recently, thanks to the advantages of the LPV modeling which offers a time-varying representation while preserving simpler dynamical system analysis, numerous works have adopted such techniques for solving quadrotor modeling problem. In [19] after linearization around the hovering point, the position dynamics depend on the heading angle that is considered a varying parameter. While [13] assumed a quasi-LPV model including the system states, control input, and estimated faults seeking an active model predictive fault-tolerant control scheme for a quadrotor.

Nevertheless, one can find a methodology proposed in [42] based on Taylor series expansion of the trigonometric functions existent in the position dynamics loop aiming at high-speed trajectory tracking. And in [12] a simple change of variables is used to calculate the required control action for position tracking. The work presented in this chapter benefits from the proposed ideas and tries to establish a rigorous model for the quadrotor UAV which represents the system dynamics precisely while being simple enough for ensuring an efficient control law design.

It is to be noted that although the methodology used in the modeling part is applied directly to a quadrotor vehicle, the same steps can be followed for modeling any aircraft including kinematics and dynamics investigation and passing by the equations governing the aircraft motion to reach the vehicle mathematical model. Depending on the particular system nature, the type of controller to be designed, and the sort of application, the mathematical model can be linearized or not in order to be presented in a more convenient form.

2.2 Quadrotor UAV

The quadrotor is a type of UAVs that consists of a rigid cross-frame equipped with four rotors pointing upwards. On seeing the vehicle structure, it comes to one's mind that it can take-off and land vertically by giving some motors speed to generate thrust force. However, the dynamic stability of such a vehicle is not as simple as it seems and requires a large research effort to be achieved as will be illustrated later. In this work the Newton-Euler formulation [43] is used to describe the quadrotor kinematics and dynamics with the following assumptions:

Structural assumptions

Assumption 1 *The structure is rigid.*

Assumption 2 *The structure is symmetric.*

Assumption 3 *The quadrotor's center of gravity (CG) coincides with the body-fixed frame origin.*

2.2.1 Newton's second law of motion

As mentioned earlier in this work, Newton-Euler formulation is the method adopted for system modeling. Basically, there are several types of forces affecting the aircraft's motion including the aerodynamic, gravitational, and propulsive forces. As any aircraft performs rotational and translational motions, the equations governing their spatial movement are deduced from Newton's second laws for linear and angular motion. Newton's second law for linear motion states that the sum of all the external forces acting upon the aircraft is equal to the time rate of change of the linear momentum, it can be described mathematically by

$$\sum \vec{\mathcal{F}} = \frac{d}{dt}(m\ \vec{v}) \tag{2.1}$$

While for angular motion, the sum of all the external moments acting upon the aircraft is equal to the time rate of change of angular momentum given by

$$\sum \vec{\mathcal{M}} = \frac{d}{dt}(\mathbf{I}\vec{w}) \tag{2.2}$$

where m is the aircraft mass, v is the aircraft velocity vector, $\mathbf{I}$ represents the aircraft moment of inertia, and w is the angular velocity vector. An important point is that equations (2.1) and (2.2) are referred to an absolute fixed frame which implies a difficulty because as the aircraft rotates the moments of inertia are varying with time with respect to these fixed axes. That's why two coordinate systems are considered, one called body frame attached to the aircraft center of gravity and rotating with it, while the other is the fixed frame called world frame, both are detailed in section 2.2.2. The vehicle velocity and angular momentum are calculated in the body frame to avoid the moment of inertia variation with time then transferred to the inertial frame to calculate the position and orientation of the aircraft as illustrated in the next sections 2.2.2 and 2.2.3. Equations (2.1) and (2.2) are represented in body axes in the following form

$$\begin{bmatrix} mI_{3*3} & 0_{3*3} \\ 0_{3*3} & \mathbf{I} \end{bmatrix} \begin{bmatrix} \dot{V}_B \\ \dot{w}_B \end{bmatrix} + \begin{bmatrix} w_B \times (mV_B) \\ w_B \times (\mathbf{I}w_B) \end{bmatrix} = \begin{bmatrix} \mathcal{F}_B \\ \mathcal{M}_B \end{bmatrix} \tag{2.3}$$

where V_B and w_B represent the linear and angular velocities in the body frame, respectively. $\mathcal{F}_B$ denotes the force vector in the body frame, and $\mathcal{M}_B$ is the moment vector in the body frame. A complete derivation for Newton's second law (2.3) governing the aircraft motion can be found in [32].

2.2.2 Kinematics

The kinematics[1] can be defined as the branch of physics that describes the motion of a body without considering the forces acting upon it. Thus, studying the system kinematics enables to establish a relation between its spatial motion and the ground control unit that's why it is beneficial in system modeling and navigation.

Figure 2.1 shows the vehicle free body diagram containing two pairs of opposite motors in a cross configuration. The figure illustrates also the two main previously mentioned coordinate systems used in the analysis, namely world frame W defined by the axes x_w ,y_w, and z_w having its origin at the ground station, besides the body frame B whose origin coincides with the CG of the body and having the axes x_B ,y_B, and z_B.

In addition, the figure indicates the principle angular rotations that are very important in motion generation see [44]. The position and orientation of the aircraft have to be referred to some inertial frame that is not moving nor rotating, in the aircraft case it is considered the world frame W and it is located at the ground control station.

[1] https://en.wikipedia.org/wiki/Kinematics

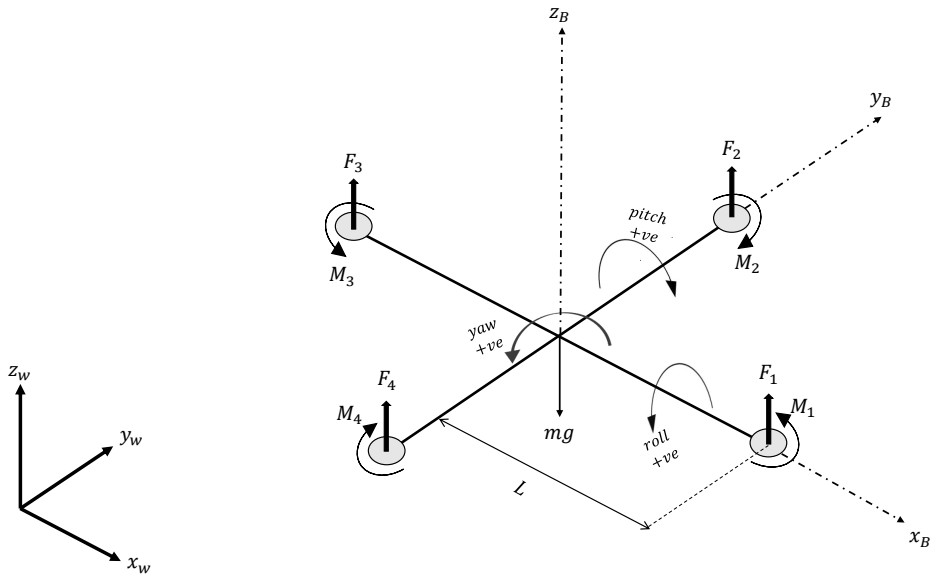

Figure 2.1: Quadrotor free body diagram

Euler angles

The relation between the world frame W and the body frame B can be described by three consecutive rotations called Euler angles. The order of rotations is very important and there exist multiple combinations but in this work we use $\psi - \theta - \phi$ Euler angles to model the rotation of the aircraft in the world frame, such a sequence consists of the following rotations:

- a rotation around z axis with an angle ψ (yaw motion)

$$R[\psi] = \begin{bmatrix} \cos\psi & -\sin\psi & 0 \\ \sin\psi & \cos\psi & 0 \\ 0 & 0 & 1 \end{bmatrix} \tag{2.4}$$

- followed by a rotation around y axis with an angle θ (pitch motion)

$$R[\theta] = \begin{bmatrix} \cos\theta & 0 & \sin\theta \\ 0 & 1 & 0 \\ -\sin\theta & 0 & \cos\theta \end{bmatrix} \tag{2.5}$$

- finally rotate around x axis with an angle ϕ (roll motion)

$$R[\phi] = \begin{bmatrix} 1 & 0 & 0 \\ 0 & \cos\phi & -\sin\phi \\ 0 & \sin\phi & \cos\phi \end{bmatrix} \tag{2.6}$$

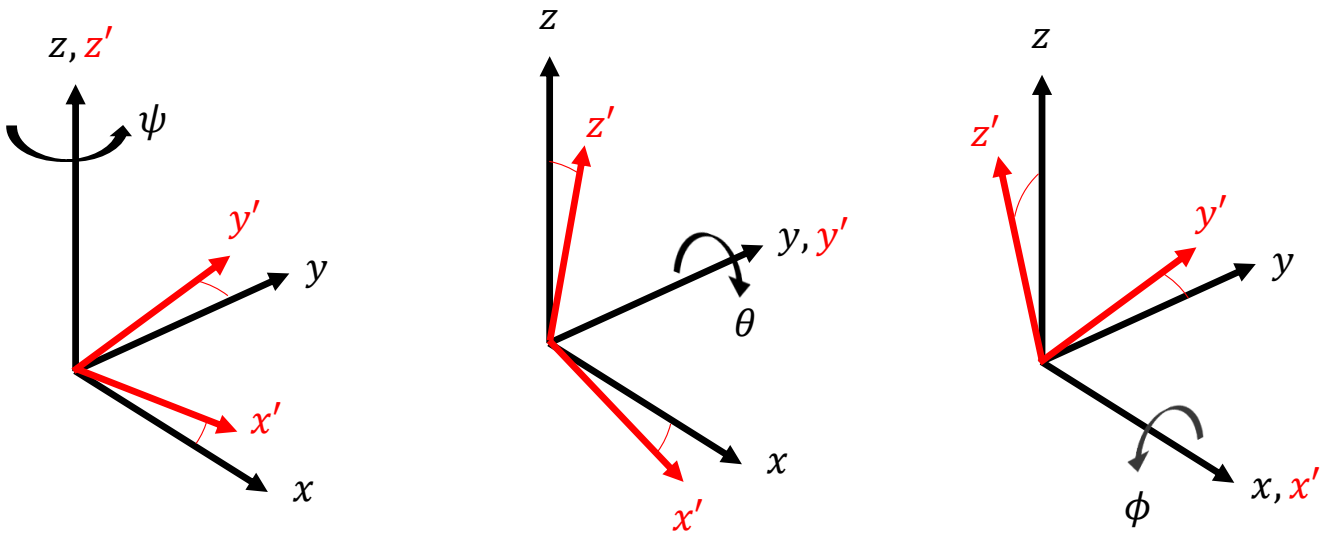

(a) rotation around z axis (b) rotation around y axis (c) rotation around x axis

Figure 2.2: Euler angles

The three rotations are illustrated in figure 2.2 and the resulting transformation matrix $R_{B\to W}$ from body frame B to world frame W is given by

$$R_{B\to W} = R[\psi]R[\theta]R[\phi] \tag{2.7}$$

$$R_{B\to W} = \begin{bmatrix} \cos\theta\cos\psi & \cos\psi\sin\theta\sin\phi - \cos\phi\sin\psi & \cos\phi\cos\psi\sin\theta + \sin\phi\sin\psi \\ \cos\theta\sin\psi & \cos\phi\cos\psi + \sin\theta\sin\phi\sin\psi & -\cos\psi\sin\phi + \cos\phi\sin\theta\sin\psi \\ -\sin\theta & \cos\theta\sin\phi & \cos\theta\cos\phi \end{bmatrix} \tag{2.8}$$

So any vector in the body frame called $A|_B$ can be expressed in the world frame as $A|_W$ by the following relation

$$A|_W = R_{B\to W}A|_B \tag{2.9}$$

Euler rates

Consider the components of the aircraft angular velocity vector in the body frame w_B along the body axes x, y, z are p, q, r respectively, then they can be related to the angular rates in the inertial frame $\dot{\phi}, \dot{\theta}, \dot{\psi}$ following the same rotation sequence $\psi - \theta - \phi$ used to obtain the rotation matrix by

$$\begin{bmatrix} p \\ q \\ r \end{bmatrix} = \begin{bmatrix} \dot{\phi} \\ 0 \\ 0 \end{bmatrix} + R[\phi]\begin{bmatrix} 0 \\ \dot{\theta} \\ 0 \end{bmatrix} + R[\phi]R[\theta]\begin{bmatrix} 0 \\ 0 \\ \dot{\psi} \end{bmatrix} \tag{2.10}$$

then

$$\begin{bmatrix} p \\ q \\ r \end{bmatrix} = \begin{bmatrix} 1 & 0 & -\sin\theta \\ 0 & \cos\phi & \sin\phi\cos\theta \\ 0 & -\sin\phi & \cos\phi\cos\theta \end{bmatrix} \begin{bmatrix} \dot{\phi} \\ \dot{\theta} \\ \dot{\psi} \end{bmatrix} \tag{2.11}$$

and

$$\begin{bmatrix} \dot{\phi} \\ \dot{\theta} \\ \dot{\psi} \end{bmatrix} = \begin{bmatrix} 1 & \sin\phi\tan\theta & \cos\phi\tan\theta \\ 0 & \cos\phi & -\sin\phi \\ 0 & \sin\phi\sec\theta & \cos\phi\sec\theta \end{bmatrix} \begin{bmatrix} p \\ q \\ r \end{bmatrix} \tag{2.12}$$

2.2.3 Dynamics

The dynamics can be considered as the complementary branch for the kinematics study as it is concerned with aircraft motion due to the applied forces. So studying system dynamics enables one to establish the relation between the affecting forces and the resulting vehicle velocity and acceleration, hence, this part is dedicated to describing the vehicle movement and how it can be produced. The quadrotor is one of the unidirectional thrusters that have 4 brushless motors pointing up, each one rotates with an angular speed Ω_i and produces a thrust force F_i and an angular moment called M_i as illustrated in figure 2.1 where i represent the actuator number and $i \in [1, \ldots, 4]$. For each motor i, the source of such thrust force F_i is the interaction between the airflow and the propeller attached to the motor hub and its airfoil shape. In addition, the moment M_i is generated following Newton's third law of motion as a reaction to the rotation of the rotor part inside the brushless DC motor around the stator part. The relation between the rotor speed and the resulting force and moment is described by

$$\begin{aligned} F_i &= K_f {\Omega_i}^2 \\ M_i &= K_m {\Omega_i}^2 \end{aligned} \tag{2.13}$$

where K_f and K_m are the thrust constant and the moment constant of the motor at steady state. This approximation is fair enough and widely deployed to represent the motor dynamics for the case of a quadrotor vehicle. However, the exact relationship between motor speed and the produced forces and moments is rather complicated and requires more investigation for the whole propulsive system including the aerodynamics of the rotor blade as illustrated in [43], which preferred finally a simplified model for motor dynamics that is more suitable for further controller design.

As the induced motor force and moment are directly related to the rotor speed, the quadrotor generates its motion by adjusting the angler velocity of each rotor Ω_i. Before proceeding with motion description it is to be mentioned that a very convenient method for studying the quadrotor motion is to divide it into two subsystems the first is the attitude subsystem having fast dynamics including the orientation angles (roll (ϕ), pitch (θ), and yaw (ψ)) and their derivatives, while the second is the translation subsystem having relatively slower varying position states (x, y, and z) and their derivatives too.

Hovering motion

Is the most important operating point of the quadrotor as it represents the equilibrium point where the required motors thrust is equal to the weight of the drone. Also, the quadrotor passes from one maneuver to another through this hovering point. As illustrated later the quadrotor motion is generated by small variations of attitude angles around the hovering condition. During hovering the quadrotor shouldn't exert any yawing action so in the motor configuration each opposite pair rotates in the same direction as shown in figure 2.3 to avoid drifting not only at hovering but also throughout the motion.

As mentioned earlier the quadrotor is an under-actuated system that performs the 6 DOF movements (3 rotations ϕ, θ, ψ and 3 translations x, y, z) using only four actuators, so the movement in each direction depends on a combination of the corresponding motor forces and moments. Altitude control is achieved by changing the total thrust of the 4 rotors such that it is increased for taking-off and going up or decreased for descending and landing as illustrated in figure 2.3.

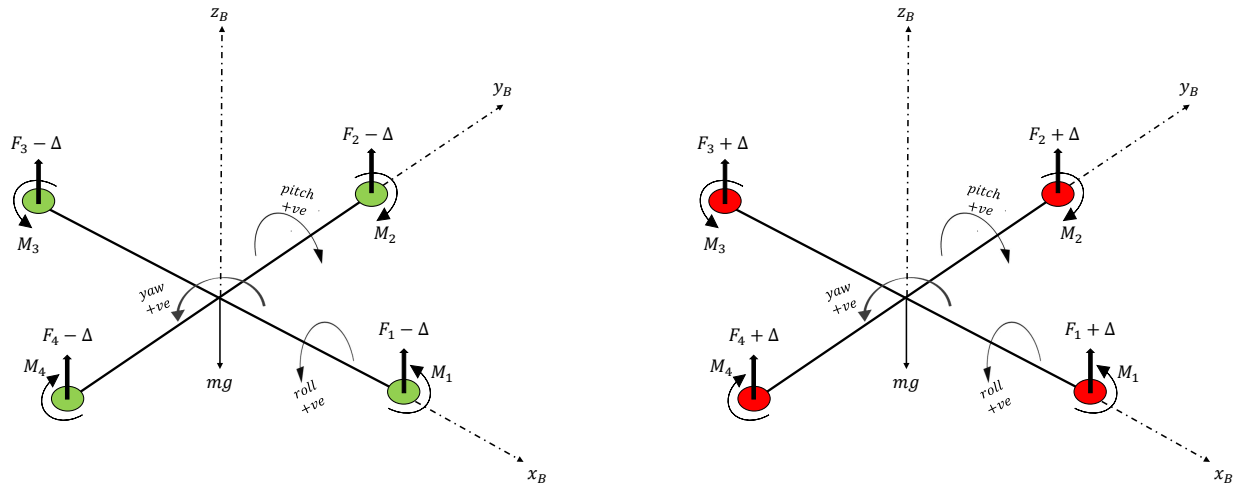

(a) moving down

(b) moving up

Figure 2.3: Movement along z axis

In addition, changing the heading angle is achieved by reducing the thrust of one set of rotors and increasing the trust of the other set while maintaining the same total thrust to hold the altitude as shown in figure 2.4. Finally, the motion along x axes is induced by a rotation around y axis by an angle θ given in figure 2.5a, and similarly, the motion along y axis is carried out by a rotation around x axis with an angle ϕ as illustrated in figure 2.5b.

Control input

As illustrated, each movement for the quadrotor depends on a combination of the 4 actuators' forces, so it is more convenient to assemble these forces to reproduce control inputs that are directly affecting the motion directions.

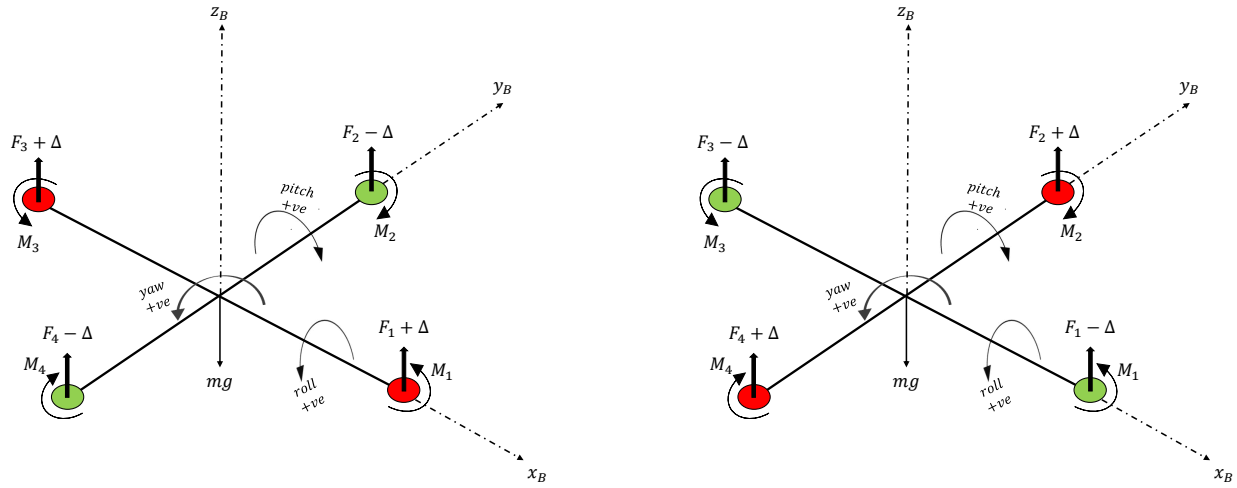

(a) positive yaw angle

(b) negative yaw angle

Figure 2.4: Heading angle control

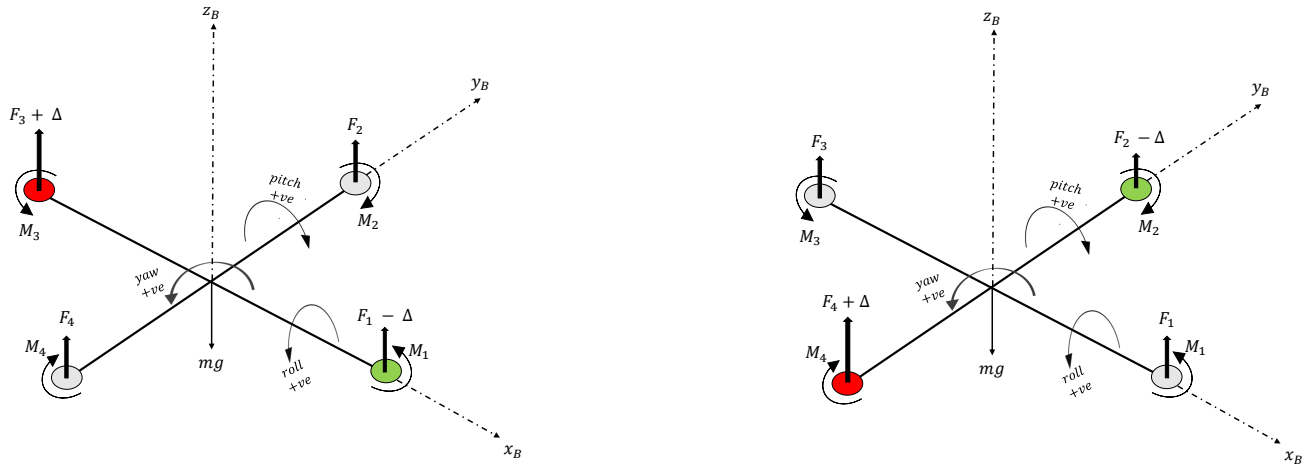

(a) moving along x axis

(b) moving along y axis

Figure 2.5: Movement in $x - y$ plane

Consider the control input vector is given by:

$$u(t) = \begin{bmatrix} u_z & u_\phi & u_\theta & u_\psi & \Omega_r \end{bmatrix}^T \tag{2.14}$$

where

$$\begin{aligned} u_z &= \sum F_i \\ u_\phi &= L(F_2 - F_4) \\ u_\theta &= L(F_3 - F_1) \\ u_\psi &= M_1 - M_2 + M_3 - M_4 \\ \Omega_r &= \Omega_1 - \Omega_2 + \Omega_3 - \Omega_4 \end{aligned} \tag{2.15}$$

So u_z is the sum of all actuators forces responsible for the motion along z axis, while u_ϕ and u_θ represent the moments around x and y axes, respectively, where L represents the quadrotor arm length illustrated in figure 2.1. Thus, u_ϕ generates a rolling rotation ϕ which induces the motion along the negative direction of y axis, along with u_θ responsible for the pitching movement with an angle θ resulting in a motion along x axis. Besides, u_ψ representing the control action in charge of changing the heading angle ψ.

Finally, Ω_r is the overall residual angular speed resulting from the four motors, this control action doesn't correspond to any of the main motion directions. However, it represents the gyroscopic effect resulting from the propeller's rotation given by equation (2.16) causing undesired angular rotation so its value has to be minimized.

$$\begin{aligned} \tau_x &= \dot{\theta} J_r \Omega_r \\ \tau_y &= -\dot{\phi} J_r \Omega_r \end{aligned} \tag{2.16}$$

where J_r is the propeller inertia constant while τ_x and τ_y represent the resulting residual torque in x and y directions, respectively.

Control allocation

The relation between the control actions $u_z, u_\phi, u_\theta, u_\psi$ and the motors angular velocities $\Omega_i, i = [1, \ldots, 4]$ can be deduced by substituting equation (2.13) into (2.15) resulting in the following equation

$$\begin{bmatrix} u_z \\ u_\phi \\ u_\theta \\ u_\psi \end{bmatrix} = T \begin{bmatrix} {\Omega_1}^2 \\ {\Omega_2}^2 \\ {\Omega_3}^2 \\ {\Omega_4}^2 \end{bmatrix}, T = \begin{bmatrix} K_f & K_f & K_f & K_f \\ 0 & K_f l & 0 & -K_f l \\ -K_f l & 0 & K_f l & 0 \\ K_m & -K_m & K_m & -K_m \end{bmatrix} \tag{2.17}$$

where T represents the control allocation matrix. It is also important to calculate its inverse especially for handling the problem of actuators faults estimation and identification, so it is given by

$$T^{-1} = \begin{bmatrix} \frac{1}{4k_f} & 0 & -\frac{1}{2Lk_f} & \frac{1}{4k_m} \\ \frac{1}{4k_f} & \frac{1}{2Lk_f} & 0 & -\frac{1}{4k_m} \\ \frac{1}{4k_f} & 0 & \frac{1}{2Lk_f} & \frac{1}{4k_m} \\ \frac{1}{4k_f} & -\frac{1}{2Lk_f} & 0 & -\frac{1}{4k_m} \end{bmatrix} \tag{2.18}$$

2.2.4 Equations of motion

After establishing a relation between earth fixed frame and vehicle body frame in addition to studying the forces and moments generated by the quadrotor motors, it is now clear how to solve Newton's second laws for linear and angular motion (2.3).

Linear motion equation

This is corresponding to the 1^{st} element of equation (2.3), and if we consider the quadrotor's center of gravity position vector in world frame denoted by $\mathbf{r}$, then it can be written as

$$m\ddot{\mathbf{r}} = \begin{bmatrix} 0 \\ 0 \\ -m.g \end{bmatrix} + R_{B\to W} \begin{bmatrix} 0 \\ 0 \\ \sum F_i \end{bmatrix} \tag{2.19}$$

where g is the acceleration of gravity, m is the vehicle mass, and $R_{B\to W}$ is the Euler rotation matrix given in equation (2.8). Benefiting from the augmented control input given by equation (2.15), the position dynamics can be given by

$$\begin{bmatrix} \ddot{x} \\ \ddot{y} \\ \ddot{z} \end{bmatrix} = \begin{bmatrix} (\cos\phi\cos\psi\sin\theta + \sin\phi\sin\psi)\frac{u_z}{m} \\ (-\cos\psi\sin\phi + \cos\phi\sin\theta\sin\psi)\frac{u_z}{m} \\ (\cos\theta\cos\phi)\frac{u_z}{m} - g \end{bmatrix} \tag{2.20}$$

Angular motion equation

It corresponds to the 2^{nd} element of equation (2.3) and can be represented in a vector form as

$$\mathbf{I}\begin{bmatrix} \dot{p} \\ \dot{q} \\ \dot{r} \end{bmatrix} = \begin{bmatrix} L(F_2 - F_4) + \tau_x \\ L(F_3 - F_1) + \tau_y \\ M_1 - M_2 + M_3 - M_4 \end{bmatrix} - \begin{bmatrix} p \\ q \\ r \end{bmatrix} \times \mathbf{I} \begin{bmatrix} p \\ q \\ r \end{bmatrix} \tag{2.21}$$

Before proceeding to deduce the quadrotor mathematical model, it has to be mentioned that by a simple analysis of the vehicle moment of inertia properties, the moment of inertia matrix $\mathbf{I}$ is found to be a diagonal matrix wihch simplifies solving equation (2.21). This is because the quadrotor has two planes of symmetry ($x-z$ and $y-z$ planes) as illustrated in figure 2.1, so the products of inertia $I_{xy} = I_{xz} = I_{yz} = 0$ and the moment of inertia matrix can be given by

$$\mathbf{I} = \begin{bmatrix} I_{xx} & 0 & 0 \\ 0 & I_{yy} & 0 \\ 0 & 0 & I_{zz} \end{bmatrix} \tag{2.22}$$

In addition, there is a special assumption concerning the case of quadrotor angular velocity, as throughout the motion the attitude angles ϕ, θ are having small values. This is a well-known assumption used in small disturbance theory which is detailed later and results in a great simplification for the Euler rates matrix (2.11) as it can be approximated by an identity matrix.

Assumption 4

The attitude angles ϕ, θ are changing with small values, so $p = \dot{\phi}, q = \dot{\theta}$, and $r = \dot{\psi}$

Benefiting the results of assumption 4, while introducing the moment of inertia as given in (2.22), then substituting equations (2.15) and (2.16) into angular motion equation (2.21) it becomes

$$\begin{bmatrix} \ddot{\phi} \\ \ddot{\theta} \\ \ddot{\psi} \end{bmatrix} = \begin{bmatrix} \frac{\dot{\theta}\dot{\psi}(I_{yy}-I_{zz})+\dot{\theta}J_r\Omega_r+u_\phi}{I_{xx}} \\ \frac{\dot{\phi}\dot{\psi}(I_{zz}-I_{xx})-\dot{\phi}J_r\Omega_r+u_\theta}{I_{yy}} \\ \frac{\dot{\phi}\dot{\theta}(I_{xx}-I_{yy})+u_\psi}{I_{zz}} \end{bmatrix} \tag{2.23}$$

2.3 Mathematical Model

The complete mathematical model for the quadrotor that represents the variation of system states with the applied input combines the translation and rotation equations (2.20) and (2.23), respectively. Consider the state vector given by

$$\mathbf{x}(t) = \begin{bmatrix} x & y & z & \phi & \theta & \psi & \dot{x} & \dot{y} & \dot{z} & \dot{\phi} & \dot{\theta} & \dot{\psi} \end{bmatrix}^T \tag{2.24}$$

Then the mathematical model takes the following nonlinear form

$$\dot{\mathbf{x}}(t) = \begin{bmatrix} \dot{x} \\ \dot{y} \\ \dot{z} \\ \dot{\phi} \\ \dot{\theta} \\ \dot{\psi} \\ (\cos\phi\cos\psi\sin\theta + \sin\phi\sin\psi)\frac{u_z}{m} \\ (-\cos\psi\sin\phi + \cos\phi\sin\theta\sin\psi)\frac{u_z}{m} \\ \cos\theta\cos\phi\frac{u_z}{m} - g \\ \frac{\dot{\theta}\dot{\psi}(I_{yy}-I_{zz})+\dot{\theta}J_r\Omega_r+u_\phi}{I_{xx}} \\ \frac{\dot{\phi}\dot{\psi}(I_{zz}-I_{xx})-\dot{\phi}J_r\Omega_r+u_\theta}{I_{yy}} \\ \frac{\dot{\phi}\dot{\theta}(I_{xx}-I_{yy})+u_\psi}{I_{zz}} \end{bmatrix} \tag{2.25}$$

2.3.1 Linearization

It is important to have a vehicle model that is representing the system fairly besides being as simple as possible to guarantee that the control law conveys the real-time implementation constraints. That's why mathematical model

linearization is a crucial step for system design since it offers a powerful method for model analysis such that the complicated nonlinear terms that have a slight effect on the system during operation can be neglected or represented in a more simplified form.

Jacobian Linearization

The method followed here is to derive the Jacobian matrix from the nonlinear model then substitute with the equilibrium point conditions. It depends on Taylor series expansion for the nonlinear differential equation representing the system dynamics around the equilibrium point. Consider equation (2.25) rewritten in the following form

$$\dot{\mathbf{x}}(t) = f(\mathbf{x}(t), u(t)) \tag{2.26}$$

If we assume that the system has an equilibrium point $(\bar{\mathbf{x}}, \bar{u})$ such that $f(\bar{\mathbf{x}}, \bar{u}) = 0$ and it is operating around this equilibrium point with small variations of states $\delta_x(t)$ and inputs $\delta_u(t)$ given by

$$\begin{aligned} \delta_x(t) &= \mathbf{x}(t) - \bar{\mathbf{x}} \\ \delta_u(t) &= u(t) - \bar{u} \end{aligned} \tag{2.27}$$

substituting in equation (2.26) we get

$$\dot{\delta}_x(t) = f(\bar{\mathbf{x}} + \delta_x(t), \bar{u} + \delta_u(t)) \tag{2.28}$$

Using Taylor series expansion with neglecting higher-order terms (this is very convenient as we consider small variations around equilibrium point) we get

$$\dot{\delta}_x(t) = \frac{\partial f}{\partial \mathbf{x}}\Big|_{\mathbf{x}=\bar{\mathbf{x}}, u=\bar{u}} \delta_x(t) + \frac{\partial f}{\partial u}\Big|_{\mathbf{x}=\bar{\mathbf{x}}, u=\bar{u}} \delta_u(t) \tag{2.29}$$

for simplicity, this equation can be written as follows

$$\dot{\mathbf{x}}(t) = \frac{\partial f}{\partial \mathbf{x}}\Big|_{\mathbf{x}=\bar{\mathbf{x}}, u=\bar{u}} \mathbf{x}(t) + \frac{\partial f}{\partial u}\Big|_{\mathbf{x}=\bar{\mathbf{x}}, u=\bar{u}} u(t) \tag{2.30}$$

keeping in mind that $\mathbf{x}(t)$ and $u(t)$ represent the states and control inputs variations. By defining the state matrix A_l and the control input matrix B_l

$$\begin{aligned} A_l &= \frac{\partial f}{\partial \mathbf{x}}\Big|_{\mathbf{x}=\bar{\mathbf{x}}, u=\bar{u}} \in \mathbb{R}^{n \times n}, \quad a_{ij} = \frac{\partial f_i}{\partial \mathbf{x}_j} \\ B_l &= \frac{\partial f}{\partial u}\Big|_{\mathbf{x}=\bar{\mathbf{x}}, u=\bar{u}} \in \mathbb{R}^{n \times m}, \quad b_{ij} = \frac{\partial f_i}{\partial u_j} \end{aligned} \tag{2.31}$$

where n and m represent the number of states and control inputs, a_{ij}, b_{ij} are the elements of matrices A_l, B_l, and i, j are the row and column number, respectively.

Then, equation (2.30) turns into the following well-known state space form

$$\dot{\mathbf{x}}(t) = A_l \mathbf{x}(t) + B_l u(t) \tag{2.32}$$

The quadrotor equilibrium point is the hovering condition described previously in 2.2.3 and can be represented mathematically by the following state space vector

$$\bar{\mathbf{x}} = \begin{bmatrix} x_h & y_h & z_h & 0 & 0 & \psi_h & 0 & 0 & 0 & 0 & 0 & 0 \end{bmatrix}^T \tag{2.33}$$

and the required control input

$$\bar{u} = \begin{bmatrix} u_{zh} & 0 & 0 & 0 & 0 \end{bmatrix}^T \tag{2.34}$$

it is to be mentioned that $u_{zh} = mg$ to maintain hovering condition, so the resulting state space matrices are as following

$$A_l = \begin{bmatrix} 0 & 0 & 0 & 0 & 0 & 0 & 1 & 0 & 0 & 0 & 0 & 0 \\ 0 & 0 & 0 & 0 & 0 & 0 & 0 & 1 & 0 & 0 & 0 & 0 \\ 0 & 0 & 0 & 0 & 0 & 0 & 0 & 0 & 1 & 0 & 0 & 0 \\ 0 & 0 & 0 & 0 & 0 & 0 & 0 & 0 & 0 & 1 & 0 & 0 \\ 0 & 0 & 0 & 0 & 0 & 0 & 0 & 0 & 0 & 0 & 1 & 0 \\ 0 & 0 & 0 & 0 & 0 & 0 & 0 & 0 & 0 & 0 & 0 & 1 \\ 0 & 0 & 0 & 0 & g & 0 & 0 & 0 & 0 & 0 & 0 & 0 \\ 0 & 0 & 0 & -g & 0 & 0 & 0 & 0 & 0 & 0 & 0 & 0 \\ 0 & 0 & 0 & 0 & 0 & 0 & 0 & 0 & 0 & 0 & 0 & 0 \\ 0 & 0 & 0 & 0 & 0 & 0 & 0 & 0 & 0 & 0 & 0 & 0 \\ 0 & 0 & 0 & 0 & 0 & 0 & 0 & 0 & 0 & 0 & 0 & 0 \\ 0 & 0 & 0 & 0 & 0 & 0 & 0 & 0 & 0 & 0 & 0 & 0 \end{bmatrix}, B_l = \begin{bmatrix} 0 & 0 & 0 & 0 & 0 \\ 0 & 0 & 0 & 0 & 0 \\ 0 & 0 & 0 & 0 & 0 \\ 0 & 0 & 0 & 0 & 0 \\ 0 & 0 & 0 & 0 & 0 \\ 0 & 0 & 0 & 0 & 0 \\ 0 & 0 & 0 & 0 & 0 \\ 0 & 0 & 0 & 0 & 0 \\ 0 & 0 & 0 & 0 & 0 \\ \frac{1}{m} & 0 & 0 & 0 & 0 \\ 0 & \frac{1}{I_{xx}} & 0 & 0 & 0 \\ 0 & 0 & \frac{1}{I_{yy}} & 0 & 0 \\ 0 & 0 & 0 & \frac{1}{I_{zz}} & 0 \end{bmatrix} \tag{2.35}$$

Although this model can represent the quadrotor dynamics throughout its motion, it limits the maneuverability of the vehicle and requires each movement to be independent of the others because of neglecting the nonlinear functions and higher-order terms. The main disadvantage of this model is neglecting the following terms

- coupling between angular velocities $\dot{\phi}, \dot{\theta}, \dot{\psi}$.
- the effect of heading angle on motion in $x - y$ plane.

So in the next part, some suggestions are to be stated which enhance the given model and increase the system maneuverability, besides introducing the expected faults and disturbances the vehicle may encounter during motion.

Small disturbance theory

Again it is obvious from the name that this linearization technique assumes small variations of the system states and the control input around the steady state condition which corresponds in our case to the hovering point. Such a methodology is detailed in [32] for an aircraft model and we use some of the proposed assumptions to handle the problem of quadrotor model linearization which are summarized as follows:

1. the system is operating around the equilibrium point $(\bar{\mathbf{x}}, \bar{u})$ defined by equations (2.33) and (2.34) with small state and input variations $\delta_x(t)$ and $\delta_u(t)$, respectively, such that

$$\begin{aligned} \mathbf{x}(t) &= \bar{\mathbf{x}} + \delta_x(t) \\ u(t) &= \bar{u} + \delta_u(t) \end{aligned} \tag{2.36}$$

2. the trigonometric functions for small angles variation in rad can be approximated as following:

$$\sin(\delta_\theta) \approx \delta_\theta, \quad \cos(\delta_\theta) \approx 1$$

$$\sin(\delta_\phi) \approx \delta_\phi, \quad \cos(\delta_\phi) \approx 1$$

3. further assumption is that the motion in $x-y$ plane is decoupled, such that the yawing angle variation term $\delta_\psi \approx 0$ so $\cos(\delta_\psi) \approx 1, \sin(\delta_\psi) \approx 0$

Linear model

Using the obtained results from small disturbance theory assumptions 2.3.1 with dropping all $\delta_{\mathbf{x}}$ to $\mathbf{x}$ for simpler representation,the obtained linear model is matching the state space model (2.32) derived in the previous section using Taylor series expansion. Such a model gives a direct interpretation for deriving the transfer functions governing the evolution of the states which are given by

$$\begin{aligned} \ddot{\phi} &= \tfrac{u_\phi}{I_{\mathrm{xx}}} \quad \rightarrow \quad \tfrac{\phi(s)}{u_\phi(s)} = \tfrac{1}{I_{\mathrm{xx}} s^2} \\ \ddot{\theta} &= \tfrac{u_\theta}{I_{\mathrm{yy}}} \quad \rightarrow \quad \tfrac{\theta(s)}{u_\theta(s)} = \tfrac{1}{I_{\mathrm{yy}} s^2} \\ \ddot{\psi} &= \tfrac{u_\psi}{I_{\mathrm{zz}}} \quad \rightarrow \quad \tfrac{\psi(s)}{u_\psi(s)} = \tfrac{1}{I_{\mathrm{zz}} s^2} \\ \ddot{x} &= g\theta \quad \rightarrow \quad \tfrac{x(s)}{\theta(s)} = \tfrac{g}{s^2} \\ \ddot{y} &= -g\phi \quad \rightarrow \quad \tfrac{y(s)}{\phi(s)} = -\tfrac{g}{s^2} \\ \ddot{z} &= \tfrac{u_z}{m} \quad \rightarrow \quad \tfrac{z(s)}{u_z(s)} = \tfrac{1}{m s^2} \end{aligned} \tag{2.37}$$

Although this model is widely deployed in the literature for solving the quadrotor modeling and control problem see [39], [43], and [45], it offers a very simplified representation for the system which is very restrictive for the vehicle maneuverability during trajectory tracking. In addition, according to Hartman–Grobman theorem [46], if the linearized model had all eigenvalues real, then it would represent the nonlinear model well around the equilibrium point. In our case, the linear model has all eigenvalues imaginary so the linearization could have an acceptable periodic behavior, but the neglected nonlinear terms can break this behavior that's why some enhancements for the linearized model are investigated in the following sections.

2.3.2 Affine model

In order to allow the system optimization for a larger flight envelope, one can linearize around each state such that each coupled term is represented twice by fixing and varying one state at each instant of time in the attitude loop. So (2.23) can be rewritten in the following form

$$\dot{\mathbf{x}}(t) = \begin{bmatrix} \dot{x} \\ \dot{y} \\ \dot{z} \\ \dot{\phi} \\ \dot{\theta} \\ \dot{\psi} \\ g\theta \\ -g\phi \\ \frac{u_z}{m} \\ \dot{\psi}\bar{\dot{\theta}}\frac{I_{yy}-I_{zz}}{2I_{xx}} + \bar{\dot{\psi}}\dot{\theta}\frac{I_{yy}-I_{zz}}{2I_{xx}} + \frac{u_\phi}{I_{xx}} \\ \dot{\psi}\bar{\dot{\phi}}\frac{I_{zz}-I_{xx}}{2I_{yy}} + \bar{\dot{\psi}}\dot{\phi}\frac{I_{zz}-I_{xx}}{2I_{yy}} + \frac{u_\theta}{I_{yy}} \\ \dot{\theta}\bar{\dot{\phi}}\frac{I_{xx}-I_{yy}}{2I_{zz}} + \bar{\dot{\theta}}\dot{\phi}\frac{I_{xx}-I_{yy}}{I_{zz}} + 2\frac{u_\psi}{I_{zz}} \end{bmatrix} \tag{2.38}$$

where the values of the states $\bar{\dot{\phi}}, \bar{\dot{\theta}}, \bar{\dot{\psi}}$ are the maximum values for the angular rates. These variables have to be predefined according to the range in which the attitude angles are evolving which directly affects the maximum values of angular velocity change. So this model covers the whole coupling effect of the nonlinear terms containing multiplied angular velocities as for example $\dot{\psi}\,\dot{\theta} < \dot{\psi}\,\bar{\dot{\theta}}$ and so on. In addition as this model is still considering small heading angle variation, so the resulting overall residual angular speed Ω_r is practically negligible that's why its effect is not included in the model. Consider the state vector given by equation (2.24) with the following control input

$$\mathbf{u}(t) = \begin{bmatrix} u_z & u_\phi & u_\theta & u_\psi \end{bmatrix}^T \tag{2.39}$$

Nominal LTI model

The model (2.38) can be rewritten as an LTI system in state space form as following

$$\begin{aligned}\dot{\mathbf{x}}(t)&= A\mathbf{x}(t) + B\mathbf{u}(t)\\ y(t)&= C\mathbf{x}(t) + D\mathbf{u}(t)\end{aligned} \tag{2.40}$$

where $\mathbf{x}(t) \in \mathbb{R}^n$, $n = 12$, $y(t) \in \mathbb{R}^{n_y}$, $n_y = 6$, and $\mathbf{u}(t) \in \mathbb{R}^{n_u}$, $n_u = 4$, represent the state vector, output vector, and control input vector, respectively. The matrices $A \in \mathbb{R}^{n\times n}, B \in \mathbb{R}^{n\times n_u}, C \in \mathbb{R}^{n_y\times n}, D \in \mathbb{R}^{n_y\times n_u}$ are the state matrix, the control input matrix, the output matrix, and the feedforward matrix, respectively, given by

$$A = \begin{bmatrix} 0_{6\times 6} & I_{6\times 6} \\ A_1 & 0_{3\times 6} \\ 0_{3\times 9} & A_2 \end{bmatrix}, \quad B = \begin{bmatrix} 0_{8\times 4} \\ B_1 \end{bmatrix} \tag{2.41}$$

$$A_1 = \begin{bmatrix} 0 & 0 & 0 & 0 & g & 0 \\ 0 & 0 & 0 & -g & 0 & 0 \\ 0 & 0 & 0 & 0 & 0 & 0 \end{bmatrix} \tag{2.42}$$

$$A_2 = \begin{bmatrix} 0 & \bar{\dot{\psi}}\frac{I_{yy}-I_{zz}}{2I_{xx}} & \bar{\dot{\theta}}\frac{I_{yy}-I_{zz}}{2I_{xx}} \\ \bar{\dot{\psi}}\frac{I_{zz}-I_{xx}}{2I_{yy}} & 0 & \bar{\dot{\phi}}\frac{I_{zz}-I_{xx}}{2I_{yy}} \\ \bar{\dot{\theta}}\frac{I_{xx}-I_{yy}}{2I_{zz}} & \bar{\dot{\phi}}\frac{I_{xx}-I_{yy}}{2I_{zz}} & 0 \end{bmatrix} \tag{2.43}$$

$$B_1 = \begin{bmatrix} \frac{1}{m} & 0 & 0 & 0 \\ 0 & \frac{1}{I_{xx}} & 0 & 0 \\ 0 & 0 & \frac{1}{I_{yy}} & 0 \\ 0 & 0 & 0 & \frac{1}{I_{zz}} \end{bmatrix} \tag{2.44}$$

Considering the system is provided with sensors to measure position and orientation, hence the states $x, y, z, \phi, \theta, \psi$ are measurable

$$C = \begin{bmatrix} I_{6\times 6} & 0_{6\times 6} \end{bmatrix}, \quad D = \begin{bmatrix} 0_{6\times 4} \end{bmatrix} \tag{2.45}$$

Faulty LTI model (actuators faults)

Consider the quadrotor is operating in an outdoor mission where it is subjected to some external disturbances and vulnerable to actuators faults. Such a situation can be described by the following model

$$\begin{aligned}\dot{\mathbf{x}}(t)&= A\mathbf{x}(t) + B\mathbf{u}(t) + E_f f(t) + E_d d(t)\\ y(t)&= C\mathbf{x}(t) + D\mathbf{u}(t)\end{aligned} \tag{2.46}$$

where the matrices $E_d \in \mathbb{R}^{n \times n_d}$, $n_d = 3$, $E_f \in \mathbb{R}^{n \times n_f}$, $n_f = 4$ are the matrices modeling disturbances and faults effect on the states, respectively. Besides $f(t) \in \mathbb{R}^{n_f}$ and $d(t) \in \mathbb{R}^{n_d}$ representing the fault and disturbance vectors, such that $d(t)$ is given by

$$d(t) = \Big[d_1(t), d_2(t), d_3(t)\Big]^T \tag{2.47}$$

where $d_1(t)$ and $d_2(t)$ represent the main wind force in y and x directions encountered while the drone is moving in the horizontal plane, with $d_3(t) = g$ representing the gravity effect on the quadrotor altitude.

$$E_d = \begin{bmatrix} E_1 \\ E_2 \end{bmatrix} \tag{2.48}$$

$$E_1 = \begin{bmatrix} 0 & .5 & 0 \\ .5 & 0 & 0 \\ 0 & 0 & 0 \\ 0.1 & 0 & 0 \\ 0 & 0.1 & 0 \\ 0 & 0 & 0 \end{bmatrix}, E_2 = \begin{bmatrix} 0 & 1 & 0 \\ 1 & 0 & 0 \\ 0 & 0 & -1 \\ .2 & 0 & 0 \\ 0 & .2 & 0 \\ 0 & 0 & 0 \end{bmatrix} \tag{2.49}$$

The matrices E_1 and E_2 contain the constant values that mask the wind effect on the system states such that the quadrotor is subjected to the outdoor wind that causes an additive body moment and force. These forces and moments result from the dynamic pressure generated around the quadrotor due to relative wind velocity. The values considered in equation (2.49) are derived based on the results obtained in [47] seeking UAV's wind field estimation through a gust field at low altitude ($50m$). In addition, it benefits from the outcome of the experimental work presented in [48] which proposes an approach for wind effect estimation of a quadrotor inside a wind tunnel by computing the coefficients of lift and drag corresponding to the applied wind speed.

For modeling actuator fault effect on the system dynamics we introduce u_f the faulty input vector related to the nominal input as following:

$$\mathbf{u}_f(t) = (I_{n_u} - \Gamma)\, T^{-1}\, \mathbf{u}(t) \tag{2.50}$$

where T is the control allocation matrix given by (2.18) and Γ represents the actuators effectiveness matrix given by

$$\Gamma = diag(\alpha_1, \alpha_2, \ldots, \alpha_m) \tag{2.51}$$

in that manner, the index $i \in \{1, .., m\}$ indicates the faulty actuator, m is the number of actuators or inputs (4 for quadrotor) and $\alpha_i = 0$, $\alpha_i = 1$ means the i^{th} input is completely healthy or faulty, respectively. This representation implies that the system fault model $E_f = -B\, \Gamma\, T^{-1}$.

2.3.3 Quadrotor Polytopic LPV framework preliminaries

As stated earlier in section 2.3.1 the deduced linear model has two major defects as it neglects the effect of both, angular velocities coupling, and nonlinear trigonometric functions. While the piecewise affine model proposed in 2.3.2 provided a solution for the coupling between angular velocities, the latter problem concerning the existence of the trigonometric functions in the position dynamics hasn't been solved yet. Keeping in mind that the model has to be simple enough for the sake of control design, the LPV framework offers an appealing solution for both nonlinear terms problems as it can express them into linearly time-varying parameters.

As mentioned in [35], there are two types of LPV systems, one where the varying parameters are exogenous signals referred to as pure or standard LPV system, and the other where system states themselves are the varying parameters named quasi-LPV which matches the quadrotor model as illustrated later. The LPV model form varies according to the state space matrices dependency on the varying parameters, in our case a convex polytopic quasi-LPV model is an appropriate representation for the nonlinear model (2.25). Such a polytopic model facilitates the system synthesis as will be illustrated in the next chapters, so consider a general LPV system in the following form

$$\begin{cases} \dot{\mathbf{x}}(t) = A(\rho(t))\mathbf{x}(t) + B(\rho(t))u(t) \\ y(t) = C(\rho(t))\mathbf{x}(t) + D(\rho(t))u(t) \end{cases} \tag{2.52}$$

where $\mathbf{x} \in \mathbb{R}^n$, $y(t) \in \mathbb{R}^{n_y}$, $u(t) \in \mathbb{R}^{n_u}$, are the state, output, and control input vectors, respectively. Besides the matrices $A(\rho(t)) \in \mathbb{R}^{n\times n}, B(\rho(t)) \in \mathbb{R}^{n\times n_u}, C(\rho(t)) \in \mathbb{R}^{n_y\times n}, D(\rho(t)) \in \mathbb{R}^{n_y\times n_u}$ representing the state matrix, the control input matrix, the output matrix, and the feedforward matrix, respectively.

In order to understand better the nature of the LPV system, the behavior of the varying parameters has to be discussed. Through the analysis of LPV systems, the time-varying parameters are assumed to have known bounds on the magnitude and rate of change, hence their values are smoothly evolving within these limits along some specific linear trajectories. Given that a varying parameter is called $\rho_i(t)$, then

$$\rho_i{}^{min} \leq \rho_i(t) \leq \rho_i{}^{max} \tag{2.53}$$

The vector $\rho^T(t) = \big(\rho_1(t), ..., \rho_{n_\rho}(t)\big)$ represents the n_ρ bounded, smoothly varying parameters such that $\rho(t) \in \Phi$ defined by

$$\Phi = \left\{ \rho(t) \in \mathbb{R}^{n_\rho} \,\middle|\, \rho_1(t) \in \left[\rho_1^{\min}, \rho_1^{\max}\right], \ldots, \rho_{n_\rho}(t) \in \left[\rho_{n_\rho}^{\min}, \rho_{n_\rho}^{\max}\right] \right\} \tag{2.54}$$

where $\rho_i^{\min}$ and $\rho_i^{\max}$, $i = 1, ..., n_\rho$ define the maximum and minimum values of the parameter $\rho_i(t)$, and similarly the time derivatives of the parameter named $\rho_i{}^{(j)}(t)$ are limited by

$$\rho_i{}^{(j)^{min}} \leq \rho_i{}^{(j)}(t) \leq \rho_i{}^{(j)^{max}}, \quad j = 1, \ldots, \nu \tag{2.55}$$

where ν is the order of the parameter derivative while the vector containing the time rates of the varying parameters $\rho^{(j)}(t)$ belong to the compact sets defined by

$$\Phi_j = \left\{ \rho^{(j)}(t) \in \mathbb{R}^{n_\rho} \middle| \rho_1^{(j)}(t) \in \left[{\rho_1^{(j)}}^{\min}, {\rho_1^{(j)}}^{\max} \right], \ldots, \rho_{n_\rho}^{(j)}(t) \in \left[{\rho_{n_\rho}^{(j)}}^{\min}, {\rho_{n_\rho}^{(j)}}^{\max} \right] \right\} \tag{2.56}$$

Notice that this assumption is always satisfied when the parameters vary continuously according to time (Lipschitz condition).

Definition 1

The polytopic system (2.52) is said to be uniformly controllable (observable) with respect to the parameter $\rho(t)$ if $\forall \rho(t) \in \Phi$, the state of the system (2.52) is controllable (observable).

Note: the concepts of controllability and observability are very essential and will be discussed in detail in the next few chapters but for now they can be described by the following definitions:

- a system is controllable if it can reach any desired final state $\mathbf{x}(t)$ from its initial state $\mathbf{x}(t_0)$ by means of unconstrained control input.
- a system is observable if every state $\mathbf{x}(t_0)$ can be estimated from the measured output $y(t)$ over a finite period of time t_1 such that $t_0 \leq t \leq t_1$

This definition is very essential while studying the stability analysis of the LPV system later on. Now after defining the limits of the varying parameters, we can proceed to describe the state space matrices dependency on the varying parameters. As illustrated, the vector of the varying parameters $\rho(t)$ evolves through a convex polytope having a number of vertices $N = 2^{n_\rho}$. Hence, at each instant of time, the value of the state space matrices depends on the interpolation between the varying parameters ultimate values described by the weighting functions $\mu_k,\ k = 1, \ldots, N$ and satisfying the following convex sum property

$$\begin{cases} 0 \leq \mu_k(\rho(t)) \leq 1, \quad \forall t, \quad \forall k = 1, \ldots, N \\ \sum_{k=1}^{N} \mu_k(\rho(t)) = 1 \end{cases} \tag{2.57}$$

then, the state space matrices in (2.52) can be represented in a polytopic form as following

$$M(\rho(t)) = \sum_{k=1}^{N} \mu_k(\rho(t)) M_k \tag{2.58}$$

where $M(\rho(t)) \in \{A(\rho(t)), C(\rho(t)), B(\rho(t)), D(\rho(t))\}$, such that the linear parameter varying matrices are combination of the sub-models derived at each vertex represented by $M_k,\ k = 1, \ldots, N$. The M_k are constant matrices can be referred to as frozen LPV system at a vertex k. After introducing the main concepts and preliminaries of LPV systems, the next part is dedicated for transforming the quadrotor nonlinear model (2.25) into a quasi-LPV form.

2.3.4 Quasi-LPV model (attitude and altitude dynamics)

In the literature of quadrotor modeling and control problem, there exists a very popular approach that adopts the idea of dividing the system into two subsystems in cascaded control design. This approach can be found in several works as [43], [49], and [50], the motive behind that is the dependence of the position dynamics on the orientation angles. Thus, it is very convenient to handle the attitude and altitude modeling and control problem separately as they represent the inner loop for the cascaded control scheme, more illustration is presented in the next chapter. Since in this section we are interested only in the attitude and altitude dynamics, consider the following reduced state vector $x_s(t)$

$$x_s(t) = \begin{bmatrix} \phi & \theta & \psi & z & \dot{\phi} & \dot{\theta} & \dot{\psi} & \dot{z} \end{bmatrix}^T \tag{2.59}$$

then the attitude and altitude dynamics extracted from the nonlinear model (2.25) is described by

$$\dot{x}_r(t) = \begin{bmatrix} \dot{\phi} \\ \dot{\theta} \\ \dot{\psi} \\ \dot{z} \\ \frac{\dot{\theta}\dot{\psi}(I_{yy}-I_{zz})+\dot{\theta}J_r\Omega_r+u_\phi}{I_{xx}} \\ \frac{\dot{\phi}\dot{\psi}(I_{zz}-I_{xx})-\dot{\phi}J_r\Omega_r+u_\theta}{I_{yy}} \\ \frac{\dot{\phi}\dot{\theta}(I_{xx}-I_{yy})+u_\psi}{I_{zz}} \\ \cos\theta\cos\phi\frac{u_z}{m} - g \end{bmatrix} \tag{2.60}$$

One can notice two types of nonlinear terms embedded in this model, angular velocity couplings ($\dot{\theta}\,\dot{\psi}, \dot{\phi}\,\dot{\psi}, \dot{\phi}\,\dot{\theta}$), and the multiplied trigonometric functions ($\cos\theta\cos\phi$). Concerning the latter, the assumption of small angle variation is still an effective solution so $\cos\theta = \cos\phi \approx 1$. However, for the angular velocities coupling it is not the same case, so these terms have to be considered as linearly varying parameters.

As increasing the number of the varying parameter increases the number of sub-models exponentially which results in a more complex model, the choice of the varying parameters is an essential step for successful and efficient representation of the system. Regarding the model (2.60) the three nonlinear terms including angular velocities multiplications can be represented in a linear form by introducing the angular rates $\dot{\theta}$, $\dot{\phi}$ as varying parameters. The maximum and minimum values for these parameters are deduced from nonlinear model simulation after designing the control law as illustrated later 3.4.3 and found to be $\dot{\theta} \in [-.5, .5]\ rad/s$, $\dot{\phi} \in [-.5, .5]\ rad/s$.

Thus, $\rho(t) = [\dot{\theta}, \dot{\phi}]$, and since the varying parameters are some of the system states, the quadrotor model is matching a quasi-LPV form. Therefore, the convex polytope through which the model evolves has 4 vertices as shown in figure 2.6. Let the vertices are called $v_{rk},\ k = 1, \ldots, 4$, then each vertex v_{rk} and the corresponding

weighting function μ_k will be defined by the limits of the parameters as follows

$$\begin{aligned} v_{r1} &\implies (\dot{\phi}^{min}, \dot{\theta}^{min}), \quad \mu_1 = \left(\frac{\dot{\phi}^{max} - \dot{\phi}(t)}{\dot{\phi}^{max} - \dot{\phi}^{min}}\right) \times \left(\frac{\dot{\theta}^{max} - \dot{\theta}(t)}{\dot{\theta}^{max} - \dot{\theta}^{min}}\right) \\ v_{r2} &\implies (\dot{\phi}^{min}, \dot{\theta}^{max}), \quad \mu_2 = \left(\frac{\dot{\phi}^{max} - \dot{\phi}(t)}{\dot{\phi}^{max} - \dot{\phi}^{min}}\right) \times \left(\frac{\dot{\theta}(t) - \dot{\theta}^{min}}{\dot{\theta}^{max} - \dot{\theta}^{min}}\right) \\ v_{r3} &\implies (\dot{\phi}^{max}, \dot{\theta}^{min}), \quad \mu_3 = \left(\frac{\dot{\phi}(t) - \dot{\phi}^{min}}{\dot{\phi}^{max} - \dot{\phi}^{min}}\right) \times \left(\frac{\dot{\theta}^{max} - \dot{\theta}(t)}{\dot{\theta}^{max} - \dot{\theta}^{min}}\right) \\ v_{r4} &\implies (\dot{\phi}^{max}, \dot{\theta}^{max}), \quad \mu_4 = \left(\frac{\dot{\phi}(t) - \dot{\phi}^{min}}{\dot{\phi}^{max} - \dot{\phi}^{min}}\right) \times \left(\frac{\dot{\theta}(t) - \dot{\theta}^{min}}{\dot{\theta}^{max} - \dot{\theta}^{min}}\right) \end{aligned} \tag{2.61}$$

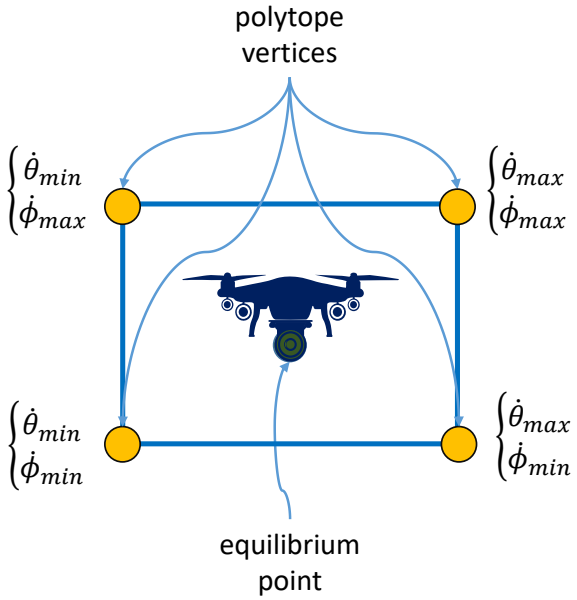

Figure 2.6: Quasi-LPV model convex polytope

Nominal quasi-LPV model

The time-varying matrices can be obtained from equation (2.58) and the LPV system corresponding to the model (2.60) takes the following state space form

$$\begin{cases} \dot{x}_s(t) = A(\rho(t))x_s(t) + B(\rho(t))u(t) \\ y(t) = C(\rho(t)x_s(t) + D(\rho(t))u(t) \end{cases} \tag{2.62}$$

where the LPV matrices are given by

$$A(\rho(t)) = \begin{bmatrix} 0_{4\times4} & I_{4\times4} \\ 0_{4\times4} & A_s \end{bmatrix}, \quad B(\rho(t)) = \begin{bmatrix} 0_{4\times5} \\ B_s \end{bmatrix} \tag{2.63}$$

$$A_s = \begin{bmatrix} 0 & 0 & \dot{\theta}\frac{I_{yy}-I_{zz}}{I_{xx}} & 0 \\ 0 & 0 & \dot{\phi}\frac{I_{zz}-I_{xx}}{I_{yy}} & 0 \\ \dot{\theta}\frac{I_{xx}-I_{yy}}{I_{zz}} & 0 & 0 & 0 \\ 0 & 0 & 0 & 0 \end{bmatrix}, \tag{2.64}$$

and

$$B_s = \left[\begin{array}{\overbrace{cccc}^{J} | c} 0 & \frac{1}{I_{xx}} & 0 & 0 & \frac{\dot{\theta}J_r}{I_{xx}} \\ 0 & 0 & \frac{1}{I_{yy}} & 0 & \frac{-\dot{\phi}J_r}{I_{yy}} \\ 0 & 0 & 0 & \frac{1}{I_{zz}} & 0 \\ \frac{1}{m} & 0 & 0 & 0 & 0 \end{array}\right] \tag{2.65}$$

The states of the quadrotor are assumed to be all measurable by sensors, while the system is strictly proper so

$$C(\rho(t)) = \left[I_{8\times 8}\right], \quad D(\rho(t)) = \left[0_{8\times 5}\right] \tag{2.66}$$

Since $C(\rho(t))$ and $D(\rho(t))$ given by equation (2.66) are independent of the varying parameters $\rho(t)$ they will be represented by the constant matrices C, D, respectively.

Faulty quasi-LPV model (actuators fault)

As the attitude and altitude dynamics include the effect of the whole control input $u(t)$ on the system, then it is evident that the actuators' faults have a direct impact on this subsystem. That's why while handling the problems concerning Fault Diagnosis or Fault-tolerant control for a quadrotor affected by actuators faults, it is convenient to consider the attitude and altitude subsystems. Now consider the quadrotor is operating in an open environment and subjected to actuators faults, such a situation can be described by the following model

$$\begin{cases} \dot{x}_s(t) = A(\rho(t))x_s(t) + B(\rho(t))u_f(t) + E(\rho(t))d(t) \\ y(t) = Cx_s(t) + Du_f(t) \end{cases} \tag{2.67}$$

where $u_f(t)$ is the faulty input signal given by

$$u_f(t) = (I_{n_u} - \Gamma)u(t) \tag{2.68}$$

where Γ is the motors efficiency matrix containing diagonal elements $(\alpha_1, \ldots, \alpha_m)$, $m = 4$ (number of rotors), α_i is the i^{th} actuator efficiency, $i \in \{1, \ldots, m\}$ and $0 \leq \alpha_i \leq 1$ indicating completely healthy and totally damaged rotor, respectively. Recalling equation (2.17) which relates the control input $u(t)$ and the rotors angular speed with the

matrix T, equation (2.68) can be written as

$$u_f(t) = u(t) - \Gamma\ T\ T^{-1}\ u(t) \tag{2.69}$$

then

$$u_f(t) = u(t) - \Gamma\ T\ \Omega^2(t) \tag{2.70}$$

By rearranging the second term of equation (2.70) and introducing this faulty input in equation (2.67) the faulty system model can have the following representation

$$\begin{cases} \dot{x}_s(t) = A(\rho(t))x_s(t) + B(\rho(t))u(t) + F(\rho(t))f(t) + E(\rho(t))d(t) \\ y(t) = Cx_s(t) + Du(t) \end{cases} \tag{2.71}$$

where $E(\rho(t)) \in \mathbb{R}^{n\times n_d}, F(\rho(t)) \in \mathbb{R}^{n\times n_f}$ and

$$F(\rho(t)) = -B_f\ T \begin{bmatrix} \bar{\Omega}_1^2 & 0 & 0 & 0 \\ 0 & \bar{\Omega}_2^2 & 0 & 0 \\ 0 & 0 & \bar{\Omega}_3^2 & 0 \\ 0 & 0 & 0 & \bar{\Omega}_4^2 \end{bmatrix}, \quad B_f = \begin{bmatrix} 0_{4\times 4} \\ J \end{bmatrix} \tag{2.72}$$

such that B_f is the faulty input matrix that allocates each rotor fault through the matrices T and J given in (2.17) and (2.65), respectively. Besides $\bar{\Omega}_i^2$ the square of nominal motor speed which is constant depending on the vehicle mass as the quadrotor motion is assumed to consist of small states variations around the hovering condition.

Note that introducing the term $\bar{\Omega}_i^2$ allows to represent each actuator fault as a time varying input signal $f(t) = [\alpha_1, \ldots, \alpha_m]^T$, $m = 4$. Such a representation facilitates introducing various kinds of actuator faults that a quadrotor may encounter which are listed in table 2.1.

faults	**disturbances**
abrupt thrust change	constant wind
intermittent motor current	acceleration of gravity
time varying fault	payload
stuck or saturated actuators	terrain induced wind
partial loss of efficiency	low altitude wind shear
complete failure	propeller vortex

Table 2.1: Popular quadrotor faults and disturbances

To calculate the value of the matrix $E(\rho(t))$ given in (2.62), one needs to specify which kind of disturbances the

quadrotor can be subjected to through its motion. Depending on the environmental conditions, sort of mission, and UAV configuration various types of disturbances can arise, some of them are listed in table 2.1. In our model, the disturbance vector $d(t)$ is given by

$$d(t) = \Big[d_1(t), d_2(t), d_3(t)\Big]^T \tag{2.73}$$

where $d_1(t)$ and $d_2(t)$ are disturbance signal representing wind force in y and x directions, respectively, while $d_3(t) = g$ modeling the effect of the acceleration of gravity on the altitude.

$$E(\rho(t)) = \begin{bmatrix} E_1 \\ E_2 \end{bmatrix} \tag{2.74}$$

$$E_1 = \begin{bmatrix} 0.1 & 0 & 0 \\ 0 & 0.1 & 0 \\ 0 & 0 & 0 \\ 0 & 0 & 0 \end{bmatrix}, E_2 = \begin{bmatrix} 1 & 0 & 0 \\ 0 & 1 & 0 \\ 0 & 0 & 0 \\ 0 & 0 & -1 \end{bmatrix} \tag{2.75}$$

As noticed the matrix $E(\rho(t))$ contains constant elements whose values are derived in a similar way to the linear model 2.3.2 based on the results of wind field estimation proposed in [47] and [48]. Since $E(\rho(t))$ and $F(\rho(t))$ contain constant elements, it is more convenient to drop their dependency on the varying parameter and rewrite them as E and F, respectively.

2.3.5 Quasi-LPV model (full quadrotor dynamics)

After proposing a quasi-LPV model representing only the attitude and altitude dynamics and showing how the quadrotor actuators' faults can be represented, it is time to investigate the whole vehicle mathematical model. As the work presented is concerned with quadrotor FTC in case of sensors or actuators faults, it has been found that dividing the quadrotor model into three subsystems, namely attitude, altitude, and position results in some advantages for further FTC implementation which can be summarized by the following points

- simplifying the process of sensors FDD, since each sensor measurements are investigated separately (the quadrotor has basically three main sensors corresponding to each subsystem, namely IMU, ultrasonic, and optical flow camera for attitude, altitude, and position states, respectively).
- enhancement of the control law design methodology such that the process of controller gains tuning for each subsystem becomes more comprehensible.
- avoiding the feasibility issues that may arise while solving the optimization problems numerically for high dimension models for observer or controller design.

Nominal model

The nominal model for each subsystem is expressed in an LPV representation following the same form of equation (2.52), in a way that each subsystem has its own state and input vectors and the corresponding parameter varying state space matrices. So we jump directly to the system model affected by the sensor faults detailed in the next section.

Faulty model (sensors faults)

As mentioned earlier the quadrotor nonlinear model given by equation (2.25) is divided into three subsystems, one describing orientation and angular rates, the second representing the altitude and rate of ascending, while the third is concerned with $x - y$ position and vehicle velocity. The connection between the three subsystems is illustrated in figure 2.7

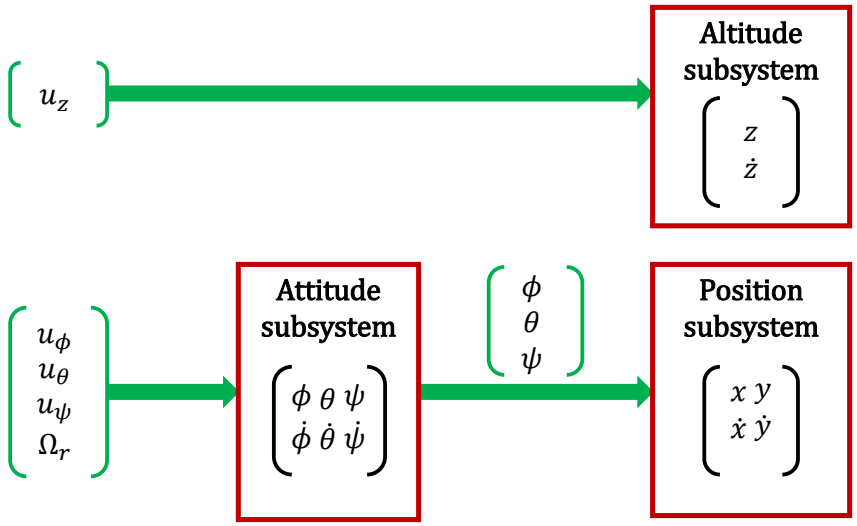

Figure 2.7: Attitude, altitude, and position subsystems

Attitude subsystem Consider the state vector $x_{at}(t)$, the input vector $u_{at}(t)$, and the disturbances vector $d_{at}(t)$ for attitude subsystem are given by

$$x_{at}(t) = \begin{bmatrix} \phi & \theta & \psi & \dot{\phi} & \dot{\theta} & \dot{\psi} \end{bmatrix}^T \tag{2.76}$$

$$u_{at}(t) = \begin{bmatrix} u_\phi & u_\theta & u_\psi & \Omega_r \end{bmatrix}^T \tag{2.77}$$

$$d_{at}(t) = \begin{bmatrix} d_1(t), d_2(t) \end{bmatrix} \tag{2.78}$$

where $d_1(t)$ and $d_2(t)$ are disturbance signals representing wind force in y and x directions, respectively. Then, the system can be represented in the following state space form

$$\begin{cases} \dot{x}_{at}(t) = A_{at}(\rho(t))x_{at}(t) + B_{at}(\rho(t))u_{at}(t) + E_{at}d_{at}(t) \\ y_{at}(t) = C_{at}x_{at}(t) + D_{at}u_{at}(t) + F_{at}f_{at}(t) \end{cases} \tag{2.79}$$

Note that the same time-varying parameters employed in the previous section are used here to model the attitude dynamics in an LPV framework so $\rho(t) = [\dot{\theta}, \dot{\phi}]$, then the state space matrices are given by

$$A_{at}(\rho(t)) = \begin{bmatrix} 0_{3\times3} & I_{3\times3} \\ 0_{3\times3} & A_{at1} \end{bmatrix}, \quad B_{at}(\rho(t)) = \begin{bmatrix} 0_{3\times4} \\ B_{at1} \end{bmatrix} \tag{2.80}$$

$$A_{at1} = \begin{bmatrix} 0 & 0 & \dot{\theta}\frac{I_{yy}-I_{zz}}{I_{xx}} \\ 0 & 0 & \dot{\phi}\frac{I_{zz}-I_{xx}}{I_{yy}} \\ \dot{\theta}\frac{I_{xx}-I_{yy}}{I_{zz}} & 0 & 0 \end{bmatrix}, \tag{2.81}$$

$$B_{at1} = \begin{bmatrix} \frac{1}{I_{xx}} & 0 & 0 & \frac{\dot{\theta}J_r}{I_{xx}} \\ 0 & \frac{1}{I_{yy}} & 0 & \frac{-\dot{\phi}J_r}{I_{yy}} \\ 0 & 0 & \frac{1}{I_{zz}} & 0 \end{bmatrix} \tag{2.82}$$

The orientation angles and the angular rates of the quadrotor are assumed to be all measurable by an IMU sensor and the disturbance vector given by (2.78) is representing wind forces and moments so

$$C_{at} = \begin{bmatrix} I_{6\times6} \end{bmatrix}, \quad D_{at} = \begin{bmatrix} 0_{6\times4} \end{bmatrix} \tag{2.83}$$

$$E_{at} = \begin{bmatrix} E_1 \\ E_2 \end{bmatrix} \tag{2.84}$$

$$E_1 = \begin{bmatrix} 0.1 & 0 \\ 0 & 0.1 \\ 0 & 0 \end{bmatrix}, E_2 = \begin{bmatrix} 1 & 0 \\ 0 & 1 \\ 0 & 0 \end{bmatrix} \tag{2.85}$$

Finally, F_{at} represents the impact of sensor faults $f_{at}(t)$ on the output $y_{at}(t)$, thus its value depends on the sensors used and their common faults. Some typical aircraft sensor faults investigated earlier in [3] are listed in table 2.2, such sensors faults can be mathematically formulated as presented in [51]. Since this work is dedicated to quadrotor sensor fault diagnosis, the main sensors are considered are IMU, ultrasonic, and optical flow camera.

sensors faults
additive bias
sensor drift
measurement freezing
loss of accuracy
calibration error

Table 2.2: Typical aircraft sensors faults

Regarding the IMU, the readings of angular rates $(\dot{\phi}, \dot{\theta}, \dot{\psi})$ are obtained from the gyroscope and magnetometer that are likely to be affected by the structural vibrations and loose fixations resulting in loss of accuracy. In addition, the readings of the gyroscope can be affected by an initial bias which if not estimated and corrected will lead to faulty measurements. Furthermore, the orientation angles (ϕ, θ) are calculated by integrating the angular rates from the gyroscope and the body accelerations obtained from the onboard accelerometer (usually an Extended Kalman filter between these two measurements is deployed to obtain adequate readings) so such measurements are vulnerable to error accumulation (drift).

A convenient way to represent all the aforementioned kinds of faults on the measurement is to have two matrices as following:

$$F_m = \begin{bmatrix} I_{3\times3} & 0_{3\times3} \end{bmatrix}, \quad F_r = \begin{bmatrix} 0_{3\times3} & I_{3\times3} \end{bmatrix} \tag{2.86}$$

such that the vector $f_{at}(t)$ contains the sensors parametric faults, then according to which sensor to be examined there are two possibilities:

- $F_{at} = F_m$, for orientation faults.
- $F_{at} = F_r$, for angular rates faults.

This is an efficient way to estimate the exact value of a sensor fault while avoiding the coupled states effect, for example, a residual in the direction of $\dot{\phi}$ is not affected by a fault of ϕ and so on.

Altitude subsystem For the sake of substituting the gravity effect on the system, an integral action is to be included in the altitude subsystem in the form of an additional state called $\tilde{z}$ such that $\dot{\tilde{z}} = -\kappa\tilde{z} + z$. This method is appealing as it enables the designed control law to adapt to the quadrotor weight if there is an extra payload according to the tuned value of the constant parameter κ. By adding this state to the altitude dynamics extracted from the nonlinear model (2.25), then the state vector $x_z(t)$ is given by

$$x_z(t) = \begin{bmatrix} z & \dot{z} & \tilde{z} \end{bmatrix}^T \tag{2.87}$$

then the altitude faulty subsystem is formulated in the following state space form

$$\begin{cases} \dot{x}_z(t) = A_z x_z(t) + B_z u_z(t) + E_z d_z(t) \\ y_z(t) = C_z x_z(t) + D_z u_z(t) + F_z f_z(t) \end{cases} \tag{2.88}$$

where the control input u_z is the first component of the input vector (2.14) and $d_z = g$ represents the acceleration of gravity on the quadrotor. Note as the assumption of small disturbance theory 2.3.1 holds the altitude subsystem doesn't include nonlinear terms so its state space matrices are all constants and are given by

$$A_z = \begin{bmatrix} 0 & 1 & 0 \\ 0 & 0 & 0 \\ 1 & 0 & -\kappa \end{bmatrix}, \quad B_z = \begin{bmatrix} 0 \\ \frac{1}{m} \\ 0 \end{bmatrix} \tag{2.89}$$

the altitude and the rate of ascending are assumed to be measurable by an ultrasonic sensor so

$$C_z = \begin{bmatrix} 1 & 0 & 0 \\ 0 & 1 & 0 \end{bmatrix}, \quad D_z = \begin{bmatrix} 0_{2\times 1} \end{bmatrix}, \quad E_z = \begin{bmatrix} -1 \end{bmatrix} \tag{2.90}$$

Concerning the ultrasonic sensor, the major problem is freezing due to range limitations and speed of data acquisition, since the fault vector $f_z(t)$ contains the sensors parametric faults, then according to which sensor to be examined there are two possibilities:

- $F_z = [1 \quad 0]^T$, for altitude faults.
- $F_z = [0 \quad 1]^T$, for ascending rates faults.

again this representation for the faulty matrix inhibits misleading fault identification that may result from the coupling of the states and their rates.

Position subsystem The previous section 2.3.4 has been considering the quadrotor attitude and altitude only and to have a complete representation for the system we need to add the position loop dynamics which is extracted from the nonlinear model (2.25) and described by the following

$$\begin{bmatrix} \ddot{x} \\ \ddot{y} \end{bmatrix} = \begin{bmatrix} \cos\phi\cos\psi\sin\theta + \sin\phi\sin\psi \\ -\cos\psi\sin\phi + \cos\phi\sin\theta\sin\psi \end{bmatrix} \frac{u_z}{m} \tag{2.91}$$

From equation (2.91), one can notice that the nonlinear terms consist of multiplied trigonometric functions of the orientation angles. As the behavior of the trigonometric functions is governed by the attitude angles values, a direct approach is to use the attitude angles as macro varying parameters to evaluate the ultimate values for the

nonlinear terms. However, considering all the attitude angles ϕ, θ, ψ as macro varying parameters is not a very efficient technique as it implies a large number of LPV system vertices. However, by taking into consideration that practically the drone operates with small state variation while moving, then the results listed below which were obtained by small disturbance theory 2.3.1 can be used.

$$\begin{cases} \cos\phi = \cos\theta \approx 1 \\ \sin\phi \approx \phi \\ \sin\theta \approx \theta \\ \frac{u_z}{m} = g \end{cases} \tag{2.92}$$

then the system (2.92) is reduced to

$$\begin{bmatrix} \ddot{x} \\ \ddot{y} \end{bmatrix} = \begin{bmatrix} \theta g \cos\psi + \phi g \sin\psi \\ -\phi g \cos\psi + \theta g \sin\psi \end{bmatrix} \tag{2.93}$$

As the position represents the outer loop for the system, the angles ϕ, θ, ψ which are the outputs of the attitude loop are considered as the position loop inputs see figure 2.7, so equation (2.93) transforms into

$$\begin{bmatrix} \ddot{x} \\ \ddot{y} \end{bmatrix} = \begin{bmatrix} g\sin\psi & g\cos\psi \\ -g\cos\psi & g\sin\psi \end{bmatrix} . \begin{bmatrix} \phi \\ \theta \end{bmatrix} \tag{2.94}$$

Since the functions $\cos\psi, \sin\psi$ are trigonometric functions, we can consider the angle ψ as a macro varying parameter. Then we have only one varying parameter which is the yawing angle $\rho(t) = \psi$ as it can not be considered as a small-angle variation (by approximating its $(\cos)$ and $(\sin)$ values) since it represents the drone heading angle.

An acceptable range for this heading angle $\psi \in [-\frac{\pi}{2}, \frac{\pi}{2}]\ rad$ in which $\sin\psi$ can be approximated by a linear relation efficiently as can be seen from figure 2.8. However, in the same range the function $\cos\psi$ can not be represented by a linear function, so a better solution is to divide the heading angle range into two regions $\psi \in [-\frac{\pi}{2}, 0]\ rad$ and $\psi \in [0, \frac{\pi}{2}]\ rad$ as for each region the two trigonometric functions can be approximated by linear functions. In this case, the LPV model of the position loop will include 3 vertices corresponding to the values of the varying parameter $\psi = [-\frac{\pi}{2}, 0, \frac{\pi}{2}]\ rad$ as illustrated in figure 2.9 such that

- if $\psi < 0$, then $\psi^{min} = -\frac{\pi}{2}$, $\psi^{max} = 0$
- if $\psi > 0$, then $\psi^{min} = 0$, $\psi^{max} = \frac{\pi}{2}$

Then we calculate the values of the trigonometric functions at ψ^{max}, ψ^{min} and their corresponding parameter varying state space matrices. Such a model is very efficient in representing the subsystem dynamics besides avoiding excessive computational time.

Taking into consideration the exogenous disturbances and sensors faults, the position subsystem dynamics

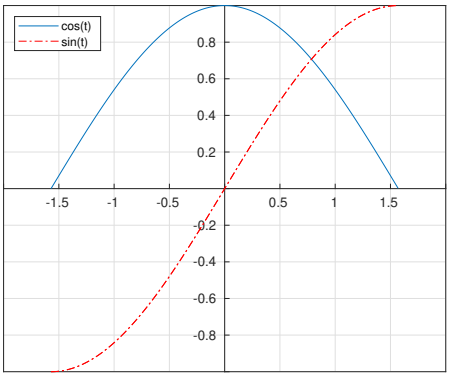

Figure 2.8: $\sin\psi$ and $\cos\psi$ functions

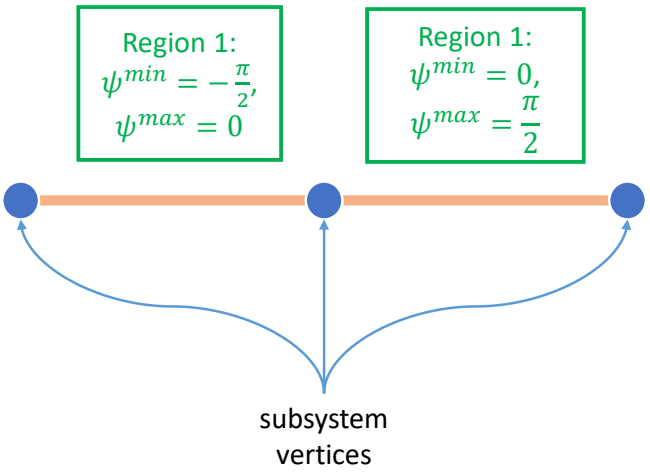

Figure 2.9: Position subsystem vertices

(2.94) can be expressed in the following LPV state space form

$$\begin{cases} \dot{x}_p(t) = A_p(\rho(t))x_p(t) + B_p(\rho(t))u_p(t) + E_p d_p(t) \\ y_p(t) = C_p x_p(t) + D_p u_p(t) + F_p f_p(t) \end{cases} \tag{2.95}$$

where the state vector $x_p(t)$ and the control input vector $u_p(t)$ are given by

$$x_p(t) = \begin{bmatrix} x & y & \dot{x} & \dot{y} \end{bmatrix}^T \tag{2.96}$$

$$u_p(t) = \begin{bmatrix} \phi & \theta \end{bmatrix}^T \tag{2.97}$$

In that way, the input of the position subsystem are the attitude angles coming from the attitude subsystem

as illustrated by figure 2.7. This problem is demonstrated more throughout next chapter while formulating the cascaded control loop design for the quadrotor in which the outer loop (position dynamics) feeds the inner loop (attitude dynamics) with the required angles. In addition, the disturbance vector $d_p(t)$ is as follows

$$d_p(t) = \begin{bmatrix} d_{p1}(t), d_{p2}(t) \end{bmatrix}^T \tag{2.98}$$

such that $d_{p1}(t), d_{p2}(t)$ representing the wind field velocity effect on y and x directions, respectively. The parameter varying state space matrices are given by

$$A_p(\rho(t)) = \begin{bmatrix} 0_{2\times2} & I_{2\times2} \\ 0_{2\times2} & 0_{2\times2} \end{bmatrix}, \quad B_p(\rho(t)) = \begin{bmatrix} 0_{2\times2} \\ B_{p1} \end{bmatrix} \tag{2.99}$$

$$B_{p1} = \begin{bmatrix} g\sin\psi & g\cos\psi \\ -g\cos\psi & g\sin\psi \end{bmatrix} \tag{2.100}$$

$$E_p = \begin{bmatrix} 0 & 0.5 \\ 0.5 & 0 \\ 0 & 1 \\ 1 & 0 \end{bmatrix} \tag{2.101}$$

The position and the velocity of the quadrotor are assumed to be measurable by an optical flow camera so

$$C_p = \begin{bmatrix} I_{4\times4} \end{bmatrix}, \quad D_p = \begin{bmatrix} 0_{2\times2} \end{bmatrix} \tag{2.102}$$

A convenient way to represent the optical flow sensor faults $f_p(t)$ on the measurement is to have two matrices as follows:

$$F_s = \begin{bmatrix} I_{2\times2} & 0_{2\times2} \end{bmatrix}, \quad F_v = \begin{bmatrix} 0_{2\times2} & I_{2\times2} \end{bmatrix} \tag{2.103}$$

such that the vector $f_p(t)$ contains the sensors parametric faults, then according to which sensor to be examined there are two possibilities:

- $F_p = F_s$, for position faults.
- $F_p = F_v$, for velocity faults.

Before concluding the main results obtained throughout this chapter it is useful to summarize the benefits and drawbacks of each model which is given in table 2.3. Since the quadrotor is a critically stable system due to the fact that its states have double poles at the origin, the open-loop simulations of the introduced models don't give

comprehensive results illustrating the differences between them. Therefore, the characteristics of each model and how the neglected dynamics through linearization affect the system response are illustrated more in the next chapter by simulations where the system is provided with a feedback control law to stabilize it.

model	**main features**	**drawbacks**
linear model 2.3.1	a simplified model which gives a direct interpretation of the system dynamics and can be easily expressed in state space or transfer function form	neglect all the nonlinearities of the model including the angular velocities coupling and trigonometric functions
affine model 2.3.2	introduces an outer envelope of the angular velocities coupling while preserving the linear form	still lacks the effect of the heading angle in 2D motion
LPV attitude and altitude 2.3.4	represents the nonlinearities of the attitude dynamics by linearly time varying parameters and since it is directly affected by the control input, it is suitable for handling actuators fault diagnosis	not including the position dynamics
LPV full vehicle dynamics 2.3.5	the same previous LPV model but the altitude loop is separated into a standalone subsystem while the position dynamics are included within a separate subsystem too in a way that facilitates the process of implementing the sensor fault diagnosis algorithm	more complicated design than the linear model

Table 2.3: Quadrotor models

2.4 Conclusions

Quadrotor modeling is a very essential task as it represents the system core upon which the control law is designed and further path planning algorithms are built. Besides that, system modeling is challenging work as it always implies a trade-off between the simplicity of the mathematical model and its accuracy in representing the system dynamics. The deduced system model has to be reasonably simple such that the designed controller can con-

vey real-time implementation constraints, that's why studying the mathematical model's possible linearization is a common procedure in system modeling.

Since the quadrotor movement consists of small states variations around the hovering point, two well-known linearization techniques, namely Jacobian linearization and small disturbance theory are proposed to obtain a simplified linear model. However, the deduced linear model has some drawbacks as it neglects completely the coupling between angular velocities and the effect of heading angle in $2D$ motion. Therefore some model enhancements are investigated which take into consideration the system faults and exogenous disturbances that the vehicle may encounter during motion.

A piecewise affine model that describes the quadrotor dynamics in an enhanced LTI form is obtained by linearizing around each state such that each coupled term is represented twice by fixing and varying one state at each instant of time. This method provides an outer envelope for the nonlinear terms in the attitude loop corresponding to multiplied angular rates, so it could improve these terms' representation in the obtained model. However, it doesn't offer a solution for the nonlinear trigonometric functions existent in the position dynamics.

Keeping in mind that the model has to be simple enough for the sake of control design, the LPV framework offers an appealing solution for both types of nonlinear terms as it can transform them into linearly time-varying parameters. After investigating the LPV modeling preliminaries, the quadrotor is found to be matching a quasi-LPV model representation. And since this work is dedicated to quadrotor FTC, a quasi-LPV model for the attitude and altitude dynamics is presented to be deployed for further actuators fault diagnosis and fault-tolerant control. The choice of such a submodel is due to the direct relation between the rotors and the attitude and altitude states which imply immediate impact in case of actuators faults.

Afterward, it has been demonstrated that an efficient approach to handle the quadrotor control and further sensors fault diagnosis, is to divide the quadrotor model into three subsystems, namely attitude, altitude, and position. According to each subsystem dynamics, a state space form is derived including the additional sensor faults and exogenous disturbances. The resulting augmented system gives a powerful means for modeling the full quadrotor dynamics and guarantees that the FTC approaches developed upon this model will comply with the real-time implementation constraints.

Chapter 3

Quadrotor Control

Chapter abstract

The quadrotor model deduced in the preceding chapter is used to build a controller that stabilizes the vehicle and guarantees adequate trajectory tracking. So initially a PID control law is designed for the simplified linear model using transfer function loop shaping technique to satisfy the required $\mathcal{H}_\infty$ norm characteristics. A linear quadratic Gaussian (LQG) control scheme is proposed in state-space form as an optimal controller that penalizes the control action according to the actuators' limitations, besides recovering the system states whose measurements are affected by Gaussian white noise. Then to ensure the effectiveness of the controller in wide areas of application where the surrounding environmental conditions are not guaranteed to be exactly modeled a robust controller based on the H_∞ technique is designed for the proposed LPV system. The simulation results show great enhancement for the performance when the system is subjected to unknown exogenous disturbances and measurement noise during following the generated trajectory using the cartesian polynomial technique.

3.1 Introduction

There is no doubt that automatic control is an essential element for aircraft and space systems design, as regardless of the vehicle type or the system automation level, it must contain a controller to steer an unmanned vehicle or to assist the pilot of manned aircraft. Therefore, such a field of engineering science has witnessed a great evolution through the last decades thanks to the concerned academic research and the validation in industrial application. Control theories can be sorted into three main branches: classical control, modern control, and robust control as stated in [31].

The classical control techniques like PID control, Bode plot, and Nyquist plot depend mainly on the root-locus and frequency response methods where the system is represented in the form of a transfer function. Although these approaches are efficient in assigning the position of the system poles and satisfying the required time response characteristics, they don't ensure the optimality of the designed control law. In addition, they are mainly adapted to SISO systems so they can't capture the system dynamics resulting from multiple input effect on the system output.

The advancements of digital computers made it possible to analyze more complex multiple input multiple output systems by formulating them in state space form resulting in modern control techniques. These techniques have been applied on both deterministic and stochastic framework so that they guarantee an optimal control action required for steering the system. Since the designed control law depends on the provided system model, so if there exists an error between the actual system and its model, the designed controller may not function as expected. The techniques that count for the modeling error and uncertainties are referred to as robust control techniques. According to [32], naming the techniques as classic and modern can give a misleading interpretation of superiority for a branch over the other, however, it is not true and the choice of the suitable control law depends on the application itself.

It is evident that quadrotors are very beneficial for several activities and industrial applications, nevertheless, they possess a complicated nonlinear model and they lack a source of control input redundancy. That's why numerous academic researches have been dedicated to the quadrotor control problem resulting in remarkable advancements that guarantee a high level of deployment of such a vehicle in various fields. The PID classical control has been introduced as an effective controller for the quadrotor model expressed in a transfer function form between the system states and the control input as can be found in [14]. Further enhancements for the PID control law have been investigated to provide the system with some robustness features based on the $\mathcal{H}_\infty$ loop shaping technique such work is presented in [52] and [15].

In [11], one can find a comparison between a PID control and an optimal control law based on Linear Quadratic Regulator (LQR) approach which didn't reach the expected results due to the quadrotor model imperfections. However, the LQR technique has experienced some improvements especially for the quadrotor control which is apparent from the experimental results introduced in [16]. By adding an optimal Linear Quadratic Estimator (LQE), the system becomes able to recover the unmeasured states to perform further fault detection as demonstrated in [21]. In addition, the work presented in [53] proposes a method to improve and evaluate the robustness level of the LQR control law.

With the rise and evolution of the LPV modeling technique, several works on state feedback control of a system modeled in an LPV framework based on $\mathcal{H}_\infty$ norm characteristics have been developed see [17]. Some recent works are concerned with quadrotor LPV control such as [18], [19], and [12], where the same design methodology is adopted using Bounded Real Lemma (BRL) to minimize the $\mathcal{H}_\infty$ norm, thus ensuring the controller robustness against exogenous signals beside the Lyapunov inequality to guarantee the desired time response characteristics.

So in this chapter, we are going to outline some of the mentioned control techniques, propose some improve-

ments to ensure the controller's robustness, and compare their performance while applied on a quadrotor model. Before proceeding with the control law discussion, it is important to mention that the quadrotor control scheme consists of nested feedback loops as shown in figure 3.1 where the outer position loop, which has slower dynamics, feeds the fast dynamics attitude loop with the desired orientation angles. This cascaded control scheme is suitable for the quadrotor mathematical model derived in chapter 2 as the position dynamics in $x-y$ plane depend on the orientation angles ϕ, θ, ψ.

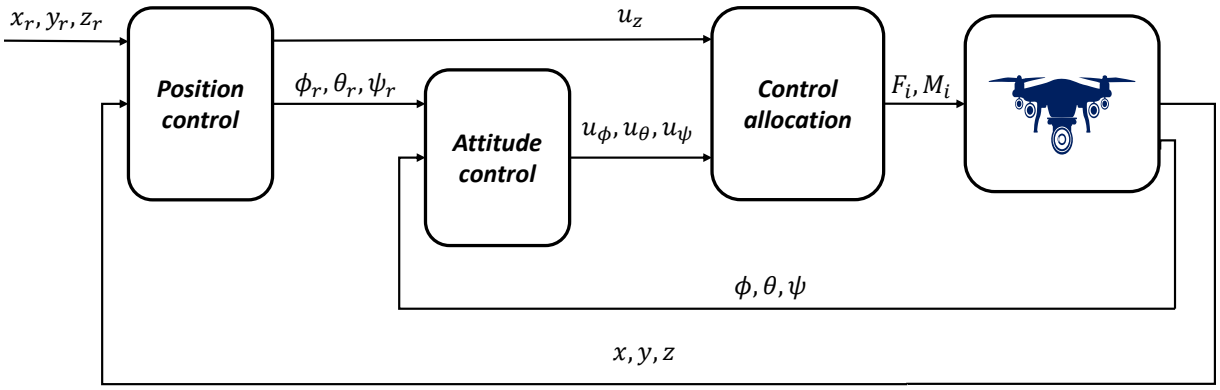

Figure 3.1: Cascaded control scheme

3.2 Classical PID control

According to [31], the PID control and its modified versions are representing more than half of the controllers used in industrial applications which proves the importance of such a technique. One of the most valuable features of the PID control is that it is very intuitive and thus the controller gains can be easily tuned to obtain the required time response characteristics. Consider the PID feedback control law in the time domain given by

$$u(t) = K_p\, e(t) + K_i \int e(t)\, dt + K_d\, \dot{e}(t) \tag{3.1}$$

where $e(t) = x_r(t) - x(t)$ is the state error. It is apparent from equation (3.1) that the proposed PID controller is a linear controller so it is applied to LTI systems which can be easily converted to a transfer function form using the convolution property of Laplace transform. So, while investigating the design of a PID control law, it is more practical to represent the system by a transfer function such that the system behavior can be anticipated based on the poles and zeros positions in the s-domain diagram. By using Laplace transform the PID control law can be represented by the following transfer function

$$G_c(s) = K_p + \frac{K_i}{s} + K_d\, s \tag{3.2}$$

where K_p is the proportional gain which is correlated to the current value of the state error $e(t)$ it is important as it urges the control action to grow rapidly when there exists a large difference between the desired and actual system state. If the open loop system is stable, then the gain K_p can be used alone to guarantee the convergence of the system to the reference value, however, there will exist a steady state error. This steady state error can be eliminated by adding the K_i gain which stands for the error accumulation in a way that gives an extra control action to substitute the error and makes the output follows the reference value precisely. Using a PI controller can give an acceptable reference tracking accompanied by a large overshoot and here comes the importance of the K_d gain which can be regarded as an anticipatory gain since it counts for the derivative of the error and increases the damping of the system during the transient response.

Figure 3.2 shows a PID closed loop control for a single-input single-output system described by a transfer function $G(s)$ where $r(t)$, $x(t)$ are the reference input and the system state, respectively.

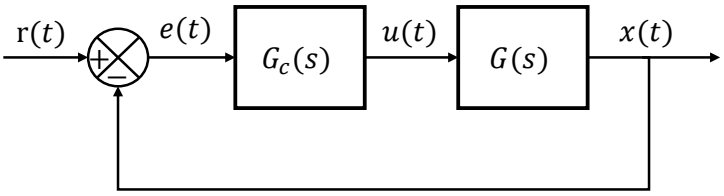

Figure 3.2: Block diagram of a PID controller

3.2.1 PID gains tuning

Choosing the values of the PID gains is a very challenging task since it depends on the plant properties and the desired time response characteristics like peak time, overshoot, settling time,.., etc. Several approaches have been proposed for tuning a PID controller, among them one can mention the Ziegler-Nichols tuning rules used in [54] based on experimental step response of the system. Although, this method is efficient in tuning the gains for unknown system model, the system may exhibit an unacceptable overshoot during the experimentation that can cause a severe damage, a detailed illustration can be found in [31].

If an accurate mathematical model of the system dynamics is established, then the tuning process can be initiated by simulation tools on a computer after which the gains can be refined through real-time experimentation. The Matlab program contains an efficient tool called '**sisotool**' which uses the root locus drawing technique to tune the primitive PID gains. It is important to mention that the root locus diagram is a method used to plot the transfer function poles and zeros position in the s-plane besides drawing the possible trajectories of their motion while changing the controller gains. This method is powerful for tuning the controller gains as the transient response of the closed loop transfer function is directly affected by the poles and zeros location in the s-plane a full illustration

for the root locus plot can be found in [31].

In order to design the PID controller by means of sisotool we need to introduce the system open loop transfer function. The quadrotor LTI model has been converted into transfer functions describing the relationship between the system states and the control input in the preceding chapter 1. Since the resulting six transfer functions (2.37) have a similar form that contains double poles at the origin, we can investigate the controller design for one transfer function then applying the same methodology for the others. Consider the open loop transfer function for the roll angle given by

$$G(s) = \frac{1}{I_{\mathrm{xx}} s^2} \tag{3.3}$$

As the transfer function has double integrators itself, it is more convenient to use a PD control law only without an integrator term. Using this controller will act as adding a zero in the root locus diagram to increase the stability of the system and enhance its time response. So the proposed controller takes the following form

$$G_c(s) = K_p + K_d\, s \tag{3.4}$$

By introducing this controller $G_c(s)$ and the transfer function $G(s)$ in Matlab sisotool function, we obtain the root locus diagram given by figure 3.3a where the blue crosses represent the open loop poles while the green crosses and the green circle represent the closed loop transfer function poles and zero, respectively. Inside the root locus diagram, we drag the poles until they reach the position that corresponds to the desired time response characteristics of the closed loop system which is illustrated by figure 3.3b.

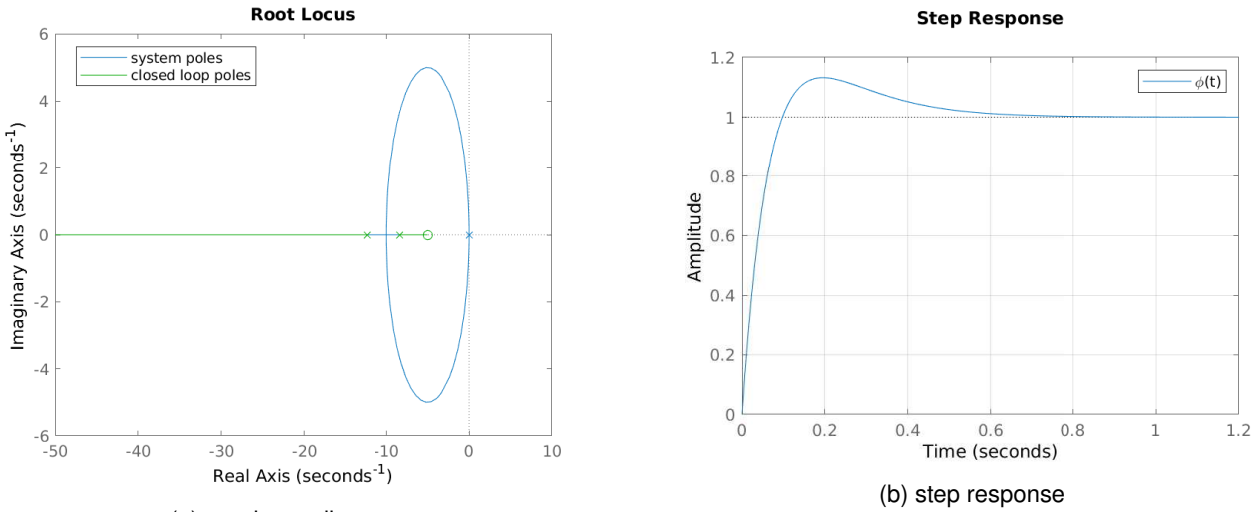

(a) root locus diagram

(b) step response

Figure 3.3: Roll angle transfer function control

We repeat the same process for the six transfer functions representing the quadrotor dynamics 2.37 such that

–	time response characteristics		PD controller gains	
–	t_s	$O_s(\%)$	K_p	K_d
$\phi\ (rad)$	$0.8s$	10	71	14.2
$\theta\ (rad)$	$0.8s$	10	71	14.2
$\psi\ (rad)$	$1s$	10	30	6
$z\ (m)$	$3s$	15	22	4.4
$x\ (m)$	$5s$	20	5	1
$y\ (m)$	$5s$	20	5	1

Table 3.1: Quadrotor states PD control

we obtain a PD control law that is able to guarantee quadrotor reference tracking. The required time response characteristics for each state and the corresponding PD gains are given in table 3.1 where t_s is the settling time and O_s is the acceptable overshoot. The values in table 3.1 indicate that the controller designed for the orientation angles ϕ, θ, ψ is more aggressive to achieve the required fast time response, however, the position states gains have smaller values as they represent the outer control loop having slower dynamics. In order to test the designed PD controller performance, it is applied to the quadrotor model described by the transfer functions (2.37) in a simulation using the Matlab Simulink program, and the obtained results are given in the next section.

3.2.2 Simulation results

The simulation environment is basically following the control scheme given by figure 3.1 where the position control unit gives the reference orientation angles to the inner attitude control loop. The PD controller gains given in the table 3.1 are used for both the linear model described by the transfer functions (2.37) and the nonlinear model (2.25) while introducing the following reference inputs

$$x_d(t) = \begin{cases} 0 & t < 20\ s \\ 2\ m & 20 \leq t \leq 40\ s \\ 0 & t > 40\ s \end{cases}, \quad y_d(t) = \begin{cases} 0 & t < 30\ s \\ 2\ m & 30 \leq t \leq 50\ s \\ 0 & t > 50\ s \end{cases}, \quad z_d(t) = \begin{cases} 0 & t < 10\ s \\ 2\ m & 10 \leq t \leq 80\ s \\ 1\ m & t > 80\ s \end{cases} \tag{3.5}$$

where x_d, y_d, z_d represent the desired spatial position of the drone. The resulting trajectory after introducing the desired position components (3.5) consists of taking off, square path, hovering, and landing. The simulation results of this trajectory are shown in figure 3.4 and it is obvious from figure 3.4a that the system is able to follow the desired trajectory precisely with the existence of an acceptable overshoot during transient response. Also, it can be noticed from figure 3.4b that however, the PD control law is a linear controller, it is very effective in achieving trajectory tracking while applied to the system nonlinear model.

Until now, the PD control law has proven its efficiency in maintaining the system stability while tracking the reference trajectory.

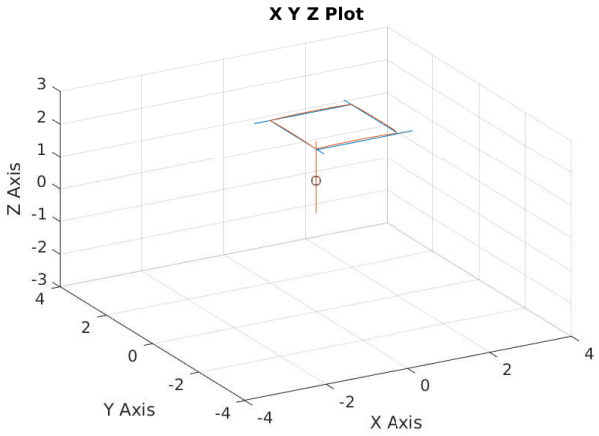

(a) PD control with the linear model

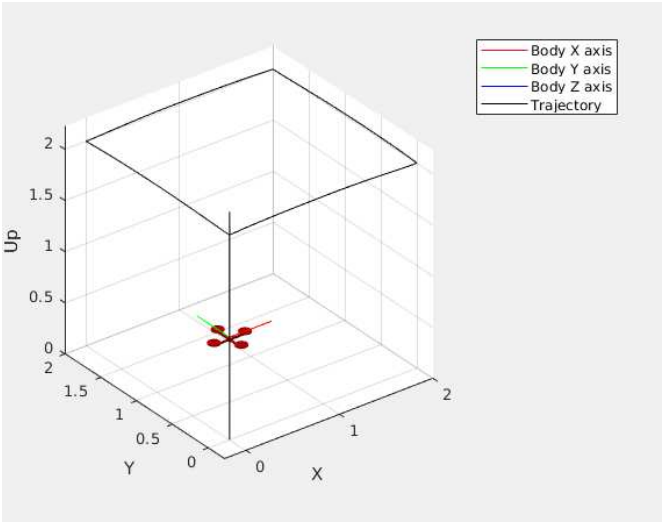

(b) PD control with nonlinear model

Figure 3.4: Square trajectory tracking

However, in an open environment, the quadrotor is likely to encounter some exogenous disturbances which are not counted for trough the design of the control law. So in order to examine the performance of the controller in the whole band of frequencies, consider the bode plot and singular values plot of the closed loop transfer function of ϕ state given by figure 3.5. In addition to the closed loop transfer function, the sensitivity $S(s)$, complementary sensitivity $T(s)$, and loop $L(s)$ transfer functions are plotted which are very important to investigate the controller robustness as illustrated in the next section 3.3. Roughly speaking, the loop transfer function $L(s) = G_c(s)\ G(s)$ should ideally look like an integrator to ensure an effective disturbance rejection and noise attenuation which is not satisfied by the PD controller.

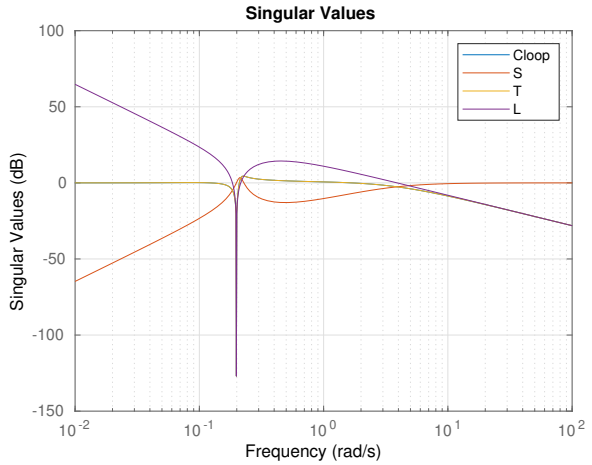

(a) singular value decomposition

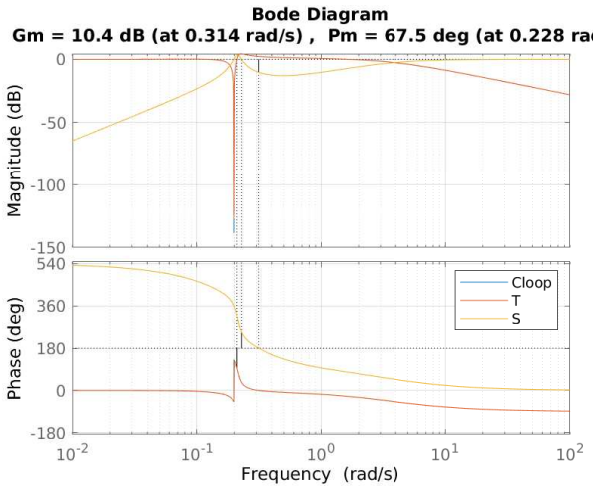

(b) Bode plot

Figure 3.5: Closed loop transfer function of ϕ state

The singular values plot in figure 3.5a illustrates how bad the controller is from the robustness point of view as

at the frequency of $0.2\ rad/s$ any disturbances will be rapidly amplified and the system may not be able to stabilize itself. In addition, the bandwidth frequency is about $4\ rad/s$ allowing more measurement noise to pass through the system response. In figure 3.5b one can notice from the bode plot of the ϕ state that at the frequency mentioned above there is a phase lag of $180°$ that's why sensitivity $|S|$ and complementary sensitivity $|T|$ functions are having very large peaks.

The results shown in figure 3.5 can be directly interpreted from the following figure 3.6 where the closed loop transfer function step response of the roll angle ϕ under disturbances effect is shown. The introduced disturbance signals are sinusoidal signals described by

$$\begin{aligned} d_1(t) &= \sin 2t\ rad/s \\ d_2(t) &= \sin 0.2t\ rad/s \end{aligned} \tag{3.6}$$

so the two disturbance signals d_1 and d_2 have the same magnitude with different frequencies. While the PD control law is able to suppress the disturbance d_1 to about 10% of its magnitude, it is not very efficient in rejecting the disturbance d_2 as it is at the critical frequency $0.2\ rad/s$ indicated earlier. So in the next section, we are going to investigate the controller design methodology that guarantees the robustness of the system.

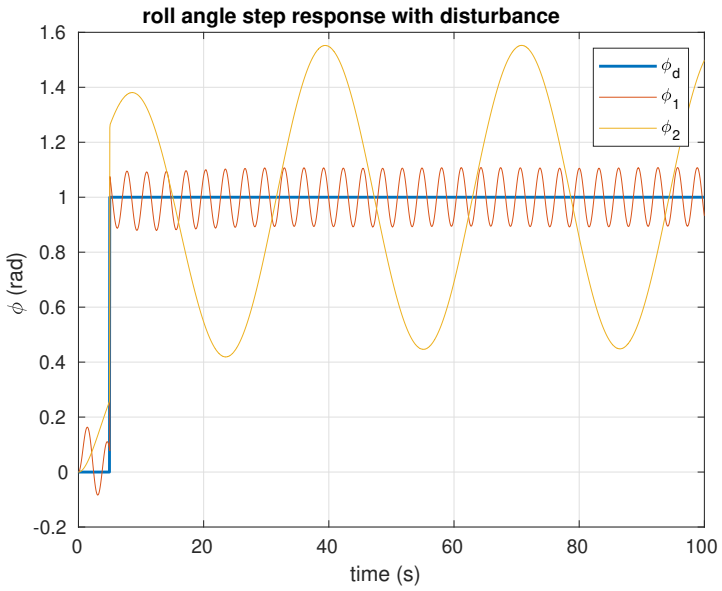

Figure 3.6: ϕ angle step response under disturbance effect

3.3 $\mathcal{H}_\infty$ loop shaping

As discussed earlier a classical PD control law could stabilize the system while tracking a specified trajectory, however, such performance is not guaranteed if there exist some external disturbances, measurement noise, or

model uncertainties. So the solution offered by the $\mathcal{H}_\infty$ loop shaping is appealing as it combines the traditional intuition of classical control methods, such as Bode's sensitivity integral, with H_∞ optimization techniques to design the controller as stated in [55]. The resulting controller stability and performance properties hold despite the probable existence of bounded differences between the nominal plant assumed in design and the true plant encountered in practice. Basically, the required robustness characteristics are described by some weighting transfer functions introduced to the plant in the frequency domain to determine the closed loop transfer function shape. Consider the feedback control system shown in figure 3.7.

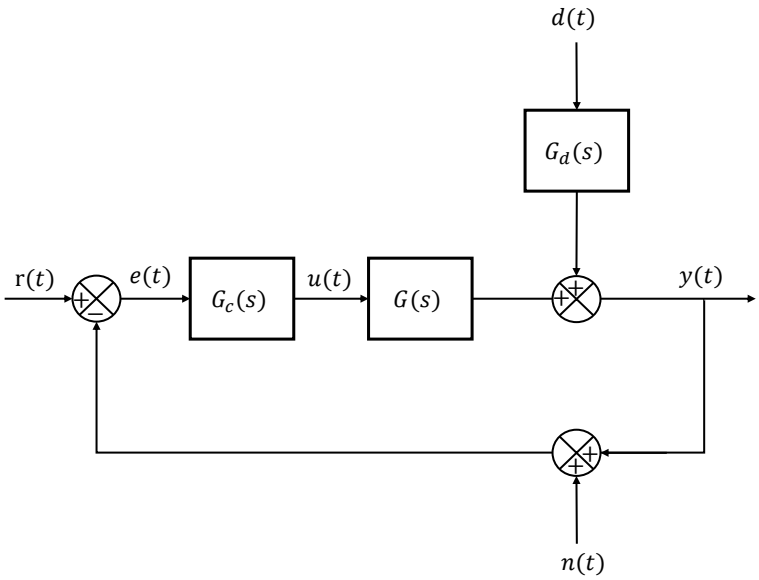

Figure 3.7: Block diagram of the system with noise and disturbance

The resulting closed-loop response is given by

$$y(t) = (I + GG_c)^{-1}GG_c\, r(t) + (I + GG_c)^{-1}G_d\, d(t) - (I + GG_c)^{-1}GG_c\, n(t) \tag{3.7}$$

where $n(t)$ represents the measurement noise. The following terminology is used to simplify the analysis

- loop transfer function: $L = GG_c$
- sensitivity function: $S = (I + GG_c)^{-1} = (I + L)^{-1}$
- complementary sensitivity function: $T = (I + GG_c)^{-1}GG_c = (I + L)^{-1}L$

Note that the relationship between the sensitivity S and complementary sensitivity T can be described by the following equation

$$S + T = I \tag{3.8}$$

which is very useful while analyzing the behavior of the two transfer functions in the frequency domain. By substi-

tuting these terms into equation (3.7), it can be rewritten as

$$y(t) = T\ r(t) + SG_d\ d(t) - T\ n(t) \tag{3.9}$$

By defining the state error by $e(t) = r(t) - y(t)$, then

$$e(t) = S\ r(t) - SG_d\ d(t) + T\ n(t) \tag{3.10}$$

such that S is representing the closed-loop transfer function from the output disturbances to the outputs, while T is the closed-loop transfer function from the reference signals to the outputs. It is obvious that the controller design aims at minimizing the error signal by achieving adequate reference tracking while preserving a high level of disturbance rejection and noise attenuation. From equation (3.10), such design criteria are impossible to be attained for the whole band of frequency as equation (3.8) implies inverse proportion between the sensitivity and complementary sensitivity transfer functions. Thus before proceeding to controller design, it is beneficial to investigate the characteristics of the reference signal r, the disturbance signal d, and the noise signal n in the frequency domain.

reference tracking (r) for sure the reference value is not changing arbitrarily at high frequency so to have good reference tracking the sensitivity function S should be kept small at low frequencies.

disturbance rejection (d) the disturbances affect the system much at low frequencies so again we need a small value for S at low frequencies.

noise attenuation (n) the noise is generally high frequency signal so we need T to be small at high frequencies such that the error due to the noise signal vanishes.

So fortunately the previously mentioned criteria can be achieved simultaneously if we design a controller G_c such that the loop gain L becomes similar to an integrator form $L \approx \omega_B/s$ where ω_B is the bandwidth frequency of the system. As if the loop gain L shape is matching an integrator form then the sensitivity function S will have a small value at low frequencies while the complementary sensitivity function T will have a small value at high frequencies. This conclusion is illustrated by the rough sketch for the transfer functions T, S, L magnitudes given in figure 3.8

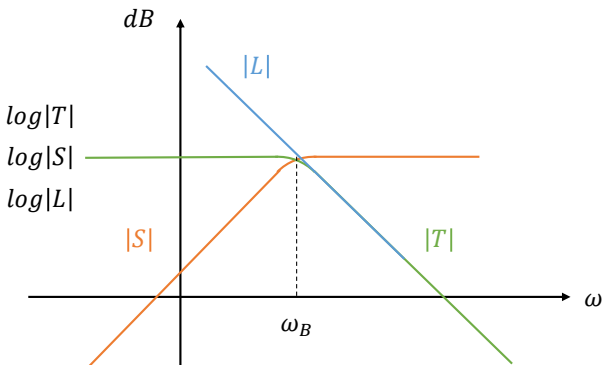

Figure 3.8: Sensitivity, complementary sensitivity, and loop transfer functions in the frequency domain

3.3.1 Open loop shaping

This is the direct approach to shape the open loop transfer function $L = G_c G$ in a form similar to an integrator at the specified bandwidth to satisfy the design requirements. Recall equation (3.10), it can be written as

$$e(t) = (I + L)^{-1}\, r(t) - (I + L)^{-1} G_d\, d(t) + (I + L)^{-1} L\, n(t) \tag{3.11}$$

the controller ideally can minimize the error to be almost zero if the following equation holds

$$e(t) \approx 0 \cdot r(t) + 0 \cdot d(t) + 0 \cdot n(t) \tag{3.12}$$

The first two terms in equation (3.12) can be achieved with $S \approx 0$ which implies $T \approx I$ due to their inverse proportion described by equation (3.8), thus the loop transfer function L must be large in magnitude at low frequency. On the other hand, to guarantee a satisfactory noise attenuation level, it is necessary to have $T \approx 0$, or equivalently, $S \approx I$ at high frequency.

It is important to define the maximum peaks of sensitivity and complementary sensitivity functions at the cross-over frequency which are given by the following two terms

$$\begin{aligned} M_S &= \max_\omega |S(j\omega)| = ||S||_\infty \\ M_T &= \max_\omega |T(j\omega)| = ||T||_\infty \end{aligned} \tag{3.13}$$

these two parameters are useful indicators for the system robustness. According to [55], the typical values for $M_S < 2\ (6\ dB)$ and $M_T < 1.25\ (2\ dB)$ to ensure good performance of the system around the desired bandwidth frequency.

For our system transfer functions (2.37) which contain two integrators, designing a lead compensator will be sufficient to guarantee the desired closed loop characteristics. The proposed lead compensator contains a zero for adjusting the phase margin hence the time response and a pole for rolling off frequency to avoid measurement noise at high frequency. Thus, the shape of the controller will be as follows

$$G_c(s) = \frac{\mathbf{b}\ s + 1}{\alpha \mathbf{b}\ s + 1} \tag{3.14}$$

Where α and $\mathbf{b}$ are constants to be chosen according to the desired phase to be added and its corresponding frequency according to the following

$$\omega_{max} = \frac{1}{\mathbf{b}\sqrt{\alpha}} \tag{3.15}$$

$$\sin(\Phi_{max}) = \frac{1 - \alpha}{1 + \alpha} \tag{3.16}$$

Where ω_{max} is the frequency at which the maximum phase is added and Φ_{max} is the maximum phase needed. Roughly speaking the relation between phase margin PM (in degrees) and system damping ratio can be given by

$$\zeta = \frac{PM}{100} \tag{3.17}$$

So the procedure for choosing the values of $\alpha, \mathbf{b}$ consists of the following steps

1. determine the required damping ratio for the system
2. from equation (3.17) calculate the needed phase margin PM
3. from the open loop system bode plot calculate the actual phase at the desired cross-over frequency ω_{max}
4. having the actual and desired phase of the system compute Φ_{max} to be added
5. from equations (3.16) and (3.15) calculate the values of α and $\mathbf{b}$
6. substitute in equation (3.14) to get the pursued controller

The results of applying the controller obtained by open loop shaping (3.14) to the roll angle transfer function (3.3) is illustrated in the next section 3.3.3.

3.3.2 Closed loop shaping

In the previous section 3.3.1 the technique focused on shaping the loop gain L such that the resulting sensitivity S and complementary sensitivity T functions are satisfying the closed loop system requirements. Here another methodology is adopted which aims at shaping the closed loop transfer functions T, S directly by introducing reasonable weights that govern their behavior in the frequency domain. Hence, the design methodology is formulated in an $\mathcal{H}_\infty$ optimal control problem which can be solved using optimization tools in Matlab.

In addition to the design requirements stated previously, we are seeking an optimal control action to limit the energy expelled by the actuators so the design criteria can be listed as follows

- adequate reference tracking
- efficient disturbance rejection
- high level of noise attenuation
- optimal control action

These criteria can be satisfied by introducing the performance weights w_P, w_T and w_u such that

$$\begin{aligned} &||w_P\ S||_\infty < 1 \\ &||w_T\ T||_\infty < 1 \\ &||w_u\ G_c\ S||_\infty < 1 \end{aligned} \tag{3.18}$$

this is called a stacking approach for which a complete derivation and illustration can be found in [55]. Assume the performance weight is a low pass weight taking the form

$$w_P(s) = \frac{s/M + \omega_B}{s + \omega_B A} \begin{cases} \text{at} \quad s \to 0 \quad w_P(s \to 0) \to 1/A \quad \Rightarrow \quad S(s \to 0) = A \\ \text{at} \quad s \to \infty \quad w_P(s \to \infty) \to 1/M \quad \Rightarrow \quad S(s \to \infty) = M \end{cases} \tag{3.19}$$

where M_S is the maximum peak magnitude of the sensitivity S, and ω_B is the desired bandwidth frequency while A represents the maximum steady-state tracking error.

This performance weight w_P ensures that the sensitivity function S has a low gain at low frequencies for good tracking performance and a high gain at high frequencies to limit overshoot. It can be thought of as a pole at $\omega_B\ A$ followed by a zero at $M\ \omega_B$ where the effect of ω_B is that it limits the maximum desired closed loop transfer function time constant. In addition, the value of M adjusts the system damping as increasing M results in less overshoot for the sensitivity function S at the bandwidth frequency. However, there exists a trade-off here as increasing M causes an increase in the response time also which is not desired. Finally, A should be kept small because it defines at which frequency starts the effect of the pole (where will the system begin disturbance rejection and reference tracking).

For the complementary sensitivity function T a high pass weight w_T which takes the following form is used

$$w_T(s) = \frac{s + \omega_B/M}{As + \omega_B} \begin{cases} \text{at} \quad s \to 0 \quad w_T(s \to 0) \to 1/M \quad \Rightarrow \quad T(s \to 0) = M \\ \text{at} \quad s \to \infty \quad w_T(s \to \infty) \to 1/A \quad \Rightarrow \quad T(s \to \infty) = A \end{cases} \tag{3.20}$$

Hence, w_T can be regarded as just the inverse of w_P due to the inverse relation between the sensitivity S and complementary sensitivity T functions (3.8). For the control action weight w_u it is sufficient to have just a constant value representing the maximum limit of the actuator which the controller will guarantee the control action won't exceed. The design procedure is as follows

1. choose the weights parameters ω_B, A, M, k_s.

2. formulate the $\mathcal{H}_\infty$ problem containing the open loop transfer function $G(s)$ and the performance weights w_P, w_T, w_u using 'augw' Matlab command.

3. solve for the robust controller $G_c(s)$ using 'hinfsyn'.

4. calculate the resulting peaks of the sensitivity and complementary sensitivity functions M_s, M_T.

5. iterate on the weights parameters until the suitable values of M_s, M_T are achieved.

3.3.3 Simulation results

Consider again the roll angle transfer function (3.3) is the one chosen to apply and validate the designed controller. By following the steps given in section 3.3.1 based on open loop shaping technique with the following requirements $\omega_{max} = 10\ \ rad/s$ and $\Phi_{max} = 85°$, the resulting controller parameters are $\alpha = 0.0038, \mathbf{b} = 1.0624$.

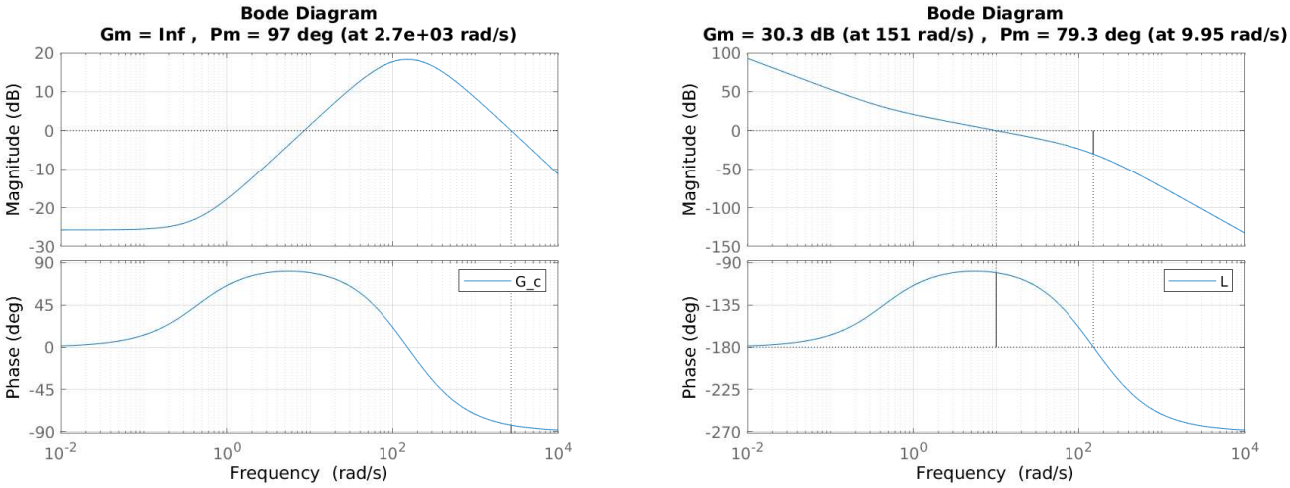

(a) lead compensator Bode plot

(b) loop gain Bode plot

Figure 3.9: Open loop shaping of roll angle transfer function

Figure 3.9b gives the bode plot of the ϕ state loop gain transfer function indicating the effect of the proposed lead compensator whose Bode plot is shown in figure 3.9a. The phase added is $85°$ at the required frequency results in a damping ratio $\zeta = .85$ so the system is overdamped which is apparent in the step response given in figure 3.11a. In addition, the performance of the lead compensator designed in 3.3.1 could be further enhanced by introducing an additional pole at high frequency $\omega = 100\ \ rad/s$ leading to a second order lead compensator. The effect of both poles appears in rolling off frequency which is about $150\ \ rad/s$ and it is sufficient for suppressing high frequency measurement noise. Figure 3.10 proves the robustness of the designed controller as it is obvious that the loop transfer function L looks like an integrator. In addition, there are no peaks for S or T at the bandwidth frequency such that the values of $M_S = 1.1136$ and $M_T = 1.0359$.

Finally, to compare the performance of the proposed controller with the PD controller deduced earlier, the following disturbance signal is introduced

$$d(t) = \sin 0.2t\ rad/s \tag{3.21}$$

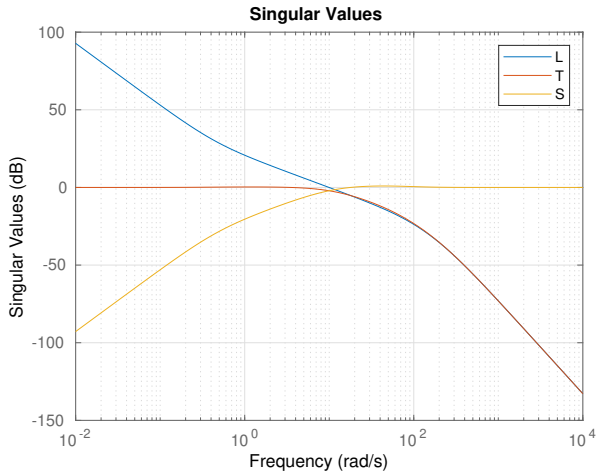

Figure 3.10: transfer functions singular values following open loop shaping

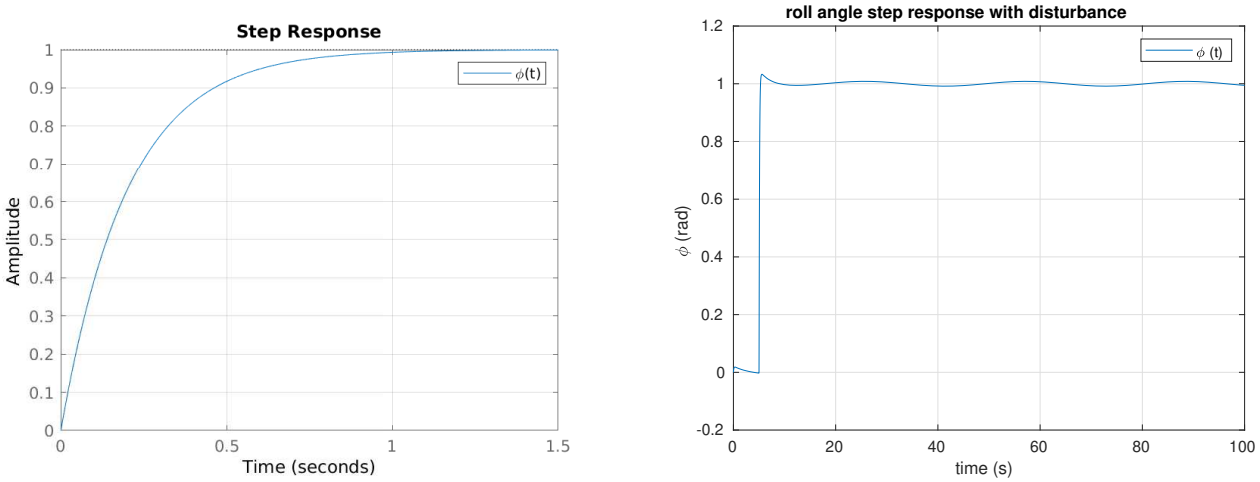

(a) roll angle step response

(b) step response under disturbance effect

Figure 3.11: Roll angle step response with and without exogenous disturbances

Figure 3.11b shows that the controller is able to reject the low frequency disturbance effectively better than the PD controller which could only minimize the disturbance effect by 40% as previously illustrated in figure 3.6.

Concerning the closed loop transfer functions S, T shaping, the design procedure given in section 3.3.2 is followed where the parameters chosen are $k_s = 2$, $A = 10^{-4}$, and $\omega_B = 9\, rad/s$. As mentioned earlier, the choice of M is an iterative process so we introduce some values of M and calculate their corresponding M_T, M_S values for the closed loop system. In addition, we evaluate the settling time t_s and the percentage of overshoot O_s, the values of M, M_T, M_S, t_s, O_s are given in table 3.2 giving a hint about the variation of the system performance with the design parameter M. This is again illustrated by figure 3.12 that shows the effect of changing the design parameter M on the closed loop step response.

After the iteration we chose $M = 1.5$ as it results in reasonable values for the peaks of the sensitivity and

M	0.5	1	1.5	2	2.5
M_T	0.98	0.99	1	1	1
M_S	1.079	1.1449	1.17	1.1904	1.1955
$t_s(s)$	0.8153	0.477	0.3802	0.3438	0.3274
$O_s(\%)$	0	0	0.0069	0.1557	0.3106

Table 3.2: Variation of the system performance with design parameter M

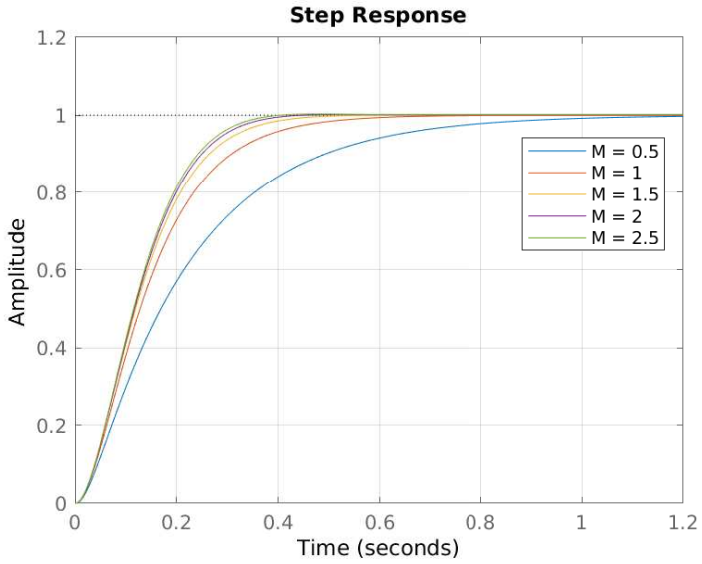

Figure 3.12: Roll angle step response variation with M

complementary sensitivity $M_S = 1, M_T = 1.17$ and preserves an acceptable transient response settling time and overshoot as $t_s = 0.3802s, O_s = 0.0069\%$. The resulting shapes of the transfer functions S, T, L are given in figure 3.13a where their magnitude is plotted with respect to the frequency. In order to get better noise attenuation, we can have a 2^{nd} order weight for the complementary sensitivity function T so the slope of the transfer function will be doubled, but this increases the settling time and for our model the response using a 1^{st} order weight was better and more suitable for the desired time response characteristics.

The H_∞ optimization problem solved using Matlab 'hinfsyn' gives a dynamic output feedback controller of a very high order containing several poles and zeros. This controller can be greatly simplified for implementation using Hankel singular values model order reduction technique which is deployed in [56]. We can maintain only the two low frequency poles and zeros that affect the system response directly where the other parts are considered as high frequency and can be easily removed. The result of gain reduction is given in figure 3.13b and indicates that the two controllers are identical in the operating frequencies of the system such that the reduced order controller can effectively achieve the required system characteristics.

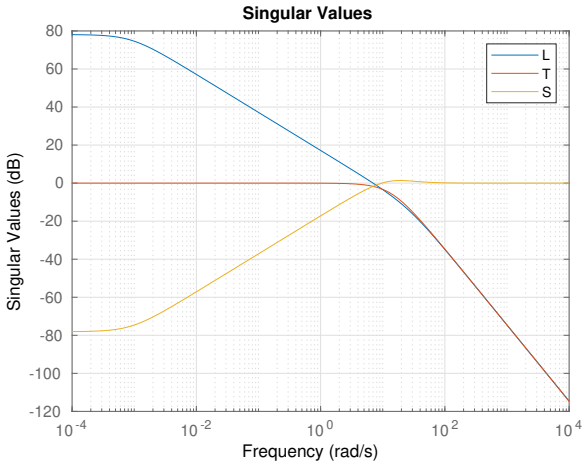

(a) singular values plot

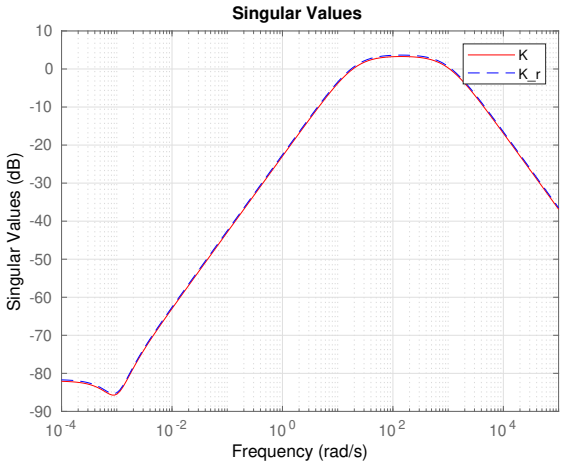

(b) reduced order controller vs derived high order controller

Figure 3.13: Roll angle closed loop shaping control

3.4 LQG control

With the continuous technological advancements, the control systems became more complex including several inputs and outputs which have to be regulated simultaneously. As mentioned in [31], it is important to reduce the complexity of the system model such that it becomes more analyzable which facilitates the controller design task. In the last sections, the linear model of the quadrotor described by the transfer functions was used to establish the controller. Although the designed control laws are able to stabilize the nonlinear model of the quadrotor, they handle each state of the system separately without considering the possible coupling effect between the multiple system inputs. Thus, it is more convenient to represent the system in state space form that gathers all system inputs and states in a simplified differential equation.

The work presented in this part is dedicated to designing a Linear Quadratic Gaussian (LQG) control law for the linear affine quadrotor model deduced in the preceding chapter 2.3.2. The term LQG refers to the capability of applying an optimal control law based on quadratic cost functions on a system with incomplete state measurement and affected by Gaussian white noise as stated in [57]. Thus, the LQG control scheme consists of a Linear Quadratic Regulator (LQR) besides a Linear Quadratic Estimator (LQE) as shown in figure 3.14. It is apparent from the figure that the state estimator takes the system output $y(t)$ to generate a full state estimation $\hat{x}(t)$ which is then transferred to the control unit to produce the control action $u(t)$ that drives the system to the desired reference trajectory $r(t)$. In addition, since the controller depends on the estimated system states, the resulting control law can be thought of as an observer-based feedback controller. The necessary conditions and the design methodology of the optimal quadratic controller and observer is presented in the following sections. Nevertheless, it has to be mentioned that the separation principle guarantees that both of them can be designed and computed independently for a linear system such as our affine LTI model.

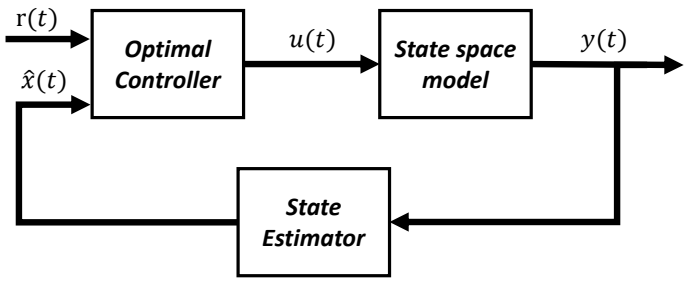

Figure 3.14: LQG control scheme

3.4.1 Quadratic optimal control law

The main advantage of such a control law is that it ensures the optimality of the control action according to the specified quadratic functions. In our case, as the drone is required to follow the desired trajectory, then the control input is not just a regulator since it includes the effect of the reference input. Consider the quadrotor piecewise affine model is described by the following LTI state space representation

$$\begin{cases} \dot{\mathbf{x}}(t) = A\mathbf{x}(t) + B\mathbf{u}(t) \\ y(t) = C\mathbf{x}(t) + D\mathbf{u}(t) \end{cases} \tag{3.22}$$

where the system matrices A, B, C, D have been derived previously in section 2.3.2, the proposed state feedback control law takes the following form

$$\mathbf{u}(t) = -K\ \mathbf{x}(t) + N_r\ r(t) \tag{3.23}$$

where $K \in \mathbb{R}^{n_u \times n}$, $N_r \in \mathbb{R}^{n_u \times n_r}$ representing the state feedback gain and the inverse of the DC gain of the system, respectively. The importance of the gain N_r is that it substitutes the difference between the reference input and the system output at the steady state. While the state feedback gain is responsible for preserving the system stability during the transient response such that it reaches the desired reference input. The application of the linear quadratic state feedback control law (3.23) on the state space model (3.22) is shown in figure 3.15. Such a feedback control diagram is very important as it represents how the controller is implemented for simulation using Matlab Simulink.

Remark 1

In order to be able to choose the value of the gain K that guarantees the optimality of the control law, the system has to be controllable or at least stabilizable.

Thus, the controllability of the system is an essential element that has to be investigated before proceeding to the controller design. In [31], one can find a good definition for the controllability and Stabilizability of the system given as follows

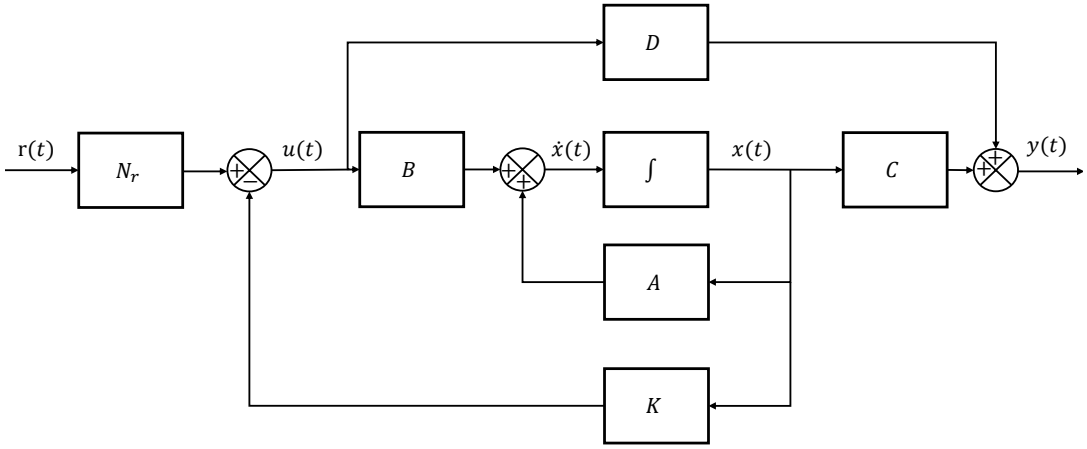

Figure 3.15: State feedback LQR control scheme

Definition 2

- a system is controllable if it can reach any desired final state $\mathbf{x}(t)$ from its initial state $\mathbf{x}(t_0)$ by means of unconstrained control input.
- concerning a partially controllable system, if the unstable states are controllable while the uncontrollable states are stable, then the system is said to be stabilizable.

There exist several methods for examining the system controllability, but for our LTI model described by equation (3.22), it is convenient to use the following controllability matrix.

$$C_o = \Big[B, AB, \ldots, A^{n-1}B\Big] \tag{3.24}$$

The system is said to be controllable if the controllability matrix C_o has full row rank, such that $rank(C_o) = n$ where n is the number of system states, a full derivation of the controllability matrix for the continuous LTI systems can be found in [31]. Fortunately, after computing the controllability matrix for our affine model, it is found to be controllable which allows designing the aspired state feedback control law. So returning back to the feedback control law (3.23), the gain matrix K has to be chosen to minimize the following cost function

$$J = \int_0^\infty (\mathbf{x}^T Q\mathbf{x} + \mathbf{u}^T R\mathbf{u})dt = \int_0^\infty ||M(t)||^2 dt \tag{3.25}$$

where $M(t)$ is the output signal used for performance evaluation defined by equation (3.26)

$$M = \begin{bmatrix} \sqrt{Q} & 0 \\ 0 & \sqrt{R} \end{bmatrix} \begin{bmatrix} \mathbf{x} \\ \mathbf{u} \end{bmatrix} \tag{3.26}$$

The matrices Q and R are positive-definite (or positive-semidefinite for Q) Hermitian or real symmetric matrices representing the weights of states variation and the control action, respectively. The values of Q and R matrices need to be tuned to accomplish the desired controller performance, a good initial guess for them can be found in [58] based on Bryson's rule which has to be further enhanced by iterations. Let the matrices Q and R taking the following form

$$Q = \begin{bmatrix} q_{11} & 0 & \dots & 0 \\ 0 & q_{22} & \dots & 0 \\ \vdots & \vdots & \ddots & \vdots \\ 0 & 0 & \dots & q_{nn} \end{bmatrix}, \quad R = \begin{bmatrix} r_{11} & 0 & \dots & 0 \\ 0 & r_{22} & \dots & 0 \\ \vdots & \vdots & \ddots & \vdots \\ 0 & 0 & \dots & r_{n_u n_u} \end{bmatrix} \tag{3.27}$$

Using Bryson's rule, an element of the Q matrix denoted q_{ii} can be regarded as the bound for the square of the state ${\mathbf{x}_i}^2$, $i \in [1, \dots, n]$ such that $q_{ii}\ {\mathbf{x}_i}^2 = 1$ (it is the nutshell result of the introduced cost function (3.25)). So an acceptable initial guess of the element q_{ii} can be given by

$$q_{ii} = \frac{1}{\bar{\mathbf{x}}_i^2} \tag{3.28}$$

where $\bar{\mathbf{x}}_i$ is the maximum acceptable value of the state $\mathbf{x}_i$. Similarly, the elements of the R matrix can have the following initial value

$$r_{ii} = \frac{1}{\bar{\mathbf{u}}_i^2} \tag{3.29}$$

where $\bar{\mathbf{u}}_i$ is the maximum available control action which the actuator can conduct. Roughly speaking, increasing elements of Q results in small variations of the corresponding states, while increasing elements of R limits the energy expended by the motors, and vice versa. After choosing the values of the weighting matrices Q, R, a common procedure to obtain the optimal feedback gain K is to solve the Algebraic Riccati Equation (ARE) given by

$$A^T\ P + P\ A - P\ B\ R^{-1}\ B^T\ P + Q = 0 \tag{3.30}$$

where P is a positive-definite Hermitian or real symmetric matrix. A full derivation of ARE can be found in [31] by substituting the state equation into the proposed cost function. However, a methodology is introduced in [53] to enhance the performance of the controller in rejecting exogenous disturbances thus increasing the robustness of the system. The idea is to replace the Riccati equation (3.30) by the Linear Matrix Inequality (LMI) (3.31) to calculate the value of the matrix P. The solution of the following LMI satisfies the ARE (3.30) which is corresponding to the LMI's first element.

$$\begin{bmatrix} A^TP + PA + Q & PB & PE_d \\ B^TP & R & 0 \\ {E_d}^TP & 0 & {\alpha_c}^2 I \end{bmatrix} \geq 0 \tag{3.31}$$

where E_d is the disturbance matrix given in section 2.3.2, then if there exists a solution for (3.31) giving a positive definite matrix P while the minimization of the value of α_c is introduced as an objective function, this will guarantee that the following inequality holds

$$\int_0^\infty ||M(t)||^2 dt \leq {\alpha_c}^2 \int_0^\infty ||d(t)||^2 dt \tag{3.32}$$

Equation (3.32) implies that the infinity norm of the transfer function from the exogenous inputs to the performance output $M(t)$ approaches minimum, then the pursued value of the optimal feedback gain matrix K can be obtained from

$$K = R^{-1}B^T P \tag{3.33}$$

then the inverse of the DC gain can be obtained from the following equation

$$N_r = -(C(A - BK)^{-1}B)^\dagger \tag{3.34}$$

3.4.2 Linear Quadratic Estimator (LQE)

As the state-feedback controller requires measurement of all system states and it is not feasible to have a sensor for each state, there is a need for an observer to have full state estimation from the states measured by sensors. As will be illustrated in the next chapter, there exist numerous methods for designing an observer for recovering the unmeasured system states.

The LQG approach deploys an LQE observer, which is an optimal observer, to provide the controller with the estimated states $\hat{\mathbf{x}}(t)$. It can be thought of as a continuous time Kalman filter as the observer gain matrix is computed using the Riccati equation to satisfy the cost function penalizing the system model and states measurement. Such a continuous time Kalman filter concerns stochastic systems affected by model uncertainty and measurement noise which are introduced as known Gaussian probability density functions. Thus, this approach enlarges the reliability of the system and improves its robustness against stochastic undesired signals and unmodeled dynamics. Let the affine LTI model described in state space form as following:

$$\begin{cases} \dot{\mathbf{x}}(t) = A\mathbf{x}(t) + B\mathbf{u}(t) + \mathbf{v}(t) \\ y(t) = C\mathbf{x}(t) + \mathbf{w}(t) \end{cases} \tag{3.35}$$

where $\mathbf{v}(t)$, $\mathbf{w}(t)$ are uncorrelated Gaussian model uncertainty and measurement noise signals having covariance matrices V and W, respectively. Hence, the proposed optimal observer takes the following form

$$\begin{cases} \dot{\hat{\mathbf{x}}}(t) = A\hat{\mathbf{x}}(t) + B\mathbf{u}(t) + L(y(t) - \hat{y}(t)) \\ \hat{y}(t) = C\hat{\mathbf{x}}(t) \end{cases} \tag{3.36}$$

where L is the gain matrix to be chosen to stabilize the estimation error $e(t)$ such that $e(t) = \mathbf{x} - \hat{\mathbf{x}}$.

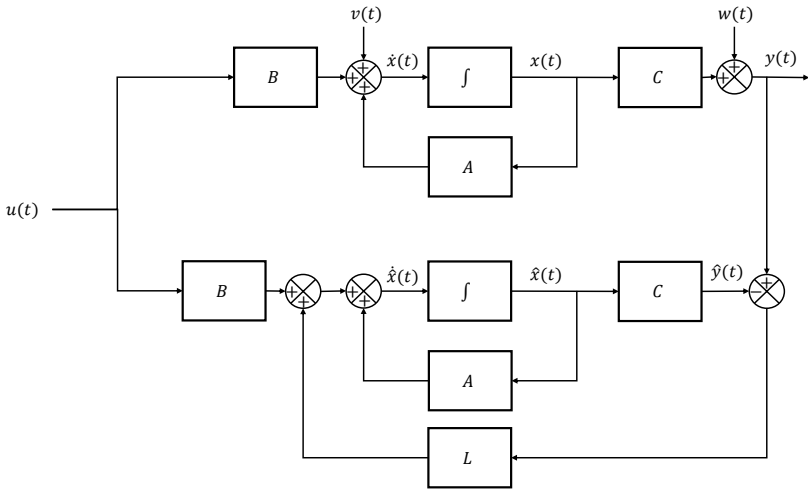

Figure 3.16: Model-based observer scheme

The figure 3.16 shows the diagram of the state space system (3.35) affected by the Gaussian measurement noise and model uncertainties and how it is connected to the observer (3.36). Now we can proceed to synthesize mathematically the application of the LQE observer on the system such that it can produce a full state estimation.

Remark 2

The system (3.35) has to be observable or at least detectable to enable assigning the value of the gain L that stabilizes the observer dynamics.

So it is important to investigate the system observability which is defined [31] as

Definition 3

- a system is observable if every state $\mathbf{x}(t_0)$ can be estimated from the measured output $y(t)$ over a finite period of time t_1 such that $t_0 \leq t \leq t_1$
- for a partially observable system, if the unobservable states are stable while the unstable states are observable, then the system is said to be detectable.

From the remarks 1, 2 and the definitions 2, 3, one can notice the duality between the system controllability and observability. This duality implies also investigating the observability of the linear system using the following

observability matrix O_b similar to the controllability matrix C_o defined before by equation (3.24)

$$O_b = \begin{bmatrix} C \\ CA \\ \vdots \\ CA^{n-1} \end{bmatrix} \tag{3.37}$$

The linear system (3.35) is said to be observable if the observability matrix O_b has full column rank, so after calculating the observability matrix, our piecewise affine model is found to be observable. Thus, the optimal value of the observer gain L can be obtained by the following Riccati equation similar to the methodology used for calculating the optimal controller gain K.

$$A\,\Lambda + \Lambda\,A^T - \Lambda\,C^T\,W^{-1}\,C\,\Lambda + V = 0 \tag{3.38}$$

where Λ is a positive definite matrix while the matrices V and W represent the weights of the model accuracy and measurement noise, respectively, and are used for solving the Riccati equation (3.38) to obtain the optimal state estimator gain L. These matrices have to be chosen carefully according to the precision of the sensors used and model uncertainties, the general behavior of the filter will be trusting the model more in case of small values of V and trusting the measurement more in case of small values of W and we can specify weights for each system state and measurement separately. After calculating the value of the matrix Λ from equation (3.38), the observer gain can be obtained by the following equation

$$L = \Lambda\,C^T\,W^{-1} \tag{3.39}$$

Remark 3

In our case, the controllability and observability matrices were sufficient to prove that the LTI affine model is completely controllable and observable, however, for partially controllable or observable systems the model has to be presented in a canonical form to investigate the stabilizability and detectability of such systems, more illustration can be found in [31].

After calculating the values of the controller and observer gains K, L from equations (3.33) and (3.39), and by replacing the actual system state $\mathbf{x}(t)$ by the estimated state $\hat{\mathbf{x}}(t)$ in the control action equation (3.23), then the augmented LQG control law can be described by the following closed-loop dynamics

$$\begin{bmatrix} \dot{x} \\ \dot{e} \end{bmatrix} = \begin{bmatrix} A - BK & BK \\ 0 & A - LC \end{bmatrix} \begin{bmatrix} x \\ e \end{bmatrix} + \begin{bmatrix} N_r \\ 0 \end{bmatrix} r \tag{3.40}$$

Equation (3.40) proves the previously mentioned fact that the gain matrices K and L can be designed independently of one another without affecting the overall stability of the system.

3.4.3 Simulation results

Using Matlab Simulink with the quadrotor parameters given in Appendix B, a square trajectory described by the following position states (3.41) is introduced to the quadrotor model affected by measurement Gaussian white noise.

$$x_r(t) = \begin{cases} 0 & t < 30\ s \\ 1\ m & 30 \leq t \leq 50\ s \\ 0 & t > 50\ s \end{cases}, \quad y_r(t) = \begin{cases} 0 & t < 20\ s \\ 1\ m & 20 \leq t \leq 40\ s \\ 0 & t > 40\ s \end{cases}, \quad z_r(t) = \begin{cases} 1\ m & t < 10\ s \\ 2.5\ m & 10 \leq t \leq 80\ s \\ 1\ m & t > 80\ s \end{cases} \tag{3.41}$$

where x_r, y_r, z_r are the reference values of the states which the system has to follow.

As mentioned earlier, The LQG feedback control law consists of an LQR controller with an LQE observer that can be designed separately. Concerning the LQR state feedback controller, the following values of the weighting matrices Q,R are obtained through successive iterations on the time response characteristics of the closed loop system states.

$$Q = diag(1, 1, 1, 1, 1, 1, 1, 1, 0.06, 0.06, 0.06) \tag{3.42}$$

$$R = 10^{-2} diag(0.4, 1.6, 1.6, 1.6) \tag{3.43}$$

For the state weighting matrix Q, the values corresponding to the angular rates $\dot{\phi}, \dot{\theta}, \dot{\psi}$ are small as they control the attitude fast dynamics. While for the control input weighting matrix R, the value corresponding to the altitude control action u_z is lower as it is the sum of all actuators' forces. After substituting by these values of Q, R matrices in (3.31) and solving the LMI for the minimum value of α^2, it is found that $\alpha = 0.75$ which guarantees an acceptable controller performance against the exogenous signals.

Regarding the observer design, after iterating on the observer time response while the system is subjected to Gaussian white noise, the values of the weighting matrices V,W are chosen as follows

$$V = 10^{-2} diag(1, 1, 1, 2, 2, 2, 1, 1, 1, 6, 6, 6) \tag{3.44}$$

$$W = diag(10, 10, 10, 10, 10, 10) \tag{3.45}$$

The measurement noise weighting matrix W has larger elements' values than model uncertainty weighting matrix V as the model has to be trusted more since the states' measurements are affected by Gaussian white noise. Afterward, the matrices V, W are introduced to the ARE (3.38) to calculate the optimal value of the observer gain matrix L. The attitude time response of the nonlinear model (2.25) after using the deduced state feedback LQR controller is shown in figure 3.17, it gives an insight about the range of the angular rates to be used in the affine LTI

model see equation (2.43). From the figure a suitable approximate value of the parameters $\bar{\dot{\phi}}, \bar{\dot{\theta}}, \bar{\dot{\psi}}$ is $0.5\ rad/s$.

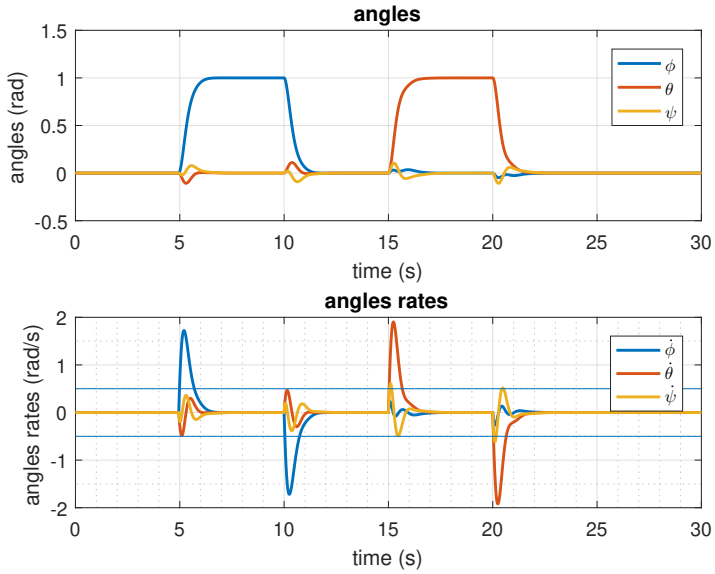

Figure 3.17: Nonlinear model LQG control

The square trajectory proposed by equation (3.41) for the piecewise affine model consists of step inputs for the system states x, y, z. Hence, The time response of the systems states is given in figures 3.18 and 3.19 where the subscripts m, r, e correspond to measured, reference, and estimated states, respectively. These figures illustrate the effectiveness of the LQG control in attenuating the measurement noise because it includes an additional Kalman filter as a state observer.

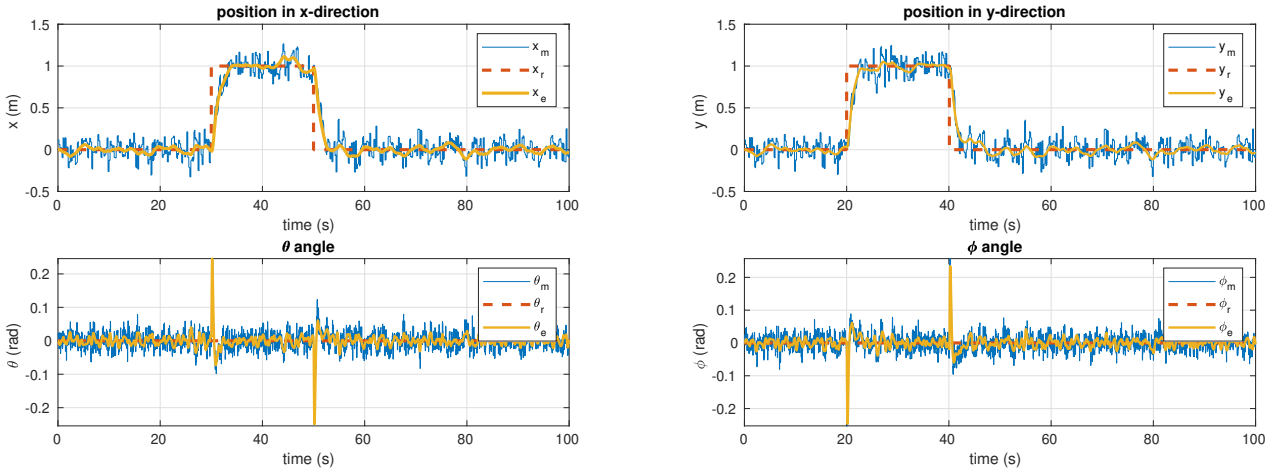

(a) x-direction

(b) y-direction

Figure 3.18: Position states step response LQR vs LQG

The coupling between the rate of change of the yaw $\dot{\psi}$, pitch $\dot{\theta}$ and roll $\dot{\psi}$ angles introduced in the piecewise affine model is apparent in yaw angle response figure 3.19a as there exist two steps, while the reference value

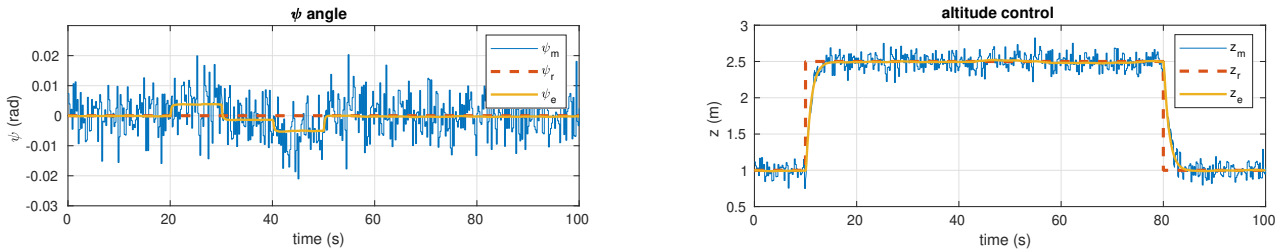

(a) yaw angle (b) z-direction

Figure 3.19: Yaw and altitude step response LQR vs LQG

is set to zero throughout the simulation. The 3D plot in figure 3.20 proves the capability of the proposed control laws in following the desired trajectory besides showing the advantage of the LQG over the LQR control in ensuring a smooth trajectory even if the system is subjected to measurement noise. Finally, to test the robustness of the controller, the closed loop MIMO system is transformed into transfer functions from each input to each output to calculate the closed loop sensitivity S and complementary sensitivity T transfer functions. By using the Matlab function 'hinfnorm', the following $\mathcal{H}_\infty$ norm values are obtained $M_S = 1.0765$ and $M_T = 1.3072$ which means that the system has an acceptable performance from the robustness point of view.

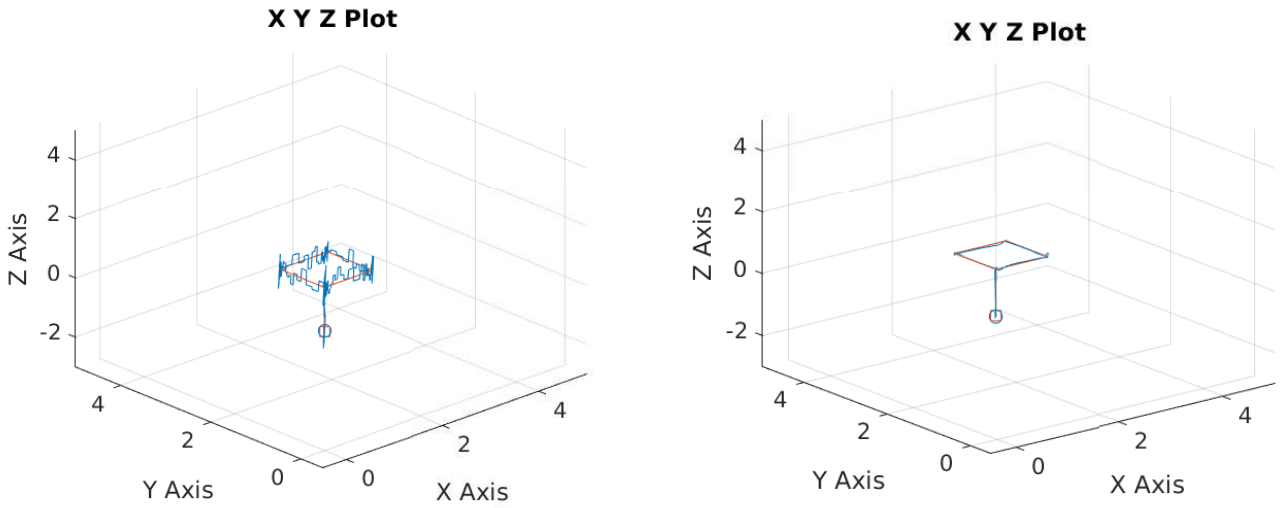

(a) LQR control (b) LQG control

Figure 3.20: Square trajectory following LQR vs LQG

3.5 Robust LPV control

The preceding sections are dedicated to design a control law based on the linearized models of the quadrotor, so in this part, the controller to be constructed is based on the LPV model of the quadrotor. Apparently, in the last chapter two LPV models have been introduced, one including the attitude and altitude dynamics only for the sake

of actuator fault diagnosis and FTC as will be illustrated later, while the other model considering the full quadrotor dynamics for handling sensors fault. So in this section, a general LPV control law design procedure is presented and then applied for each subsystem of the model in simulation using Matlab Simulink. The proposed LPV controller aims at ensuring the closed loop system robustness besides achieving the required time response characteristics. Consider the quadrotor subsystem dynamics is expressed in the following LPV form

$$\begin{cases} \dot{\mathbf{x}}(t) = A(\rho(t))\mathbf{x}(t) + B(\rho(t))u(t) \\ y(t) = C(\rho(t))\mathbf{x}(t) + D(\rho(t))u(t) \end{cases} \tag{3.46}$$

this is the model given before by equation (2.52) having the same state vectors and matrices dimensions. After verifying the controllability of the pair $(A(\rho(t)), B(\rho(t)))$ following the results of definition 2 and benefiting the convexity property of the LPV model, the proposed LPV state feedback control law takes the following form

$$u(t) = -K_c(\rho(t))\mathbf{x}(t) \tag{3.47}$$

where $K_c(\rho(t))$ is representing the feedback gain whose value has to be chosen carefully to ensure the closed loop stability of the system during the transient response while preserving the desired design requirements.

3.5.1 Controller design

As mentioned earlier there are two main objectives of the pursued LPV control law, the first is the robustness of the resulting closed loop system, and the other is the exact time response of the system. The first objective can be attained by analyzing the system stability during the existence of the controller using the following quadratic Lyapunov function

$$\mathbf{V}(\mathbf{x}) = \mathbf{x}^T \, P_c \, \mathbf{x}, \quad P_c = {P_c}^T > 0 \tag{3.48}$$

where P_c is a symmetric positive definite matrix such that the Lyapunov function given in (3.48) is guaranteed to be positive definite $\mathbf{V}(\mathbf{x}) > 0$. The Lyapunov function can be regarded as the system energy, thus the second condition of Lyapunov theory is satisfied when $\dot{\mathbf{V}}(\mathbf{x}) < 0$ which ensures the convergence of the system. So consider the derivative of the Lyapunov function obtained by differentiating equation (3.48) given by

$$\dot{\mathbf{V}}(\mathbf{x}) = \dot{\mathbf{x}}^T \, P_c \, \mathbf{x} + \mathbf{x}^T \, P_c \, \dot{\mathbf{x}} \tag{3.49}$$

Then by substituting the controller (3.47) into the system (3.46) and further using the resulting state dynamics

into (3.49) the derivative of the Lyapunov function becomes as follows

$$\dot{\mathbf{V}}(\mathbf{x}) = \mathbf{x}^T \left(\big(A(\rho(t)) - B(\rho(t))K_c(\rho(t))\big)^T P_c + P_c\big(A(\rho(t)) - B(\rho(t))K_c(\rho(t))\big) \right) \mathbf{x} \tag{3.50}$$

Since $\dot{\mathbf{V}}(\mathbf{x})$ is in quadratic form, the following LMI implies that $\dot{\mathbf{V}}(\mathbf{x})$ is negative definite

$$\big(A(\rho(t)) - B(\rho(t))K_c(\rho(t))\big)^T P_c + P_c\big(A(\rho(t)) - B(\rho(t))K_c(\rho(t))\big) + 2\zeta_c P_c < 0 \tag{3.51}$$

where ζ_c is a positive scalar representing the decay rate such that increasing its value shifts the closed loop system poles to the left half s-plane and makes the response faster. It is also important to mention that the inequality (3.51) is only sufficient but not necessary because if it is satisfied, the asymptotic stability of the system can be concluded, however, if it is not satisfied this doesn't prove that the system is unstable.

The second objective can be satisfied by solving the Bounded Real Lemma (BRL) (3.52) to ensure the closed loop system quadratic $\mathcal{H}_\infty$ performance as illustrated in [17].

$$\begin{pmatrix} \big(A(\rho(t)) - B(\rho(t))K_c(\rho(t))\big)^T P_c + P_c\big(A(\rho(t)) - B(\rho(t))K_c(\rho(t))\big) & P_c B(\rho(t)) & C(\rho(t))^T \\ B(\rho(t))^T P_c & -I & D(\rho(t))^T \\ C(\rho(t)) & D(\rho(t)) & -{\gamma_c}^2 I \end{pmatrix} < 0 \tag{3.52}$$

while γ_c is the system $\mathcal{H}_\infty$ norm bound, then the system can be said to have a quadratic $\mathcal{H}_\infty$ performance level γ_c if an only if there exists a unique positive definite matrix P_c satisfying the inequality (3.52) for all admissible values of the time varying parameters $\rho(t)$. The existence of such a matrix P_c implies that the Lyapunov function (3.48) guarantees asymptotic stability of the system while ensuring that the L_2 gain between the input and output is bounded by γ_c such that

$$||y(t)||_2 < \gamma_c ||u(t)||_2 \tag{3.53}$$

along all the possible trajectories of the parameters $\rho(t)$. To sum up, solving the two inequalities (3.51) and (3.52) simultaneously for a positive definite matrix P_c results in an optimal feedback gain $K_c(\rho(t))$ which ensures the quadratic $\mathcal{H}_\infty$ performance γ_c of the system besides the desired time constant ζ_c. There are two main challenges emerging while solving the two inequalities listed below

- First problem is that both inequalities (3.51) and (3.52) are not in a linear form as they contain terms including variables multiplication. This is tackled by a simple change of variables that converts the two inequalities into LMIs that can be solved using a semi-definite programming solver called 'SEDUMI' see [59]. A full derivation of the LMIs can be found in Appendix A, in addition, a full review of the Bilinear matrix inequalities (BMIs) and LMIs used in control applications can be found in [60].

- Second problem is related to the time varying nature of the resulting LMIs with respect to the varying parameters $\rho(t)$ which imposes an infinite number of LMIs to cover all possible trajectories of $\rho(t)$. A solution for such a problem is proposed by [17] based on the convexity of the polytopic LPV system representation and is summarized by the following theorem

Theorem 1

Based on the polytopic LPV model convexity property (2.57), if the inequalities (3.51) and (3.52) hold at the LPV model vertices $v_{rk},\ k = 1, \ldots, N$, then it is a sufficient condition to guarantee that they hold for all possible values of $\rho(t)$.

The results of theorem 1 affirm that the number of LMIs to be solved is reduced from infinity to be equal to the number of the LPV model vertices N. Thus, the gain matrix $K_c(\rho(t))$ can be calculated in the following the general polytopic form as in (2.58)

$$K_c(\rho(t)) = \sum_{k=1}^{N} \mu_k(\rho(t)) K_{ck} \tag{3.54}$$

where $\mu_k(\rho(t))$ is the weighting functions as illustrated in section 2.3.3 and K_{ck} are the gain matrices at the polytopic model vertices to be calculated to ensure asymptotic stability of the system (3.46). It is apparent that the controller design is identical to the gain scheduling where the controller gain matrix depends on the varying parameters vector $\rho(t)$ so it can be defined as a self-scheduled $\mathcal{H}_\infty$ control law as stated in [19].

Finally, to eliminate the steady state error and ensure precise reference tracking, the following term is added to the control law

$$u(t) = -K_c(\rho(t))\mathbf{x}(t) + V_c(\rho(t))\eta(t) \tag{3.55}$$

where $V_c(\rho(t))$ is representing the parameter varying inverse of the DC gain following the polytopic form presented by (2.58) while its values at the polytope vertices $V_{cj}, j = 1, \ldots, N$ are calculated as follows

$$V_{cj} = -\Big(C_k\big[A_k - B_k K_{cj})\big]^{-1} B_k\Big)^{\dagger}, \quad j, k = 1, \ldots, N \tag{3.56}$$

where $X^{\dagger}$ denotes the pseudo-inverse of the matrix X and $\eta(t)$ represents the reference input signal.

3.5.2 Simulation results

In order to reveal the effectiveness of the proposed controller, it is applied in simulation on the nominal quadrotor LPV model derived in the preceding chapter 2.3.5. As illustrated the LPV model consists of three subsystems one for attitude dynamics, another for altitude dynamics, while the third is describing the position dynamics and it is fed by the attitude angles in a cascaded form. For each subsystem, an LPV controller is designed according to the

methodology presented in 3.5.1 with the desired time response characteristics. Choosing the constants values is an iterative process according to the system model and desired response characteristics, in our case the following design parameters are used $\kappa = 2,\ \zeta_{at} = 6,\ \zeta_{al} = 1.5,\ \zeta_p = 0.5$ where κ is the altitude integral action constant while $\zeta_{at},\ \zeta_{al}$, and ζ_p are representing the attitude, altitude, and position decay rates, respectively, that have to be introduced in the solving the Lyapunov inequalities (3.51). By using Matlab Simulink with quadrotor parameters detailed in B, the LPV controller shows great performance in following the desired trajectory given by

$$x_r(t) = \begin{cases} 0 & t < 19\ s \\ 4(t-19)\ m & 19 \le t < 20\ s \\ 4\ m & 20 \le t < 40\ s \\ 4 - 4(t-40)\ m & 40 \le t < 41\ s \\ 0 & t \ge 41\ s \end{cases}, \quad y_r(t) = \begin{cases} 0 & t < 20\ s \\ 4(t-20)\ m & 20 \le t < 21\ s \\ 4\ m & 21 \le t < 41\ s \\ 4 - 4(t-41)\ m & 41 \le t < 42\ s \\ 0 & t \ge 42\ s \end{cases} \tag{3.57}$$

$$z_r(t) = \begin{cases} 0 & t < 5\ s \\ 0.4(t-5)\ m & 5 \le t < 10\ s \\ 2\ m & 10 \le t < 48\ s \\ 2 - 0.4(t-48)\ m & 48 \le t < 53\ s \\ 0 & t \ge 53\ s \end{cases}, \quad \psi_r(t) = \begin{cases} 0 & t < 19.5\ s \\ -40(t-19.5)^\circ & 19.5 \le t < 20\ s \\ -20 + 40(t-20)^\circ & 20 \le t < 20.5\ s \\ 0 & 20.5 \le t < 40.5\ s \\ -40(t-40.5)^\circ & 40.5 \le t < 41\ s \\ -20 + 40(t-41)^\circ & 41 \le t < 41.5\ s \\ 0 & t \ge 41.5\ s \end{cases} \tag{3.58}$$

where x_r, y_r, z_r, ψ_r are the reference values of the states which the system has to follow.

The quadrotor is able to execute the required task precisely despite the existence of sinusoidal disturbances and measurement noise affecting the system states. The disturbance vectors $d_1(t), d_2(t)$ affecting the attitude states given by equation (2.78) are sinusoidal waves with a magnitude 3 and frequency $0.5\ rad/s$ while the disturbance vectors $d_{p1}(t), d_{p2}(t)$ introduced in (2.98) affecting the position states are assumed to be sinusoidal also but having a magnitude of 2 and frequency $0.8\ rad/s$. Through the simulation, these disturbances start at $t = 20\ s$ representing the wind force that the quadrotor encounter during motion. Finally, the additive measurement noise $n_s(t) \in [-0.03, 0.03]$ and $n_v(t) \in [-.06, .06]$ represent states and their derivatives noise having a sample time of $0.1, 0.08\ s$, respectively.

The results demonstrated by figures 3.21b and 3.21a show how effectively the system states are able to follow the desired values despite the existence of the measurement noise. One of the main advantages of the LPV controller is that it counts for the effect of the heading angle on the position states which is completely ignored in linear models. The controller enables the system to perform a rotational movement around $z-axis$ while preserving its motion in x and y directions as seen from figure 3.22b. For a linear system, each of these movements had to be

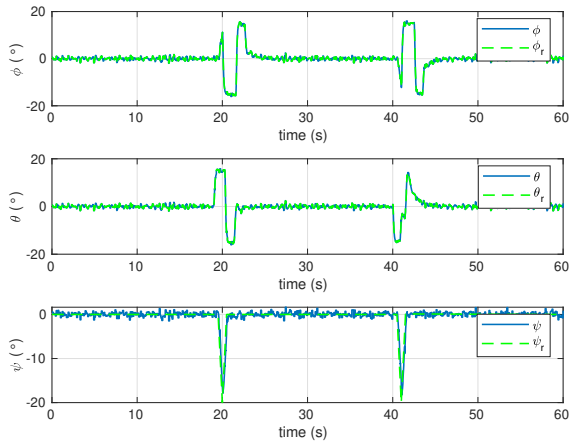

(a) attitude states

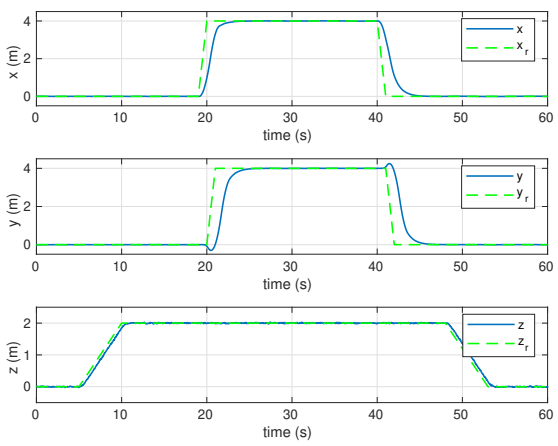

(b) position states

Figure 3.21: Time response of the system states using LPV controller

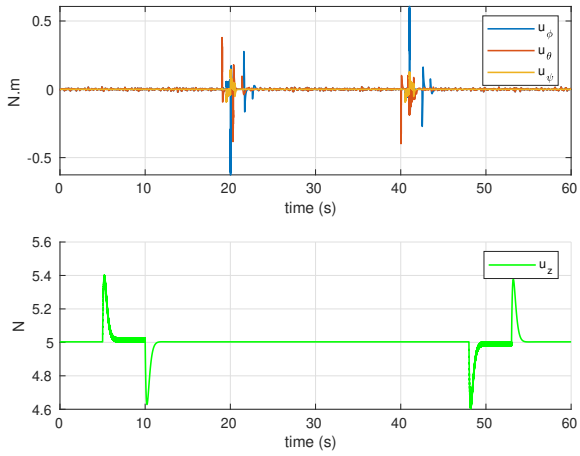

(a) control inputs

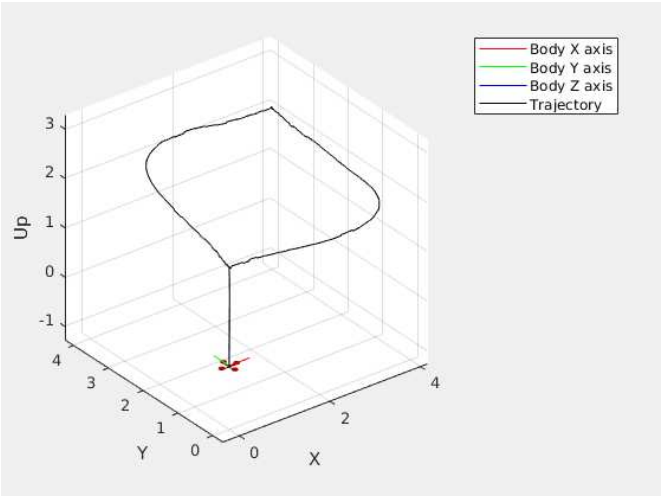

(b) trajectory tracking

Figure 3.22: Trajectory tracking using LPV controller and the required control action

done separately in a successive way that limits the implementation of the desired trajectory which can be real-time varying according to the environmental obstacles.

In addition, the LPV control law is proven to be cost-efficient as it produces an acceptable control action which the quadrotors actuators can supply throughout the motion. As depicted from figure 3.22a, the control action in the direction of altitude u_z has a nominal value around $5\ N$ to counteract the gravity effect and it changes its value within a bound of $0.4\ N$ to reach the required altitude. While the other control inputs u_ϕ, u_θ, u_ψ responsible for the rotations are kept zero throughout the simulation except for the instants when a directional motion is desired their values change within a limit of $0.5\ N.m$ which can be attained by varying the speeds of the opposite rotors.

Finally, the robustness of the LPV control law is revealed through comparing its performance with that designed using LQR control technique. The procedure given in section 3.4.1 based on solving the Riccati equation for as-

signing the controller gain matrix is applied to the quadrotor LPV model 2.3.5 where the controller gain is calculated at each vertex then the LPV controller gain is calculated from equation 3.54. By applying both control laws on the quadrotor model to follow the same reference trajectory indicated in equations (3.57) and (3.58), the results shown in figure 3.23 are obtained. Despite the slight difference between the system states resulting from the robust LPV and the LQR controllers shown in figure 3.23a, the 3D trajectory tracking response displayed in figure 3.23b prove that the LPV controller is able to reject the exogenous disturbance effect more efficiently in a way that ensures a more accurate trajectory following.

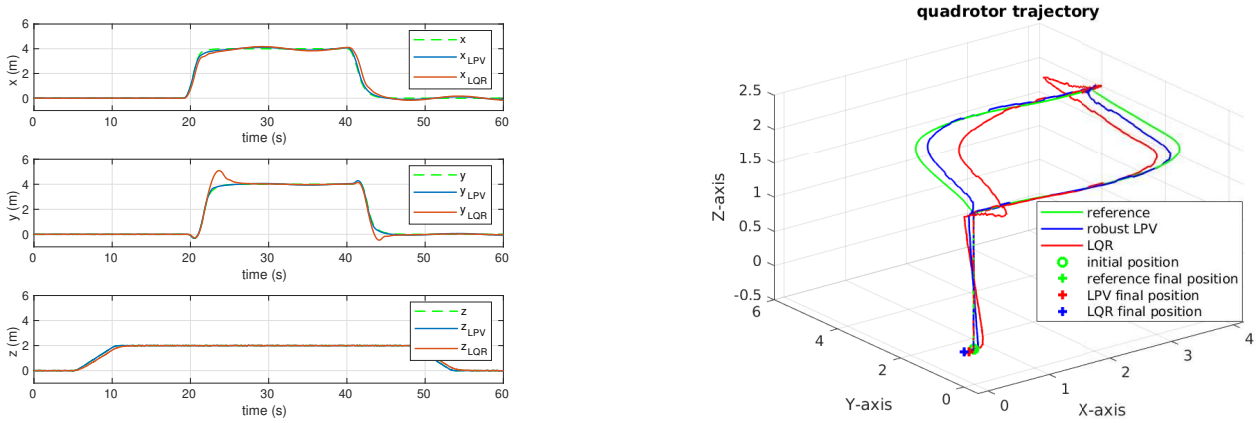

(a) position states

(b) trajectory tracking

Figure 3.23: Robust LPV vs LQR controllers

The same results can be depicted from figure 3.24 which includes a comparison between both controllers performance through following a reference cartesian polynomial trajectory illustrated in C. In addition to the trajectory following accuracy, it can be seen that the LPV controller guarantees a precise final position of the drone despite the existence of strong exogenous wind disturbances.

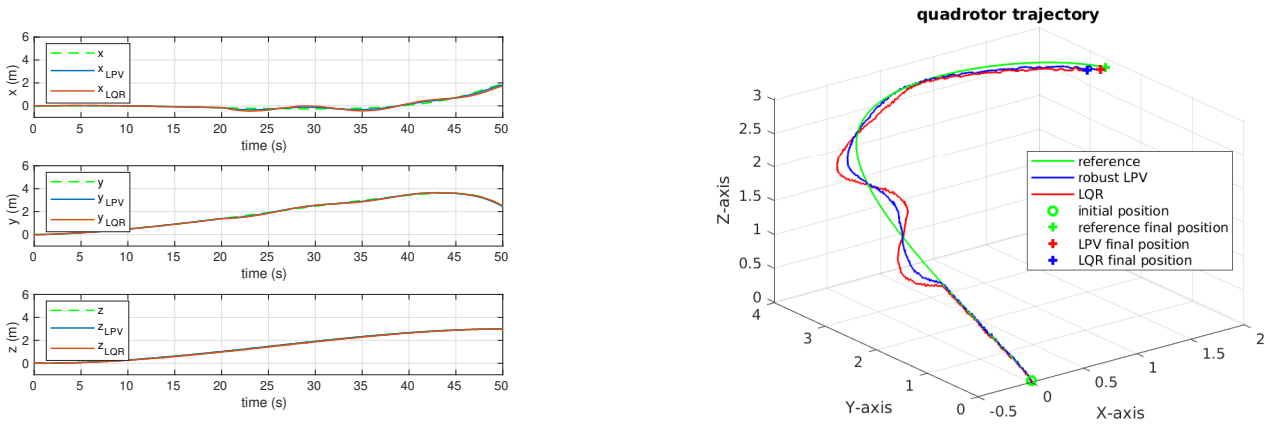

(a) position states

(b) trajectory tracking

Figure 3.24: Robust LPV vs LQR controllers

3.6 Conclusions

In this chapter, the problem of quadrotor control is addressed and investigated in multiple ways depending on the system models derived through the preceding chapter. Despite the simplicity of such a drone configuration, the controller design is a crucial task that enables stabilizing the system and prepare it to perform the desired autonomous missions such as surveillance and path following. The compromise between simplicity and accuracy leads us to describe the nonlinear model dynamics by transfer functions once, then by an LTI model, and finally, by an LPV model, each of them is suitable for some specific tasks. Thus, it is reasonable to design an adaptable control law for each model which is compatible with the model nature and the available drone microcontroller for real-time implementation.

At first, a PID control law is proposed for the linear model described by single-input single-output SISO transfer functions where the controller gains are tuned using the root locus method to satisfy the required time response characteristics. Although the designed PID controller could efficiently make the system follow the desired trajectory, it didn't ensure an admissible level of robustness and the closed loop system has experienced a great influence of exogenous disturbances.

That's why another technique for controller design based on $\mathcal{H}_\infty$ loop shaping is adopted that is able to meet the time response requirements besides securing an acceptable robustness degree. Two methods are proposed for choosing the controller transfer function, the first depends on shaping the open loop transfer functions of the system, while the other aims at shaping the closed loop sensitivity and complementary sensitivity functions directly. The two methods demonstrate a great performance in disturbance rejection and noise attenuation while preserving the time response criteria as depicted from their frequency response and further simulations using Matlab Simulink.

For the state space affine LTI model, an LQG control scheme is developed consisting of an LQE as a state observer in addition to the LQR feedback controller. After tuning the observer and controller weighting matrices using an initial guess based on Bryson's rule, an LMI is introduced to the controller gain calculation instead of the Riccati equation to enhance the system robustness by ensuring a quadratic $\mathcal{H}_\infty$ performance level of the system against the undesired inputs. While the observer gain is computed using ARE to attain an optimal value and provide the controller with smooth states readings free from the measurement noise.

The last control law proposed is a self-scheduled LPV controller for each subsystem of the quasi-LPV model of the quadrotor. It is shown that the convexity feature of the quadrotor quasi-LPV model could facilitate the controller synthesis and limit the number of LMIs to be satisfied during the calculation of the controller gain. By introducing the controller design parameters, the optimal time varying feedback control gain is derived through solving the Lyapunov inequality besides the BRL to ensure a quadratic $\mathcal{H}_\infty$ performance in addition to the adequate time response of the closed loop system. Such performance is tested in simulation which proves the capabilities of the LPV controller in suppressing the exogenous disturbance effect while following the required path.

Also, the controller is able to provide smoother trajectories thanks to the heading angle dynamics embedded in the positioning subsystem which prepare the whole system for a dynamic real-time trajectory in applications like tracking a moving object. Such a feature has facilitated the implementation of the proposed technique for path planning based on parametric curves in which the position states are varying freely without a restriction on the directional movement order. Nevertheless, the LPV controller exhibits a high level of disturbance rejection which makes it a perfect choice for applications including navigation within unknown environment conditions where the drone has to avoid the encountered obstacles.

Chapter 4

Fault Detection and Diagnosis

Chapter abstract

In order to provide the quadrotor with an efficient active FTC scheme, a fault detection and diagnosis (FDD) unit is proposed to identify the fault based on some residual signals generated by a model-based observer. According to the observer design, it may give just fault detection or fault isolation with the aid of a bank of observers. In addition, the observer structure can empower the system to perform fault detection, estimation, and identification simultaneously. Thus, three types of observer design are investigated, namely Lunberger observer which considers a deterministic system model, Kalman filter dedicated to stochastic systems affected by model uncertainties and measurement noise, and robust observer based on $\mathcal{H}_-/\mathcal{H}_\infty$ notion for maximizing fault impact and minimizing other signals effect on the residual signals. Since the latter two approaches provide better robust results, a comparison between their performance is conducted by applying them to a quadrotor LTI model affected by actuator faults and subjected to measurement noise and exogenous disturbances.

Afterward, a new approach alternative to the $\mathcal{H}_-/\mathcal{H}_\infty$ technique is proposed aiming to decouple exogenous signals from the system fault. This approach is developed for actuators fault estimation and is extended to identify sensors faults through adding an integral action to the system output. It is illustrated that under some structural conditions, the faults can be estimated exactly while the perturbations are completely decoupled from the residual signals. However, if exact convergence is not ensured, some relaxed conditions are provided to maintain asymptotic fault estimation. Finally, the worst-case where the perturbations cannot be decoupled is presented and handled using a generalized $\mathcal{H}_-/\mathcal{H}_\infty$ approach which is further enhanced utilizing the auxiliary output. A general design procedure is provided which unifies the presented different cases according to the system output relative degree, then applied in simulation to a quadrotor LPV model to illustrate the effectiveness of the proposed approach in identifying precisely the sensors and actuators faults.

4.1 Introduction

Concerning the solution of fault diagnosis problem, several methods have been introduced some of them are signal-based analysis in time or frequency domains while others are model-based using the concept of observer design for state estimation. The idea of model-based residual generation is to check the conformity between the actual output of the system and the expected output of its trusted model, thus identifying a system defect in case of different outputs. Model-based observer design for fault diagnosis is an extremely large research area including numerous efficient approaches like fuzzy techniques, sliding mode observers and adaptive observers, etc. The particular case of quadrotor has a huge share of this research work for example the sliding mode observer technique is used in [61] for actuators faults and in [62] for sensors faults. However, in this study, only the observer design based on $\mathcal{H}_\infty$ strategies and the relevant approaches will be addressed aiming to propose an efficient solution for quadrotor actuators and sensors fault identification.

Luenberger observer presented in [63] is a deterministic approach that has been employed in a wide range of applications one of them is fault diagnosis. Taking into account the existence of model mismatch in real practice, the work in [64] proposes an observer analyzed in the frequency domain to ensure robustness against disturbances and model uncertainty. To avoid linearization errors an adaptive approach is introduced in [65] for fault diagnosis of a class of non-linear systems. However, a generalized non-linear Takagi-Sugeno (TS) representation is given in [66] combining a system of linear observers to comply with real-time application constraints. Luenberger type observer is also used for fault detection in [20] dedicated to multirotor UAVs with a bank of observers for fault isolation and in [67] for a quadrotor beside an augmented variable observer for fault estimation.

Kalman filter can be used in the observation context for fault diagnosis as a stochastic model-based residual generator assuming Gaussian probability density functions for both measurement noise and model uncertainty. Such observers had evolved and benefited from the unknown-input decoupling technique in generating multiple subsystems and their corresponding filters for fault isolation see [68]. While in [69] a bank of Kalman filters is used in a dedicated observer scheme (observer sensitive to specific fault) to identify faults of aircraft gas turbine engines modeled in a linear form. A two stage Kalman filter is used for simultaneous actuator fault detection and estimation in [21] offering an extra step of measurement correction to identify precisely the size and type of fault and further extended in [40] to include sensor faults. Other types of Kalman filters are used for fault detection of nonlinear systems such as dual unscented Kalman filter (DUKF) [70] and adaptive Kalman filter [71].

Eigenstructure assignment by introducing a weighting matrix for the residual signal, the observer eigenvectors can be assigned in such a way that it decouples the state estimation error from disturbances see [72], thus the observer is able to perform state estimation besides fault diagnosis. However, as the problem is seeking reliable residuals indicating fault occurrence, a solution is provided in [73] focusing on decoupling the disturbances from the resulting residual signal rather than the state estimation.

Unknown Input Observer (UIO) is an observer that results in a state estimation error approaching zero asymptotically regardless of the presence of the unknown input (disturbance) in the system as mentioned in [74]. It is another Luenberger type observer aiming at decoupling the estimated states from the exogenous disturbances, such decoupling is ensured by introducing some parametric expressions for system and observer matrices as in [75]. The concept of UIO has expanded to deal with non-linear systems satisfying some Lipschitz constraints in [76] with a bank of nonlinear UIOs for fault isolation. By investigating the output relative degree some algebraic conditions can be satisfied resulting in an enhanced UIO performance not only in state estimation decoupling from unknown disturbance but also in estimating the exogenous disturbance itself. Such work is presented in [77] with a general application for systems modeled in the LPV framework. By relaxing the state estimation decoupling inequality constraints a new UIO is introduced in [78] that is compatible with a larger class of systems having LPV outputs not necessarily Linear Time-Invariant (LTI). The UIO structure is utilized in [79] for quadrotor sensor fault detection and is further combined with the eigenstructure assignment approach in [80] to solve the quadrotor actuators fault detection problem.

$\mathcal{H}_-/\mathcal{H}_\infty$ *technique* is one of the most useful $\mathcal{H}_\infty$ norm-based strategies for fault detection and diagnosis which allows maximizing the fault effect and minimizing the effect of the disturbance on the residual signal simultaneously, a comparison between such an observer and a stochastic continuous-time Kalman filter can be found in [81]. The signal to be minimized includes model uncertainty, exogenous disturbance, and measurement noise see [82] where the $\mathcal{H}_\infty$ norm is formulated into a Linear Matrix Inequality (LMI) form while the $\mathcal{H}_-$ norm feasibility is ensured through satisfying a quadratic constraint. In [83] a solution is presented in the frequency domain to ensure the ratio between the $\mathcal{H}_-$ and $\mathcal{H}_\infty$ norms is larger than one hence the observer is more sensitive to faults. The solution is achieved by iterating the values of the weighting matrix (introduced in the observer scheme) and the performance index to reach its optimal value.

Later on, the idea of constructing a separate model for estimating the fault effect on an uncertain LTI system had been proposed in [84]. Such a concept uses two observers, one for plant state estimation, while the other for fault estimation. The observer design problem is presented in an LMI optimization form to guarantee acceptable performance values for $\mathcal{H}_\infty$ norms of faults and disturbances effect on the residual signal. The worst-case fault sensitivity $\mathcal{H}_-$ index is formulated as ARE (Algebraic Riccati Equation) and an LMI dual to the well-known Bounded Real Lemma (BRL) for the whole frequency spectrum in [85]. Furthermore, a weighting matrix is introduced to guarantee a feasible solution for a strictly proper system infinite frequency range, such work was developed [22] to include exogenous disturbances and deployed in [86] for uncertain LTI systems.

An observer scheme is proposed in [87] which is able to cancel the system dynamics such that the residual signal is only affected by disturbances and faults, moreover, the observer gain matrices are chosen according to the number of faults in a way that achieves fault isolation. A post-bandpass weighting filter is introduced in [88] to overcome the problem of modeling fault effect on the output such that the minimum fault sensitivity level is larger

than the maximum disturbance $\mathcal{H}_\infty$ norm over a finite frequency domain. The min/max problem is presented in [89] as a ratio between the two norms by multiplying the $\mathcal{H}_\infty$ norm of disturbances by the inverse of $\mathcal{H}_-$ norm of faults and minimizing this resulting norms ratio.

The $\mathcal{H}_-/\mathcal{H}_\infty$ technique has been later used for fault detection of wind turbines in [90] and further developed for LPV systems in [91]. A method has been proposed in [92] for discrete-time Takagi-Sugeno fuzzy systems considering sensor faults as auxiliary state variables and applying the min/max problem for the augmented system, then it was further developed to include model uncertainty in [93]. In [94], the difference between the two norms introduced as a linear optimization criterion for solving the $\mathcal{H}_-/\mathcal{H}_\infty$ problem with the application of the developed algorithm to a car lateral dynamics control. In addition, a solution is provided for sensor fault detection of descriptor LPV systems in [95] by introducing unmeasurable scheduling functions and in [96] over a finite frequency domain.

Nevertheless, the min/max problem could be further reformulated in [23] to a simple minimization problem, for linear systems, by introducing a reference model to shape the residual signal. This approach is extended for Takagi-Sugeno systems [24] introducing a perturbation term in the outputs in order to satisfy the regularity assumption [25] needed for the minimization of the $\mathcal{H}_\infty$ gain. In addition, one can find a two-stage observer for state and fault estimation in [97] with the application to discrete-time descriptor switched systems. A deep study has been provided in [26] by exploiting the relative degree notion [28] giving a way to avoid the added virtual perturbation and the difficulty of fault effect modeling.

Fortunately, intensive research and several algorithms have been proposed through the last decade, which allows estimating robustly the time derivatives of a noisy signal. One can cite the algebraic differentiators [27] and high-gain differentiators [98] which provide non-asymptotic time derivatives estimation without any knowledge of statistical properties of the noise affecting the signal to be differentiated. Thanks to these tools, the $\mathcal{H}_-/\mathcal{H}_\infty$ observer performance has been highly enhanced based on the differentiated output signal see [99]. Recently, there exists the algorithm presented in our work [100] which is benefiting from the previously cited techniques particularly $\mathcal{H}_-/\mathcal{H}_\infty$ and UIO and uses the auxiliary system output to provide a generalized approach for a robust residual generation in case of actuator faults.

To give an overview of the aspects covered in this chapter, we begin with an investigation for different model-based observer design methodologies dedicated to solving the problem of fault detection and diagnosis by generating trustful residual signals. A Lunberger type observer is introduced for handling actuator faults detection accompanied by a bank of similar observers for fault identification and isolation. Afterward, the previously discussed LQE observer 3.4.2 is presented as an optimal continuous-time Kalman filter dedicated to the stochastic piecewise affine system affected by model uncertainties and measurement noise. Later on, an observer is designed for fault detection based on $\mathcal{H}_-/\mathcal{H}_\infty$ such that it minimizes the exogenous disturbance effect and maximizes the fault effect on the residual signal. Since the latter two techniques are suitable to uncertain systems affected by noise and disturbance, they provide a wider range of applicability in real-time. So, a comparison between the residual

signals obtained by each method is conducted by simulating their response through different quadrotor actuators fault scenarios using Matlab-Simulink in the presence of exogenous disturbances and measurement noise.

The conclusions of the preceding work urged investigating further enhancements for the $\mathcal{H}_-/\mathcal{H}_\infty$ technique in actuator fault diagnosis. Thus, a generalized approach for such a problem is introduced based on the differentiated system output where it is shown with a simple analysis, that the $\mathcal{H}_-/\mathcal{H}_\infty$ presents the worst-case scenario for fault estimation and some structural conditions, if satisfied, allow to enhance the solutions proposed. By introducing a virtual residual vector, two notions, namely, exact and asymptotic residual convergence, are defined and further analyzed resulting in some imperative algebraic conditions to be satisfied. The existence of such a virtual residual empowers the residual generator to perform fault detection, estimation, and isolation simultaneously which is a valuable feature.

Later on, the $\mathcal{H}_-/\mathcal{H}_\infty$ technique is discussed with some improvements thanks to the auxiliary output which satisfied the regularity condition that is essential for ensuring the observer design feasibility. For each case, the corresponding design methodology is given followed by simulation for academic examples considering LTI and LPV system representation to prove the generality and applicability of the developed algorithm. Then, the effectiveness of the proposed approach is demonstrated by simulation on the quadrotor LPV model affected by actuator faults with comparison to the classical $\mathcal{H}_-/\mathcal{H}_\infty$ concept.

This technique is further used for sensor fault diagnosis in presence of exogenous disturbances and measurement noise by adding an integral action for the system output as in [101]. The system model has first to satisfy a proposed ranking condition that ensures the observability of the constructed augmented system including the integral action. In that manner, the sensors faults are remodeled in the resulting augmented system to be affecting the system states directly thus the auxiliary output will contain the effect of the sensors faults besides the exogenous disturbance as illustrated in [102]. The proposed methodology is tested for LTI and LPV examples and applied for the quadrotor LPV model in simulation to reveal its effectiveness in estimating sensors faults.

4.2 Fault detection

This part is dedicated to system fault detection based on checking the conformity between the observer estimated output and the actual system output as illustrated in figure 4.1. The idea is to introduce a residual signal representing the difference between the observed states and the system output denoted $r(t)$ such that its value vanishes asymptotically in the fault-free case and deviates from zero in case of fault occurrence see [20]. That's why the model-based observer used for fault detection can be referred to as a residual generator and the observer design methodology affects directly the accuracy of the residuals. According to the system model and the nature of the operating environment, an observer can be established in a way to produce trustful residual signals indicating the system malfunction precisely.

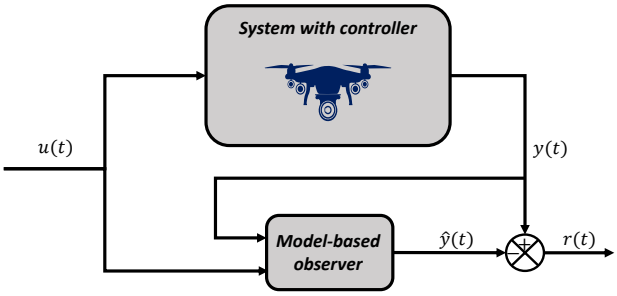

Figure 4.1: Fault detection scheme

4.2.1 Deterministic approach (Lunberger observer)

The methodology offered here for designing the residual generator is similar to the Luenberger observer scheme addressed for handling a deterministic system model fault detection problem utilized in [20]. So consider the affine LTI model of the quadrotor affected by actuator faults is given by

$$\begin{aligned} \dot{\mathbf{x}}(t) &= A\mathbf{x}(t) + B\mathbf{u}(t) + E_f f(t) \\ y(t) &= C\mathbf{x}(t) \end{aligned} \tag{4.1}$$

where $\mathbf{x}(t) \in \mathbb{R}^n$, $y(t) \in \mathbb{R}^{n_y}$, $\mathbf{u}(t) \in \mathbb{R}^{n_u}$, and, $f(t) \in \mathbb{R}^{n_f}$ represent the state vector, output vector, control input vector, and fault vector, respectively, having the dimensions illustrated in 2.3.2. The effect of the disturbance is eliminated as the proposed Luenberger observer is designed for a deterministic system model. It is important to mention that as the residual generator is dedicated for actuator faults so the output matrix is as follows

$$C = \begin{bmatrix} I_{4\times 4} & 0_{4\times 8} \end{bmatrix} \tag{4.2}$$

In that way, the observed states are attitude angles ϕ, θ, ψ and the altitude measurement z. After checking the observability of the pair (A, C), the system (4.1) is found to be observable as explained previously in 3.4.2. So an observer can be proposed as a residual generator taking the following form

$$\begin{cases} \dot{\hat{\mathbf{x}}}(t) = A\hat{\mathbf{x}}(t) + B\mathbf{u}(t) + L(y(t) - \hat{y}(t)) \\ \hat{y}(t) = C\hat{\mathbf{x}}(t) \\ r(t) = y(t) - \hat{y}(t) \end{cases} \tag{4.3}$$

where L is the observer gain matrix which represents a weighting matrix to the correction term $L(y(t) - \hat{y}(t))$ responsible for driving the observer state $\hat{\mathbf{x}}(t)$ to match the system state $\mathbf{x}(t)$. Since the attitude and altitude are the observed system states, the observer scheme 4.3 allows to obtain four residual signals namely, $r_\phi, r_\theta, r_\psi, r_z$ corresponding to the estimated directions which are mainly affected by the actuators faults.

Consider the error signal of the observer is denoted $e(t)$, where $e(t) = \mathbf{x}(t) - \hat{\mathbf{x}}(t)$, then the error dynamics $\dot{e}(t)$ can be described by

$$\dot{e}(t) = \dot{\mathbf{x}}(t) - \dot{\hat{\mathbf{x}}}(t) \tag{4.4}$$

By substituting the system dynamics (4.1) and the observer dynamics (4.3) into equation (4.4), hence the error dynamics $\dot{e}(t)$ can be given by

$$\dot{e}(t) = (A - L\,C)e(t) + E_f f(t) \tag{4.5}$$

Thus, the observer gain L has to be chosen such that the matrix $(A - L\,C)$ is stable and consequently the error converges to zero asymptotically $e(t) = 0$ in fault-free case $f(t) = 0$. The value of the matrix L can be assigned by solving the following characteristic equation for the desired observer response time.

$$|sI - A + LC| = 0 \tag{4.6}$$

The observer response becomes faster when the eigenvalues of the matrix $(A - L\,C)$ are shifted more to the left-hand side of $s-$plane. Then, in case of actuator fault the error signal $e(t)$ deviates from zero and similarly the residual signal vary from zero to some value indicating fault occurrence since $r(t) = C\,e(t)$. The results of using such an observer for actuators fault detection are illustrated by simulation in 4.2.5.

4.2.2 Stochastic approach (continuous-time Kalman filter)

The work presented in this section aims at using the continuous-time Kalman filter introduced before as an optimal estimator in the preceding chapter 3.4.2 as a residual generator for fault detection. Such a methodology has been deployed in [21] for actuator fault detection of discrete-time systems, while in this work it is dedicated to the piecewise affine LTI model of the quadrotor. As mentioned before, the Kalman filter concerns stochastic systems affected by model uncertainty and measurement noise which are introduced as known Gaussian probability density functions. Let the quadrotor affine LTI model including the actuators fault effect is described in state space form as following:

$$\begin{cases} \dot{\mathbf{x}}(t) = A\mathbf{x}(t) + B\mathbf{u}(t) + E_f f(t) + \mathbf{v}(t) \\ y(t) = C\mathbf{x}(t) + \mathbf{w}(t) \end{cases} \tag{4.7}$$

As illustrated in section 3.4.2, the pair (A, C) is found to be observable so the previously proposed scheme for the residual generator in 4.2.1 can be reused. But this time the observer gain matrix L is calculated through solving the following Riccati equation for a positive definite matrix Λ

$$A\,\Lambda + \Lambda\,A^T - \Lambda\,C^T\,W^{-1}\,C\,\Lambda + V = 0 \tag{4.8}$$

to minimize the error covariance matrix $\Lambda = \mathbb{E}\left[(\mathbf{x}(t) - \hat{\mathbf{x}}(t))\ (\mathbf{x}(t) - \hat{\mathbf{x}}(t))^T\right]$ in fault-free case $f(t) = 0$, then the observer gain can be calculated from

$$L = \Lambda\ C^T\ W^{-1} \tag{4.9}$$

As illustrated in 3.4.2, such that the obtained residual generator is able to attenuate the measurement noise and model uncertainty effects on the residual signals while stabilizing the error dynamics in an optimal way.

4.2.3 Robust $\mathcal{H}_-/\mathcal{H}_\infty$ observer

The work introduced here follows [94] for the observer design methodology with application to a quadrotor helicopter. The main purpose of such an observer is to minimize the effect of all perturbing signals including exogenous disturbances, model uncertainty, and measurement noise while maximizing fault effect to ensure adequate fault detection. The $\mathcal{H}_-$ index can be defined as the worst fault sensitivity level, this norm has been further developed and formulated as an ARE (Algebraic Riccati Equation) and an LMI (Linear Matrix Inequality) dual to BRL (Bounded Real Lemma) in [85] and extended to include the whole bandwidth of frequency. Nevertheless, the $\mathcal{H}_\infty$ norm can be thought of as the peak influence (maximum amplification) of the exogenous signals on the residual signal. Thus the observer design aims at maintaining the $\mathcal{H}_-$ norm above a certain level β which is larger than the highest value of the $\mathcal{H}_\infty$ norm defined by the constant γ. Consider the following quadrotor affine model representation with introducing the effect of system faults and disturbances.

$$\begin{cases} \dot{\mathbf{x}}(t) = A\mathbf{x}(t) + B\mathbf{u}(t) + E_d d(t) + E_f f(t) \\ y(t) = C\mathbf{x}(t) + D\mathbf{u}(t) + F_d d(t) + F_f f(t) \end{cases} \tag{4.10}$$

where E_d , E_f , F_d , F_f are constant matrices modeling the fault and disturbance effect on the system and measurement, respectively, while $d(t)$, $f(t)$ are the disturbance and fault vectors. Since the pair (A, C) is observable, then by using the residual generator scheme given by (4.3) and defining state error $e(t) = \mathbf{x}(t) - \hat{\mathbf{x}}(t)$ then the error dynamics $\dot{e}(t) = \dot{\mathbf{x}}(t) - \dot{\hat{\mathbf{x}}}(t)$ will be as follows

$$\begin{cases} \dot{e}(t) = A^* e(t) + {E_d}^* d(t) + {E_f}^* f(t) \\ r(t) = Ce(t) + F_d d(t) + F_f f(t) \end{cases} \tag{4.11}$$

Where $A^* = A - LC$, ${E_d}^* = E_d - LF_d$, ${E_f}^* = E_f - LF_f$. The resulting sensitivity functions of fault and disturbances to the residual

$$\begin{cases} T_{rf}(s) = C(sI - A^*)^{-1}{E_f}^* + F_f \\ T_{rd}(s) = C(sI - A^*)^{-1}{E_d}^* + F_d \end{cases} \tag{4.12}$$

The objective of the $\mathcal{H}_-/\mathcal{H}_\infty$ fault detection observer is achieved under the following conditions

$$\begin{cases} ||T_{rd}||_\infty \leq \gamma \\ ||T_{rf}||_- \geq \beta \end{cases} \tag{4.13}$$

The problem is to find the matrix L such that the observer is stable while maximizing β and minimizing γ (β and γ are positive scalars), this is achieved through the following procedure.

Problem formulation

- 1^{st} objective, stability of the observer

  From Lyaponouv stability criteria for a square matrix A if there exist a symmetric positive definite matrix $P > 0$ and a positive scalar $\zeta_o > 0$ such that

  $$A^T P + PA + 2\zeta_o P < 0 \tag{4.14}$$

  Then all the eigenvalues of A will be less than $-\zeta_o$, applying in our case where $A^* = A - LC$ with introducing the variable $U = -PL$ to transform this matrix inequality into an LMI results in the following

  $$A^T P + PA + UC + C^T U^T + 2\zeta_o P < 0 \tag{4.15}$$

- 2^{nd} objective, disturbance rejection

  According to [94], the first inequality of equation (4.13) can be rewritten in the following form

  $$\left[\begin{array}{c|c} A^{*T}P + PA^* + C^T C & PE_d{}^* + C^T F_d \\ \hline E_d{}^{*T}P + F_d{}^T C & F_d{}^T F_d - \gamma^2 I \end{array}\right] \leq 0 \tag{4.16}$$

  by introducing the values $A^*, E_d{}^*$ and U as given before in the inequality (4.16) the following LMI is obtained.

  $$\left[\begin{array}{c|c} A^T P + PA + C^T C + C^T U^T + UC & PE_d + UF_d + C^T F_d \\ \hline E_d{}^T P + F_d{}^T U^T + F_d{}^T C & F_d{}^T F_d - \gamma^2 I \end{array}\right] \leq 0 \tag{4.17}$$

- 3^{rd} objective, maximizing the fault effect

  Similarly, the second inequality of equation (4.13) can be represented by

  $$\left[\begin{array}{c|c} A^{*T}P + PA^* - C^T C & PE_f{}^* - C^T F_f \\ \hline E_f{}^{*T}P - F_f{}^T C & \beta^2 I - F_f{}^T F_f \end{array}\right] \leq 0 \tag{4.18}$$

and by substituting the values $A^*, {E_f}^*$ and U, we obtain the following LMI.

$$\left[\begin{array}{c|c} A^TP + PA - C^TC + C^TU^T + UC & PE_f + UF_f - C^TF_f \\ \hline {E_f}^TP + {F_f}^TU^T - {F_f}^TC & \beta^2 I - {F_f}^TF_f \end{array}\right] \leq 0 \tag{4.19}$$

Problem solution

Mathematically the set of LMIs described before by (4.15),(4.17), and (4.19) is solved using SeDuMi solver with optimization criterion to maximize $(\beta^2 - \gamma^2)$ under the mentioned LMI constraints to find the values of P and U. Then the observer gain matrix is calculated from $L = -P^{-1}U$, the resulting observer should give:

1. correct time response for fault detection
2. robustness against perturbations
3. sensitivity towards faults

Unfortunately, in the case of strictly proper systems in which there is no effect of the fault on the outputs, hence, F_f is equal to zero, there is no feasible solution for the third LMI as we can see from element $(2,2)$ in (4.19) the condition is $\beta^2 I - {F_f}^TF_f \leq 0$, thus this inequality can't be solved [85]. Therefore the robust $\mathcal{H}_-/\mathcal{H}_\infty$ can theoretically be designed for systems with faults on measurements (sensors faults) but obviously, the fault in actuators has its impact on the measured outputs so we assume here constant values for the elements of the matrix F_f but a solution for this problem will be presented in the next section based on the relative degree of the system output.

4.2.4 Fault isolation

After studying the design of model-based observers such that they can be used for system fault detection, it is evident that they are able to indicate the fault occurrence and its time. Although by a simple analysis of the resulting residual signals, they can lead to an initial guess of the fault location, however, it is not practical to depend on these results and their implications. Therefore, another technique can be adopted for fault isolation that is based on augmenting the system with a bank of σ observers, σ: number of actuators, illustrated by figure 4.2 such that each observer contains the faulty model of the corresponding faulty actuator see [20]. In that manner, during the faulty situation, at least one of the isolation observers is consistent with the behavior of the corresponding faulty plant such that this observer has all the residuals signals approaching zero.

Consider again the LTI model affected by actuators faults given by

$$\begin{aligned} \dot{\mathbf{x}}(t) &= A\mathbf{x}(t) + B\mathbf{u}(t) + E_f f(t) \\ y(t) &= C\mathbf{x}(t) \end{aligned} \tag{4.20}$$

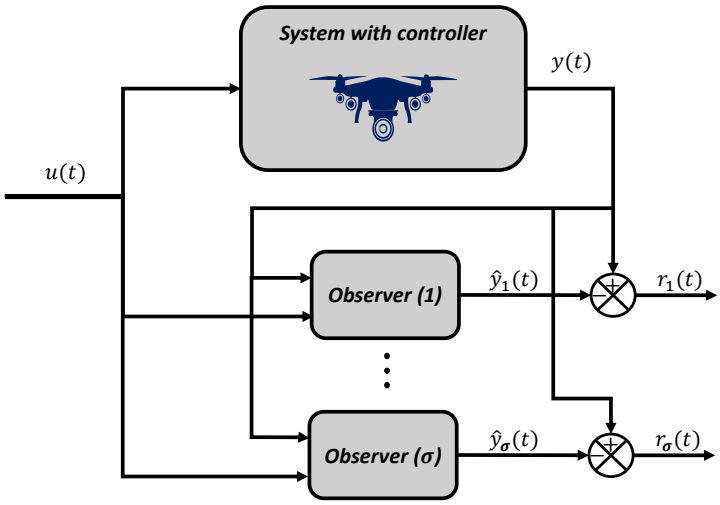

Figure 4.2: Fault isolation scheme

In that way, this state space LTI model is representing the quadrotor affine LTI model detailed in 2.3.2 while the output matrix C is given by equation (4.2). As previously mentioned, each one of the isolation observers(i), $i \in \{1, \ldots, \sigma\}$ shown in figure 4.2 includes the system model subjected to a fault in the corresponding actuator(i) so the observer takes the following form

$$\begin{cases} \dot{\hat{\mathbf{x}}}_i(t) = A\hat{\mathbf{x}}_i(t) + B\mathbf{u}(t) + E_f f_i(t) + L(y(t) - \hat{y}_i(t)) \\ \hat{y}_i(t) = C\hat{\mathbf{x}}_i(t) \\ r_i(t) = y(t) - \hat{y}_i(t) \end{cases} \tag{4.21}$$

where the fault vectors $f_i(t), i \in \{1, \ldots, \sigma\}$ consists of number of elements $j, j \in \{1, \ldots, \sigma\}$ given by

$$f_i(j) = \begin{cases} f_{ai} & i = j \\ 0 & i \neq j \end{cases} \tag{4.22}$$

where f_a is the actuator's(i) magnitude of fault which is assumed to be formerly known. Consider now the error signal of the i^{th} observer is denoted $e_i(t) = \mathbf{x}(t) - \hat{\mathbf{x}}_i(t)$, then the error dynamics $\dot{e}_i(t)$ can be described by

$$\dot{e}_i(t) = \dot{\mathbf{x}}(t) - \dot{\hat{\mathbf{x}}}_i(t) \tag{4.23}$$

by substituting equations (4.21) and (4.20) into (4.23) we obtain the error dynamics as follows

$$\dot{e}_i(t) = (A - L\,C)e_i(t) + E_f(f(t) - f_i(t)) \tag{4.24}$$

The observer gain matrix L can be chosen to stabilize the error dynamics according to the observer type following one of the presented methods 4.2.1, 4.2.2, or 4.2.3. Then, the residual signal $r_i(t) = Ce_i(t)$ has a value far from zero while the system is not experiencing any fault $(f(t) = 0)$, however, it approaches zero asymptotically when the system is subjected to an actuator fault $f(t) = f_i(t)$. The effectiveness of using such a technique for actuators fault isolation is illustrated by simulations in section 4.2.5. However, further enhancements have to be introduced to reduce the conservatism of such an approach resulting from the necessity of having prior knowledge about the fault intensity.

4.2.5 Simulation results

In this part, the quadrotor affine LTI model accompanied with the LQR controller and having the parameters given in B is simulated using Matlab-Simulink to test the performance of the presented observers in actuator fault detection and isolation. The simulation environment varies according to the utilized approach such that it may include exogenous disturbances and measurement noise to verify the capabilities of the proposed robust observers in handling such situations during the fault existence.

Luenberger observer for fault detection

In order to test the response of the observer in different cases, four actuators fault scenarios are introduced as shown in figure 4.3. Figure 4.3a indicates the residual generator response through the first fault scenario including a loss of efficiency by 20% of the 1^{st} actuator that takes place at a time instant $t = 50\ s$. It is apparent from the figure that during the fault-free situation $t < 50\ s$ the behavior of the detection observer is said to be consistent with the nominal plant and therefore the detection residual $r(t)$ vanishes asymptotically. However, after the occurrence of a fault the detection residual $r(t)$ deviates from zero as seen in the figure at $t > 50\ s$ the residual signal has some value indicating the existence of actuator or actuators malfunction.

Although the observer's main contribution is detecting actuators fault, by further analysis of the resulting residual signal in addition to the knowledge about the nature of the system configuration, some hints about the location of the fault can be obtained. In figure 4.3a the residual r_θ is having a value much larger than that of the other residuals, and knowing that the set of actuators responsible for controlling θ angle are motor 1 and motor 3, we can roughly deduce that one of these two actuators is experiencing some malfunction. Furthermore, the sign of the residual r_θ can point out precisely which actuator is faulty as since r_θ is positive this means that an additional positive pitch angle $\theta > 0$. The only possibility for being in such a situation is that the force from motor 3 is greater than motor 1 such that $F_3 > F_1$ see figure 2.5a which means the faulty actuator is motor 1.

The same results can be depicted from figure 4.3b which gives the residual signal $r(t)$ in case of a loss of efficiency by 20% of the 2^{nd} motor. One can notice that the residual having a large value is r_ϕ which indicates a

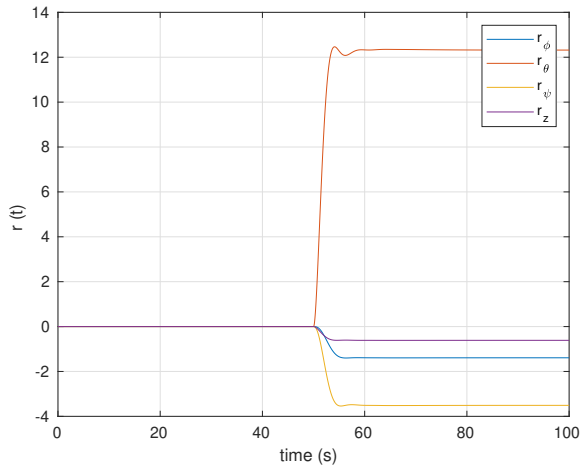

(a) 20% efficiency loss in 1^{st} actuator

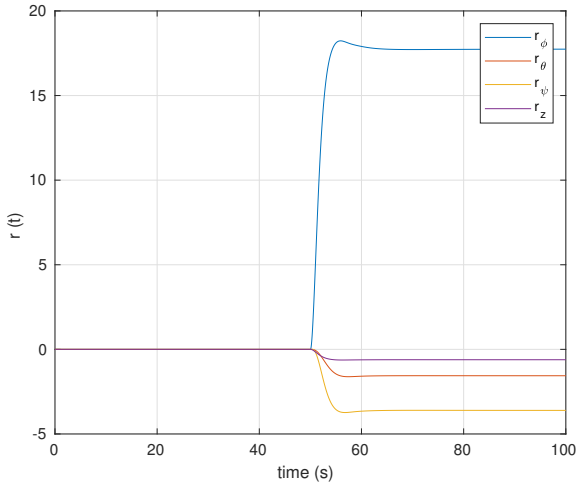

(b) 20% efficiency loss in 2^{nd} actuator

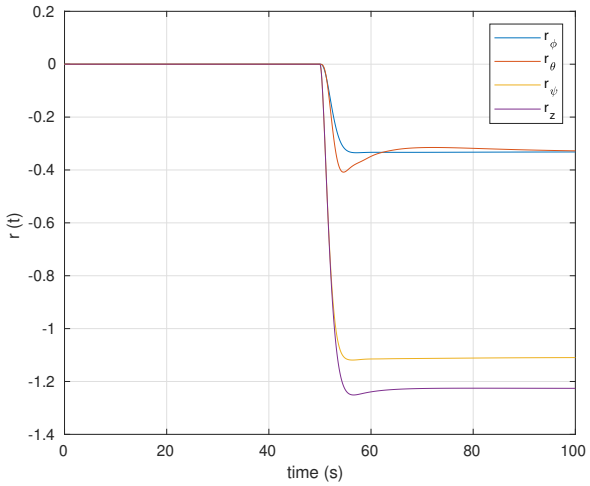

(c) 20% efficiency loss in two opposite actuators

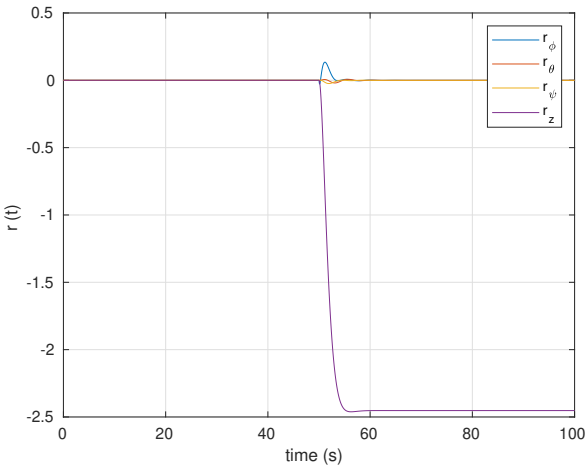

(d) 20% efficiency loss in the four actuators

Figure 4.3: Fault detection using Luenberger observer

fault of the motor set $2, 4$ and since r_ϕ has a positive value, the faulty actuator is motor 2. The ability of the residual generator to give a rough indication of the fault location is revealed by the residual signal shown in figure 4.3c. It can be seen in the figure that two residuals namely, r_ψ, and r_z are having large values due to a 20% loss of efficiency in the two opposite actuators $1, 3$. These motors deficiency cause a loss of altitude represented by the high residual value of r_z besides a defect in rotation angle control demonstrated by the high value of the residual signal r_ψ. Finally, when the 4 actuators are experiencing a loss of efficiency of 20%, the residual generator response is given in figure 4.3d. And as expected in this case, the orientation stability is preserved while the altitude state is highly affected resulting in a large value of r_z. The nutshell of the preceding analysis with the aid of further simulation scenarios is summarized in table 4.1 giving a methodology for deducing the fault location using the detection residuals, however, within the next sections another robust approach for precise fault estimation and identification will be deployed.

Residual	Fault location
$r_\phi \gg 0$	1^{st} actuator
$r_\phi \ll 0$	3^{rd} actuator
$r_\theta \gg 0$	2^{nd} actuator
$r_\theta \ll 0$	4^{th} actuator
$r_\psi \ll 0$	1^{st} & 3^{rd} actuators
$r_\psi \gg 0$	2^{nd} & 4^{th} actuators
$r_z \ll 0$	4 actuators

Table 4.1: Actuators fault detection analysis

Luenberger observer for actuators fault isolation

Despite the capability of the model-based observer to give a hint about the fault location, it is not very practical to depend on these results and their further analysis only. Thus, actuators fault identification or isolation can be attained automatically through the use of a bank of observers each one is consistent with the behavior of a faulty actuator model as indicated in 4.2.4.

Figure 4.4 shows the response of the 4 observers and the corresponding residual signals in case of a loss of efficiency by 20% in 1^{st} actuator starting at time instant $t = 50\ s$. It is apparent that in the fault-free case none of the isolation observers is consistent with the behavior of the nominal plant and thus the values of the residual signals are far from zero at $t < 50\ s$. While in the faulty case, at least one of the isolation observers is consistent with the behavior of the corresponding faulty plant such that this observer has all the residuals signals approaching zero. In our case, as the fault is introduced in the 1^{st} actuator, the 1^{st} observer residuals vanish after $t = 50s$ while the residuals of the other observers 2 to 4 are having some value indicating that they aren't matching the faulty model.

These results are illustrated by the decision logical table 4.2 where the value 0 correspond to a zero residual while the value 1 correspond to non-zero residual. We obtain from each isolation observer(i) 4 residuals in the observed directions namely $r_{\phi_i}, r_{\theta i}, r_{\psi_i}, r_{zi}$ whose values should be zero when the system is subjected to a fault of i^{th} actuator. So in our simulation scenario when the fault of 1^{st} takes place at $t \geq 50s$, the values of the residuals

-	r_{ϕ_1}	r_{ϕ_2}	r_{ϕ_3}	r_{ϕ_4}	$r_{\theta 1}$	$r_{\theta 2}$	$r_{\theta 3}$	$r_{\theta 4}$	r_{ψ_1}	r_{ψ_2}	r_{ψ_3}	r_{ψ_4}	r_{z1}	r_{z2}	r_{z3}	r_{z4}
$f_1(t)$	0	1	1	1	0	1	1	1	0	1	1	1	0	1	1	1
$f_2(t)$	1	0	1	1	1	0	1	1	1	0	1	1	1	0	1	1
$f_3(t)$	1	1	0	1	1	1	0	1	1	1	0	1	1	1	0	1
$f_4(t)$	1	1	1	0	1	1	1	0	1	1	1	0	1	1	1	0

Table 4.2: Actuators fault isolation logical decision

follow ten to reach the values indicated in the table $r_{\phi_1} = r_{\theta 1} = r_{\psi_1} = r_{z1} = 0$. In this case the fault is said to be perfectly isolable because none of the other residuals vanishes at the same time which means the expected fault magnitude is matched exactly. Since this case is very difficult to achieve through practical applications, another approach for the observer formulation is discussed in the next sections for precise fault estimation and isolation.

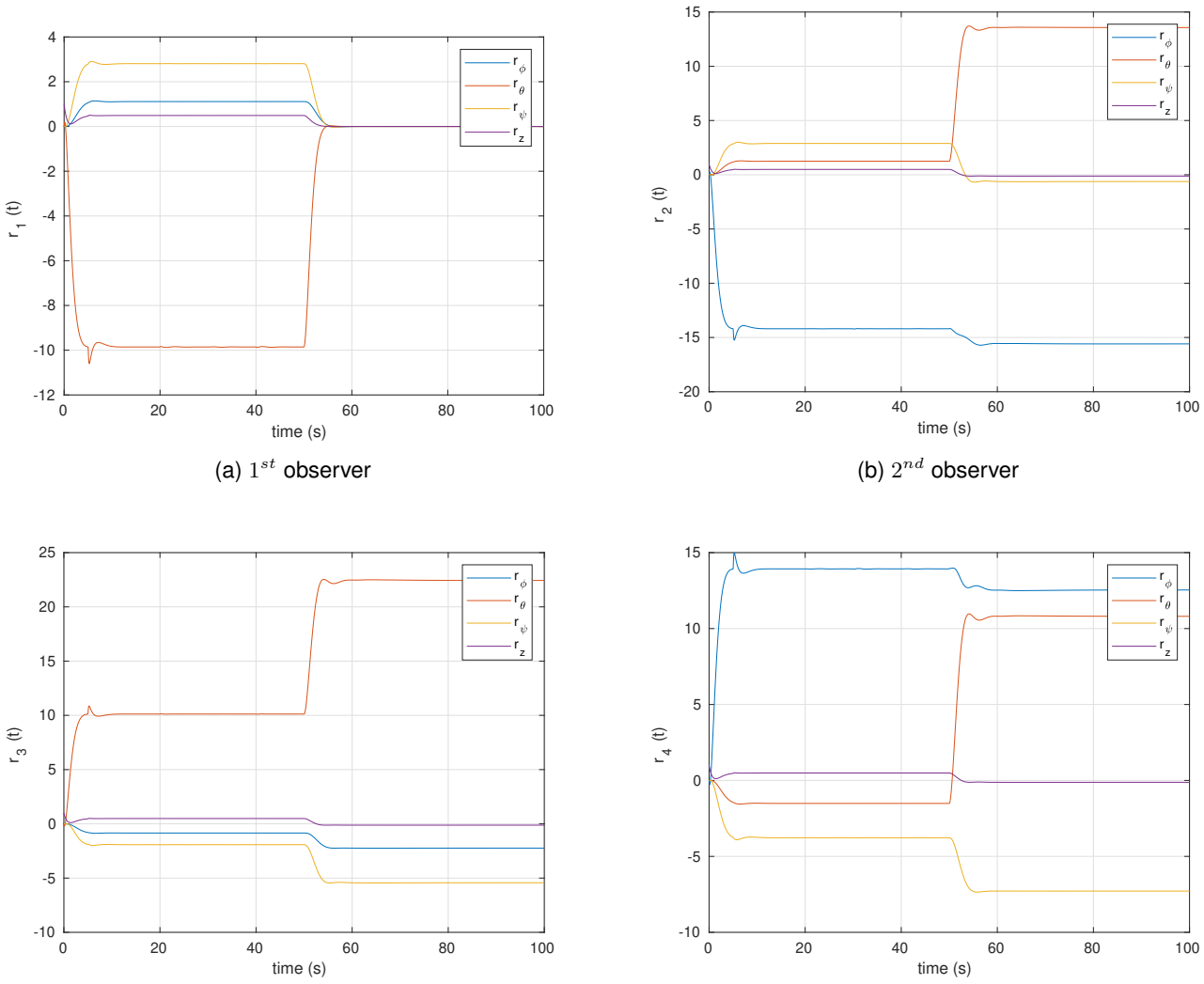

(a) 1^{st} observer

(b) 2^{nd} observer

(c) 3^{rd} observer

(d) 4^{th} observer

Figure 4.4: Fault isolation using a bank of Luenberger observers

Fault detection (Kalman filter vs $\mathcal{H}_-/\mathcal{H}_\infty$ observer)

This work is motivated by the existence of numerous techniques for actuators fault detection where the idea is to compare the performance of two well-known and widely employed observers one based on a stochastic approach (Kalman filter) while the other depending on system robustness ($\mathcal{H}_-/\mathcal{H}_\infty$). For the sake of evaluating the efficiency of the two observers, a simulation is performed on the quadrotor affine LTI model provided with an LQR controller

as illustrated in figure 4.5 and having the parameters given in B using Matlab-Simulink. The simulation environment in both cases contains the same exogenous wind disturbances and measurement noise after which the results are analyzed according to different aspects: noise attenuation level, disturbance rejection, response time, etc. The drone is subjected to different scenarios of actuators faults, for each one, the two observers' responses (residual signals) are listed and analyzed leading to the final conclusions.

The weighting matrices chosen for solving the ARE (4.8) to obtain the optimal value of the Kalman filter gain matrix are given by

$$\begin{cases} V = 10^{-2} * diag(1,1,1,2,2,2,1,1,1,6,6,6) \\ W = diag(10,10,10,10,10,10) \end{cases} \tag{4.25}$$

As the simulation considers white Gaussian noise applied on the measured output vector, the model is to be trusted more so the values of the V matrix are of a small order of magnitude compared to the W matrix. In addition, for solving the 3 LMIs proposed in section 4.2.3 to obtain a robust residual generator the value of the time constant is chosen to be $\zeta_o = 2.5$, and the fault modeling matrix is introduced as $F_f = diag(10,10,10,10)$. Finally, the additive measurement noise $n_s(t) \in [-0.03, 0.03]$ and $n_v(t) \in [-.06, .06]$ represent states and their derivatives noise having a sample time of $0.2, 0.05\ s$, respectively, as the velocity signals are more sensitive to higher frequency noise.

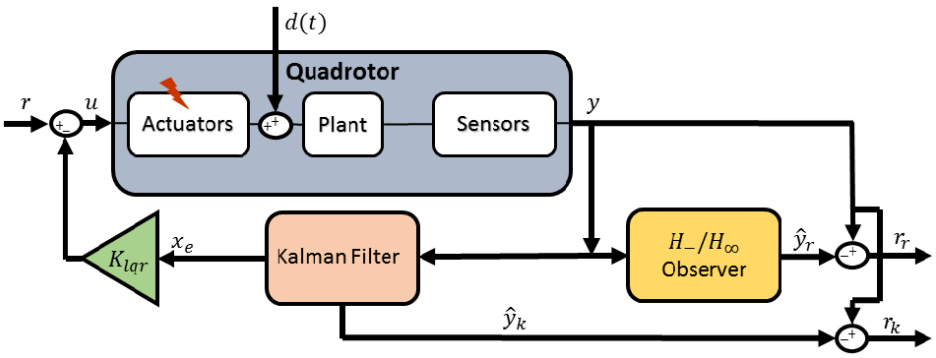

Figure 4.5: Schematic of observers comparison in fault detection

Figure 4.6 shows the simulation results for cases of no-fault and loss of efficiency by 20% in one, two opposite or the four actuators beginning at time $t = 60s$ and compares the response of the two observers. Again the residuals considered are $r_\phi, r_\theta, r_\psi, r_z$ since they are the main directions affected by actuators faults and the subscripts r and k represent robust observer and Kalman filter, respectively. Throughout the simulation, the quadrotor is subjected to constant equal wind gusts in x and y directions beginning at time $t = 20s$ and vanishing at $t = 40s$.

So the disturbance vectors given by equation (2.47) are described by

$$\begin{cases} d_1(t) = 0.2 & 20 < t < 40s \\ d_2(t) = 0.2 & 20 < t < 40s \end{cases} \tag{4.26}$$

After solving the convex optimization problem, the resulting values of β^2 and γ^2 are 1.24 and 1.0924, respectively. However, the robust observer will need to be enhanced in the aspect of noise attenuation such that it becomes able to suppress the Gaussian white noise introduced in the simulation as effectively as the Kalman filter.

The response of the two observers in the fault-free case ($f(t) = 0$) is given in figure 4.6a showing that the $\mathcal{H}_-/\mathcal{H}_\infty$ observer is highly effective in minimizing the effect of the exogenous disturbances on the system. This is evident from the residual response for the disturbances which has a value about 10% of the value of residuals generated by Kalman filter. However, it is more sensitive to the measurement noise which is an important point to be taken into consideration in future work.

Figure 4.6b shows the simulation of the first scenario where there exist a loss of efficiency in 1 actuator by 20% given by equation (4.27) from which one can comprehend the same observer response for fault and disturbances in ϕ and θ residuals. However, the residuals from the robust observer have much larger values in ψ and z directions indicating the sensitivity of the residuals to the fault even if the two observers give almost the same residual in the main fault direction ϕ.

$$f(t) = \begin{cases} 0.2 & t > 60\ s \\ 0 & t \geq 0 \\ 0 & t \geq 0 \\ 0 & t \geq 0 \end{cases} \tag{4.27}$$

In figure 4.6c the case of two opposite rotors loss of efficiency is demonstrated where the imposed fault is given by equation (4.28), so the expected direction to have maximum residual is ψ which is confirmed. Nevertheless, it is apparent in directions of ϕ and θ how the observer is much more robust than the Kalman filter for the wind disturbance (disturbance effect value is about 10% compared to that obtained from Kalman filter).

$$f(t) = \begin{cases} 0.2 & t > 60\ s \\ 0 & t \geq 0 \\ 0.2 & t > 60\ s \\ 0 & t \geq 0 \end{cases} \tag{4.28}$$

While figure 4.6d shows the case of efficiency loss in the four actuators corresponding to the maximum residual in altitude direction, again the two observers give almost the same residual value in z direction. But the proposed observer residuals response for the wind gust in the remaining directions ϕ, θ, ψ are about $9\%, 9\%, 1\%$ of the values

of the Kalman filter residuals, respectively. In that manner, the residuals generated by the $\mathcal{H}_-/\mathcal{H}_\infty$ point out how efficient the observer is in defining the direction of fault while suppressing the effect of the exogenous disturbances which will be the milestone for further fault estimation.

$$f(t) = \begin{cases} 0.2 & t > 60\ s \\ 0.2 & t > 60\ s \\ 0.2 & t > 60\ s \\ 0.2 & t > 60\ s \end{cases} \tag{4.29}$$

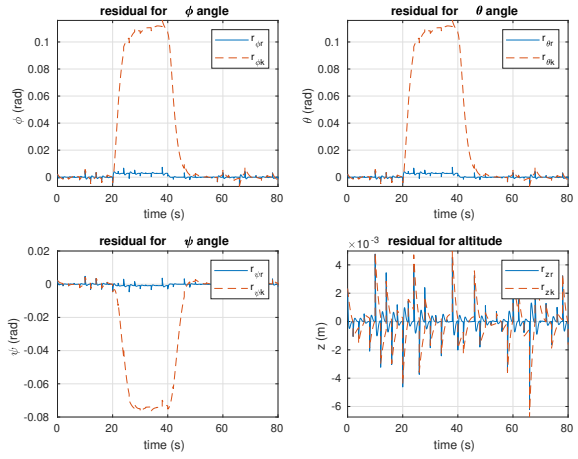

(a) Fault free case

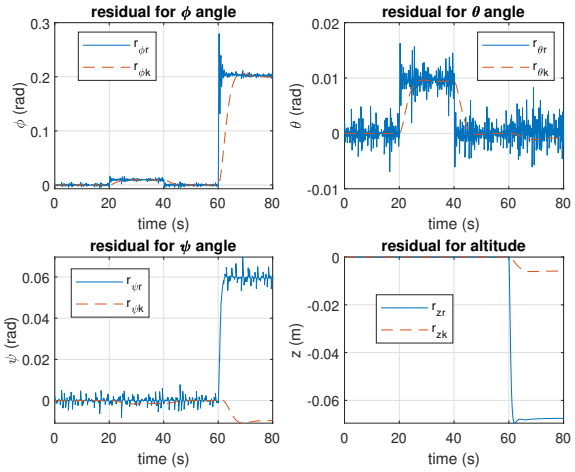

(b) 20% efficiency loss in 1^{st} actuator

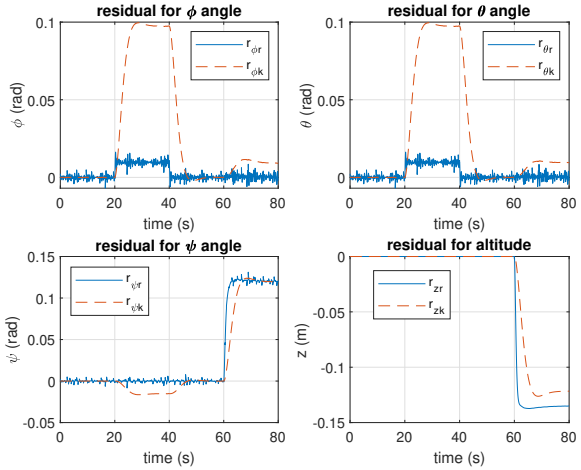

(c) 20% efficiency loss in two opposite actuators

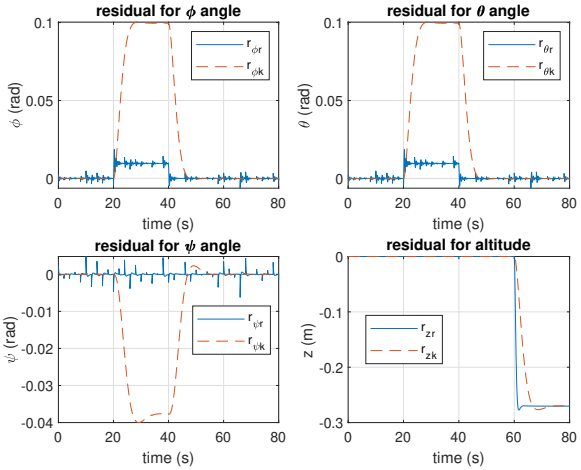

(d) 20% efficiency loss in the four actuators

Figure 4.6: Kalman filter vs H_-/H_∞ observer for LTI system

4.3 Fault diagnosis

The work presented in this section benefits from the concept of eigenstructure assignment [73], Unknown Input Observer (UIO) design [77], beside the $\mathcal{H}_\infty$ norm-based strategy [26] aiming to provide a unified algorithm for residual generator design which is able to achieve robust actuators and sensors fault diagnosis: detection, isolation, and estimation. In addition, the proposed residual generator is based on the system differentiated output signal and its relative degree that will be discussed later. Classically, the problem of actuator fault diagnosis is tackled by using the well-known $\mathcal{H}_-/\mathcal{H}_\infty$ approach [81] which aspires to minimize the effect of the perturbation $d(t)$ and to maximize the effect of the fault $f(t)$ on the residual signals. This approach was further developed based on the system relative degree in [99] to satisfy the regularity condition similar to the general idea behind the work produced here. However, the residual generator scheme and the fault weighting matrix proposed allows to estimate the fault precisely, thus the resulting residual signals are more robust than those obtained in [99] as will be illustrated by numerical examples. Notice that the $\mathcal{H}_-/\mathcal{H}_\infty$ approach deals with the worst case (minimum $\mathcal{H}_-$ and maximum $\mathcal{H}_\infty$ norms) but with a simple study of the system, more interesting properties may be obtained which enhance the performances of the residual generator. However, the proposed approach is designed for systems modeled in the LPV framework, the methodology followed can be also applied for Linear Time-Invariant (LTI) systems as they can be seen as frozen LPV systems at a specific vertex.

4.3.1 Introduction to the relative degree of LPV systems

In this section, the basic concepts and definitions of the LPV system output relative degree are discussed, so it can be considered as a continuation of the LPV framework preliminaries introduced before in section 2.3.3. Let us consider the LPV systems including the effect of the faults and the disturbances described by

$$\begin{cases} \dot{x}(t) = A\left(\rho(t)\right) x(t) + F\left(\rho(t)\right) f(t) + E\left(\rho(t)\right) d(t) \\ y(t) = C\left(\rho(t)\right) x(t) \end{cases} \tag{4.30}$$

where $x(t) \in \mathbb{R}^n$, $f(t) \in \mathbb{R}^{n_f}$, $d(t) \in \mathbb{R}^{n_d}$ and $y(t) \in \mathbb{R}^{n_y}$ are the state vector, the fault vector, the disturbance vector and the output of the system, respectively. The matrices $A(\rho(t))$, $F(\rho(t))$, $E(\rho(t))$, $C(\rho(t))$ are parameter varying state matrices with appropriate dimensions while $\rho^T(t) = \left(\rho_1, ..., \rho_{n_\rho}\right)$ represents the vector of n_ρ time-varying parameters which are sufficiently smooth and bounded as discussed earlier in 2.3.3 which means that $\rho(t) \in \Phi$ where Φ is an hyper-rectangle defined by

$$\Phi = \left\{ \rho(t) \in \mathbb{R}^{n_\rho} \left| \rho_1(t) \in \left[\rho_1^{\min}, \rho_1^{\max}\right], \ldots, \rho_{n_\rho}(t) \in \left[\rho_{n_\rho}^{\min}, \rho_{n_\rho}^{\max}\right] \right. \right\} \tag{4.31}$$

where $\rho_i^{\min}$ and $\rho_i^{\max}$, $i = 1, ..., n_\rho$ define the upper and lower bounds of the parameter $\rho_i(t)$. Similarly the time derivatives of the parameter named ${\rho_i}^{(j)}(t)$ belong to the compact sets Φ_j defined by

$$\Phi_j = \left\{ \rho^{(j)}(t) \in \mathbb{R}^{n_\rho} \middle| \rho_1^{(j)}(t) \in \left[{\rho_1^{(j)}}^{\min}, {\rho_1^{(j)}}^{\max} \right], \ldots, \rho_{n_\rho}^{(j)}(t) \in \left[{\rho_{n_\rho}^{(j)}}^{\min}, {\rho_{n_\rho}^{(j)}}^{\max} \right] \right\} \tag{4.32}$$

where j defines the order of the time derivative of the parameters while ${\rho_i^{(j)}}^{\max}$ and ${\rho_i^{(j)}}^{\min}$ represent the maximum and minimum values of the parameter derivative $\rho_i^{(j)}$. Notice that this assumption is always satisfied when the parameters vary continuously according to time (Lipschitz condition see [103]). Assume that the Linear parameter varying matrices are defined in a polytopic form as follows

$$M(\rho(t)) = \sum_{k=1}^{N} \mu_k(\rho(t)) M_k \tag{4.33}$$

where $M(\rho(t)) \in \{A(\rho(t)), C(\rho(t)), E(\rho(t)), F(\rho(t))\}$ and μ_k are weighting functions previously defined by equation (2.57). It follows that the time derivative of $M(\rho(t))$ can be expressed as follows

$$\frac{dM(\rho(t))}{dt} = \sum_{k=1}^{N} \dot{\mu}_k(\rho(t)) M_k \tag{4.34}$$

Definition 4

Given the system (4.30), the integer number r_{ij} is called a relative degree of the i^{th} output $y_i(t)$ with respect to the j^{th} fault $f_j(t),\ j = 1, ..., n_f$ if the fault $f_j(t)$ appears in the equation of the r_{ij}^{th} time derivative of the output ($y_i^{(r)}(t)$) [28]. It is called a uniform relative degree if it appears in the r_{ij}^{th} time derivative if it is constant and the same $\forall \rho(t) \in \Phi$ and $\forall \rho^{(j)} \in \Phi_j$.

In order to illustrate the relative degree concept mathematically, consider again the LPV system given by equation (4.30) whose output matrix is independent of the varying parameter (matching the quadrotor LPV models 2.3.5 and 2.3.4) is as follows

$$\begin{cases} \dot{x}(t) = A\left(\rho(t)\right) x(t) + F\left(\rho(t)\right) f(t) + E\left(\rho(t)\right) d(t) \\ y(t) = Cx(t) \end{cases} \tag{4.35}$$

Consider the system (4.35) having the following r^{th} output derivative

$$y^{(r)}(t) = Cx^{(r)}(t) \tag{4.36}$$

It is clear that calculating the output derivatives of the LPV system is more difficult than the LTI one as the state matrices are varying with time. In addition, in this work, we are interested in the output derivative which is affected

by the encountered fault, so we can expand equation (4.36) as follows

$$\dot{y}(t) = C\dot{x}(t) = CA_\rho x(t) + CF_\rho f(t) + CE_\rho d(t) \tag{4.37}$$

where each parameter varying matrix $X(\rho(t))$ is replace by its reduced form X_ρ so $X(\rho(t)) \rightarrow X_\rho$ to reduce the size of equations. Recall the general output relative degree definition 4, we can conclude that the fault (disturbance) relative degree to the output $\lambda_f(\lambda_d)$ is the number of output successive derivatives until the fault (disturbance) effect begins to emerge. So in equation (4.37), if $CF_\rho \neq 0$, then the fault signal is affecting the first derivative of the output such that $\lambda_f = 1$. Otherwise the fault relative degree is greater than one $\lambda_f > 1$ and we need to differentiate the output signal another time. Note that the disturbance relative degree can be obtained in a similar way by checking the value of the matrix CE_ρ.

Consider the case when $CF_\rho = CE_\rho = 0$, then we proceed to calculate the second time derivative of the output as follows

$$\ddot{y}(t) = C\frac{d}{dt}(\dot{x}(t)) = C\frac{d}{dt}(A_\rho x(t)) = C(\dot{A}_\rho x(t) + A_\rho \dot{x}(t)) \tag{4.38}$$

$$\ddot{y}(t) = C(\dot{A}_\rho + A^2{}_\rho)x(t) + CA_\rho F_\rho f(t) + CA_\rho E_\rho d(t) \tag{4.39}$$

then we check the relative degrees of the fault and disturbance λ_f, λ_d through calculating the values of the matrices $CA_\rho F_\rho, CA_\rho E_\rho$ as earlier and so on for higher output derivatives.

Assumption 5

Throughout this work, we assume that the relative degree is well defined in the compact sets Φ and Φ_j defined in (4.31) and (4.32). It means that the time variations of the parameters and their successive time derivatives do not affect the value of the relative degree r of the output with respect to fault. We refer to the notion of uniform relative degree r_{ij} on Φ and Φ_j.

4.3.2 Auxiliary output approach for fault diagnosis

In order to construct the residual generator according to the vector relative degree of the output $y(t)$, a new output vector denoted the auxiliary output $\tilde{y}(t)$ is generated. Of course, this auxiliary output is obtained from time derivatives of the output and some linear parameter varying combinations of them. These time derivatives can be robustly obtained by the recent algorithms of signal differentiation, see for example Non-Asymptotic Algebraic Differentiators [27]. Clearly, this work is motivated by the quality of the obtained time derivatives of a signal which are robust with respect to noises compared to the classical differentiation function based on difference computation. Utilizing the

output derivative (4.36), the auxiliary output can be defined by

$$\tilde{y}(t) = \big(y(t), \dot{y}(t), \ldots, y^{(r)}(t)\big)^T \tag{4.40}$$

Notice that for the construction of the auxiliary output, since the relative degree of each output with respect to each fault is exploited, three cases are considered corresponding to the presence or not of the disturbance and its derivatives in the auxiliary output vector. Recall λ_d and λ_f represent the relative degrees of each output with respect to disturbance and fault vectors, respectively, then according to the system we may have

C(1) $\lambda_f < \lambda_d \rightarrow$ output relative degree to the faults is less than that for the disturbances

C(2) $\lambda_f = \lambda_d \rightarrow$ the relative degree to the faults is equal to the disturbances

C(3) $\lambda_f > \lambda_d \rightarrow$ output relative degree to the fault is greater than that for the disturbance

Since MIMO systems are studied, it may happen that a combination of these three cases appears in the system for simplicity the system (4.30) can be written in the following form through representing each parameter varying matrix $X(\rho(t))$ by its reduced form X_ρ

$$\begin{cases} \dot{x}(t) = A_\rho x(t) + F_\rho f(t) + E_\rho d(t) \\ y(t) = Cx(t) \end{cases} \tag{4.41}$$

The auxiliary output vector contains the system output and its successive time derivatives (more detailed in [26]) and is calculated for each case as follows:

- case1 $\tilde{y}(t) = C_{\bar{\rho}} x(t) + R_{\bar{\rho}} f(t)$
- case2 $\tilde{y}(t) = C_{\bar{\rho}} x(t) + R_{\bar{\rho}} f(t) + D_{\bar{\rho}} d(t)$
- case3 $\tilde{y}(t) = C_{\bar{\rho}} x(t) + R_{\bar{\rho}} f(t) + D_{\bar{\rho}} \bar{d}(t)$

where $\bar{\rho}(t)$ represents the vector of the parameters $\rho(t)$ and their time derivatives according to the relative degrees. The new output $\tilde{y}(t)$ called auxiliary output is designed in such a way to ensure that the matrix $R_{\bar{\rho}}$ is of full column rank $\forall \bar{\rho}(t)$. And $\bar{d}(t)$ contains the disturbance $d(t)$ and its time derivatives. Notice that for this last case, additional assumptions on boundedness of the time derivatives of the disturbance $d(t)$ are needed (One can restrict the class of disturbances to the signals belonging in a Sobolev space).

Residual generator

For the preceding three cases, the following residual generator is proposed

$$\begin{cases} \dot{\hat{x}}(t) = A_\rho \hat{x}(t) + L_{1\bar{\rho}} \left(y(t) - \hat{y}(t)\right) + L_{2\bar{\rho}} \left(\tilde{y}(t) - \hat{\tilde{y}}(t)\right) \\ \hat{y}(t) = C\hat{x}(t) \\ \hat{\tilde{y}}(t) = C_{\bar{\rho}}\hat{x}(t) \\ r(t) = M_{\bar{\rho}} \left(\tilde{y}(t) - \hat{\tilde{y}}(t)\right) \end{cases} \tag{4.42}$$

Then, the objective is to design the gain matrices $L_{1\bar{\rho}}$, $L_{2\bar{\rho}}$ and $M_{\bar{\rho}}$ in order to ensure robust actuator fault diagnosis (detection, estimation and isolation). Alternatively to the $\mathcal{H}_-/\mathcal{H}_\infty$ technique, the adopted approach is to transform this min/max strategy to only a minimization problem if necessary (Especially in cases 2 and 3). So let us first define the reference residual vector $r_r(t)$ as follows

$$r_r(t) = Qf(t) \tag{4.43}$$

where Q is a weighting matrix playing a crucial role in the performances of the residual generator. A judicious choice of such a matrix may realize fault detection, fault isolation and fault estimation as follows.

1. If $Q \in \mathbb{R}^{1\times n_f}$, only one residual signal is generated which performs fault detection
2. If $Q \in \mathbb{R}^{n_f\times n_f}$ is a diagonal matrix with entries $Q_{i,i} = q_{ii} > 1, i = 1, ..., n_f$, fault isolation is performed, in addition, since $q_{ii} > 1$ the effect of the faults are amplified on the residual signals which avoid the fact that the effect of faults is masked due to measurement noises, especially for faults with small magnitudes.
3. Finally, if $Q = I_{n_f}$ where I_{n_f} represents the identity matrix of dimension $n_f \times n_f$, the fault estimation problem is performed.

In addition, we introduce the following virtual residual vector $r_e(t)$ which has great importance in the residual generator analysis as illustrated later

$$r_e(t) = r(t) - r_r(t) \tag{4.44}$$

Important definitions

Definition 5 *The residual generator is said to be exact convergent if*

$$r(t) = Qf(t) \tag{4.45}$$

Definition 6 *The residual generator is said to be asymptotic convergent if*

$$\lim_{t\to+\infty} r(t) = Qf(t) \tag{4.46}$$

Main results

Since we are seeking the optimal values of the residual generator (4.42) gain matrices, two main notions are investigated namely, exact, and asymptotic convergence of the residual signals to the fault. Each methodology requires the system model to satisfy some decoupling ranking conditions which are stated and discussed to obtain the corresponding residual generator gains. However, if the system is not satisfying any of the addressed decoupling conditions, then the robust $\mathcal{H}_-/\mathcal{H}_\infty$ is introduced as a worst-case scenario for fault diagnosis. In order to ensure the generality of the proposed theorems for a wide range of system models, they are applied for the three system cases mentioned before based on its output relative degree with respect to faults and disturbances.

Exact convergence

Theorem 2

Given a non-singular diagonal matrix $Q \in \mathbb{R}^{n_f \times n_f}$, the residual vector $r(t)$ converges exactly to the reference residual vector $r_r(t) = Qf(t)$, thus $r_e(t) = 0$ if the following condition holds

$$rank\left(\begin{bmatrix} C_{\bar{\rho}} & R_{\bar{\rho}} \\ 0 & Q \end{bmatrix}\right) = rank\left(\begin{bmatrix} C_{\bar{\rho}} & R_{\bar{\rho}} \end{bmatrix}\right), \forall \bar{\rho}(t) \in \bar{\Phi} \tag{4.47}$$

Solution to case1 For this first case, it is assumed that each output has a relative degree with respect to the faults $f(t)$ less than the relative degrees with respect to the disturbances $d(t)$. Then, the state error $e(t) = x(t) - \hat{x}(t)$ obeys the differential equation

$$\begin{cases} \dot{e}(t) = (A_\rho - L_{1\bar{\rho}}C - L_{2\bar{\rho}}C_{\bar{\rho}})\, e + (F_\rho - L_{2\bar{\rho}}R_{\bar{\rho}})\, f(t) + E_\rho d(t) \\ r(t) = M_{\bar{\rho}}C_{\bar{\rho}}e(t) + M_{\bar{\rho}}R_{\bar{\rho}}f(t) \end{cases} \tag{4.48}$$

$$\begin{cases} \dot{e}(t) = (A_\rho - L_{1\bar{\rho}}C - L_{2\bar{\rho}}C_{\bar{\rho}})\, e + (F_\rho - L_{2\bar{\rho}}R_{\bar{\rho}})\, f(t) + E_\rho d(t) \\ r_e(t) = M_{\bar{\rho}}C_{\bar{\rho}}e(t) + (M_{\bar{\rho}}R_{\bar{\rho}} - Q)\, f(t) \end{cases} \tag{4.49}$$

If the system satisfies the condition of Theorem 2, then the matrix $M_{\bar{\rho}}$ value can be assigned to guarantee exact convergence of the residual to fault $r_e(t) = 0$ as follows:

$$\begin{cases} M_{\bar{\rho}}C_{\bar{\rho}} = 0 \\ M_{\bar{\rho}}R_{\bar{\rho}} - Q = 0 \end{cases} \tag{4.50}$$

Proof 1 *under the rank condition in Theorem 2, there exists a matrix $M_{\bar{\rho}}$ such that*

$$M_{\bar{\rho}} \begin{bmatrix} C_{\bar{\rho}} & R_{\bar{\rho}} \end{bmatrix} = \begin{bmatrix} 0 & Q \end{bmatrix} \tag{4.51}$$

Therefore, under these conditions, we will have $r_e(t) = 0$, thus $r(t) = Qf(t)$ which implies exact convergence of the residual signal to its reference.

Some remarks

Remark 4 *It can be seen that under the condition of Theorem 2, the residual vector $r(t)$ does not depend on $e(t)$, then, even if the state estimation error $e(t)$ is not stable, the fault diagnosis is performed. This is obtained if the time derivatives of the outputs and the parameters are known exactly which is true only theoretically. In such a case, the matrix $L_{1\bar{\rho}}$ can be fixed to zero, in addition, the observability of the system is not a necessary condition for fault estimation. However, in practical applications, the time derivatives are obtained after a transient phase, in this case we need to consider the stability of the system:*

- *if the system is stable, the matrix $L_{1\bar{\rho}}$ can be fixed to zero and fault estimation can be performed.*
- *if the system is not stable or there is a large difference of the observer initial conditions, it is necessary to assign the value of the matrix $L_{1\bar{\rho}}$ (using pole placement or any other technique) in order to stabilize the state estimation error, hence in this case the system has to be observable or at least detectable.*

Remark 5 *Notice also that if the condition of Theorem 2 is satisfied, the perturbation $d(t)$ does not affect the residual vector $r(t)$ which illustrates the interest of this property compared to the $\mathcal{H}_-/\mathcal{H}_\infty$ approach (see examples 1, 2).*

Thus, if a system is matching case1 while satisfying the condition of Theorem 2, the matrix $M_{\bar{\rho}}$ can be obtained as follows for

$$M_{\bar{\rho}} = \begin{bmatrix} 0 & Q \end{bmatrix} \begin{bmatrix} C_{\bar{\rho}} & R_{\bar{\rho}} \end{bmatrix}^{\dagger} \tag{4.52}$$

where $X^{\dagger}$ denotes the pseudo-inverse of the matrix X. Since, theoretically (see remark 4), the observability or the detectability of the system are not required, the matrices $L_{1\bar{\rho}}$ and $L_{2\bar{\rho}}$ can be fixed to zero. However in practical situations, the time derivatives are obtained after a finite time, then, if the system is unstable, the matrix $L_{1\bar{\rho}}$ should be designed in such a way to stabilize the state estimation error dynamics. Consequently, this case requires that the pair (A_ρ, C) is observable or at least detectable such that the gain matrix $L_{1\bar{\rho}}$ can be chosen by pole placement method previously discussed in 4.2.1.

Solution to case2 by combining the residual generator 4.42 with the system corresponding to case2, the following state estimation error is obtained

$$\begin{cases} \dot{e}(t) = (A_\rho - L_{1\bar{\rho}}C - L_{2\bar{\rho}}C_{\bar{\rho}})\, e + (F_\rho - L_{2\bar{\rho}}R_{\bar{\rho}})\, f(t) + (E_\rho - L_{2\bar{\rho}}D_{\bar{\rho}})\, d(t) \\ r_e(t) = M_{\bar{\rho}}C_{\bar{\rho}}e(t) + (M_{\bar{\rho}}R_{\bar{\rho}} - Q)\, f(t) + M_{\bar{\rho}}D_{\bar{\rho}}d(t) \end{cases} \tag{4.53}$$

Similar to the result of Theorem2, exact convergence is achieved if following rank condition holds

$$rank\left(\begin{bmatrix} C_{\bar{\rho}} & R_{\bar{\rho}} & D_{\bar{\rho}} \\ 0 & Q & 0 \end{bmatrix}\right) = rank\left(\begin{bmatrix} C_{\bar{\rho}} & R_{\bar{\rho}} & D_{\bar{\rho}} \end{bmatrix}\right), \forall \bar{\rho}(t) \in \bar{\Phi} \tag{4.54}$$

Proof 2 *under the rank condition in* (4.54)*, there exists a matrix* $M_{\bar{\rho}}$ *such that*

$$M_{\bar{\rho}}\begin{bmatrix} C_{\bar{\rho}} & R_{\bar{\rho}} & D_{\bar{\rho}} \end{bmatrix} = \begin{bmatrix} 0 & Q & 0 \end{bmatrix} \tag{4.55}$$

which will guarantee exact convergence of the residual signal to the reference residual resulting in $r_e(t) = 0$.

Then the gain matrix can be obtained as follows

$$M_{\bar{\rho}} = \begin{bmatrix} 0 & Q & 0 \end{bmatrix}\begin{bmatrix} C_{\bar{\rho}} & R_{\bar{\rho}} & D_{\bar{\rho}} \end{bmatrix}^{\dagger} \tag{4.56}$$

while the gain matrix $L_{1\bar{\rho}}$ can be obtained by pole placement for the eigenvalues of $(A_\rho - L_{1\bar{\rho}}C)$ such that it ensures the residual generator is stable.

Solution to case3 the same conditions are valid for case3 with replacing the disturbance signal $d(t)$ by the differentiated disturbance signal $\bar{d}(t)$ so the gain matrices can be obtained in a similar way to case2. However, an additional assumption on $\bar{d}(t)$ should be ensured since $\bar{d}(t)$ contains $d(t)$ and its successive time derivatives up to a finite order, it is necessary that all these time derivatives are bounded, which means that $d(t)$ belongs to a corresponding Sobolev space.

Example 1 *Let an LTI system affected by actuator faults takes the following form which is similar to the LPV model given in* (4.41)

$$\begin{cases} \dot{x}(t) = Ax(t) + Ff(t) + Ed(t) \\ y(t) = Cx(t) \end{cases} \tag{4.57}$$

where the system matrices are given by

$$A = \begin{pmatrix} 0 & 1 & 3 \\ 0 & 0 & 1 \\ -3 & -3 & -3 \end{pmatrix}, F = \begin{pmatrix} 4 \\ 1 \\ 0 \end{pmatrix}, E = \begin{pmatrix} 0 \\ 1 \\ 0 \end{pmatrix}, C = \begin{pmatrix} 1 & 0 & 0 \\ 0 & 0 & 1 \end{pmatrix} \tag{4.58}$$

The same previous analysis is applied and the gain matrices are calculated for the LTI model by replacing the varying matrices X_ρ with their reciprocal constant matrices X. By calculating the auxiliary output $\tilde{y}(t)$, the system is found to have a relative degree 1, corresponding to case1, and satisfying the condition of Theorem 2 so the gain matrix M is calculated from (4.52) *and given by*

$$M = \begin{pmatrix} \frac{1}{6} & -\frac{1}{3} & \frac{1}{2} & \frac{1}{6} \end{pmatrix} \tag{4.59}$$

While L_1 and L_2 are fixed to zero, the results are shown in figure 4.7 where the disturbance introduced and system output are given in figure 4.7a while the resulting residual signal is illustrated in figure 4.7b proving the hypothesis of Theorem 2 which implies exact convergence of the residual to the fault and showing the role played by the weighting matrix Q in fault isolation. Despite the exact convergence of the residual signal, figure 4.7c shows that the state estimation error is not converging to zero when the L_1, L_2 gains are fixed to zeros, however, it is apparent in figure 4.7d that by calculating the gain matrix L_1 by a simple pole placement the residual generator can work as a state estimator such that the estimation error converges to zero.

Example 2 *Consider now the LPV system* (4.41) *defined by the following matrices*

$$A_\rho = \begin{pmatrix} 0 & 1 & \rho(t) \\ 0 & 0 & 1 \\ -\rho(t) & -3 & -\rho(t) \end{pmatrix}, F_\rho = \begin{pmatrix} 2\rho(t) \\ 1 \\ 0 \end{pmatrix}, E_\rho = \begin{pmatrix} 0 \\ 1 \\ 0 \end{pmatrix}, C = \begin{pmatrix} 1 & 0 & 0 \\ 0 & 0 & 1 \end{pmatrix} \tag{4.60}$$

and $\rho(t) \in [1, 3]$, this example corresponds to case1 and the condition of Theorem 2 is fulfilled which implies that the exact residual property is guaranteed. The matrix $M_{\bar{\rho}}$ is computed from (4.52) *and given by*

$$M_{\bar{\rho}} = \begin{pmatrix} \frac{1}{6} & -\frac{1}{3} & \frac{1}{2\rho(t)} & \frac{1}{6\rho(t)} \end{pmatrix} \tag{4.61}$$

Since the exact residual convergence is satisfied, the gains $L_{1\bar{\rho}}$ and $L_{2\bar{\rho}}$ are fixed to zero. The results are given in figure 4.8 where figure 4.8a shows the varying parameter, the introduced perturbations, and the resulting system output. Figure 4.8b proves the exact convergence and complete decoupling of the residual signal from disturbances and fault through fault estimation $Q = 1$ (red dashed line) or fault isolation $Q = 5$ (cyan dashed line). Note that to guarantee the correct response of the residual generator another varying-parameter $\eta(t) = \frac{1}{\rho(t)}$, $\eta(t) \in [\frac{1}{3} \;\; 1]$, have

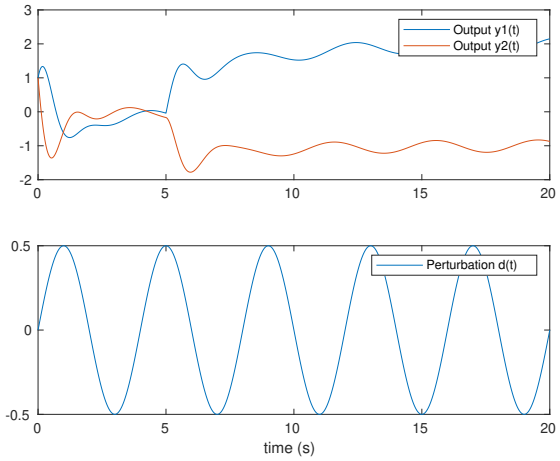

(a) disturbance and system output

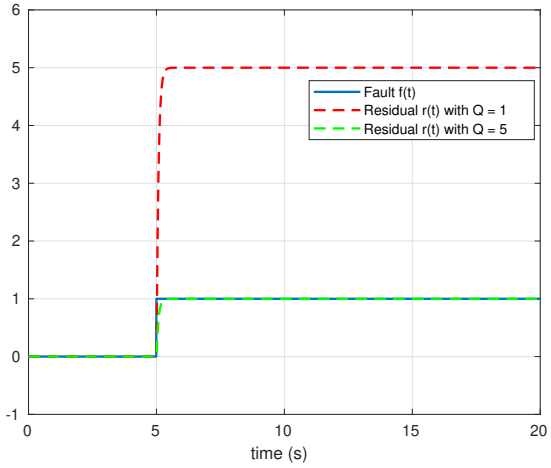

(b) resulting residual signal

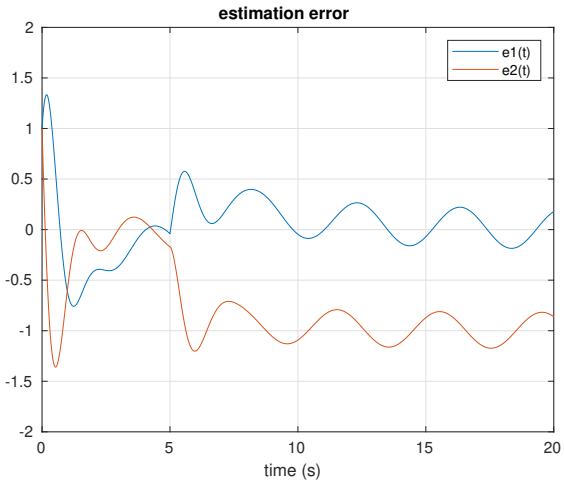

(c) estimation error with L_1, L_2 are zeros

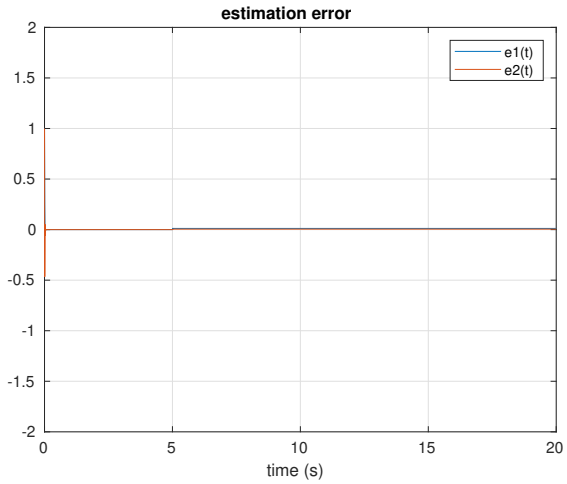

(d) estimation error with gain matrix L_1

Figure 4.7: Solution following Theorem 2 for LTI system

to be introduced to calculate the gain matrices $M_{\bar{\rho}}, L_{1\bar{\rho}}, L_{2\bar{\rho}}$. In addition, to reveal the effectiveness of the proposed approach, the gains of the residual generator are calculated using the $\mathcal{H}_-/\mathcal{H}_\infty$ which will be discussed in detail in section 4.3.2. The residual signal shown in figure 4.8b with dashed green line is obtained by applying the $\mathcal{H}_-/\mathcal{H}_\infty$ technique and appears to be affected by the disturbance signal which is completely decoupled using 2.

Asymptotic convergence

When the condition of Theorem 2 is not satisfied, exact residual convergence is no longer ensured. However, under some conditions, asymptotic residual convergence can be recovered as stated in the following Theorem 3.

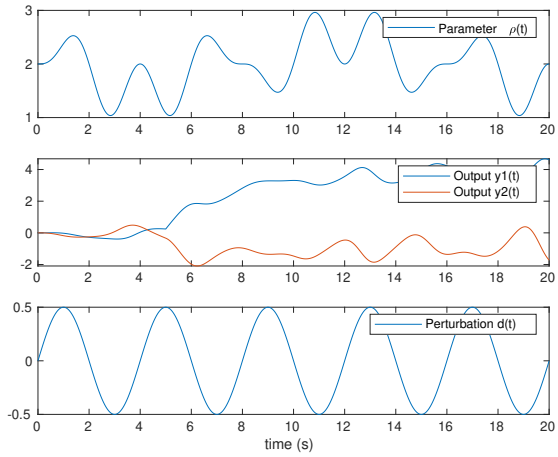

(a) varying parameter, output, and disturbance

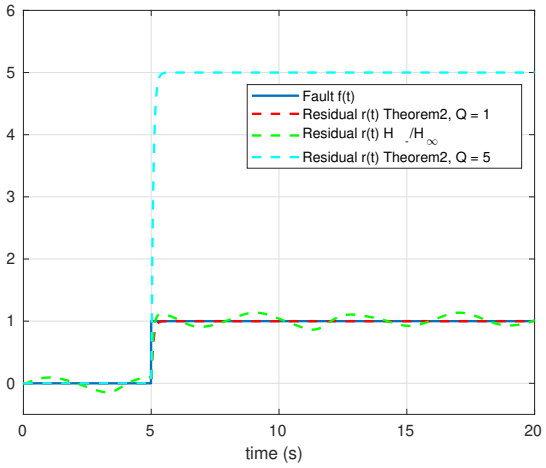

(b) resulting residual signal

Figure 4.8: Solution following Theorems 2 for LPV system

Theorem 3

Given a non-singular diagonal matrix $Q \in \mathbb{R}^{n_f \times n_f}$. If the conditions

$$rank\left(R_{\bar{\rho}}\right) = n_f, \quad rank\left(\begin{bmatrix} F_\rho \\ R_{\bar{\rho}} \end{bmatrix}\right) = rank\left(F_\rho\right) \tag{4.62}$$

hold $\forall \rho(t) \in \Phi, \forall \bar{\rho}(t) \in \bar{\Phi}$, and the pair $(A_\rho - L_{2\bar{\rho}} C_{\bar{\rho}}, C)$ is observable, or at least detectable, then there exist matrices $M_{\bar{\rho}}$, $L_{1\bar{\rho}}$ and $L_{2\bar{\rho}}$ such that

$$\begin{cases} \lim\limits_{t \to +\infty} r(t) = Qf(t) & d = 0 \\ \|r(t) - Qf(t)\|_2 < \gamma \|d(t)\|_2 & d \neq 0 \end{cases} \tag{4.63}$$

Proof 3 *Under the rank conditions of Theorem 3, there exist two parameter varying matrices $M_{\bar{\rho}}$ and $L_{2\bar{\rho}}$ such that*

$$\begin{cases} M_{\bar{\rho}} R_{\bar{\rho}} = Q \\ L_{2\bar{\rho}} R_{\bar{\rho}} = F_\rho \end{cases} \tag{4.64}$$

By satisfying these conditions the fault effect can be decoupled from the resulting error dynamics, then the asymptotic convergence of the state error is ensured to be bounded by a quadratic $\mathcal{H}_\infty$ limit γ which is formulated as an LMI feasibility problem illustrated next.

Remark 6

The gain matrix $L_{1\bar{\rho}}$ is very beneficial specially in this case, as although the matrices $M_{\bar{\rho}}$ and $L_{2\bar{\rho}}$ are fixed, it gives a margin to choose the gain value such that the observer is able to recover the system states precisely while achieving the required quadratic $\mathcal{H}_\infty$ performance level.

It is important to highlight that the observability of the pair $(A_\rho - L_{2\bar{\rho}}C_{\bar{\rho}}, C)$ is a necessary condition to guarantee the applicability of Theorem 3. Recall the general definition of the system observability 3, the observability of an LTI system could be verified by checking the rank of the observability matrix (3.37). However, for an LPV system it is not the case as the state matrices are varying with time so it is considered as a family of Linear Time Varying (LTV) systems whose state transition matrix Ψ is dependent on the varying parameters $\rho(t)$. For example, consider the LPV system given by equation (4.41), the solution of such a differential equation will result in a state transition matrix $\Psi(t, t_0, \rho(t))$ which is not easy to solve. Note for an LTI system, the solution of the differential equation is simple as the state matrix A is constant so the state transition matrix becomes $\Psi(t, t_0) = e^{A(t-t_0)}$ which facilitates the derivation of the observability matrix (3.37) as illustrated in [31].

Thus, to check the observability of the LPV system it has to be handled as an LTV system so it should satisfy the following theorem 4 presented in [104].

Theorem 4

Consider a general LPV system given by

$$\begin{cases} \dot{x}(t) = A_\rho x(t) \\ y(t) = C_\rho x(t) \end{cases} \tag{4.65}$$

The system (4.65) is completely observable if $rank(\mathcal{O}) = n, \forall \rho(t) \in \Phi$ where n: is the number of system states

$$\mathcal{O} = \begin{bmatrix} o_1^T & o_2^T \dots o_n^T \end{bmatrix} \tag{4.66}$$

where $o_1 = C_\rho$ and $o_{i+1} = o_i A_\rho + \dot{o}_i, \quad i \in [1, \dots, n-1]$

Applying the results of theorem 4 for the pair $(A_\rho - L_{2\bar{\rho}}C_{\bar{\rho}}, C)$, we can calculate the matrices $o_i, i \in [1, \dots, n]$ as follows

$$\begin{cases} o_1 = C \\ o_2 = C(A_\rho - L_{2\bar{\rho}}C_{\bar{\rho}}) \\ o_3 = C\big[(A_\rho - L_{2\bar{\rho}}C_{\bar{\rho}})^2 + \dot{A}_\rho - \dot{L}_{2\bar{\rho}}C_{\bar{\rho}} - L_{2\bar{\rho}}\dot{C}_{\bar{\rho}}\big] \\ \vdots \\ o_n = o_{n-1}(A_\rho - L_{2\bar{\rho}}C_{\bar{\rho}}) + \dot{o}_{n-1} \end{cases} \tag{4.67}$$

Note that the matrix $\mathcal{O}$ is analogical to the observability matrix of LTI systems (3.37) but the main difference lies behind the nature of the LPV systems whose parameters are varying with time such that it depends on the parameters and their successive time derivatives. To reduce the computation of the LPV observability matrix (4.66), it has to satisfy the rank condition $rank(\mathcal{O}) = n, \forall \rho(t) \in \Phi$ within the compact set Φ representing the hyper rectangle within which the varying parameters evolve. In [77], the same methodology is followed by calculating the derivatives of the output to extend the designed continuous time LPV observer for arbitrary relative degree of the unknown input. After checking the observability of the pair $(A_\rho - L_{2\bar{\rho}}C_{\bar{\rho}}, C)$, we can proceed to assign the gain matrices of the residual generator according to theorem 3 for each of the previously cited cases.

Solution to case1 consider the system corresponding to case1 accompanied with the residual generator 4.42, then the error dynamics will be as follows

$$\begin{cases} \dot{e}(t) = (A_\rho - L_{1\bar{\rho}}C - L_{2\bar{\rho}}C_{\bar{\rho}})\, e + (F_\rho - L_{2\bar{\rho}}R_{\bar{\rho}})\, f(t) + E_\rho d(t) \\ r_e(t) = M_{\bar{\rho}}C_{\bar{\rho}}e(t) + (M_{\bar{\rho}}R_{\bar{\rho}} - Q)\, f(t) \end{cases} \tag{4.68}$$

by applying the results of Theorem 3, the error dynamics (4.68) reduces to

$$\begin{cases} \dot{e}(t) = (A_\rho - L_{1\bar{\rho}}C - L_{2\bar{\rho}}C_{\bar{\rho}})\, e + E_\rho d(t) \\ r_e(t) = M_{\bar{\rho}}C_{\bar{\rho}}e(t) \end{cases} \tag{4.69}$$

Then under the detectability condition of the pair $(A_\rho - L_{2\bar{\rho}}C_{\bar{\rho}}, C)$, it can be concluded that there exists a parameter varying gain matrix $L_{1\bar{\rho}}$ such that the state estimation error $e(t)$ is asymptotically stable when $d(t) = 0$ which implies that $\lim_{t\to+\infty} r_e(t) = 0$, consequently, $r(t)$ converges asymptotically to $r_r(t) = Qf(t)$. When $d(t) \neq 0$ but bounded, the boundedness property $\|r(t) - Qf(t)\|_2 < \gamma \|d(t)\|_2$ is obtained. By minimizing γ, the distance between $r(t)$ and $Qf(t)$ is minimized which allows to obtain more accurate results.

So when the system satisfies the conditions of Theorem 3, the residual generator gain matrices $L_{2\bar{\rho}}, M_{\bar{\rho}}$ are obtained as follows

$$\begin{cases} M_{\bar{\rho}} = QR_{\bar{\rho}}^{\dagger} \\ L_{2\bar{\rho}} = F_\rho R_{\bar{\rho}}^{\dagger} \end{cases} \tag{4.70}$$

Then, in order to ensure the asymptotic convergence of the residual generator, the matrix $L_{1\bar{\rho}}$ should be designed in such a way to stabilize the matrix $(A_\rho - L_{1\bar{\rho}}C - L_{2\bar{\rho}}C_{\bar{\rho}})$ while preserving the minimum influence of $d(t)$ when $d(t) \neq 0$. Before proceeding to calculate the observer gain matrix $L_{1\bar{\rho}}$, it is important to consider the implications of the next Bounded Real Lemma (BRL)

Lemma 1

consider the following system

$$\begin{cases} \dot{e}(t) = A_{e_\rho} e(t) + E_{d_\rho} d(t) \\ r_e(t) = C_{e_\rho} e(t) + F_{d_\rho} d(t) \end{cases} \tag{4.71}$$

The system (4.71) is stable and satisfying $\|r_e(t)\|_2 < \gamma \|d(t)\|_2$ if the following LMI is satisfied

$$\begin{pmatrix} {A_{e_\rho}}^T P + P A_{e_\rho} & P E_{d_\rho} & {C_{e_\rho}}^T \\ {E_{d_\rho}}^T P & -\gamma^2 I & {F_{d_\rho}}^T \\ C_{e_\rho} & F_{d_\rho} & -I \end{pmatrix} < 0 \tag{4.72}$$

with P, a symmetric positive definite matrix.

So the gain matrix $L_{1\bar{\rho}}$ can be calculated by applying the results of BRL 1 to the error dynamics (4.69) to guarantee a quadratic performance level γ with respect to exogenous disturbance which imposes the following inequality.

$$\begin{pmatrix} (A_\rho - L_{1\bar{\rho}} C - L_{2\bar{\rho}} C_{\bar{\rho}})^T P + P(A_\rho - L_{1\bar{\rho}} C - L_{2\bar{\rho}} C_{\bar{\rho}}) & P E_\rho & (M_{\bar{\rho}} C_{\bar{\rho}})^T \\ {E_\rho}^T P & -\gamma^2 I & 0 \\ M_{\bar{\rho}} C_{\bar{\rho}} & 0 & -I \end{pmatrix} < 0 \tag{4.73}$$

As the values of $L_{2\bar{\rho}}, M_{\bar{\rho}}$ are calculated before from (4.70), then the inequality (4.73) can be transformed into an LMI and solved for the minimum value of γ using an optimization tool. This can be done by introducing a new variable $U_1 = -P L_{1\bar{\rho}}$ to the inequality (4.73) as previously done in 4.2.3 and then solve the resulting LMI for the minimum γ such that P is a positive definite matrix. Finally, the gain matrix $L_{1\bar{\rho}}$ can be obtained from

$$L_{1\bar{\rho}} = -P^{-1} U_1 \tag{4.74}$$

Solution to case2 in a similar way, by combining the residual generator (4.42) with the system model matching case2, the error dynamics becomes as follows

$$\begin{cases} \dot{e}(t) = (A_\rho - L_{1\bar{\rho}} C - L_{2\bar{\rho}} C_{\bar{\rho}})\, e + (F_\rho - L_{2\bar{\rho}} R_{\bar{\rho}})\, f(t) + (E_\rho - L_{2\bar{\rho}} D_{\bar{\rho}})\, d(t) \\ r_e(t) = M_{\bar{\rho}} C_{\bar{\rho}} e(t) + (M_{\bar{\rho}} R_{\bar{\rho}} - Q)\, f(t) + M_{\bar{\rho}} D_{\bar{\rho}} d(t) \end{cases} \tag{4.75}$$

If the system satisfies the rank conditions of Theorem 3, then there exist two parameter varying gain matrices $M_{\bar{\rho}}$ and $L_{2\bar{\rho}}$ which can be calculated from (4.70) such that the fault effect is decoupled from the error dynamics and

the differential equation (4.75) reduces to

$$\begin{cases} \dot{e}(t) = (A_\rho - L_{1\bar{\rho}}C - L_{2\bar{\rho}}C_{\bar{\rho}})\, e + (E_\rho - L_{2\bar{\rho}}D_{\bar{\rho}})\, d(t) \\ r_e(t) = M_{\bar{\rho}}C_{\bar{\rho}}e(t) + M_{\bar{\rho}}D_{\bar{\rho}}d(t) \end{cases} \tag{4.76}$$

Under the observability (or at least detectability) of the pair $(A_\rho - L_{2\bar{\rho}}C_{\bar{\rho}}, C)$, there exists a parameter varying matrix $L_{1\bar{\rho}}$ such that $\|r(t) - Qf(t)\|_2 < \gamma \|d(t)\|_2$. In addition, when $d(t)$ is minimized the transfer from $d(t)$ to $r_e(t)$ is minimized and then the distance between $r(t)$ and $Qf(t)$ is minimized as well. Similar to the previous case the gain matrix $L_{1\bar{\rho}}$ can be calculated by applying the results of BRL 1 on the error dynamics (4.76) to obtain the following inequality

$$\begin{pmatrix} (A_\rho - L_{1\bar{\rho}}C - L_{2\bar{\rho}}C_{\bar{\rho}})^T P + P(A_\rho - L_{1\bar{\rho}}C - L_{2\bar{\rho}}C_{\bar{\rho}}) & P\,(E_\rho - L_{2\bar{\rho}}D_{\bar{\rho}}) & (M_{\bar{\rho}}C_{\bar{\rho}})^T \\ (E_\rho - L_{2\bar{\rho}}D_{\bar{\rho}})^T P & -\gamma^2 I & (M_{\bar{\rho}}D_{\bar{\rho}})^T \\ M_{\bar{\rho}}C_{\bar{\rho}} & M_{\bar{\rho}}D_{\bar{\rho}} & -I \end{pmatrix} < 0 \tag{4.77}$$

The same change of variables trick can be used by introducing a new variable $U_1 = -PL_{1\bar{\rho}}$ which transforms the inequality (4.77) to an LMI and solve it for a positive definite matrix P which implies the minimum value of γ as an optimization function.

Solution to case3 can be tackled in a similar way to case2 using $\bar{d}(t)$ instead of $d(t)$ and ensuring that $d(t)$ again belongs to Sobolev space as mentioned before.

$\mathcal{H}_-/\mathcal{H}_\infty$ **technique** If the system is not convenient with any of theorems 2 or 3 (the faults and disturbances can't be decoupled from the model), the problem can be solved using the $\mathcal{H}_-/\mathcal{H}_\infty$ technique. The idea is to maximize the fault effect on the residual while minimizing the effect of exogenous disturbances by ensuring a lower bound for the $\mathcal{H}_-$ norm from fault to residual which is larger than the upper bound of the $\mathcal{H}_\infty$ norm from the disturbances to residual. The problem of regularity assumption mentioned previously in 4.2.3 that arises in case of actuators faults only while solving the problem of $\mathcal{H}_-/\mathcal{H}_\infty$ no longer exists, as the auxiliary output $\tilde{y}(t)$ obtained after differentiating the output signal according to the relative degree notion, is directly affected by the actuators fault.

The algorithm presented here is similar to that discussed before in 4.2.3 but here it is investigated for an LPV system model. In order to demonstrate the fundamentals of this technique consider the error dynamics resulting from applying the residual generator (4.42) to any of the previously cited cases is given in the following general form

$$\begin{cases} \dot{e}(t) = A_{e_\rho}e(t) + E_{f_\rho}f(t) + E_{d_\rho}d(t) \\ r_e(t) = C_{e_\rho}e(t) + F_{f_\rho}f(t) + F_{d_\rho}d(t) \end{cases} \tag{4.78}$$

Then, the objective of the $\mathcal{H}_-/\mathcal{H}_\infty$ fault detection observer is achieved under the following conditions

$$\begin{cases} ||T_{rd}||_\infty \leq \gamma_r \\ ||T_{rf}||_- \geq \beta \end{cases} \tag{4.79}$$

Thus, the problem is to find the matrices $L_{1\bar{\rho}}, L_{2\bar{\rho}}$ and $M_{\bar{\rho}}$ that maximizes β and minimizes γ_r such that the observer is stable. Such a problem can be expressed mathematically by the following three LMIs.

1. adequate time response

$$A_{e\rho}{}^T P + P A_{e\rho} + 2\zeta_o P < 0 \tag{4.80}$$

   where ζ_o is a positive scalar to be chosen to determine the observer time constant.

2. disturbance effect minimization $||T_{rd}||_\infty \leq \gamma$

$$\begin{pmatrix} A_{e\rho}{}^T P + P A_{e\rho} & P E_{d\rho} & C_{e\rho}{}^T \\ E_{d\rho}{}^T P & -\gamma_r^2 I & F_{d\rho}{}^T \\ C_{e\rho} & F_{d\rho} & -I \end{pmatrix} < 0 \tag{4.81}$$

3. fault effect maximization $||T_{rf}||_- \geq \beta$

$$\begin{pmatrix} A_{e\rho}{}^T P + P A_{e\rho} & P E_{f_\rho} & -C_{e\rho}{}^T \\ E_{f_\rho}{}^T P & \beta^2 I & -F_{f_\rho}{}^T \\ -C_{e_\rho} & -F_{f_\rho} & I \end{pmatrix} < 0 \tag{4.82}$$

Thanks to the convexity property of the proposed LPV model, if the stated LMIs are satisfied at the LPV model vertices, then they hold for all possible trajectories of the varying parameter $\rho(t)$ see Theorem 1. In addition, the existence of the inequality (4.80) within the solution ensures the quadratic detectability of the LPV system see [104]. The solution based on $\mathcal{H}_-/\mathcal{H}_\infty$ for each of the previously cited system cases follows the same procedure. First, we combine the residual generator (4.42) with the system model to calculate the error dynamics differential equation. Then, we evaluate the error dynamics matrices by comparing (4.78) with the obtained error dynamics. Finally, the set of LMIs presented in 4.3.2 is solved using a semi-definite programming tool like YALMIP [59] based on a solver as SeDuMi or Mosek. This procedure is well known in LPV systems after transforming it in a polytopic form with a change of variables to establish the corresponding LMI constraints (the reader can refer to [26]). The results of deploying such an approach in quadrotor sensors and actuators fault diagnosis is demonstrated by simulation in section 4.3.5.

Example 3 *consider again the LTI system* (4.57) *with the same matrices in* (4.58) *except for* E *which is given by*

$$E_\rho = \begin{pmatrix} 1 \\ 0 \\ 0 \end{pmatrix} \tag{4.83}$$

Now the system corresponds to case2 satisfying the conditions of Theorem 3 so the gain matrices L_1, L_2, M *are calculated twice, once according to Theorem 3 while the other following* $\mathcal{H}_-/\mathcal{H}_\infty$ *giving the results shown in figure 4.9. Figures 4.9a and 4.9b give similar responses for fault estimation where the exact convergence is achieved in the absence of the disturbances (dashed red line). While the obtained residual signal during the disturbance existence (dashed green line) indicates that their magnitude is reduced to about* 30% *of their real value which proves the capabilities of the proposed algorithms. However, the calculation time of the gain matrices according to Theorem 3 is very worthy and promising for the real-time application of such a residual generator.*

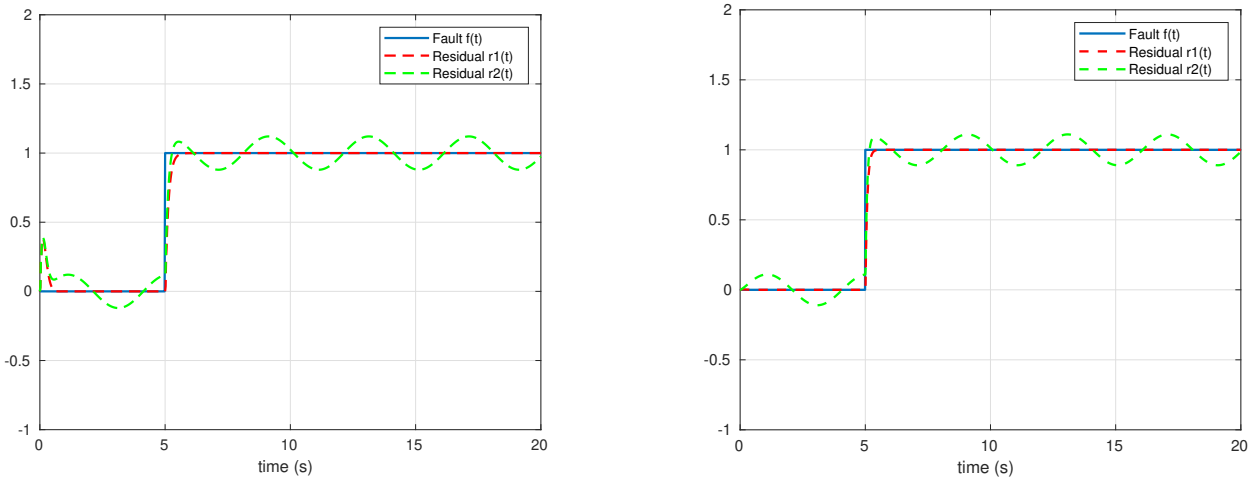

(a) Theorem 3

(b) $\mathcal{H}_-/\mathcal{H}_\infty$ technique

Figure 4.9: Fault estimation for LTI system

Example 4 *consider again the LPV system* (4.41) *with the same matrices in* (4.60) *except for* E_ρ *which will be as following*

$$E_\rho = \begin{pmatrix} 1 \\ 0 \\ 0 \end{pmatrix} \tag{4.84}$$

Now the system corresponds to case2 satisfying the conditions of Theorem 3 so the same procedure is followed as for the LTI system by calculating the gain matrices twice using Theorem 3 and $\mathcal{H}_-/\mathcal{H}_\infty$ *technique. The results shown in figure 4.10 prove that while the disturbance is set to be zero the residual signal (dashed red line) converges*

precisely to the fault. However, in case of disturbance existence, the residual signal (dashed green line) converges asymptotically to the fault with minimization to the disturbance effect. Moreover, the residual signal is affected in this case by the behavior of the varying parameter on which the fault matrix depend but such an effect doesn't prohibit the fault estimation performed.

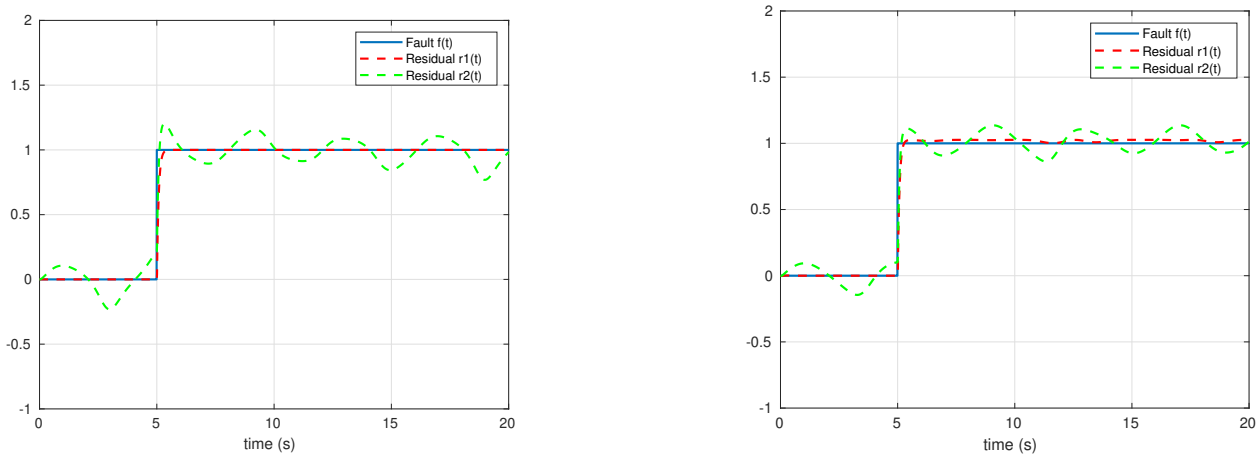

(a) Theorem 3

(b) $\mathcal{H}_-/\mathcal{H}_\infty$ technique

Figure 4.10: Fault estimation for LPV system

4.3.3 Quadrotor actuators fault diagnosis

In this section, we aim to apply the results obtained in section 4.3.2 for analyzing and estimating the quadrotor possible actuator faults during the existence of exogenous perturbations and measurement noise as illustrated by the schematic shown in figure 4.11. As previously mentioned, while investigating actuators faults it is practical to consider the attitude and altitude dynamics only as they are directly influenced by the control inputs.

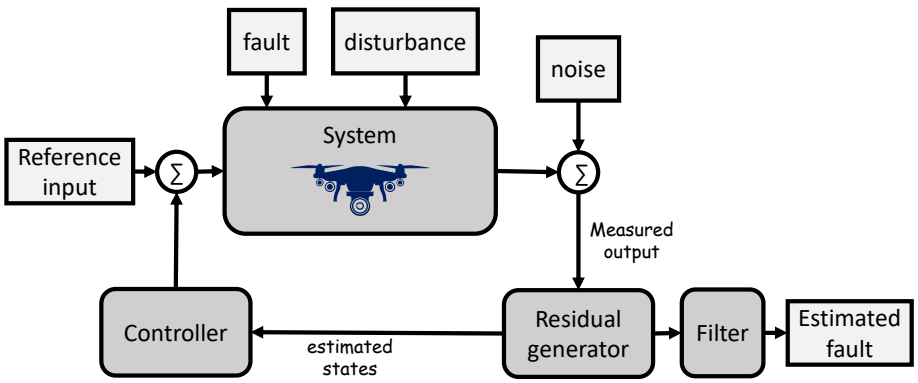

Figure 4.11: Actuators fault diagnosis schematic

So consider the quadrotor quasi-LPV model representing the attitude and altitude dynamics including the effect of actuators fault and exogenous disturbance detailed in 2.3.4 is given by the following state space form

$$\begin{cases} \dot{x}(t) = A_\rho x(t) + B_\rho u(t) + Ff(t) + Ed(t) \\ y(t) = Cx(t) + Du(t) \end{cases} \tag{4.85}$$

where the state vectors and the varying parameter matrices are demonstrated in section 2.3.4. Note that the work presented here is limited for a strictly proper system (which coincides with the quadrotor model that doesn't have a direct effect on the input on the output) to avoid input signal differentiation, thus the feed-forward matrix $D = 0$. After calculating the fault and disturbance relative degrees following 4.3.1, it is found that $\lambda_f = \lambda_d = 1$ so the system is following case2 where the fault and disturbance effect appear in the first derivative of the output which is described by

$$\dot{y}(t) = C\dot{x}(t) = CA_\rho x(t) + CB_\rho u(t) + CFf(t) + CEd(t) \tag{4.86}$$

Fortunately, the fault relative degree $\lambda_f = 1$ such that the control input signal doesn't have to be differentiated, however, if this not the case, the control input derivatives should be estimated for calculating the auxiliary output as illustrated in [26]. Thus, the auxiliary output vector can be given by

$$\tilde{y}(t) = \begin{bmatrix} y(t) \\ \dot{y}(t) \end{bmatrix} = \begin{bmatrix} Cx(t) \\ CA_\rho x(t) + CB_\rho u(t) + CFf(t) + CEd(t) \end{bmatrix} \tag{4.87}$$

or represented in the following compact form

$$\tilde{y}(t) = C_{\bar{\rho}} x(t) + B_{\bar{\rho}} u(t) + R_{\bar{\rho}} f(t) + D_{\bar{\rho}} d(t) \tag{4.88}$$

where

$$C_{\bar{\rho}} = \begin{bmatrix} C \\ CA_\rho \end{bmatrix}, B_{\bar{\rho}} = \begin{bmatrix} 0 \\ CB_\rho \end{bmatrix}, R_{\bar{\rho}} = \begin{bmatrix} 0 \\ CF \end{bmatrix}, D_{\bar{\rho}} = \begin{bmatrix} 0 \\ CE \end{bmatrix} \tag{4.89}$$

are auxiliary output matrices with appropriate dimensions and $\bar{\rho}(t)$ represents the vector of the parameters $\rho(t)$ and their time derivatives. Hence, the proposed residual generator for fault diagnosis is similar to (4.42) but including the control input vector $u(t)$ and can be given by

$$\begin{cases} \dot{\hat{x}}(t) = A_\rho \hat{x}(t) + B_\rho u(t) + L_{1\bar{\rho}} \left(y(t) - \hat{y}(t) \right) + L_{2\bar{\rho}} \left(\tilde{y}(t) - \hat{\tilde{y}}(t) \right) \\ \hat{y}(t) = C\hat{x}(t) \\ \hat{\tilde{y}}(t) = C_{\bar{\rho}} \hat{x}(t) + B_{\bar{\rho}} u(t) \\ r(t) = M_{\bar{\rho}} \left(\tilde{y}(t) - \hat{\tilde{y}}(t) \right) \end{cases} \tag{4.90}$$

By checking the conditions of theorems 2 and 3 using the deduced state matrices, the system is found to be satisfying the conditions of Theorem 3 only. So exact convergence of the residual signal is not ensured, however, asymptotic convergence of the residual signal to the fault is guaranteed by applying the results of Theorem 3. Through combining the system model (4.85) and the residual generator (4.90), the resulting error dynamics is matching that obtained before while investigating the application of Theorem 3 results on a system of case2. So the solution provided in 4.3.2 can be used to obtain the gain matrices $L_{1\bar{\rho}}, L_{2\bar{\rho}}$ and $M_{\bar{\rho}}$ which result in asymptotic convergence of the residual signal to the fault.

Post band-pass filter

As one can notice from figure 4.11, there exists a post-filter dedicated for further refinement of the residual signal obtained to indicate precisely the system faults. The idea of using a post filter is presented in [97] where the model-based observer is designed for state estimation only then the filter is introduced to the augmented system dynamics such that it can perform fault estimation. It is obviously not the same case as the residual generator presented here since it can successfully estimate the fault directly thanks to the existence of the virtual residual signal. However, the system may encounter two or more simultaneous actuator faults so the proposed post band-pass filter is used to identify the expected fault upon the knowledge of system behavior and environment nature. For example, the brushless motors of the quadrotor can induce a high-frequency vibration noise due to their high rotation speeds. The effect of such vibration can be regarded by the residual generator as an actuator fault, but this is not an accurate result. Therefore, the existence of such a filter will prohibit the misleading implications of faults that are out of the band-pass filter bandwidth. Consider the band-pass filter is given by the following state space form

$$\begin{cases} \dot{x}_h(t) = A_h x_h(t) + B_h r(t) \\ r_f(t) = C_h x_h(t) + D_h r(t) \end{cases} \tag{4.91}$$

where r_f is the filtered residual signal, x_h is the filter state vector and the matrices A_h, B_h, C_h, D_h are filter gains whose values depend on the chosen cutoff frequencies as following. Consider the band-pass filter has a second order transfer function given by

$$\frac{r_f(s)}{r(s)} = \frac{2\zeta\omega_n s}{s^2 + 2\zeta\omega_n s + \omega_n^2} \tag{4.92}$$

where ω_n is the filter natural frequency and ζ is the filter damping factor. By means of state space realization the filter gain matrices in (4.91) are found to be as following

$$A_h = \begin{bmatrix} 0 & 1 \\ -\omega_n^2 & -2\zeta\omega_n \end{bmatrix}, B_h = \begin{bmatrix} 0 \\ 2\zeta\omega_n \end{bmatrix} \tag{4.93}$$

$$C_h = \begin{bmatrix} \frac{\omega_n}{2\zeta} & 0 \end{bmatrix}, D_h = \begin{bmatrix} 0 \end{bmatrix} \tag{4.94}$$

The use of such a filter will allow the system to cutoff or minimize the signals that have a frequency out of the filter bandwidth which is given by $B_w = \zeta\omega_n$. The importance of using such a band-pass filter is demonstrated through the simulation deducted in section 4.3.5 where the system is able to distinguish effectively between two simultaneous faults imposed on it.

4.3.4 Quadrotor sensors fault diagnosis

After investigating how to apply the methodology proposed for fault diagnosis to estimate actuators faults, it is practical to deploy the same algorithm for sensors fault diagnosis. The problem addressed here is illustrated by the schematic shown in figure 4.12 where the residual generator aims to identify sensors faults in presence of exogenous disturbances and measurement noise.

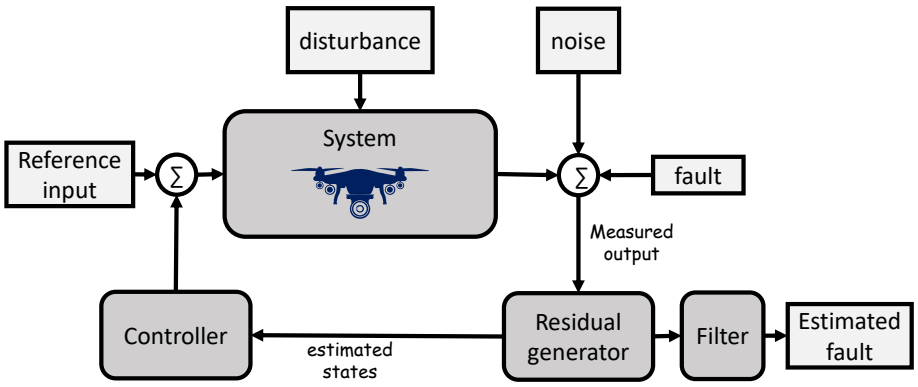

Figure 4.12: Sensors fault diagnosis schematic

As discussed earlier in section 2.3.5, as the quadrotor LPV model contains 3 subsystems, it is useful to handle each subsystem sensor faults separately. Such that a unique residual generator is introduced for each of the subsystems considering the specified faulty submodel dynamics presented in 2.3.5. In order to apply the auxiliary output approach presented in 4.3.2 for sensor fault diagnosis, consider the following general state space representation of the LPV subsystem

$$\begin{cases} \dot{x}(t) = A_\rho x(t) + B_\rho u(t) + Ed(t) \\ y(t) = Cx(t) + Ff(t) \end{cases} \tag{4.95}$$

where the state vectors and varying parameter matrices are detailed in section 2.3.5 for each subsystem of the quadrotor model. Note that since the altitude subsystem doesn't include varying parameters it can be handled as

an LTI subsystem corresponding to a frozen LPV model during residual generator synthesis. by defining a new state $\epsilon(t) = \int_0^t y(\tau)\, d\tau, \epsilon(t) \in \mathbb{R}^{n_y}$ such that

$$\dot{\epsilon}(t) = Cx(t) + Ff(t) \tag{4.96}$$

Through combining the system (4.95) with the proposed integral state, the following augmented system can be constructed

$$\begin{cases} \dot{x}_a(t) = \bar{A}_\rho x_a(t) + \bar{B}_\rho u(t) + \bar{E}_\rho d(t) + \bar{F}_\rho f(t) \\ y_a(t) = \bar{C}_\rho x_a(t) \end{cases} \tag{4.97}$$

where

$$x_a(t) = \begin{bmatrix} x(t) \\ \epsilon(t) \end{bmatrix}, \bar{A}_\rho = \begin{bmatrix} A_\rho & 0 \\ C & 0 \end{bmatrix}, \bar{B}_\rho = \begin{bmatrix} B_\rho \\ 0 \end{bmatrix}, \bar{E}_\rho = \begin{bmatrix} E \\ 0 \end{bmatrix}, \bar{F}_\rho = \begin{bmatrix} 0 \\ F \end{bmatrix}, \bar{C}_\rho = \begin{bmatrix} 0 & I_{n_y} \end{bmatrix} \tag{4.98}$$

represent the augmented system state vector and parameter varying matrices with appropriate dimensions.

This procedure is deployed in [101] to design an observer with an additive integral action while the observability of the pair $(\bar{A}_\rho, \bar{C}_\rho)$ is checked by theorem 4. In addition, as will be illustrated later, the methodology followed in this section to assign the observer gains is based on $\mathcal{H}_-/\mathcal{H}_\infty$ approach 4.3.2. Through this approach since the obtained feasible solution includes satisfying the Lyapunov inequality (4.80), the LPV system is guaranteed to be quadratically detectable.

Using such an integral action results in the following two main advantages for the residual generator design:

- better representation of the disturbances effect on the system measurement.
- avoiding the fault signal derivative estimation for auxiliary output computing (another approach for fault derivative estimation using Proportional Multiple Integral (PMI) can be found in [105])

As mentioned before, to minimize $\mathcal{H}_\infty$ norm the regularity assumption should be satisfied, the common way adopted is to introduce a term modeling the disturbance effect on the output. However, a promising method proposed in [26] based on an extended output of the system containing the output and its time derivatives named the auxiliary output $\tilde{y}(t)$. Such output provides more realistic impact of the disturbances, while these time derivatives can be robustly attained by the recent algorithms of signal differentiation, see for example high-gain differentiators [98]. Consider the augmented system (4.97) its auxiliary output $\tilde{y}(t)$ is given by

$$\tilde{y}(t) = \begin{bmatrix} y_a(t) \\ \dot{y}_a(t) \end{bmatrix} = \begin{bmatrix} \bar{C}_\rho x_a(t) \\ \bar{C}_\rho \dot{x}_a(t) \end{bmatrix} \tag{4.99}$$

or in another form

$$\tilde{y}(t) = C_{\bar{\rho}} x_a(t) + B_{\bar{\rho}} u(t) + R_{\bar{\rho}} f(t) + D_{\bar{\rho}} d(t) \tag{4.100}$$

where

$$C_{\bar{\rho}} = \begin{bmatrix} \bar{C}_\rho \\ \bar{C}_\rho \bar{A}_\rho \end{bmatrix}, B_{\bar{\rho}} = \begin{bmatrix} 0 \\ \bar{C}_\rho \bar{B}_\rho \end{bmatrix}, R_{\bar{\rho}} = \begin{bmatrix} 0 \\ \bar{C}_\rho \bar{F}_\rho \end{bmatrix}, D_{\bar{\rho}} = \begin{bmatrix} 0 \\ \bar{C}_\rho \bar{E}_\rho \end{bmatrix} \tag{4.101}$$

are system matrices with appropriate dimensions and $\bar{\rho}(t)$ represents the vector of the parameters $\rho(t)$ and their time derivatives.

Since sensor faults are considered, then their effect appear in the 1^{st} output time derivative (relative degree of fault to output is $\lambda_f = 1$). Fortunately regarding the quadrotor LPV model the disturbance affect the 1^{st} output time derivative, thus the regularity condition is satisfied in the auxiliary output (4.99). Note if another system has a relative degree from disturbance to output $\lambda_d > 1$, then it is necessary to estimate input and fault derivatives, such an issue can be interesting for future work. So after defining the augmented system affected by sensors faults (4.97) and its auxiliary output (4.100), then the residual generator proposed is similar to the general form presented in (4.42) and given by

$$\begin{cases} \dot{\hat{x}}_a(t) = \bar{A}_\rho \hat{x}_a(t) + \bar{B}_\rho u(t) + L_{1\bar{\rho}} \left(y_a(t) - \hat{y}_a(t) \right) + L_{2\bar{\rho}} \left(\tilde{y}(t) - \hat{\tilde{y}}(t) \right) \\ \hat{y}_a(t) = \bar{C}_\rho \hat{x}_a(t) \\ \hat{\tilde{y}}(t) = C_{\bar{\rho}} \hat{x}_a(t) + B_{\bar{\rho}} u(t) \\ r(t) = M_{\bar{\rho}} \left(\tilde{y}(t) - \hat{\tilde{y}}(t) \right) \end{cases} \tag{4.102}$$

After computing the auxiliary output $\tilde{y}(t)$ for the quadrotor model subsystems defined in section 2.3.5, each subsystem is found to have equal relative degrees for fault and disturbances as illustrated earlier. Thus, the subsystems are matching a system auxiliary output represented by case2 where the faults and disturbances appear together in the differentiated system output. However, the subsystems are not satisfying either the conditions of Theorem 2, nor Theorem 3 which implies that the residual generator can't ensure exact or asymptotic convergence of the residual signal to the fault. Therefore, the $\mathcal{H}_-/\mathcal{H}_\infty$ approach presented in section 4.3.2 is used to obtain the gain matrices $L_{1\bar{\rho}}, L_{2\bar{\rho}}$, and $M_{\bar{\rho}}$ in a way that guarantees minimum effect of the disturbance on the residual signal. The same band-pass filter introduced in 4.3.3 is used for refinement of the resulting residual signal such that it is affected only by sensors faults which have a frequency within the filter's bandwidth. The results of deploying such an approach in quadrotor sensors fault estimation is demonstrated by simulation in section 4.3.5.

4.3.5 Simulation results

Actuators fault estimation

After computing the auxiliary output $\tilde{y}(t)$ for the quasi-LPV quadrotor model, the system is found to be matching case2 with relative degrees $\lambda_f = \lambda_d = 1$ and satisfying the conditions of Theorem 3, so the solution provided in section 4.3.2 can be used to obtain the gain matrices $L_{1\bar{\rho}}, L_{2\bar{\rho}}$ and $M_{\bar{\rho}}$. Note that the system may satisfy conditions

of theorem 2 or correspond to any of the three cases mentioned before based on the matrices $F(\rho(t)), E(\rho(t))$ and $C(\rho(t))$, thus depending on the system model besides the types of faults and disturbances considered, that's why a general solution was provided in section 4.3.2.

The simulation conducted here is based on the quasi-LPV quadrotor model including attitude and altitude dynamics 2.3.4 and accompanied by a self-scheduled LPV controller proposed in 3.5. In order to reveal the effectiveness of the new approach the same gains are calculated using $\mathcal{H}_-/\mathcal{H}_\infty$ technique given in 4.3.2 providing some constants to guarantee the controller, the observer, and the filter stability. Choosing the values of the constants is an iterative process according to the system model and desired response characteristics, in our case we reached the following design parameters, $\rho^{min} = -0.5\ rad/s, \rho^{max} = 0.5 rad/s, \kappa = 1.1, \zeta_o = 4, \zeta = 2$, and $\omega_n = 20\ Hz$. After introducing the selected constants and following the proposed methodology for solving the LMIs presented in sections 4.3.2 and 4.3.2 using YALMIP-MOSEK optimization solver, the obtained disturbance rejection levels from the auxiliary output approach and $\mathcal{H}_-/\mathcal{H}_\infty$ technique are $\gamma = 1.0532, \gamma_r = 1.0925$, respectively, while the minimum fault effect is $\beta = 1.1957$

For the sake of testing the performance of the proposed approaches the simulation is done with initial conditions of the state vector $x(0) = [0\ 0\ 0\ 1\ 0\ 0\ 0\ 0]^T$ and estimated state vector $\hat{x}(0) = .5$, the disturbance vectors $d_1(t), d_2(t)$ are sinusoidal waves with a magnitude 0.5 and frequency $0.8\ rad/s$ and finally the additive measurement noise $n_s(t) \in [-0.03, 0.03]$ and $n_v(t) \in [-.06, .06]$ represent states and their derivatives noise having a sample time of $0.03, 0.01\ s$, respectively. In addition, the reference values of the states which the system has to follow are given by

$$\phi_r(t) = \begin{cases} 0 & t < 4\ s \\ 1\ rad & 4 \leq t \leq 7\ s \\ 0 & t > 7\ s \end{cases}, \quad \theta_r(t) = \begin{cases} 0 & t < 15\ s \\ 1\ rad & 15 \leq t \leq 18\ s \\ 0 & t > 18\ s \end{cases}, \quad z_r(t) = \begin{cases} 0 & t < 2\ s \\ 2\ m & t > 2\ s \end{cases} \tag{4.103}$$

Firstly, the residual generator is simulated in the fault-free case to test its power in recovering system states, attenuating measurement noise, and rejecting exogenous disturbance. The results shown in figure 4.13 prove the capabilities of the observer in providing the controller with estimated states $\hat{x}(t)$ smooth enough to achieve adequate reference tracking which is indicated in figure 4.13a.

In figure 4.13b, the estimation error is affected by the measurement noise, however, it converges asymptotically to zero after a while due to the initial conditions of the system. The shown response time of the observer is suitable for control and can be further decreased by increasing the value of the parameter ζ_o, but this comes at cost of higher overshoot. As per figure 4.13c, the main task of the residual generator is well accomplished as the residual signals are slightly affected (order of magnitude 10^{-3}) by both initial conditions and exogenous disturbance beginning at time $t = 20s$, thus in case of actual fault these effects will completely disappear compared to the fault magnitude as we can notice from figure 4.14a.

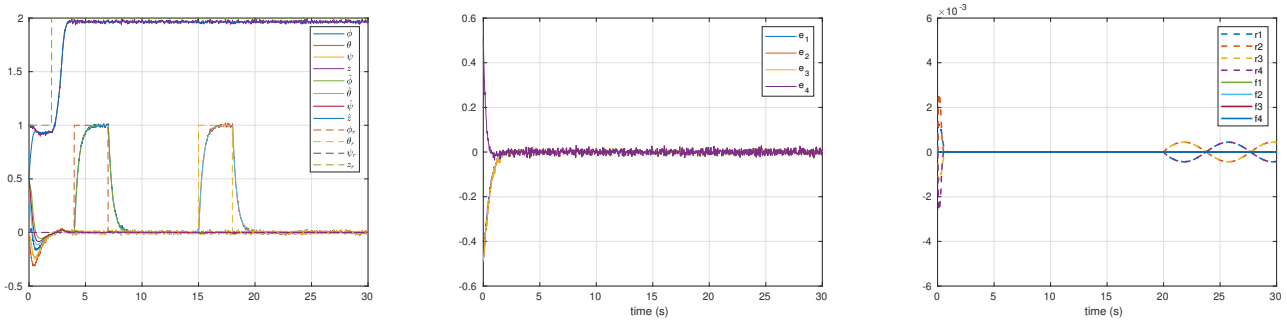

(a) system states (b) estimation error (c) faults vs residuals

Figure 4.13: Fault free case

In figure 4.14, one can find the response of the residual generator for fault estimation in case of 40% loss of efficiency in the $1st$ actuator indicated by equation (4.104) using both the new proposed approach and $\mathcal{H}_-/\mathcal{H}_\infty$ technique. The emerging sinusoidal wave after fault occurrence illustrates that the residual generator based on $\mathcal{H}_-/\mathcal{H}_\infty$ technique shown in figure 4.14b is highly affected by the instability of the system due to actuator loss of efficiency which is eliminated by the newly developed approach. A simple comparison between the two approaches is given in table 4.3 based on synthesizing the simulation results.

$$f_1(t) = \begin{cases} 0 & t < 4\ s \\ 0.4 & 4 \leq t \leq 6\ s \\ 0 & t > 6\ s \end{cases} \tag{4.104}$$

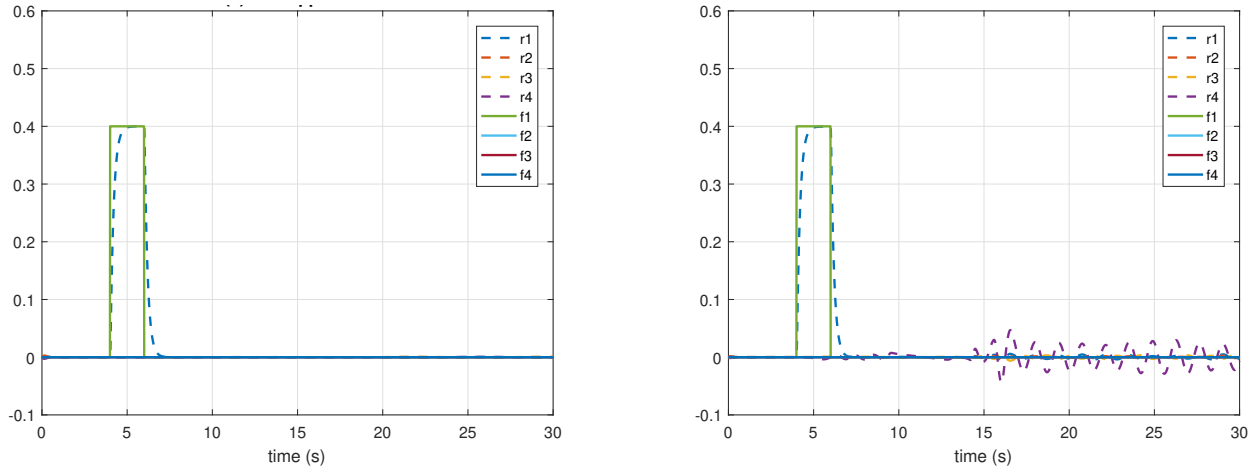

(a) Solution following Theorem 3 (b) $\mathcal{H}_-/\mathcal{H}_\infty$ technique

Figure 4.14: New approach vs $\mathcal{H}_-/\mathcal{H}_\infty$ technique

One very essential problem of quadrotors is battery level degradation during flight, the residual generator proposed here provides a powerful means to estimate exactly the battery level as indicated in figure 4.15, thus it enables substituting the loss of thrust and altitude during the whole operational time which is automatically provided by the

	New approach	$\mathcal{H}_-/\mathcal{H}_\infty$ technique
computational time	less	long
code optimization	shorter	long
state recovery	exact	exact
noise attenuation	enhanced	acceptable
fault estimation	enhanced	acceptable

Table 4.3: New approach vs $\mathcal{H}_-/\mathcal{H}_\infty$ technique

FTC law discussed in the next chapter.

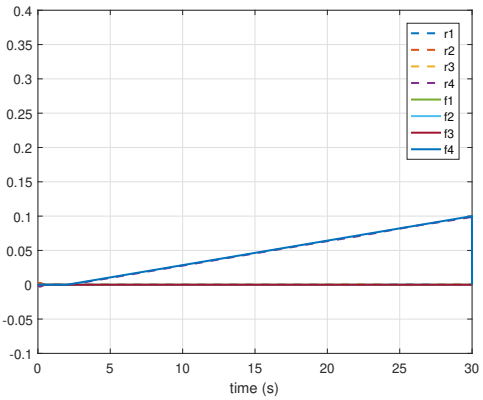

Figure 4.15: Battery level estimation

Until now the proposed residual generator has proven its capability in fault diagnosis, but what about the case when two different faults come together? Here arises the importance of the post-band-pass filter. Figure 4.16 shows the case of a loss of efficiency by 40% from $4s$ to $6s$ followed by a sinusoidal fault with a magnitude of 0.1 and high frequency $50\ Hz$ as demonstrated by equation (4.105). The results illustrate that while using the filter, however, there is a slight time delay, the second undesired fault is minimized to a magnitude of 0.01 highlighting the main step fault which lies in the expected band of frequencies.

$$f_1(t) = \begin{cases} 0 & t < 4\ s \\ 0.4 & 4 \leq t \leq 6\ s \\ 0 & 6 \leq t \leq 15\ s \\ 0.1 \sin 50t & t > 15\ s \end{cases} \tag{4.105}$$

Sensors fault estimation

Note as the quadrotor model doesn't convey theorems 2 and 3, the following two LPV system examples are investigated to check the validity of these assumptions while handling the sensors faults.

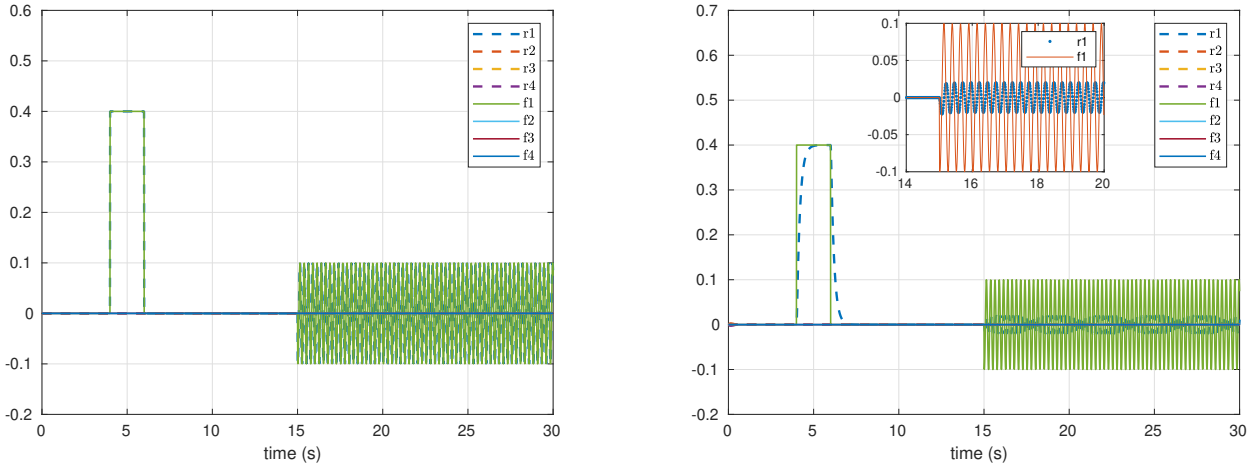

(a) without filter

(b) with filter

Figure 4.16: Filtered vs non-filtered residual signal

Example 5 *Consider now the LPV system* (4.95) *defined by the following matrices*

$$A_\rho = \begin{pmatrix} 2 & 1 & \rho(t) \\ 3 & 0 & 6 \\ -\rho(t) & -5 & -\rho(t) \end{pmatrix}, B_\rho = \begin{pmatrix} 0 \\ 1 \\ 0 \end{pmatrix}, E = \begin{pmatrix} 0 \\ 0 \\ 1 \end{pmatrix}, C = \begin{pmatrix} 0 & 0 & 0 \\ 0 & 0 & 1 \end{pmatrix}, F = \begin{pmatrix} 1 \\ 1 \end{pmatrix} \tag{4.106}$$

and $\rho(t) \in [10, 12]$*, after following the procedure illustrated in 4.3.4 by introducing the integral action and calculating the auxiliary output, the model presented in this example is found to be corresponding to case1 and the condition of Theorem 2 is fulfilled which implies that the exact residual property is guaranteed. The matrix* $M_{\bar{\rho}}$ *is computed from* (4.52) *and given by*

$$M_{\bar{\rho}} = \begin{pmatrix} 0 & 0 & 1 & 0 \end{pmatrix} \tag{4.107}$$

As demonstrated earlier, since the exact residual convergence is satisfied, the gains $L_{1\bar{\rho}}$ *and* $L_{2\bar{\rho}}$ *can be fixed to zero. However, to ensure stability of the observer the value of the gain matrix is assigned using pole placement such that the matrix* $\left(\bar{A}_\rho - L_{1\bar{\rho}}\bar{C}_\rho - L_{2\bar{\rho}}C_{\bar{\rho}}\right)$ *has negative real eigenvalues. The results are given in figure 4.17 where figure 4.17a shows the varying parameter, the introduced perturbations, and the estimated system output which converges to the real system output despite the instability of the model. While figure 4.17b proves the exact convergence during fault estimation and complete decoupling of the residual signal from the sinusoidal disturbance when the virtual residual weighting matrix* $Q = 1$ *(dashed red line). In addition, when the weighting matrix* $Q = 5$*, the residual signal (dashed green line) confirm the ability of the residual generator to isolate the fault.*

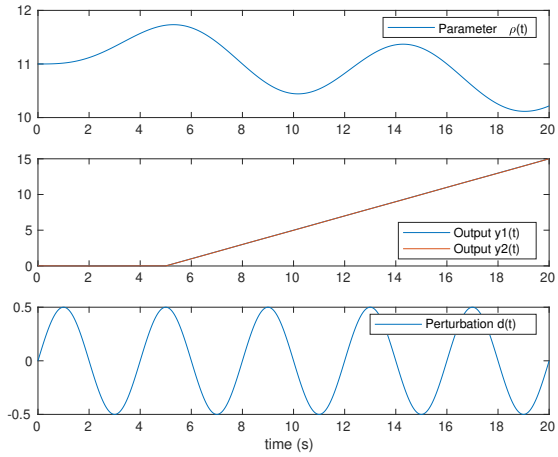

(a) varying parameter, output, and disturbance

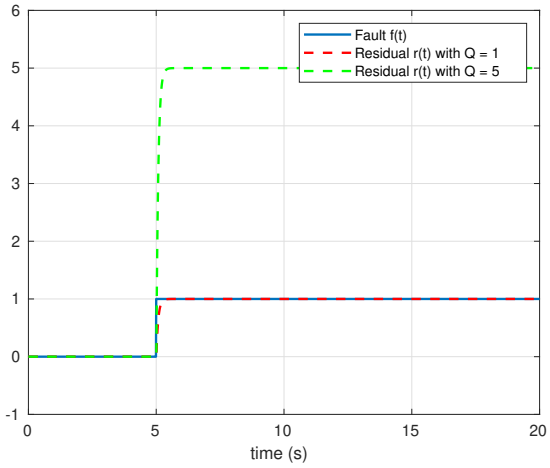

(b) resulting residual signal

Figure 4.17: Solution following Theorems 2 for LPV system

Example 6 *consider again the LPV system* (4.95) *with the same matrices in* (4.106) *except for* E *which is given by*

$$E_\rho = \begin{pmatrix} 1 \\ 0 \\ 1 \end{pmatrix} \tag{4.108}$$

Again by introducing the integral action and calculating the system auxiliary output as indicated in 4.3.4, the system is found to be corresponding to case2 satisfying the conditions of Theorem 3. So the procedure presented in 4.3.2 is followed to calculate the residual generator gain matrices. The results shown in figure 4.18 prove that while the disturbance is set to be zero (dashed red line) the residual signal convergences precisely to the fault. However, in case of disturbance existence, the residual signal converges asymptotically to the fault with minimization to the disturbance effect.

Now after discussing the advantages of the proposed auxiliary output approach for fault diagnosis, we can proceed to apply the obtained results to the quadrotor vehicle. By using Matlab Simulink with quadrotor model having the parameters detailed in B and accompanied by the LPV controller proposed in 3.5, some interesting results of the proposed residual generator are demonstrated. After computing the auxiliary output $\tilde{y}(t)$ for each of the quadrotor model subsystems presented in 2.3.5, they are found to have equal relative degrees for fault and disturbances as illustrated earlier, however, they are not satisfying the conditions of theorems 2 and 3 so the $\mathcal{H}_-/\mathcal{H}_\infty$ approach presented in section 4.3.2 is used to obtain the gain matrices $L_{1\bar{\rho}}, L_{2\bar{\rho}}$, and $M_{\bar{\rho}}$.

Choosing the constants of the Lyapunov inequalities (4.80) for each subsystem is an iterative process according to the system model and desired response characteristics, in our case we reached the following design parameters $\zeta_{o_{at}} = 6,\ \zeta_{o_{al}} = 4,\ \zeta_{o_p} = 2.4$ where $\zeta_{o_{at}},\ \zeta_{o_{al}}$, and ζ_{o_p} are representing the attitude, altitude, and position residual

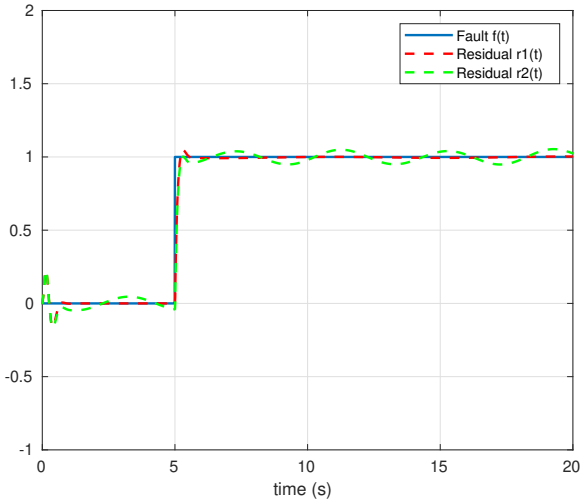

Figure 4.18: Fault estimation for LPV system

generators' decay rates, respectively. To test the performance of the proposed approach the simulation is done with initial conditions of the state vectors $x_{at}(t) = x_z = x_p = 0$ mentioned in equations (2.76), (2.87), and (2.96), respectively, while the estimated state vectors $\hat{x}_{at}(t) = .1$, $\hat{x}_z(t) = .1$, and $\hat{x}_p(t) = .05$. In addition, the additive measurement noise $n_s(t) \in [-0.03, 0.03]$ and $n_v(t) \in [-.06, .06]$ represent states and their derivatives noise having a sample time of $0.03, 0.01\ s$, respectively. Finally, the attitude and position disturbance vectors mentioned in equations 2.78 and 2.98 are described by

$$d_1(t) = \begin{cases} 0 & t \leq 20\ s \\ 0.5 \sin 0.8t & t > 20\ s \end{cases}, \quad d_2(t) = \begin{cases} 0 & t \leq 20\ s \\ 0.5 \sin 1.2t & t > 20\ s \end{cases} \tag{4.109}$$

$$d_{p1}(t) = \begin{cases} 0 & t \leq 20\ s \\ 0.1(t-20) & 20 < t < 25\ s \\ 0.5 & t \geq 25\ s \end{cases}, \quad d_{p1}(t) = \begin{cases} 0 & t \leq 20\ s \\ 0.05(t-20) & 20 < t < 25\ s \\ 0.25 & t \geq 25\ s \end{cases} \tag{4.110}$$

Such that the attitude states are subjected to sinusoidal disturbance waves while the position states are affected by wind gust disturbance.

Firstly, the residual generator is simulated in the fault-free case to test its power in recovering system states, attenuating measurement noise, and rejecting exogenous disturbance. By choosing the fault matrices such that they represent the faults of the state as illustrated in 2.3.5, The results shown in figure 4.19 prove the capabilities of the observer in providing the controller with estimated states $\hat{x}(t)$ smooth enough to achieve adequate reference tracking despite the existence of measurement noise as demonstrated by figure 4.19a.

In addition, the main task of the residual generator is well accomplished as the residual signals are very slightly affected by both initial conditions (order of magnitude $(10^{-1})^\circ$ for attitude angles and $(10^{-3})\ m$ for position states)

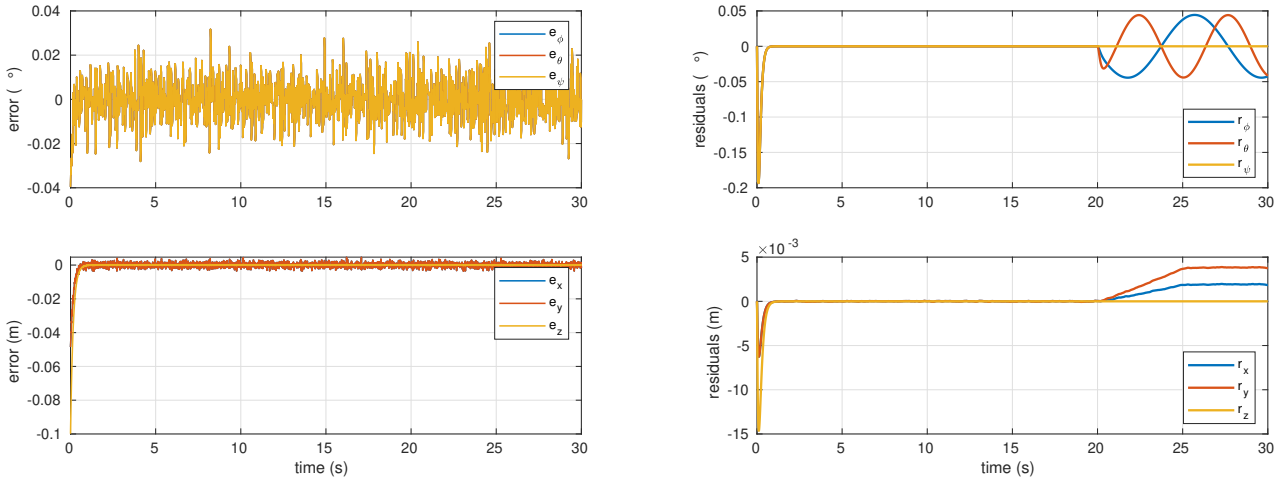

(a) estimation error

(b) residual signals

Figure 4.19: Fault free case

as indicated in figure 4.19b. While exogenous disturbance effect beginning at $20s$ is reduced to have an order of magnitude $(10^{-2})^{\circ}$ for attitude angles and $(10^{-3})\ m$ for position states, thus in case of actual fault these effects will completely disappear compared to the fault magnitude.

In order to reveal the effectiveness of the proposed $\mathcal{H}_{-}/\mathcal{H}_{\infty}$ technique 4.3.2 in fault estimation, consider the fault modeling matrix is given by $F_{at} = F_m$ mentioned in equation (2.86) such that the orientation angles states are subjected to the following sensors faults

$$f(t) = \begin{cases} 2^{\circ} & t > 10\ s \\ (2 + 0.4t)^{\circ} & t > 10\ s \\ 5^{\circ} & 10 \leq t \leq 15\ s \end{cases} \tag{4.111}$$

The fault signal (4.111) represents a bias in the reading of (ϕ), a drift of (θ) (which as mentioned before likely to happen as the IMU integrates the ($\dot{\theta}$) measurement provided by the gyroscope), and a sudden abrupt change of (ψ). The results shown in figure 4.20a demonstrate the capabilities of the residual generator in fault detection and estimation of simultaneous different faults affecting the orientation angles despite the existence of exogenous disturbances and the initial condition difference between the real system measurement and the residual generator.

Furthermore, by considering $F_{at} = F_r$ given in (2.86), the angular rates are subjected to the sensors faults given by (4.112). Such faults represent time varying gyroscope malfunction of $\dot{\phi}$ and $\dot{\theta}$ due to the structure vibrations and loose fixations of the onboard sensor while $\dot{\psi}$ is affected by sudden finite time abrupt change. Again the results shown in figure 4.20b illustrate the great potential of the proposed algorithm for the gyroscope time varying and abrupt faults estimation in spite of the large overshoot which can be reduced by choosing smaller value of the

observer time constant $\zeta_{o_{at}}$ but this will come a a cost of slower response time of the residual generator.

$$f(t) = \begin{cases} (5\sin 0.8t + 2\cos 2.4t)^\circ/s & t > 10\ s \\ (4\sin 0.5t + 3\cos t)^\circ/s & t > 10\ s \\ 10^\circ/s & 5 \leq t \leq 7\ s \end{cases} \tag{4.112}$$

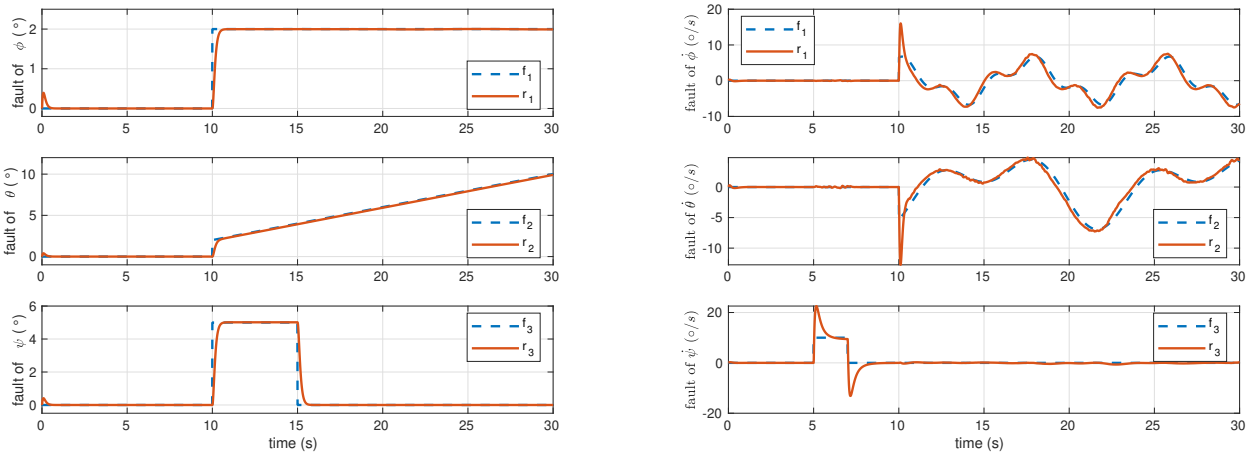

(a) attitude angles faults

(b) angular rates faults

Figure 4.20: Faults vs residuals of attitude states

After investigating the ability of the proposed residual generator in estimating the attitude angles and the angular rates faults represented by different IMU sensor malfunction scenarios, we can proceed to verify the obtained results for position sensors. As mentioned earlier, the quadrotor is commonly provided with an optical flow camera giving the 2D plane coordinates along with an ultrasonic sensor for altitude measuring. By considering the position subsystem fault modeling matrix given in equation (2.103) $F_p = F_s$ and altitude fault matrix (2.88) $F_z = [1\ 0]^T$, then the location measurements (x, y, z) are subjected to parametric sensors faults given by the following equation

$$f(t) = \begin{cases} .02\ \hat{x}\ (m) & t > 20\ s \\ .1(m) & t > 20\ s \\ -\hat{z} + \hat{z}(t_f)\ (m) & 7 \leq t \leq 9\ s \end{cases} \tag{4.113}$$

The fault signal described by equation (4.113) represent a calibration error which begins at time instant $t = 20s$ such that the x position measurement is linearly affected by a constant error value. Also the measurement in $y-$direction is influenced by a sudden bias fault beginning at time $t = 20s$ and continue until the end of simulation time. In addition, the altitude z is subjected to freezing fault given by f_3 where $t_f = 7s$ is the start time, such fault is common for ultrasonic sensors due to their measuring range limits depending on the speed of sound. For these three simultaneous faults, the residual generator results are demonstrated by figure 4.21a where the residual signals

are following the x, y position faults precisely. Also, during the existence of the freezing fault in altitude measurement, the overall system tries to stabilize itself and keeps tracking the reference altitude. Since the commanded altitude is linearly increasing at the time instant where the freezing fault emerges as indicated from equation (4.114), there is a sinusoidal behavior until the system becomes free from the fault and reaches the required altitude.

$$z_r(t) = \begin{cases} 0 & 0 \leq t \leq 5\ s \\ 0.2(t-5)\ (m) & 5 \leq t \leq 10\ s \\ 1\ (m) & t > 10\ s \end{cases} \tag{4.114}$$

On the other hand, when the freezing fault is introduced while the quadrotor is hovering at a specific altitude it doesn't affect the system and consequently the residual signal is kept zero. Finally, for testing the performance of the residual generator in estimating the velocity measurements $\dot{x}, \dot{y}, \dot{z}$, the fault modeling matrices for the altitude and position subsystems descried by equations (2.88) and (2.103) are given by $F_p = F_r$ and $F_z = [0\ 1]^T$. Consider the following fault vector

$$f(t) = \begin{cases} 0.2\ (m/s) & 15 \leq t \leq 20\ s \\ 0.1\ (m/s) & 5 \leq t \leq 10\ s \\ 0.2\ (m/s) & 10 \leq t \leq 15\ s \end{cases} \tag{4.115}$$

In this manner, the sensors' faults illustrated by equation (4.115) represent abrupt bias measurement for a finite time of $5\ s$. The results shown in figure 4.21b indicate that the residual signals are following the sensors' faults precisely despite the large overshoot which reaches 50% in $\dot{x}, \dot{y}$ residuals due to sudden change of measurement value. In addition, although the gravity effect is modeled as a disturbance on the system, it doesn't prohibit asymptotic convergence of the residual signal to the fault. The results obtained here are very promising for further sensor fault tolerant control design as the residual generator is able to identify the amount and location of fault precisely.

4.4 Conclusions

This chapter is dedicated to studying the problem of fault detection and diagnosis aiming to produce an efficient model-based observer which is able to identify the fault occurrence precisely. The purpose of such an observer is to check the conformity between the output of the nominal system model and its real output so that in case of a system fault both outputs won't have the same values. The difference between both outputs is commonly referred to as residual signals indicating the existence of system faults so the main goal of the observer design process is to develop the most accurate residual signals. After performing a detailed literature review of the methods proposed for observer design such that it can be used as a residual generator, it has been found that three types of observers and their modified forms are widely deployed while dealing with the problem of fault detection and diagnosis.

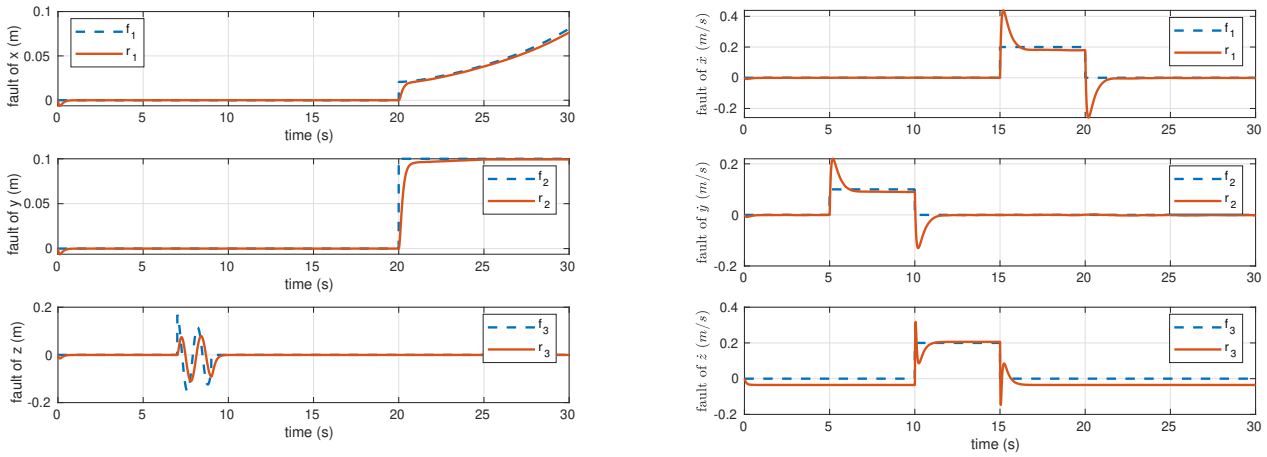

(a) position states faults

(b) velocities faults

Figure 4.21: Faults vs residuals of position states

These three observers are Lunberger type observer dedicated to the deterministic system model, Kalman filter for stochastic systems affected by Gaussian measurement noises and model uncertainties, and robust observer-based on synthesizing the $\mathcal{H}_\infty$ norm characteristics of the targeted signals. The Luenberger observer is introduced as a residual generator for the affine LTI model of the quadrotor and has proven its capabilities in fault detection through simulations where the residual signals deviate from zero indicating fault existence. Furthermore, it has been demonstrated that by advanced analysis of the magnitude and direction of the residual signals, the fault location can be specified. However, to provide an automated approach for fault isolation, a bank of Luenberger type observers are presented each one corresponding to one actuator faulty model. The idea behind the use of a bank of observers is that when the system is subjected to a fault, the residuals generated from at least on of these observers will match the faulty system model and thus the residuals generated from this observer will vanish indicating the faulty actuator. This concept is validated by a simulation of a fault scenario of the quadrotor represented by a loss of efficiency of one actuator where the main observer residuals could precisely detect the fault while the bank of observers results specify which actuator is experiencing the fault.

Despite the acceptable results obtained by a residual generator based on a Luenberger observer, it is designed to handle a deterministic system model. To ensure a wider range of applicability of the residual generator in different operating situations, one needs to consider possible model uncertainties, measurement noises, and exogenous disturbance that may affect the system during performing its task. So another approach is utilized for the design of the residual generator following the structure of a continuous-time Kalman filter. The design procedure involves penalizing the sensors' measurements or the system model through introducing weighting matrices to solve the algebraic Riccati equation seeking an optimal value of the observer gain matrix. Such a methodology produces very efficient residual signals for fault detection and isolation despite the existence of measurement noise. However, it

is more convenient for the system affected by Gaussian white measurement noise and model uncertainties which again limits its applicability for a system experiencing an unknown signal influence.

In order to design a robust observer which is powerful enough to overcome the effect of exogenous signals, the quadratic performance of the system under the effect of such signals has to be taken into consideration. So a residual generator is designed aiming at minimization the $\mathcal{H}_\infty$ norm from disturbances to residuals and maximization of the $\mathcal{H}_-$ norm from fault to residuals results in more robustness against perturbations and sensitivity towards faults. In that manner, the residual generator guarantees that the minimum effect of the fault on the residuals is higher than the exogenous signals effect such that the observer can define correctly whether the vehicle is subjected to some external temporary disturbances or it is experiencing an actuator partial or complete loss. Consequently, a wind effect model besides actuators fault effect model is introduced for the states and outputs of the system to satisfy the regularity condition which is essential for ensuring the feasibility of the proposed LMIs that characterize the quadratic performance of the observer. The effectiveness of the proposed observer is demonstrated by simulations with a comparison to the results obtained from the Kalman filter proving that it is very promising to use not only for fault detection but for further fault estimation and isolation.

After investigating the various methodologies proposed in the literature for fault detection and isolation, we could conclude that a model-based observer design utilizing the quadratic $\mathcal{H}_\infty$ norm characteristics is very advantageous for the problem of fault detection and diagnosis. Thus, by a deep study for the $\mathcal{H}_-/\mathcal{H}_\infty$ technique, it has been found that there are two major points that need to be enhanced for improving the design procedure besides the obtained residual signals as well. The first point is related to the regularity condition which is satisfied by introducing constant matrices modeling fault and disturbance effect on the system states and outputs. While the second problem is concerning the residual generator scheme which can perform only fault detection with a bank of observers for fault isolation.

So a new observer-based residual generator design methodology is proposed which, under some structural properties of the system, allows to ensure exact or asymptotic residual to fault convergence. Some algebraic criteria are stated proving mathematically that the classical residual generators design based on $\mathcal{H}_-/\mathcal{H}_\infty$ techniques can be regarded as the worst-case scenario for system fault diagnosis when the decoupling conditions can't be satisfied. The regularity condition, which is essential to guarantee proposed algorithms applicability, is fulfilled benefiting the differentiated output signal leading to enhanced stable techniques. Furthermore, the observability of the LPV system is investigated to ensure the feasibility of the methodology followed through observer's gain assignment as it represents a necessary condition for the validity of the introduced LMIs. In addition, the proposed residual generator scheme empowers the system to conduct a complete fault diagnosis: detection, estimation, and isolation thanks to the offered virtual residual signal and its weighting matrix. Nevertheless, the scheme used in residual generator design provides a margin to adjust time response characteristics such that it recovers the system states precisely, hence acting efficiently as a state estimator during the absence of system faults. The results are validated

on a quadrotor modeled as a quasi LPV system and provided with a robust output feedback controller showing the effectiveness of the proposed algorithms in actuators fault diagnosis, which are considered the milestone for powerful reliable fault-tolerant control.

After ensuring the maturity of the developed methodology by testing its performance for LTI and LPV academic examples other than the quadrotor model, the algorithm proposed for the residual generator design is reused for handling the sensors fault diagnosis problem. Where it is proven that, under some structural condition of the system, it can be augmented with an additive integral action, which allows exploiting the same suggested procedure for sensor fault diagnosis. Nevertheless, such an approach promotes the ability of the system to model the effect of the disturbances on the measurements, in a way that increases its robustness. Moreover, augmenting the system with an integral action helps to avoid the problem resulting from the control input and the fault differentiation. Finally, the introduced algorithm results are validated on the quadrotor LPV model subjected to sensor faults and exogenous disturbances. The precise fault estimation results exhibit the great potential of the proposed residual generator to be further used along with the actuator faults residual generator in active fault-tolerant control.

Chapter 5

Fault-Tolerant Control

Chapter abstract

Benefiting the results obtained from the actuator FDD unit proposed in the preceding chapter, an active fault-tolerant control law is proposed to overcome the actuators loss of efficiency. After fault estimation, the performance of the faulty system is evaluated to check the ability of the FTC law to overcome the actuator malfunction in a way that ensures a precise trajectory tracking. Through computing the controllability gramian matrix and the eigenvalues of the faulty system, the controller reconfiguration unit becomes able to decide whether the actuators damage can be contained or not. Therefore, if the actuators experience a partial loss of efficiency, the proposed FTC law will provide an additional control action to preserve the stability of the system and keep track of the required path. The efficiency of the proposed FTC law is demonstrated through simulation of the quadrotor LPV model subjected to various actuators fault scenarios and provided with the FTC law.

5.1 Introduction

Indeed, it is an essential feature for automated systems to be provided with FTC algorithms such that they can maintain an acceptable performance in case of degraded system functionality due to a hardware or even a software damage. As previously mentioned, the FTC techniques can be categorized into two main branches, one where no information about the fault is available referred to as passive FTC, while the other includes an FDD or FDI residual generator besides a controller reconfiguration unit see [3]. The results obtained in [35] through evaluating the performance of different passive and active FTC schemes prove the ability of the latter method to guarantee the system stability while being subjected to larger fault magnitude, thus increasing the system reliability. Hence, the work presented here benefits from the results achieved in the preceding chapter for actuators and sensors fault diagnosis and tries to establish an efficient FTC law for the quadrotor UAV.

Such a topic has been widely investigated in academic research targeting a mature methodology that can be deployed on a large scale in the software development of quadrotors. Among these works, one can cite [106] which proposes an active model reference FTC law that combines the system dynamics and the actuator faults within a single framework and evaluates the overall system performance through some indicators that compare the reference states and their corresponding actual outputs. Nevertheless, in [107] an observer-based FTC scheme is introduced where the faults are inserted as scheduling functions for the controller gain such that it adapts to the actuator fault. In addition, an exponential time function is utilized to ensure a smooth transition between the nominal controller gain and the modified one during the presence of the actuator fault. Furthermore, the idea of observer-based FTC is presented in other works like [30] and [108] where an augmented system including the observer and FTC law dynamics is analyzed in a way that guarantees the stability of the overall system during the presence of quadrotor actuator faults.

Another efficient solution for the problem of active FTC law design can be found in [29] for a general Takagi-Sugeno system. Throughout this work it is proven that the FTC law is able make the faulty states converge exactly to the healthy model states if the Takagi-Sugeno model premise variable belong to the system states or the output. As our quadrotor LPV model matches this case, such an approach is adopted for the FTC law design in a way that ensures the faulty system stability and reference tracking given that the residual generator is able to deliver precise fault estimation as shown in the last chapter.

5.2 Actuators FTC

Thanks to the results obtained in the preceding chapter concerning actuators fault diagnosis, an observer-based FTC law can be designed in a dynamic way to ensure a precise fault compensation in case of actuators' loss of efficiency. As previously discussed, the quadrotor control law takes the formulation of cascaded feedback loops where the inner loop (attitude and altitude dynamics) assigns the required motors thrust force to stabilize the vehicle. Hence, it is practical to consider only the quasi-LPV model of the attitude and altitude dynamics presented in 2.3.4 while designing the FTC law. Recall the nominal system model (2.62) which is described by the following state space representation

$$\begin{cases} \dot{x}_s(t) = A(\rho(t))x_s(t) + B(\rho(t))u(t) \\ y(t) = C(\rho(t)x_s(t) + D(\rho(t))u(t) \end{cases} \tag{5.1}$$

where $x_s(t), u(t), y(t)$ are the state vectors, while $A(\rho(t)), B(\rho(t)), C(\rho(t), D(\rho(t))$ represent the parameter varying matrices of appropriate dimensions detailed in 2.3.4. Consider now the system affected by actuators loss of

efficiency presented also in 2.3.4 given in state space form as follows

$$\begin{cases} \dot{x}_f(t) = A(\rho(t))x_f(t) + B(\rho(t))u_T(t) + F(\rho(t))f(t) \\ y_f(t) = C(\rho(t))x_f(t) + D(\rho(t))u_T(t) \end{cases} \tag{5.2}$$

such that the subscript f indicates the faulty signals while $u_T(t)$ stands for the modified control law to be designed in a way that ensures the stability of the system during the presence of actuators faults. It is important to mention that the varying parameters vector $\rho(t)$ in equation (5.2) should be denoted $\rho_f(t)$ since the varying parameters will be affected by the fault as well. However, knowing that the quadrotor model is quasi-LPV, hence the varying parameters belong to the system states $x_f(t)$ and by designing the FTC law such that it ensures the convergence of the system states $x_f(t)$ to the nominal ones $x_s(t)$, we can assume that at steady state $\rho_f(t)$ converges to $\rho(t)$. For other types of LPV systems where the varying parameters are not among the system states, the exact convergence of the faulty states to their nominal values is not ensured during steady state, more illustration can be found in [29].

5.2.1 Tolerant control law design

The nature of the designed active FTC law benefits from the information provided by the fault diagnosis unit so the reconfigured controller has to include an additive term depending on the estimated fault to compensate for its effect as shown in figure 5.1.

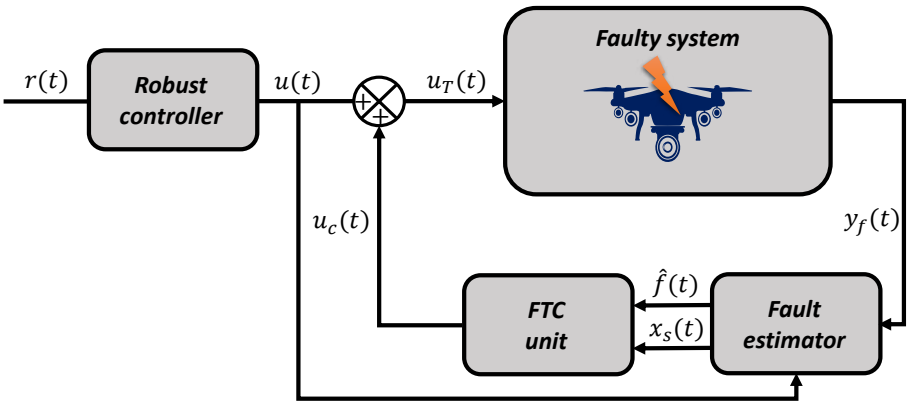

Figure 5.1: Actuators FTC schematic

Consider the modified control law $u_T(t)$ is given by

$$u_T(t) = u(t) + u_c(t) \tag{5.3}$$

where $u(t)$ is the nominal control input of the system introduced before in 3.5 and $u_c(t)$ is the complementary control

action that emerges in case of actuator fault calculated from

$$u_c(t) = -B^{\dagger}(\rho(t))\ F(\rho(t))\ r(t) + K_c(\rho(t))\ (x_s(t) - x_f(t)) \tag{5.4}$$

where $r(t)$ is the residual signal obtained from the fault diagnosis unit (4.90) and $K_c(\rho(t))$ is the nominal state feedback gain matrix given in (3.54). The existence of the second term in (5.4) ensures the stability of the system during the transient phase while switching to the FTC law due to the fault presence as the gain matrix $K_c(\rho(t))$ tends to minimize the error between the nominal and faulty system states $x_s(t)$ and $x_f(t)$, respectively. Consider the state error is given by $\varepsilon(t) = x_s(t) - x_f(t)$, then the error dynamics resulting from combining the nominal (5.2) and faulty (5.2) system dynamics is given by the following differential equation

$$\dot{\varepsilon}(t) = \dot{x}_s(t) - \dot{x}_f(t) = A(\rho(t))\varepsilon(t) + B(\rho(t))\big[u(t) - u_T(t)\big] - F(\rho(t))f(t) \tag{5.5}$$

By substituting the complementary and modified control inputs $u_c(t), u_T(t)$ from equations (5.3) and (5.4) into equation (5.5), the error dynamics is transformed into the following form

$$\dot{\varepsilon}(t) = \big[A(\rho(t)) - B(\rho(t))\ K_c(\rho(t))\big]\varepsilon(t) + F(\rho(t))\big[r(t) - f(t)\big] \tag{5.6}$$

Concerning the second term of equation (5.6), the gains of the residual generator proposed in 4.3.3 are assigned following the results of Theorem 3 to ensure asymptotic convergence of the residual signal $r(t)$ to the fault signal $f(t)$ described mathematically by

$$\begin{cases} \lim\limits_{t \to +\infty} r(t) = Qf(t) & d = 0 \\ \|r(t) - Qf(t)\|_2 < \gamma \|d(t)\|_2 & d \neq 0 \end{cases} \tag{5.7}$$

where the weighting matrix Q is chosen to be $Q = I_{n_f \times n_f}$ such that the residual generator performs fault estimation. Thus, the second term in equation (5.6) converges to zero at a steady state in the absence of exogenous disturbance effect. Nevertheless, during the disturbance's existence, the residual signal converges to the fault within a limit that doesn't exceed the constant γ. Recall the error dynamics given by equation (5.6), since the feedback controller gain $K_c(\rho(t))$ is computed in section 3.5.1 to ensure the quadratic stability of the system, then the FTC law is proven to be able to stabilize the error dynamics $\dot{\varepsilon}(t)$ as the homogeneous solution of the differential equation (5.6) when the disturbance is equal to zero will be

$$\varepsilon(t) = e^{\varrho(t)}\ \varepsilon(0) \tag{5.8}$$

where $\varrho(t) = \int_0^t \big(A(\rho(\tau)) - B(\rho(\tau))\ K_c(\rho(\tau))\big)\, d\tau$ is the closed loop state transition matrix whose eigenvalues are ensured to be in the left half plane of Laplace domain through the controller design 3.5.1. Moreover, through the

presence of the disturbance effect, the error dynamics $\dot{\varepsilon}(t)$ will have the nonhomogeneous differential equation form represented by (5.6) whose solution is given by

$$\varepsilon(t) = e^{\varrho(t)}\,\varepsilon(0) + e^{\varrho(t)} \int_0^t e^{-\varrho(t)} F(\rho(\tau)) \big[r(\tau) - f(\tau)\big]\, d\tau \tag{5.9}$$

such that the first term on the right-hand side is the response due to the initial condition which converge to zero thanks to the controller gain matrix $K_c(\rho(t))$. While the second term represent the response due to the difference between the fault and the residual signals for which the disturbance effect is minimized to the quadratic performance level γ following the results of equation (5.7) thanks to the residual generator design technique discussed before. So in the latter case where the system is subjected to some exogenous perturbations the error $\varepsilon(t)$ doesn't converge completely to zero as it will be slightly affected by the disturbance existence which doesn't prohibit the FTC law from performing its main task. Hence, the complementary control input given in equation (5.4) is able to bring the system to stability in case of actuator fault occurrence by driving the faulty states $x_f(t)$ to reach their nominal values $x_s(t)$.

5.2.2 System recoverability

While investigating actuator fault-tolerant control law design, it is extremely important to pay attention for the controllability of the system during the existence of the fault since they affect directly the control input of the system. Instead of using the controllability matrix (3.24), another approach is employed based on the controllability gramian which doesn't only check the system controllability but in addition signifies the degree of controllability along each direction. The controllability gramian matrix denoted W_c can be calculated by solving the following Laypunov equation:

$$\varrho_k W_c + W_c {\varrho_k}^T + B_{f_k} {B_{f_k}}^T = 0, \quad k = 1, \ldots, N \tag{5.10}$$

where B_{f_k} is the faulty input matrix at the vertex k. There exist several methods for analyzing the controllability gramian matrix W_c among them one can find the work in [109] which tracks the minimum measure of the Hankel Singular Value (HSV) of the matrix W_c.

In this work, we are interested in the evolution of all the controllability gramian eigenvalues as they indicate how the system performance degrades when it is subjected to actuator faults. Roughly speaking, the largest eigenvalues correspond to the most controllable directions and obviously the least eigenvalues correspond to the least controllable states. The idea is to calculate the controllability gramian matrix W_c from the LMI (5.10) for varying actuator loss of efficiency faults and plot the eigenvalues of the W_c with their corresponding magnitude of the faults. The results shown in figure 5.2 demonstrate how the system performance is affected by the actuator faults as the decrease of the eigenvalues proves that the system becomes less controllable until it reaches the complete failure where the system becomes uncontrollable (fault $= 100\%$). It can be depicted from the figures 5.2a and 5.2b that the

system can guarantee an acceptable performance while subjected to actuators loss of efficiency up to $= 80\%$ after which the system won't be able to recover the required states as in the nominal case.

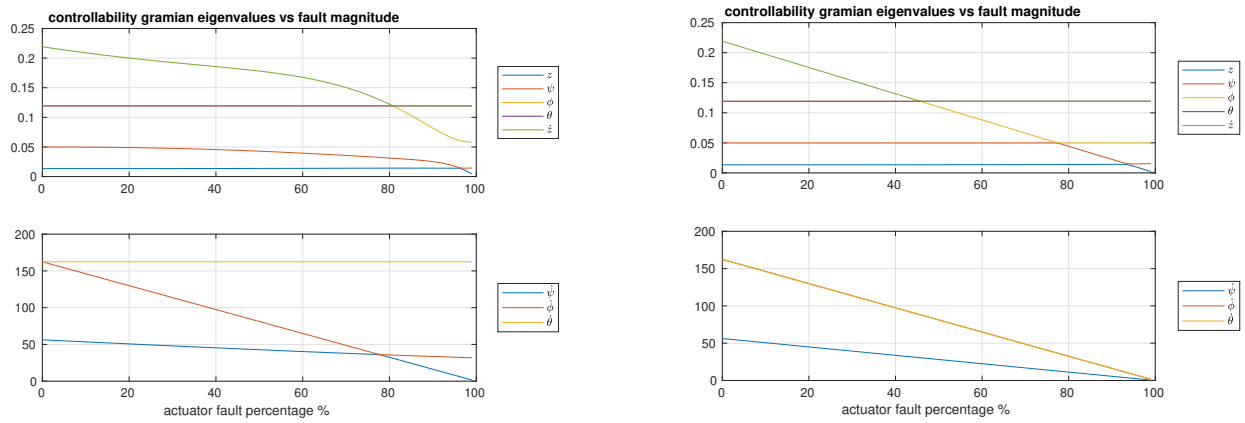

(a) two opposite actuators

(b) the four actuators

Figure 5.2: Eigenvalues of W_c evolution with actuators loss of efficiency of

On the other hand, there exist another very important measure for the system performance and its transient time response characteristics during the presence of actuators fault which is the eigenvalues of the closed loop state transition matrix $\varrho(t)$. It has been shown in section 5.2.1 how influential this matrix is to the FTC law design and how the error dynamics depend directly on it. It is clear from equations (5.8) and (5.9) that the larger the negative eigenvalues of the matrix $\varrho(t)$ are, the faster the faulty system converges to the nominal one.

So it is very useful to track the eigenvalues evolution of the matrix $A(\rho(t)) - B_f(\rho(t))\ K_c(\rho(t))$ with time during the fault existence where $B_f(\rho(t))$ represents the faulty input matrix after fault estimation. In that manner, it is expected that due to the actuator faults the closed loop system poles will be fairly shifted towards the right hand side of Laplace domain resulting in higher settling time of the system. The effect of the actuators faults on the system poles and state transition matrix eigenvalues is demonstrated through simulation in section 5.3 justifying the degraded performance of the system which can lead to a complete system instability and proves the effectiveness of the proposed FTC law in handling such problems.

5.2.3 Input redundancy

The limitation of the proposed FTC law lies behind the fact that the quadrotor is an underactuated system where there doesn't exist any physical input redundancy as each input is responsible for controlling the motion along a specific direction as shown earlier. Thus, the faulty actuator can not be replaced by other motors using the proposed FTC law, hence it can handle a maximum loss of efficiency of 50% of each actuator. This is evident as beyond this limit the actuators will not be able to provide the sufficient thrust demanded by the FTC law since the available thrust force $T_a = .5\ T$ where T is the maximum available thrust in the nominal case.

The problem of further loss of efficiency or complete failure of one or multiple actuators $50\% < f_i < 100\%, i \in [1, \ldots, 4]$, it is not addressed in this work and obviously can not be handled using the proposed approach as it depends mainly on the controllability of the system during the functioning of the quadrotor four actuators. Such a problem can be very interesting for future work based on the fault estimation provided by the fault diagnosis unit but the main idea will be to give up the nominal model used for controller design and propose a reduced model which sacrifices the yaw angle control targeting the position stability as in [110], [111], and [112].

For evaluating the performance of the proposed approach for FTC law design, it is applied to the quadrotor LPV model in simulation considering different actuator fault scenarios in 5.3. The simulation results prove the capabilities of the deployed technique where the system is able to overcome the actuator fault and continue the required task while giving an adequate indicator for system malfunction to avoid a complete system failure.

5.3 Simulation results

In order to reveal the effectiveness of the proposed approaches for fault-tolerant control, a simulation is performed using Matlab-Simulink program where the quadrotor LPV model is subjected to exogenous disturbances and measurement noise. The drone is required to follow a 3D Cartesian polynomial trajectory discussed in C between an initial configuration $[0, 0, 0, 30^\circ]$ and a final configuration $[2, 2, 3, 0^\circ]$ such that a trajectory configuration is defined by the position and heading states $[x, y, z, \psi]$. Throughout the drone path it encounters various scenarios of actuators faults which are handled by the FTC law in a way that ensures not only the system stability but also a successful completion of the required task.

While investigating actuators fault scenarios the quasi-LPV model including attitude and altitude dynamics 2.3.4 is considered since it is affected directly by the actuators fault. The attitude states are extracted from the output vector and are inserted as the inputs for the position loop (cascaded control scheme 3.1) such that one can be able to recognize the actuators fault effect on the position states. To give a better understanding of the simulation environment, the initial condition of the state vector in (2.59) is $x(0) = 0$ and its estimated value is given by $\hat{x}(0) = 0.1$. While the included disturbances are low-frequency sinusoidal gust wind given by

$$\begin{cases} d_1(t) = 0.5 \sin 0.8t & t > 10s \\ d_2(t) = 0.5 \cos 0.8t & t > 10s \end{cases} \tag{5.11}$$

Finally, the measured attitude, altitude, angular rates, and rate of ascending are subjected to white Gaussian noises $n_s(t) \in [-0.03, 0.03]$ and $n_v(t) \in [-.06, .06]$ having a sample time of $0.03, 0.01\ s$, respectively.

Scenario(1) abrupt fault of one actuator

In this scenario the 1^{st} actuator of the quadrotor is experiencing an abrupt loss of efficiency of 50% while the remaining three actuators are healthy with no fault. This case can be described by considering the fault vector in equation (2.71) is given by

$$f(t) = \begin{cases} 0.5 & 5 < t < 20\ s \\ 0 & 0 < t < 20\ s \\ 0 & 0 < t < 20\ s \\ 0 & 0 < t < 20\ s \end{cases} \tag{5.12}$$

The results shown in figure 5.3a illustrate that the residual generator is able to estimate the imposed fault precisely in a way that permits the designed FTC law to recover the system states and enable it to complete the required reference trajectory as can be depicted from figure 5.3b. In that figure, one can find the fault free, the system response without FTC, and its trajectory with the FTC law in green, blue, and red continuous lines, respectively. The figure proves the capability of the proposed FTC law as the quadrotor could reach the required final configuration despite the fault existence. However, when the system is not provided with any FTC law it goes far from the required trajectory and couldn't reach the expected final destination. The simulation time is only $20s$ and one can see how the system diverges from its nominal path which points out the importance of such an additive control law for real time deployment of such a drone through outdoor missions.

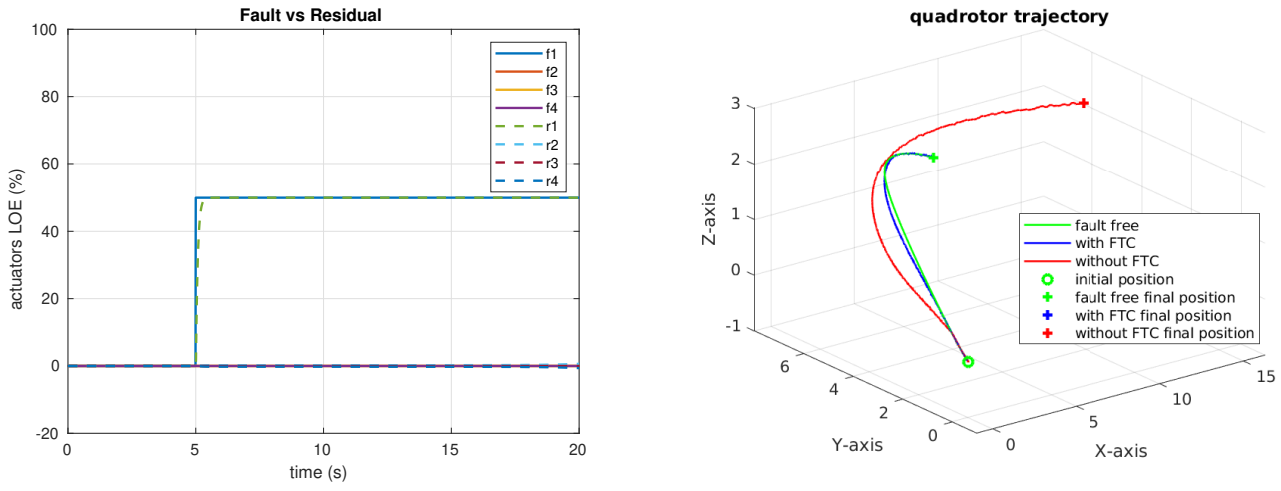

(a) actuator faults and residual signals

(b) Cartesian polynomial trajectory

Figure 5.3: 1^{st} actuator fault and the resulting trajectory

In figure 5.4 the attitude and position states are demonstrated while the system is subjected to the mentioned abrupt fault (5.12). It can be noticed that the system provided with the FTC law response (continuous blue line) is keeping track of the reference inputs (dashed green line) but the system without an FTC law response (dotted red line) is not able to follow the desired states and diverges with time.

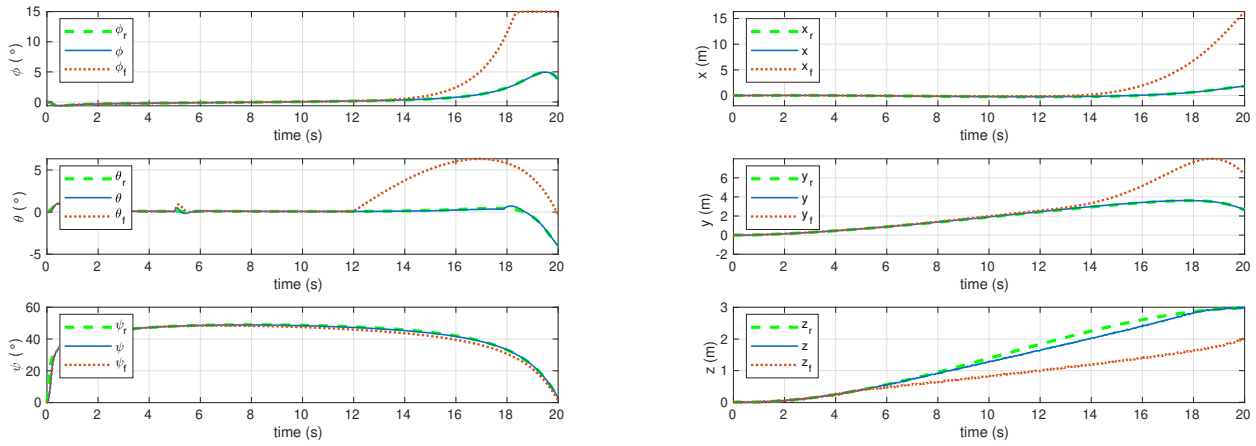

(a) attitude states (b) position states

Figure 5.4: 1^{st} actuator fault corresponding attitude and position states

The reason of such a degraded performance of the system during the absence of an FTC law can be depicted from the evolution of the closed loop system eigenvalues with time shown in figure 5.5a. Instead of plotting all the state transition matrix eigenvalues, we take their average knowing that whenever this average value gets smaller magnitude, the time response of the system is deteriorated. This is a direct implication of the shift occurred to the closed loop system poles due to the fault existence shown in figure 5.5b.

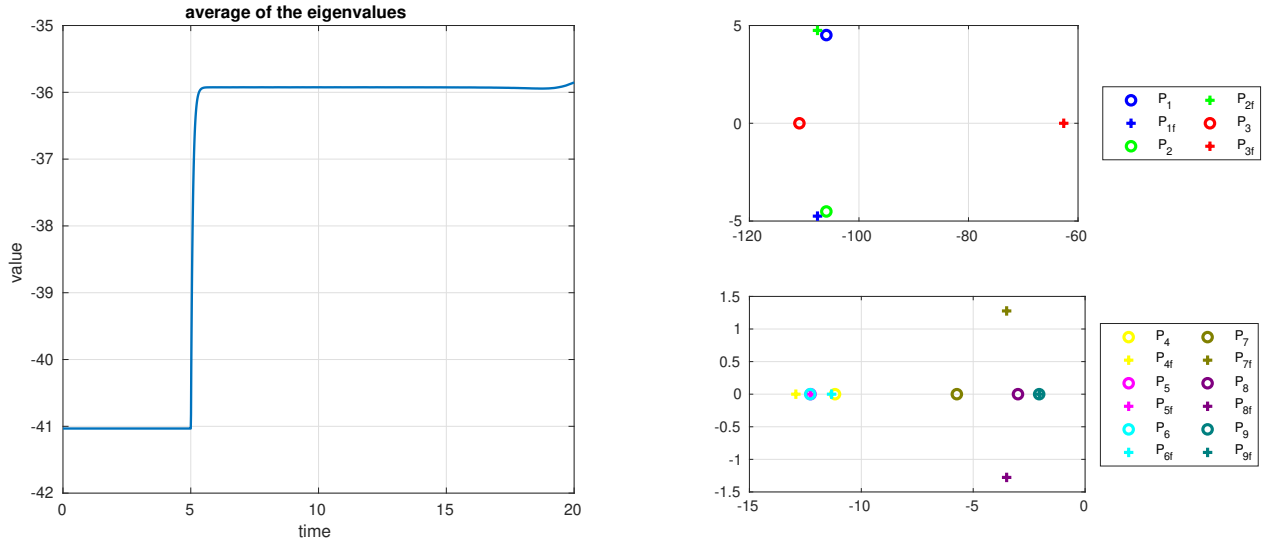

(a) eigenvalues (b) poles position

Figure 5.5: 1^{st} actuator fault closed loop poles and eigenvalues evolution

In that figure, the poles are divided into two sets, one with large values representing the fast dynamics of the attitude states, while the other contains the remaining position states, their time derivatives, and the attitude rates. Keeping in mind that the "o", "$+$" symbols represent the poles nominal and faulty positions, respectively, one can

notice that the time response is degraded not only because of the shift that happened to the pole(3) in red which results in slower response, but also because of the conversion of the poles(7,8) from pure real poles to include an imaginary component which degrades the system damping.

Scenario(2) abrupt and linear time varying actuators faults

Throughout this actuators fault scenario, the simulation parameters discussed before describing the noises and disturbances are kept unchanged while the system is experiencing two simultaneous actuators faults given by

$$f(t) = \begin{cases} 0.5 & 5 < t < 20\ s \\ \frac{10}{3}(t-5) & 5 < t < 20\ s \\ 0 & 0 < t < 20\ s \\ 0 & 0 < t < 20\ s \end{cases} \tag{5.13}$$

In that manner, the fault vector defined by equation (5.13) represents an abrupt loss of efficiency of the 1^{st} actuator by 50% while the adjacent 2^{nd} actuator is subjected to a constant performance degradation with time starting at $t = 5s$. It is obvious from figure 5.6a that the fault diagnosis unit is able to deliver an adequate fault estimation for both types of faults which empowers the FTC unit to handle such a faulty situation and make the system reach the required final point in addition to following the desired trajectory precisely as shown in figure 5.6b.

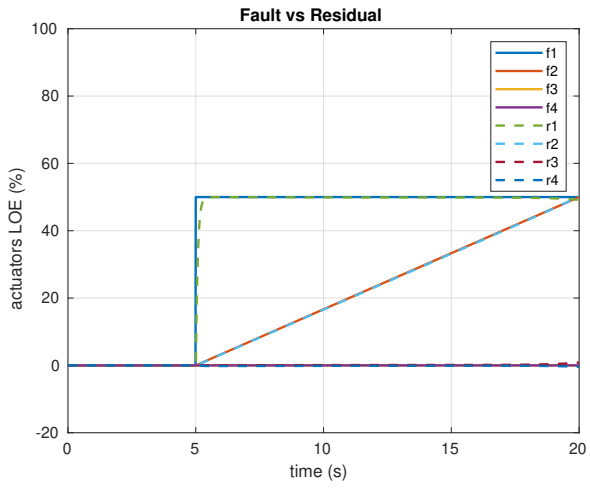

(a) actuator faults and residual signals

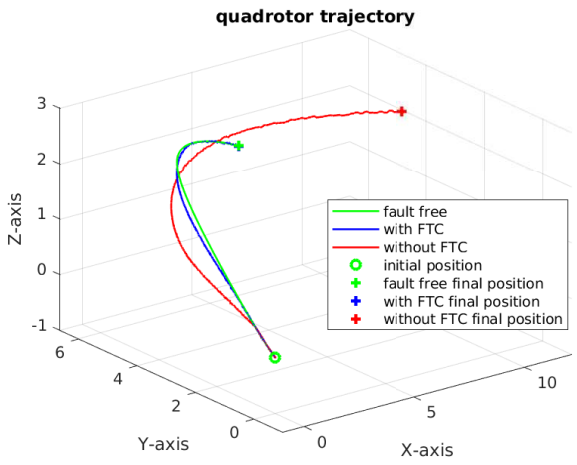

(b) Cartesian polynomial trajectory

Figure 5.6: Two adjacent actuators faults and the resulting trajectory

Furthermore, it is interesting to investigate the eigenvalues average evolution during the faults existence which is demonstrated by figure 5.7a to indicate the degraded performance of the nominal controller represented by the continuous red line in figure 5.6b. The results shown in figure 5.7a display how the actuators faults affect the eigenvalues and shift them more to the right hand side of the s-domain where the initial shift at $t = 5s$ is due to

the abrupt fault while the magnitude of the eigenvalues average keeps decreasing by cause of the second linearly increasing fault. In addition, the plot of closed loop system poles at nominal ($t = 2s$) and faulty ($t = 12s$) performance situations represented by "o" and "$+$" symbols, respectively, shown in figure 5.7b justifies the degradation of the eigenvalues average. One can notice that the poles corresponding to the attitude states are shifted to the right hand side leading to a longer time response of the attitude subsystem which explains why the system with a nominal controller is not able to follow the desired trajectory during the fault presence.

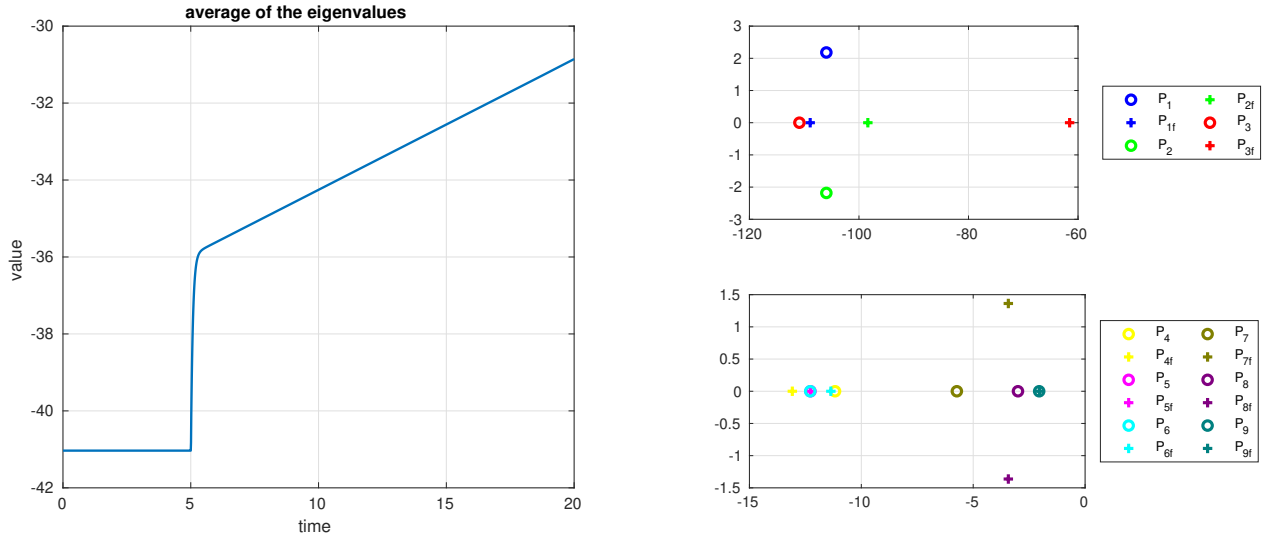

(a) eigenvalues (b) poles position

Figure 5.7: Two adjacent actuators faults closed loop poles and eigenvalues evolution

Scenario(3) abrupt and sinusoidal time varying actuators faults

For the third scenario, the system is subjected to the following fault vector

$$f(t) = \begin{cases} 0.5 & 5 < t < 20\ s \\ 0 & 0 < t < 20\ s \\ 0.25 + 0.25\sin 4t & 10 < t < 15\ s \\ 0 & 0 < t < 20\ s \end{cases} \tag{5.14}$$

Thus, in this case two opposite actuators namely, 1, and 3 are subjected to an abrupt and a sinusoidal time varying faults, respectively. Again the results shown in figure 5.8 prove the capability of the fault diagnosis unit in fault estimation beside the effectiveness of the proposed FTC law in recovering the system states during the fault existence.

Nevertheless, the influence of the two actuators faults appear on the eigenvalues average shown in figure 5.9a which is initially decreased at $t = 5s$ when the 1^{st} actuator loses 50% of its efficiency suddenly. Furthermore, at

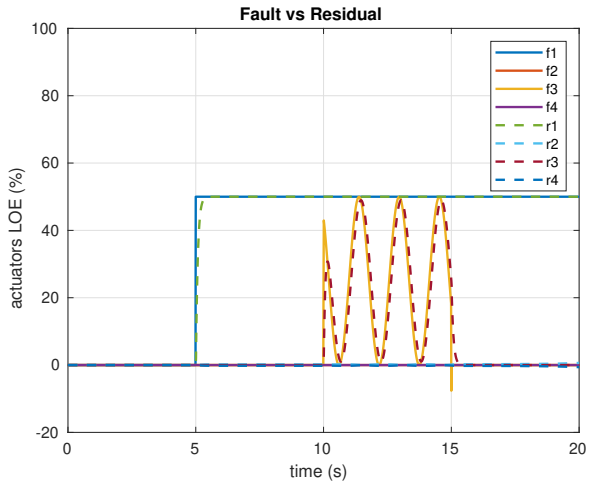

(a) actuators faults and residual signals

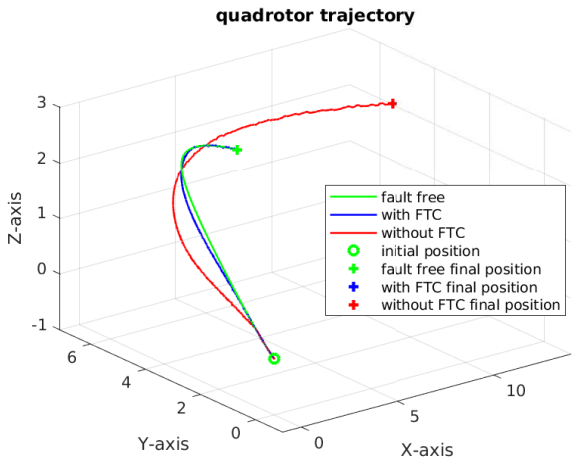

(b) Cartesian polynomial trajectory

Figure 5.8: Two opposite actuators faults and the resulting trajectory

$t = 10s$ the eigenvalues average begins to fluctuate under the impact of the sinusoidal fault of the 3^{rd} actuator explaining the degraded performance of the nominal controller. While as figure 5.9b illustrate the effect of the sinusoidal fault on the attitude angles which prohibit the nominal controller from retrieving and following the desired trajectory shown in figure 5.8b.

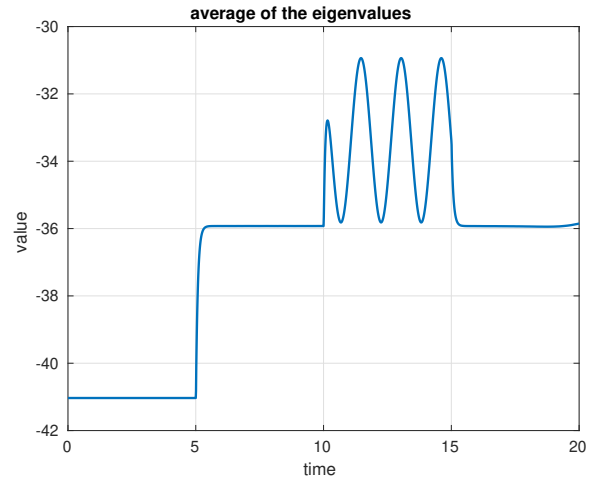

(a) eigenvalues

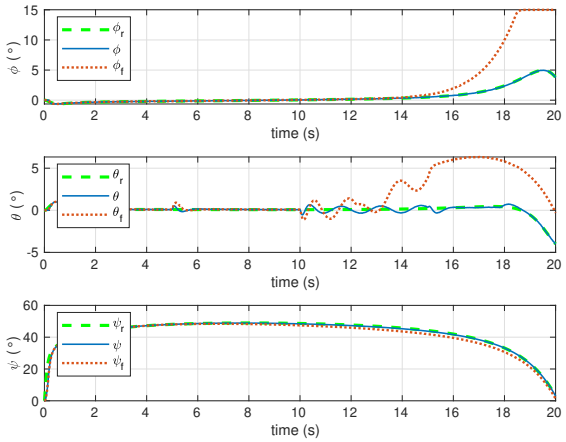

(b) attitude states

Figure 5.9: Eigenvalues evolution and attitude states corresponding to two opposite actuators faults

5.4 Conclusions

In this chapter a FTC law is proposed benefiting the results obtained from the developed residual generator concerning fault estimation. It is shown through analyzing the error dynamics between the faulty system and the healthy

model that the convergence of the residual signal to the fault implies the convergence of the faulty system states to their nominal value. The robust state feedback gain calculated for nominal system control is reused to guarantee a smooth transition of the control action when the system encounter a sudden fault in addition to ensuring the convergence of the error dynamics.

Since the main condition of the applicability of the designed FTC law is the system controllability, a detailed investigation of the controllability gramian and its eigenvalues degradation with the increase of actuator loss of efficiency percentage is provided. In addition, in order to understand clearly the behavior of the faulty system and the impact of actuator faults on its stability, the average of the eigenvalues of the closed loop faulty system is deployed as a measure of how the system's transient response is affected by the fault existence.

The fact that the quadrotor is an underactuated system implies another limitation on the FTC law applicability as the system doesn't exhibit any mechanical redundancy. Which means that in case of a complete loss of one or more actuators, the nominal behavior of the system is no more attainable and other approaches should be adopted aiming to achieve partial tracking of the system states and sacrificing one degree of freedom at least. Finally, to evaluate the performance of the FTC law, it is added to the quadrotor LPV model in simulation environment where the drone model is subjected to various actuators fault scenarios. The simulation results prove that the system provided with such a controller reconfiguration unit is able to insure a higher reliability level while following the desired trajectory even when the system is experiencing actuator fault.

Chapter 6

General Conclusion and Perspectives

6.1 Conclusions

The work presented in this thesis aims at providing a powerful solution for the problem of Fault-Tolerant Control (FTC) of a quadrotor UAV. It is demonstrated how much such vehicles are important for various applications in our daily life in a way that motivates several academic research to develop methods and algorithms to increase their safety and reliability. The quadrotor vehicle is one of the most beneficial UAVs thanks to its lightweight, low power consumption, and ability to take off and land vertically. However, the quadrotors don't possess any hardware redundancy and are usually equipped with IMU and GPS sensors for state estimation which can be vulnerable to drift and inaccuracy errors. In addition, the nature of these UAVs being autonomous systems urges the investigation of FTC law design to evaluate and locate the system fault whenever it takes place besides modifying the control action required to overcome such fault. After performing a detailed investigation of the literature, it is found that such a problem can be tackled through some fundamental steps beginning by modeling the system dynamics then designing a control law to stabilize the vehicle and achieve reference tracking. Afterward, a Fault Detection and Diagnosis (FDD) unit has to be constructed and integrated with the controller reconfiguration unit in an active FTC law formulation.

Concerning the system modeling, there exist numerous methods for representing the vehicle dynamics as the deduced model depends on the vision of the designer and the tasks which the vehicle is required to perform. The methodology adopted in this work is based on Newton-Euler formulation for describing the system kinematics and dynamics followed by a linearization technique to simplify the obtained nonlinear model. Despite the advantage of the full linear model deduced regarding its simplicity and ease of analysis, it can't guarantee optimal performance of the system due to the neglected nonlinear dynamics. An affine model can provide an ultimate value for the angular velocities coupling effect while preserving the linear representation of the system but it still lacks the heading angle degree of freedom during motion. Thus, modeling the system in LPV framework is an appealing solution as it

offers to embed the nonlinear terms as linearly time-varying parameters between their extremum values which are anticipated based on the knowledge of their evolution with time. Such a solution presents an accurate description of the nonlinear model while preserving a simpler analysis during controller design and further FTC unit establishment.

Since the quadrotor model is an open-loop unstable system, a controller has to be designed in a way that provides the stability of the system and ensures its ability to achieve trajectory tracking. While considering the linear model of the vehicle, a PID classical controller presents a suitable solution to reach the required time response characteristics of the closed-loop system. In addition, from the robustness point of view, the controller can be constructed based on loop shaping of the system's sensitivity and complementary sensitivity transfer functions such that it becomes able to reject the effect of the exogenous disturbance besides improving the noise attenuation level. On the other hand, an optimal control law is designed using Linear Quadratic Regulator (LQR) technique for the MIMO LTI model of the system which gives a direct influence on the control action required and the resulting state variations through the cost function minimization. Furthermore, by adding an optimal state observer, a Linear Quadratic Gaussian (LQG) control law is formulated which enables the system to trust the model or the measurement according to the uncertainty and noise weightings introduced. Afterward, a self-scheduled feedback LPV controller is designed to benefit the results realized through establishing and analyzing the control laws for the linear systems and the polytopic convexity of the obtained quasi-LPV model. So as to ensure the robustness of the system and its adequate time response, the quadratic Lyapunov inequality and the Bounded Real Lemma (BRL) are formulated into an LMI feasibility problem to assign the feedback gain value. The performance of such a controller is evaluated in different simulation scenarios where the system was able to follow the desired trajectory precisely despite the existence of the effect of a strong disturbance.

As previously illustrated, the FDD unit is an essential element to construct an active FTC law as it provides information about the fault occurrence time, its magnitude, and location. In this work, the FDD unit consists of a model-based observer acting as a residual generator for fault diagnosis. Three approaches are introduced to assign the state observer's gain matrix namely, Luenberger observer, continuous-time Kalman filter, and a robust observer based on $\mathcal{H}_-/\mathcal{H}_\infty$ technique. Since the latter two approaches provide a wider range of applicability thanks to their ability to suppress the measurement noise effect, a comparison between both of them is held in simulation. The obtained results prove that the observer designed using $\mathcal{H}_-/\mathcal{H}_\infty$ technique is more sensitive to the system faults and provides a higher level of robustness against exogenous disturbances. Afterward, an approach is proposed to enhance the performance of the residual generator design such that it becomes able to achieve fault detection, estimation, or isolation according to the introduced virtual residual weighting matrix. Such a methodology is based on an auxiliary output of the system that is computed after investigating the system output relative degree to faults and disturbances. This auxiliary output satisfies the regularity condition necessary to ensure the feasibility of the presented LMIs in addition to offering an extra degree of freedom to the assignment of the observer's gain matrix. Through synthesizing the proposed residual generator design, some algebraic conditions are introduced to ensure

exact or asymptotic residual to fault convergence. Finally, when the system doesn't convey any of the decoupling conditions, the $\mathcal{H}_-/\mathcal{H}_\infty$ technique is deployed for gains assignment.

The developed algorithm is applied in simulation to the quadrotor LPV model subjected to actuators faults giving outstanding results in fault estimation which proves the capabilities of the proposed approach. By means of adding an integral action to the system and verifying the observability of the constructed augmented system, the same approach is implemented in the quadrotor's sensors faults estimation. A simulation is then conducted in which the vehicle is subjected to some common and likely to occur IMU and GPS faults that can influence the system's behavior during trajectory tracking. Again the simulation results demonstrate the great potential of the methodology adopted and its ability to provide the controller reconfiguration unit with precise information during fault existence. Based on these results an active FTC law is introduced to handle the problem of actuators' loss of efficiency which benefits from the residual generator output to provide the system with the control action necessary to maintain its stability. The outcome of deploying such an FTC law presents a worthy contribution to the problem of quadrotor control as it doesn't require excessive computational time yet it enables the system to overcome faulty situations successfully. Thus, the proposed theoretical work in this thesis introduces an efficient solution hoping to be integrated with the recently developed algorithms to boost the capabilities of drones. In that way, we will be able to see powerful commercial drones performing professional tasks efficiently in an autonomous way.

6.2 Perspectives

The work presented in this thesis can be considered as a milestone for future advancements in the domain of FTC and its applicability to the market drones. Therefore, in this section, we provide some ideas which can benefit from the obtained results and further improve them in a way that increases the maturity and robustness of the proposed approaches.

6.2.1 Sensor FTC

The output of the proposed residual generator for sensors faults diagnosis is highly promising to be integrated with an active FTC law to overcome the sensors malfunction. Through investigating the literature, several approaches are suggested to handle the problem of sensors faults based on the precise estimation of their magnitude and location. The idea of introducing a virtual sensor that compensates for the sensor defect is widely deployed in works like [113] and [114] where the validity of the approach is based on the ranking condition of the faulty output matrix. In the same sense, the techniques presented in [115] and [116] integrate the fault estimation results with the system dynamics so that the control law compensates for the sensors malfunction and stabilizes the system dynamics simultaneously. Another methodology is adopted in [117] which the system states are assumed to be observable

from each output. Then, some weightings are introduced depending on the fault magnitude affecting each output of the system such that the weighting value corresponding to a faulty output approaches zero. This approach is applied to handle vehicle dynamics subjected to sensors faults in [9] where the results prove the effectiveness of such an approach in preserving an accurate trajectory tracking during faults presence.

6.2.2 Output signal differentiation

While investigating the output relative degree, some assumptions are considered to simplify the residual generator design and analysis in LPV framework that are summarized by:

- In section 4.3.1, the output matrix is considered independent of the varying parameter so its value is constant while deriving the successive output differentiation. Thus, Further analysis can be dedicated to computing the auxiliary output of a system whose output matrix is a varying parameter matrix to generalize the applicability of such a residual generator.

- The disturbances introduced to the quadrotor model is found to be having the same relative degree as the faults such that $\lambda_d = \lambda_f$ and the quadrotor model matches a system of case2 as illustrated in 4.3.2. However, if other types of disturbances are considered whose effect appears before the system fault corresponding to case3 ($\lambda_d < \lambda_f$), the boundedness of these disturbances must be checked carefully to apply the proposed algorithm.

- In addition, the quadrotor model is strictly proper which doesn't exhibit a direct effect from the input to the output as demonstrated in section 4.3.3 so no input signal differentiation is needed to calculate the auxiliary output. Otherwise, if the system is not strictly proper, an intermediate system should be introduced to avoid computing input signal derivatives as proposed in [26].

6.2.3 Correlation between faults of sensors and actuators

It is evident that the basic condition for constructing a residual generator in the form of a model-based observer is the observability of the system. Thus, extra research should be devoted to the cases when sensors are experiencing complete loss as they don't only affect the measurements of the system but can hide probable damage of one or more actuators. A solution can be presented using the concept of observability gramian to demonstrate which are the most affected directions of state estimation and their corresponding responsible actuators during the presence of sensors faults.

6.2.4 Actuators failure

In this work, we presented a solution for the problem of actuators' loss of efficiency based on the residual signal obtained from the FDD unit. However, when one or more actuators experience a complete failure, the classical control methods are no longer efficient because the quadrotor is an underactuated system and doesn't possess any input redundancy as discussed before. So an effective solution is proposed in [118] whose idea is to sacrifice the yaw angle control targeting the position stability. This work is further extended in [110] to give a relaxed hovering condition of various multicopters despite a complete loss of actuators or large misalignment of the vehicle center of mass with the center of the body axes. Nevertheless, the work presented in [119] benefits from an FDI unit to construct an active FTC law based on an incremental nonlinear dynamic inversion (INDI) approach that overcomes the complete loss of one actuator. In addition, the outcome of the hybrid nonlinear FTC law proposed in [111] is promising as it could stabilize the quadrotor in high-speed flight performed in a wind tunnel despite the complete loss of one actuator. The same problem of complete actuator failure could be handled in LPV framework in the works of [120] and [112] in a way that is convenient with the methodology produced in this thesis and shows great potential to be deployed in future work.

Appendices

Appendix A

LMI preliminaries

The procedure for solving the two inequalities (3.51) and (3.52) is well known in LPV systems after transforming them in a polytopic form with a change of variables to establish the corresponding LMI constraints see [121]. Consider the inequality (3.51) can be expressed at the polytopic model vertex by

$$(A_k - B_k K_{cj})^T P_c + P_c(A_k - B_k K_{cj}) + 2\zeta_c P_c < 0, \quad k, j = 1, \ldots, N \tag{A.1}$$

or in an expanded form

$$A_k{}^T P_c - K_{cj}{}^T B_k{}^T P_c + P_c A_k - P_c B_k K_{cj} + 2\zeta_c P_c < 0, \quad k, j = 1, \ldots, N \tag{A.2}$$

Lemma 2 *consider the inequality $Q_c < 0$, if there exists a symmetric and positive definite matrix X_c, then the following conditions are equivalent*

(i) $Q_c < 0$

(ii) $X_c\, Q_c\, X_c < 0$

Applying the results of the congruence lemma 2, the inequality (A.2) is multiplied by the matrix $Q_c = P_c{}^{-1}$ from left to give

$$Q_c A_k{}^T P_c - Q_c K_{cj}{}^T B_k{}^T P_c + A_k - B_k K_{cj} + 2\zeta_c < 0, \quad k, j = 1, \ldots, N \tag{A.3}$$

then multiply again by $Q_c = P_c{}^{-1}$ from right to obtain

$$Q_c A_k{}^T - Q_c K_{cj}{}^T B_k{}^T + A_k Q_c - B_k K_{cj} Q_c + 2\zeta_c Q_c < 0, \quad k, j = 1, \ldots, N \tag{A.4}$$

By a change of variables, the inequality (A.4) can be transformed into an LMI the idea is to introduce another

variable let's say $U_{cj} = K_{cj}Q_c$ and substitute in (A.4) to get

$$Q_c{A_k}^T - {U_{cj}}^T{B_k}^T + A_kQ_c - B_kU_{cj} + 2\zeta_cQ_c < 0, \quad k, j = 1, \ldots, N \tag{A.5}$$

The same procedure is followed to transform the inequality (3.52) into an LMI form, consider the following BRL at the polytope vertex

$$\begin{pmatrix} (A_k - B_kK_{cj})^TP_c + P_c(A_k - B_kK_{cj}) & P_cB_k & {C_k}^T \\ {B_k}^TP_c & -I & {D_k}^T \\ C_k & D_k & -{\gamma_c}^2I \end{pmatrix} < 0 \tag{A.6}$$

then by left and right multiplication of the inequality (A.6) by the following diagonal matrix

$$\begin{bmatrix} {Q_c}_{n\times n} & 0 & 0 \\ 0 & I_{n_u\times n_u} & 0 \\ 0 & 0 & I_{n_y\times n_y} \end{bmatrix} \tag{A.7}$$

where $Q_c = {P_c}^{-1}$ and n, n_u, n_y represent the states, inputs, and outputs number, respectively, after that the same variable $U_{cj} = K_{cj}Q_c$ is introduced to obtain the following LMI

$$\begin{pmatrix} Q_c{A_k}^T - {U_{cj}}^T{B_k}^T + A_kQ_c - B_kU_{cj} & B_k & Q_c{C_k}^T \\ {B_k}^T & -I & {D_k}^T \\ C_kQ_c & D_k & -{\gamma_c}^2I \end{pmatrix} < 0 \tag{A.8}$$

By solving the LMIs (A.5) and (A.8) for the matrices $Q_c > 0$ and U_{cj} then the controller gains at the vertices w can be obtained from

$$K_{cj} = U_{cj}{Q_c}^{-1} \tag{A.9}$$

Appendix B

Quadrotor's parameters

The parameters used throughout the simulations performed in the thesis are borrowed from the work of [41] and are listed in the following table.

parameter	**symbol**	**value**	**units**
mass	m	1.1	Kg
moments of inertia around x, y axes	$I_{xx} = I_{yy}$	0.0196	$Kg\ m^2$
moments of inertia around z axis	I_{zz}	0.0264	$Kg\ m^2$
propeller inertia	J_r	8.5×10^{-4}	$Kg\ m^2$
motor's thrust coefficient	K_f	9.29×10^{-5}	$N\ s^2$
motor's moment coefficient	K_m	1.1×10^{-6}	$N\ m\ s^2$

Table B.1: Quadrotor parameters

Appendix C

Path planning

The methodology adopted in path planning is based on polynomial trajectories generated in cartesian space for describing the curved path the drone follows along each direction. This technique is very popular for generating parametric curves see [122] by interpolation between the initial and final conditions such that the resulting trajectory is independent of the path curvature focusing only on the boundaries configuration. Thus, the degree of the trajectory polynomial is defined according to the provided information about the path initial and final conditions which are used for calculating the polynomial constants. By assuming the aircraft 3D path is a function of time and can be described by the following polynomials

$$\begin{cases} x(t) = a_{x_n} t^n + a_{x_{n-1}} t^{n-1} + \cdots + a_{x_1} t + a_{x_0} \\ y(t) = a_{y_n} t^n + a_{y_{n-1}} t^{n-1} + \cdots + a_{y_1} t + a_{y_0} \\ z(t) = a_{z_n} t^n + a_{z_{n-1}} t^{n-1} + \cdots + a_{z_1} t + a_{z_0} \end{cases} \tag{C.1}$$

where t is the time, and n representing the polynomial degree. Then, the curved path can be fully defined by calculating the polynomial constants $a_{xn}, \ldots, a_{x0}$ and so on for the other directions. For each of the position components, there must exist a number of boundary values equal to $n+1$ to enable calculating the n-degree polynomial constants. Apparently, increasing the number of boundary conditions allows for a higher polynomial degree, however, in this method it's preferable to use cubic or at most quintic polynomials to avoid inflection points through the path as indicated in [123]. In our case, a cubic polynomial having a degree $n = 3$ is used for fitting the proposed curved path and the polynomial constants are calculated such that generated trajectory satisfies automatically the boundary conditions on x, y, z. For determining the 3^{rd} order polynomial constants, we need 4 boundary conditions in addition to one equation for calculating the required time for completing the trajectory denoted by T_f. The later equation concerning arrival time is derived based on the vehicle velocity and acceleration limits to ensure a feasible smooth path free from deflections. Regarding the boundary conditions, consider the

following simplified model governing the dynamics of the aircraft 3D motion

$$\begin{cases} \dot{x} = \mathcal{V}\cos\theta\cos\psi \\ \dot{y} = \mathcal{V}\cos\theta\sin\psi \\ \dot{z} = \mathcal{V}\sin\theta \end{cases} \tag{C.2}$$

this model imposes additional boundary conditions on the vehicle velocity such that the values of the states are sufficient to calculate the polynomials constants. As an example, the path along $x-$direction is described by a cubic polynomial as follows

$$x(t) = a_{x3}t^3 + a_{x2}t^2 + a_{x1}t + a_{x0} \tag{C.3}$$

and its derivatives

$$\dot{x}(t) = 3a_{x3}t^2 + 2a_{x2}t + a_{x1} \tag{C.4}$$

$$\ddot{x}(t) = 6a_{x3}t + 2a_{x2} \tag{C.5}$$

Assuming the initial configuration given by the states $x_i, y_i, z_i, \mathcal{V}_i, \theta_i, \psi_i$ while the final configuration described by the states $x_f, y_f, z_f, \mathcal{V}_f, \theta_f, \psi_f$ and utilizing equation (C.2), the boundary conditions related to $x-$direction can be given by

- initial conditions $x(0) = x_i, \quad \dot{x}(0) = \mathcal{V}_i\cos\theta_i\cos\psi_i$
- final conditions $x(T_f) = x_f, \quad \dot{x}(T_f) = \mathcal{V}_f\cos\theta_f\cos\psi_f$

By substituting these boundary conditions in equations (C.3) and (C.4), then the constants $a_{x0}, \ldots, a_{x3}$ are given by

$$\begin{cases} a_{x0} = x_i \\ a_{x1} = \mathcal{V}_i\cos\theta_i\cos\psi_i \\ a_{x2} = \frac{1}{2{T_f}^2}\Big(-2T_f\mathcal{V}_f\cos\theta_f\cos\psi_f - 4T_f\mathcal{V}_i\cos\theta_i\cos\psi_i + 6(x_f - x_i)\Big) \\ a_{x3} = \frac{1}{{T_f}^3}\Big(T_f(\mathcal{V}_i\cos\theta_i\cos\psi_i + \mathcal{V}_f\cos\theta_f\cos\psi_f) - 2(x_f - x_i)\Big) \end{cases} \tag{C.6}$$

The final step to determine the value of the constants is to calculate the predicted arrival time T_f required for completing the path following. As mentioned earlier, the execution time depends on the drone velocity and acceleration limits thus, it has to be chosen such that none of these constraints are saturated during motion. Consider the drone maximum velocity on $x-$direction is denoted by u_{max}, then following the polynomial path (C.3), the drone reaches its maximum velocity when the next condition is satisfied

$$u_{max} \rightarrow \ddot{x}(t) = 0 \tag{C.7}$$

substituting in equation (C.5), we obtain

$$t|_{u_{max}} = -\frac{a_{x2}}{3a_{x3}} \tag{C.8}$$

where $t|_{u_{max}}$ is the time instant at which the velocity reaches its maximum value. Afterward, we can substitute $t|_{u_{max}}$ and u_{max} in equation (C.4) which is then transformed into an equation in one variable T_f. By solving this equation we obtain the expected arrival time that satisfies the velocity limit denoted T_{vel}. For checking the arrival time that complies with the acceleration constraint called a_{max}, the same steps are followed as

$$a_{max} \rightarrow x^{(3)}(t) = 0 \tag{C.9}$$

considering the 3^{rd} time derivative of the position x given by

$$x^{(3)}(t) = 6a_{x3} \tag{C.10}$$

then the condition (C.9) is satisfied when $a_{x3} = 0$ which implies

$$t|_{a_{max}} = \frac{2(x_f - x_i)}{\mathcal{V}_i \cos\theta_i \cos\psi_i + \mathcal{V}_f \cos\theta_f \cos\psi_f} \tag{C.11}$$

Afterward, by substituting $t|_{a_{max}}$ and a_{max} into equation (C.5), the arrival time which guarantees that the maximum acceleration a_{max} is not exceeded denoted T_{acc} can be calculated. Finally, the arrival time T_f required to complete the path is chosen such that $T_f > max(T_{vel}, T_{acc})$. In that manner, the feasibility of the proposed polynomial path between the initial and final configurations is ensured as the drone is guaranteed not to exceed the velocity and acceleration limitations.

Having the polynomial constants (C.6) and the predicted arrival time T_f, then the cubic polynomial describing the movement along $x-$direction is fully defined. By repeating the same procedure for the other two directions y, z, one can obtain an entire 3D cartesian trajectory between the starting point and the desired arrival point. Throughout the drone path, the heading angle ψ can be calculated based on equation (C.2) as follows

$$\psi = \arctan\left(\frac{\dot{y}}{\dot{x}}\right) \tag{C.12}$$

By using Matlab-Simulink to simulate the generated 3D trajectory on the quadrotor LPV model which possesses the proposed self-scheduled feedback controller presented in 3.5, the results given in figure C.1 are obtained. Figure C.1b shows the 3D trajectory of the quadrotor between the initial point $(0, 0, 0)$ and the final point $(2, 2, 3)$, while figure C.1a demonstrates the response of the system position states. Despite the overshoot existing in x, y states response, the two figures prove the capabilities of the controller in making the system follow the desired curved trajectory precisely.

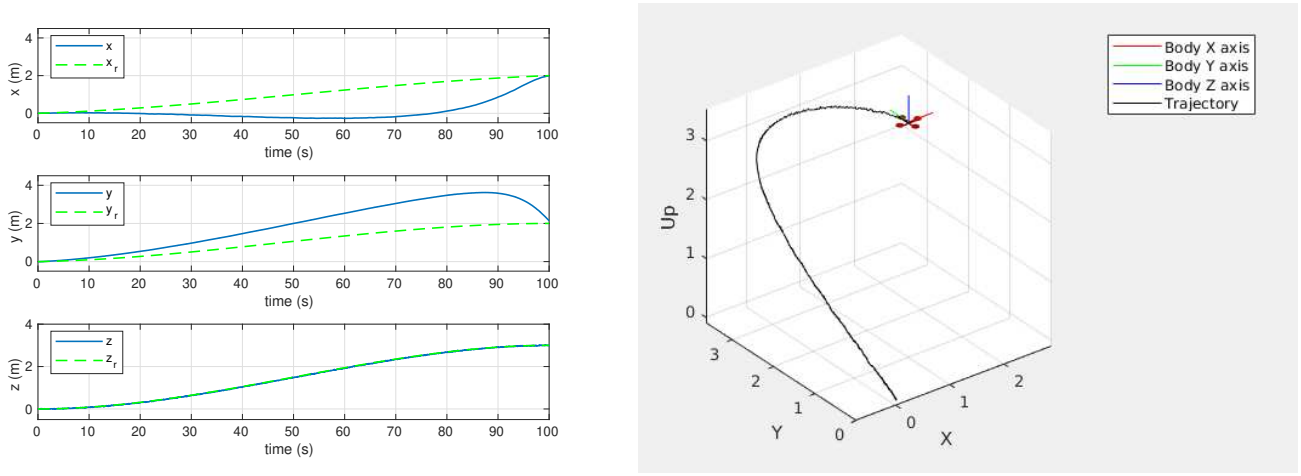

(a) position states

(b) polynomial trajectory tracking

Figure C.1: Cartesian polynomial trajectory tracking using LPV controller

Bibliography

[1] Mogens Blanke, W Christian Frei, Franta Kraus, J Ron Patton, and Marcel Staroswiecki. What is fault-tolerant control? *IFAC Proceedings Volumes*, 33(11):41–52, 2000.

[2] Youmin Zhang and Jin Jiang. Bibliographical review on reconfigurable fault-tolerant control systems. *Annual reviews in control*, 32(2):229–252, 2008.

[3] Halim Alwi, Christopher Edwards, and Chee Pin Tan. Fault tolerant control and fault detection and isolation. In *Fault Detection and Fault-Tolerant Control Using Sliding Modes*, pages 7–27. Springer, 2011.

[4] Zhiwei Gao, Carlo Cecati, and Steven X Ding. A survey of fault diagnosis and fault-tolerant techniques—part i: Fault diagnosis with model-based and signal-based approaches. *IEEE Transactions on Industrial Electronics*, 62(6):3757–3767, 2015.

[5] Julien Marzat, Hélène Piet-Lahanier, Frédéric Damongeot, and Eric Walter. Model-based fault diagnosis for aerospace systems: a survey. *Proceedings of the Institution of Mechanical Engineers, Part G: Journal of aerospace engineering*, 226(10):1329–1360, 2012.

[6] Matthew T DeGarmo. Issues concerning integration of unmanned aerial vehicles in civil airspace. *Center for Advanced Aviation System Development*, 4, 2004.

[7] Enrico Petritoli, Fabio Leccese, and Lorenzo Ciani. Reliability and maintenance analysis of unmanned aerial vehicles. *Sensors*, 18(9):3171, 2018.

[8] Remus C Avram, Xiaodong Zhang, and Jonathan Muse. Quadrotor sensor fault diagnosis with experimental results. *Journal of Intelligent & Robotic Systems*, 86(1):115–137, 2017.

[9] Dalil Ichalal, Benoît Marx, José Ragot, Said Mammar, and Didier Maquin. Sensor fault tolerant control of nonlinear takagi–sugeno systems. application to vehicle lateral dynamics. *International Journal of Robust and Nonlinear Control*, 26(7):1376–1394, 2016.

[10] Farid Sharifi, Mostafa Mirzaei, Brandon W Gordon, and Youmin Zhang. Fault tolerant control of a quadrotor uav using sliding mode control. In *2010 conference on control and Fault-Tolerant Systems (SysTol)*, pages 239–244. IEEE, 2010.

[11] Samir Bouabdallah, Andre Noth, and Roland Siegwart. Pid vs lq control techniques applied to an indoor micro quadrotor. In *2004 IEEE/RSJ International Conference on Intelligent Robots and Systems (IROS)(IEEE Cat. No. 04CH37566)*, volume 3, pages 2451–2456. IEEE, 2004.

[12] Carlos Trapiello, Vicenç Puig, and Bernardo Morcego. Position-heading quadrotor control using lpv techniques. *IET Control Theory & Applications*, 13(6):783–794, 2019.

[13] Damiano Rotondo, Fatiha Nejjari, and Vicenç Puig. Robust quasi-lpv model reference ftc of a quadrotor uav subject to actuator faults. *International Journal of Applied Mathematics and Computer Science*, 25(1), 2015.

[14] Hossein Bolandi, Mohammad Rezaei, Reza Mohsenipour, Hossein Nemati, and Seed Majid Smailzadeh. Attitude control of a quadrotor with optimized pid controller. 2013.

[15] RA Garcia, FR Rubio, and MG Ortega. Robust pid control of the quadrotor helicopter. *IFAC Proceedings Volumes*, 45(3):229–234, 2012.

[16] Oktaf Agni Dhewa, Andi Dharmawan, and Tri Kuntoro Priyambodo. Model of linear quadratic regulator (lqr) control method in hovering state of quadrotor. *vol*, 9:135–143, 2017.

[17] Pierre Apkarian, Pascal Gahinet, and Greg Becker. Self-scheduled $\mathcal{H}_\infty$ control of linear parameter-varying systems: a design example. *Automatica*, 31(9):1251–1261, 1995.

[18] Samarathunga LMD Rangajeeva and James F Whidborne. Linear parameter varying control of a quadrotor. In *2011 6th International Conference on Industrial and Information Systems*, pages 483–488. IEEE, 2011.

[19] Iman Sadeghzadeh, Abbas Chamseddine, Didier Theilliol, and Youmin Zhang. Linear parameter varying control synthesis: State feedback versus $\mathcal{H}_\infty$ technique with application to quadrotor ua v. In *2014 International Conference on Unmanned Aircraft Systems (ICUAS)*, pages 1099–1104. IEEE, 2014.

[20] Daniel Vey and Jan Lunze. Experimental evaluation of an active fault-tolerant control scheme for multirotor uavs. In *2016 3rd Conference on Control and Fault-Tolerant Systems (SysTol)*, pages 125–132. IEEE, 2016.

[21] M Hadi Amoozgar, Abbas Chamseddine, and Youmin Zhang. Experimental test of a two-stage kalman filter for actuator fault detection and diagnosis of an unmanned quadrotor helicopter. *Journal of Intelligent & Robotic Systems*, 70(1-4):107–117, 2013.

[22] Jian Liang Wang, Guang-Hong Yang, and Jian Liu. An lmi approach to $\mathcal{H}_-$ index and mixed $\mathcal{H}_-/\mathcal{H}_\infty$ fault detection observer design. *Automatica*, 43(9):1656–1665, 2007.

[23] Emmanuel Mazars, Imad M Jaimoukha, and Zhenhai Li. Computation of a reference model for robust fault detection and isolation residual generation. *Journal of control science and engineering*, 2008, 2008.

[24] Dalil Ichalal, Benoît Marx, José Ragot, and Didier Maquin. Fault detection, isolation and estimation for takagi–sugeno nonlinear systems. *Journal of the Franklin Institute*, 351(7):3651–3676, 2014.

[25] Amr M Pertew, Horacio J Marquez, and Qing Zhao. $\mathcal{H}_\infty$ observer design for lipschitz nonlinear systems. *IEEE Transactions on Automatic Control*, 51(7):1211–1216, 2006.

[26] D Ichalal, B Marx, D Maquin, and J Ragot. Actuator fault diagnosis: $\mathcal{H}_\infty$ framework with relative degree notion. *IFAC-PapersOnLine*, 49(5):321–326, 2016.

[27] Michel Fliess, Cédric Join, and Hebertt Sira-Ramirez. Non-linear estimation is easy. *International Journal of Modelling, Identification and Control*, 4(1):12–27, 2008.

[28] Alberto Isidori, J van Schuppen, E Sontag, M Thoma, and M Krstic. Communications and control engineering. *Nonlinear control systems*, 1995.

[29] Dalil Ichalal, Benoit Marx, José Ragot, and Didier Maquin. Observer based actuator fault tolerant control for nonlinear takagi-sugeno systems: an lmi approach. In *18th Mediterranean Conference on Control and Automation, MED'10*, pages 1278–1283. IEEE, 2010.

[30] Xiaohong Nian, Weiqiang Chen, Xiaoyan Chu, and Zhiwei Xu. Robust adaptive fault estimation and fault tolerant control for quadrotor attitude systems. *International Journal of Control*, 93(3):725–737, 2020.

[31] Ogata Katsuhiko. *Modern control engineering*. 2010.

[32] Robert C Nelson et al. *Flight stability and automatic control*, volume 2. WCB/McGraw Hill New York, 1998.

[33] M Ravi Tailor and PH Bhathawala. Linearization of nonlinear differential equation by taylor's series expansion and use of jacobian linearization process. *International Journal of Theoretical and Applied Science*, 4(1):36–38, 2011.

[34] Jeff S Shamma. *Analysis and design of gain scheduled control systems*. PhD thesis, Massachusetts Institute of Technology, 1988.

[35] Damiano Rotondo, Fatiha Nejjari, Abel Torren, and Vicenc Puig. Fault tolerant control design for polytopic uncertain lpv systems: Application to a quadrotor. In *2013 Conference on Control and Fault-Tolerant Systems (SysTol)*, pages 643–648. IEEE, 2013.

[36] Jeff S Shamma. An overview of lpv systems. *Control of linear parameter varying systems with applications*, pages 3–26, 2012.

[37] Sara Ifqir, N Ait Oufroukh, Dalil Ichalal, and Saïd Mammar. Interval observer for lpv systems: Application to vehicle lateral dynamics. *IFAC-PapersOnLine*, 50(1):7572–7577, 2017.

[38] Bei Lu, Fen Wu, and SungWan Kim. Switching lpv control of an f-16 aircraft via controller state reset. *IEEE transactions on control systems technology*, 14(2):267–277, 2006.

[39] Tarek N Dief, Shiego Yoshida, and Mohamed Abdelhady. Attitude and altitude stabilization of quad rotor using parameter estimation and self-tuning controller. In *AIAA Atmospheric Flight Mechanics Conference*, page 2392, 2015.

[40] Majid Moghadam and Fikret Caliskan. Actuator and sensor fault detection and diagnosis of quadrotor based on two-stage kalman filter. In *2015 5th Australian Control Conference (AUCC)*, pages 182–187. IEEE, 2015.

[41] Kostas Alexis, George Nikolakopoulos, Yannis Koveos, and Antonios Tzes. Switching model predictive control for a quadrotor helicopter under severe environmental flight conditions. *IFAC Proceedings Volumes*, 44(1):11913–11918, 2011.

[42] Pablo SG Cisneros, Christian Hoffmann, Marcus Bartels, and Herbert Werner. Linear parameter-varying controller design for a nonlinear quad-rotor helicopter model for high speed trajectory tracking. In *2016 American Control Conference (ACC)*, pages 486–491. IEEE, 2016.

[43] Samir Bouabdallah. Design and control of quadrotors with application to autonomous flying. Technical report, Epfl, 2007.

[44] Gauthier Rousseau. *Optimal trajectory planning and predictive control for cinematographic flight plans with quadrotors*. PhD thesis, Université Paris-Saclay, 2019.

[45] Daniel Vey and Jan Lunze. Structural reconfigurability analysis of multirotor uavs after actuator failures. In *2015 54th IEEE Conference on Decision and Control (CDC)*, pages 5097–5104. IEEE, 2015.

[46] BORIS HASSELBLATT. The hartman–grobman theorem, 2004.

[47] Jack W Langelaan, Nicholas Alley, and James Neidhoefer. Wind field estimation for small unmanned aerial vehicles. *Journal of Guidance, Control, and Dynamics*, 34(4):1016–1030, 2011.

[48] Fabrizio Schiano, Javier Alonso-Mora, Konrad Rudin, Paul Beardsley, Roland Y Siegwart, and Bruno Siciliano. Towards estimation and correction of wind effects on a quadrotor uav. In *IMAV 2014: International Micro Air Vehicle Conference and Competition 2014*, pages 134–141. International Micro Air Vehicle Conference and Competition 2014 (IMAV 2014), 2014.

[49] Moussa Labbadi and Mohamed Cherkaoui. Robust integral terminal sliding mode control for quadrotor uav with external disturbances. *International Journal of Aerospace Engineering*, 2019, 2019.

[50] Chun Kiat Tan, Jianliang Wang, Yew Chai Paw, and Teng Yong Ng. Tracking of a moving ground target by a quadrotor using a backstepping approach based on a full state cascaded dynamics. *Applied soft computing*, 47:47–62, 2016.

[51] Jovan D Bošković and Raman K Mehra. Failure detection, identification and reconfiguration in flight control. In *Fault Diagnosis and Fault Tolerance for Mechatronic Systems: Recent Advances*, pages 129–167. Springer, 2003.

[52] Ming Chen and Mihai Huzmezan. A simulation model and h (loop shaping control of a quad rotor unmanned air vehicle. In *Modelling, Simulation, and Optimization*, pages 320–325, 2003.

[53] MM Komnatska. Flight control system design via static output feedback: Lmi-approach. In *2013 IEEE 2nd International Conference Actual Problems of Unmanned Air Vehicles Developments Proceedings (APUAVD)*, pages 184–186. IEEE, 2013.

[54] Brian R Copeland. The design of pid controllers using ziegler nichols tuning. *Internet: http://educypedia. karadimov. info/library/Ziegler_Nichols. pdf*, 2008.

[55] Sigurd Skogestad and Ian Postlethwaite. *Multivariable feedback control: analysis and design*, volume 2. Citeseer, 2007.

[56] Wil Schilders. Introduction to model order reduction. In *Model order reduction: Theory, research aspects and applications*, pages 3–32. Springer, 2008.

[57] Lebao Li, Lingling Sun, and Jie Jin. Survey of advances in control algorithms of quadrotor unmanned aerial vehicle. In *2015 IEEE 16th International Conference on Communication Technology (ICCT)*, pages 107–111. IEEE, 2015.

[58] Joao P Hespanha. Lqg/lqr controller design. *Undergraduate Lecture Notes, University of California, Santa Barbara, California, USA*, 2007.

[59] J. Löfberg. Yalmip : A toolbox for modeling and optimization in matlab. In *In Proceedings of the CACSD Conference*, Taipei, Taiwan, 2004.

[60] Jeremy G VanAntwerp and Richard D Braatz. A tutorial on linear and bilinear matrix inequalities. *Journal of process control*, 10(4):363–385, 2000.

[61] Ngoc Phi Nguyen and Sung Kyung Hong. Sliding mode thau observer for actuator fault diagnosis of quadcopter uavs. *Applied Sciences*, 8(10):1893, 2018.

[62] Remus C Avram, Xiaodong Zhang, Jacob Campbell, and Jonathan Muse. Imu sensor fault diagnosis and estimation for quadrotor uavs. *IFAC-PapersOnLine*, 48(21):380–385, 2015.

[63] David Luenberger. Observers for multivariable systems. *IEEE Transactions on Automatic Control*, 11(2):190–197, 1966.

[64] Ron J Patton and Jie Chen. Observer-based fault detection and isolation: Robustness and applications. *Control Engineering Practice*, 5(5):671–682, 1997.

[65] Aiping Xu and Qinghua Zhang. Nonlinear system fault diagnosis based on adaptive estimation. *Automatica*, 40(7):1181–1193, 2004.

[66] Dalil Ichalal, Benoit Marx, José Ragot, and Didier Maquin. Fault diagnosis for takagi-sugeno nonlinear systems. *IFAC Proceedings Volumes*, 42(8):504–509, 2009.

[67] Liguo Qin, Xiao He, Yan Zhou, and Donghua Zhou. Fault-tolerant control for a quadrotor unmanned helicopter subject to sensor faults. In *2016 International Conference on Unmanned Aircraft Systems (ICUAS)*, pages 1280–1286. IEEE, 2016.

[68] Damien Koenig and Ron J Patton. New design of robust kalman filters for fault detection and isolation. *IFAC Proceedings Volumes*, 32(2):7926–7931, 1999.

[69] Wei Xue, Ying-qing Guo, and Xiao-dong Zhang. A bank of kalman filters and a robust kalman filter applied in fault diagnosis of aircraft engine sensor/actuator. In *Second International Conference on Innovative Computing, Informatio and Control (ICICIC 2007)*, pages 10–10. IEEE, 2007.

[70] Ling Ma and Youmin Zhang. Dukf-based gtm uav fault detection and diagnosis with nonlinear and lpv models. In *Proceedings of 2010 IEEE/ASME International Conference on Mechatronic and Embedded Systems and Applications*, pages 375–380. IEEE, 2010.

[71] Qinghua Zhang. Adaptive kalman filter for actuator fault diagnosis. *Automatica*, 93:333–342, 2018.

[72] Ron J Patton and Jie Chen. Robust fault detection using eigenstructure assignment: A tutorial consideration and some new results. In *Proceedings of the 30th IEEE Conference on Decision and Control*, volume 3, pages 2242–2247, 1991.

[73] Ron J Patton and Jie Chen. On eigenstructure assignment for robust fault diagnosis. *International Journal of Robust and Nonlinear Control: IFAC-Affiliated Journal*, 10(14):1193–1208, 2000.

[74] Jie Chen, Ron J Patton, and Hong-Yue Zhang. Design of unknown input observers and robust fault detection filters. *International Journal of control*, 63(1):85–105, 1996.

[75] Guang-Ren Duan and Ron J Patton. Robust fault detection using luenberger-type unknown input observers-a parametric approach. *International Journal of Systems Science*, 32(4):533–540, 2001.

[76] Weitian Chen and Mehrdad Saif. Fault detection and isolation based on novel unknown input observer design. In *2006 American Control Conference*, pages 6–pp. IEEE, 2006.

[77] Dalil Ichalal and Saïd Mammar. On unknown input observers for lpv systems. *IEEE Transactions on Industrial Electronics*, 62(9):5870–5880, 2015.

[78] Benoît Marx, Dalil Ichalal, José Ragot, Didier Maquin, and Saïd Mammar. Unknown input observer for lpv systems. *Automatica*, 100:67–74, 2019.

[79] Laifeng Zuo, Lina Yao, and Yunfeng Kang. Uio based sensor fault diagnosis and compensation for quadrotor uav. In *2020 Chinese Control And Decision Conference (CCDC)*, pages 4052–4057. IEEE, 2020.

[80] Lebsework Negash, Sang-Hyeon Kim, and Han-Lim Choi. An eigenstructure assignment embedded unknown input observe approach for actuator fault detection in quadrotor dynamics. *IFAC-PapersOnLine*, 49(17):426–431, 2016.

[81] Eslam Abouselima, Dalil Ichalal, and Saïd Mammar. Quadrotor control and actuator fault detection: Lqg versus robust $\mathcal{H}_-/\mathcal{H}_\infty$ observer. In *2019 4th Conference on Control and Fault Tolerant Systems (SysTol)*, pages 86–91. IEEE, 2019.

[82] Ming Hou and Ron J Patton. An lmi approach to $\mathcal{H}_-/\mathcal{H}_\infty$ fault detection observers. *UKACC International Conference on CONTROL*, 1996.

[83] J Chen and RJ Patton. $\mathcal{H}_\infty$ formulation and solution for robust fault diagnosis. *IFAC Proceedings Volumes*, 32(2):7808–7813, 1999.

[84] Maiying Zhong, Steven X Ding, Tang Bingyong, T Jeinsch, and M Sader. An lmi approach to design robust fault detection observers. In *Proceedings of the 4th World Congress on Intelligent Control and Automation (Cat. No. 02EX527)*, volume 4, pages 2705–2709. IEEE, 2002.

[85] Jian Liu, Jian Liang Wang, and Guang-Hong Yang. An lmi approach to minimum sensitivity analysis with application to fault detection. *Automatica*, 41(11):1995–2004, 2005.

[86] HB Wang, JL Wang, and J Lam. Robust fault detection observer design: iterative lmi approaches. *Journal of Dynamic Systems, Measurement, and Control*, 2007.

[87] Imad M Jaimoukha, Zhenhai Li, and Emmanuel Mazars. Fault isolation filter with linear matrix inequality solution to optimal decoupling. In *2006 American Control Conference*, pages 6–pp. IEEE, 2006.

[88] Zhenhai Li, Emmanuel Mazars, Ze Zhang, and Imad M Jaimoukha. State–space solution to the $\mathcal{H}_-/\mathcal{H}_\infty$ fault-detection problem. *International Journal of Robust and Nonlinear Control*, 22(3):282–299, 2012.

[89] Ze Zhang and Imad M Jaimoukha. An optimal solution to an $\mathcal{H}_-/\mathcal{H}_\infty$ fault detection problem. In *2011 50th IEEE Conference on Decision and Control and European Control Conference*, pages 903–908. IEEE, 2011.

[90] Xiukun Wei and Michel Verhaegen. Fault detection of large scale wind turbine systems: A mixed $\mathcal{H}_\infty/\mathcal{H}_-$ index observer approach. In *2008 16th Mediterranean Conference on Control and Automation*, pages 1675–1680. IEEE, 2008.

[91] X Wei and M Verhaegen. Lmi solutions to the mixed $\mathcal{H}_-/\mathcal{H}_\infty$ fault detection observer design for linear parameter-varying systems. *International Journal of Adaptive Control and Signal Processing*, 25(2):114–136, 2011.

[92] Mohammed Chadli, Ali Abdo, and Steven X Ding. $\mathcal{H}_-/\mathcal{H}_\infty$ fault detection filter design for discrete-time takagi–sugeno fuzzy system. *Automatica*, 49(7):1996–2005, 2013.

[93] Sabrina Aouaouda, Mohammed Chadli, Peng Shi, and Hamid-Reza Karimi. Discrete-time $\mathcal{H}_-/\mathcal{H}_\infty$ sensor fault detection observer design for nonlinear systems with parameter uncertainty. *International Journal of Robust and Nonlinear Control*, 25(3):339–361, 2015.

[94] Ahmad Farhat and Damien Koenig. $\mathcal{H}_-/\mathcal{H}_\infty$ robust fault detection observer for uncertain switched systems. In *2015 European Control Conference (ECC)*, pages 3174–3179. IEEE, 2015.

[95] FR López Estrada, Jean Christophe Ponsart, Didier Theilliol, and Carlos-Manuel Astorga-Zaragoza. Robust $\mathcal{H}_-/\mathcal{H}_\infty$ fault detection observer design for descriptor-lpv systems with unmeasurable gain scheduling functions. *International Journal of Control*, 88(11):2380–2391, 2015.

[96] Zhenhua Wang, Peng Shi, and Cheng-Chew Lim. $\mathcal{H}_-/\mathcal{H}_\infty$ fault detection observer in finite frequency domain for linear parameter-varying descriptor systems. *Automatica*, 86:38–45, 2017.

[97] Damien Koenig, Benoît Marx, and Sébastien Varrier. Filtering and fault estimation of descriptor switched systems. *Automatica*, 63:116–121, 2016.

[98] Salim Ibrir. Online exact differentiation and notion of asymptotic algebraic observers. *IEEE transactions on Automatic control*, 48(11):2055–2060, 2003.

[99] Meng Zhou, Mickael Rodrigues, Yi Shen, and Didier Theilliol. $\mathcal{H}_-/\mathcal{H}_\infty$ fault detection observer design based on generalized output for polytopic lpv system. In *Journal of Physics: Conference Series*, volume 783, page 012002. IOP Publishing, 2017.

[100] Eslam Abouselima, Dalil Ichalal, and Said Mammar. Robust actuator fault diagnosis for lpv systems: Application to quadrotor. In *2021 American Control Conference (ACC)*, pages 4938–4945. IEEE, 2021.

[101] Jian Zhang, Akshya Kumar Swain, and Sing Kiong Nguang. *Robust observer-based fault diagnosis for nonlinear systems using MATLAB®*. Springer, 2016.

[102] Eslam Abouselima, Dalil Ichalal, and Said Mammar. Robust sensor fault estimation for lpv systems: Application to quadrotor uav. In *2021 9th International Conference on Systems and Control (ICSC)*, pages 373–379. IEEE, 2021.

[103] Hassan K Khalil. *Nonlinear control*. Pearson Higher Ed, 2014.

[104] Olivier Sename, Peter Gaspar, and József Bokor. *Robust control and linear parameter varying approaches: application to vehicle dynamics*, volume 437. Springer, 2013.

[105] Dalil Ichalal, Benoit Marx, José Ragot, and Didier Maquin. Simultaneous state and unknown inputs estimation with pi and pmi observers for takagi sugeno model with unmeasurable premise variables. In *2009 17th Mediterranean conference on control and automation*, pages 353–358. IEEE, 2009.

[106] Damiano Rotondo, Fatiha Nejjari, and Vicenç Puig. Model reference quasi-lpv control of a quadrotor uav. In *2014 IEEE Conference on Control Applications (CCA)*, pages 736–741. IEEE, 2014.

[107] Zhixiang Liu, Chi Yuan, and Youmin Zhang. Active fault-tolerant control of unmanned quadrotor helicopter using linear parameter varying technique. *Journal of Intelligent & Robotic Systems*, 88(2-4):415, 2017.

[108] Younes Al Younes, Hassan Noura, Abdelhamid Rabhi, and Ahmed El Hajjaji. Actuator fault-diagnosis and fault-tolerant-control using intelligent-output-estimator applied on quadrotor uav. In *2019 International Conference on Unmanned Aircraft Systems (ICUAS)*, pages 413–420. IEEE, 2019.

[109] Maryamsadat Tahavori and Agus Hasan. Fault recoverability for nonlinear systems with application to fault tolerant control of uavs. *Aerospace Science and Technology*, 107:106282, 2020.

[110] Mark W Mueller and Raffaello D'Andrea. Relaxed hover solutions for multicopters: Application to algorithmic redundancy and novel vehicles. *The International Journal of Robotics Research*, 35(8):873–889, 2016.

[111] Sihao Sun, Leon Sijbers, Xuerui Wang, and Coen de Visser. High-speed flight of quadrotor despite loss of single rotor. *IEEE Robotics and Automation Letters*, 3(4):3201–3207, 2018.

[112] Ahmed Khattab, Halim Alwi, and Christopher Edwards. Mitigating total rotor failure in quadrotor using lpv based sliding mode control scheme. In *2019 4th Conference on Control and Fault Tolerant Systems (SysTol)*, pages 98–103. IEEE, 2019.

[113] Saul Montes de Oca and Vicenc Puig. Fault-tolerant control design using a virtual sensor for lpv systems. In *2010 Conference on Control and Fault-Tolerant Systems (SysTol)*, pages 88–93. IEEE, 2010.

[114] Damiano Rotondo, Fatiha Nejjari, and Vicenç Puig. A virtual actuator and sensor approach for fault tolerant control of lpv systems. *Journal of Process Control*, 24(3):203–222, 2014.

[115] Marcin Pazera, Mariusz Buciakowski, and Marcin Witczak. Robust multiple sensor fault-tolerant control for dynamic non-linear systems: Application to the aerodynamical twin-rotor system. *International Journal of Applied Mathematics and Computer Science*, 28(2), 2018.

[116] Mariella Maia Quadros, Iury Valente de Bessa, Valter JS Leite, and Reinaldo Martinez Palhares. Fault tolerant control for linear parameter varying systems: an improved robust virtual actuator and sensor approach. *ISA transactions*, 104:356–369, 2020.

[117] Dalil Ichalal, Benoît Marx, Didier Maquin, and José Ragot. Nonlinear observer based sensor fault tolerant control for nonlinear systems. *IFAC Proceedings Volumes*, 45(20):1053–1058, 2012.

[118] Mark W Mueller and Raffaello D'Andrea. Stability and control of a quadrocopter despite the complete loss of one, two, or three propellers. In *2014 IEEE international conference on robotics and automation (ICRA)*, pages 45–52. IEEE, 2014.

[119] Peng Lu and Erik-Jan van Kampen. Active fault-tolerant control for quadrotors subjected to a complete rotor failure. In *2015 IEEE/RSJ International Conference on Intelligent Robots and Systems (IROS)*, pages 4698–4703. IEEE, 2015.

[120] Johannes Stephan, Lorenz Schmitt, and Walter Fichter. Linear parameter-varying control for quadrotors in case of complete actuator loss. *Journal of Guidance, Control, and Dynamics*, 41(10):2232–2246, 2018.

[121] Ryan James Caverly and James Richard Forbes. Lmi properties and applications in systems, stability, and control theory. *arXiv preprint arXiv:1903.08599*, 2019.

[122] Antonio Barrientos, Pedro Gutiérrez, and Julián Colorado. Advanced uav trajectory generation: Planning and guidance. In *Aerial Vehicles*, pages 55–82. InTech, 2009.

[123] Yasmina Bestaoui Sebbane. *Planning and decision making for aerial robots*. Springer, 2014.

Résumé de thèse

Depuis plusieurs années, les systèmes autonomes sont largement déployés dans des domaines differents de notre vie quotidienne. C'est pourquoi, contrôle tolérant aux fautes (FTC) des systèmes autonomes a suscité un réel intérêt surtout pour les drones autonomes. En effet, si le système est doté d'une unité FTC, il sera capable dès la détection d'un défaut d'alerter les parties impactées tout en préservant une performance acceptable pour accomplir la tâche requise. Dans cette thèse, nous soulignons l'importance de concevoir un algorithme FTC robuste pour un quadrotor pour maintenir son fonctionnement dans des conditions défectueuses.

Pour resoudre ce problème, on commence par l'établissement d'un modèle fiable pour le système représentant la dynamique physique. Ainsi, la formule de Newton-Euler est utilisée pour modéliser le quadrotor, ce qui donne un modèle mathématique qui décrit la dynamique du système. Le modèle obtenu est ensuite linéarisé autour du point d'équilibre en appliquant la théorie des petites perturbations, mais comme le modèle résultant est excessivement simplifié, d'autre proposition a été étudiée. La méthode adoptée est intéressante car le système est modélisé dans un cadre LPV où les termes non linéaires sont considérés comme variant linéairement dans le temps dans les limites des paramètres donnés.

Le modèle déduit est ensuite utilisé pour construire un contrôleur qui stabilise le quadrotor et garantit un suivi de trajectoire plus précis. Une loi de commande PID est donc conçue pour le modèle linéaire simplifié en utilisant la technique de mise en forme de la boucle de la fonction de transfert pour satisfaire les caractéristiques de la norme $\mathcal{H}_\infty$ requise. Ensuite, pour assurer l'efficacité du contrôleur dans de vastes domaines d'application où les conditions environnementales ne sont pas garanties d'être exactement modélisées, un contrôleur robuste basé sur la technique $\mathcal{H}_\infty$ est conçu pour le système LPV proposé.

Afin de fournir au quadrotor un schéma FTC efficace, une unité de détection et de diagnostic des fautes (FDD) est proposée pour identifier les détails des fautes tels que: la quantité, l'emplacement. L'unité FDD contient un observateur basé sur un modèle qui génère des signaux résiduels indiquant l'apparition de la faute. Ainsi, un observateur est conçu sur la base de $\mathcal{H}_-/\mathcal{H}_\infty$ visant à maximiser la sensibilité de la faute au résidu en utilisant les propriétés de l'indice $\mathcal{H}_-$ et en minimisant la norme $\mathcal{H}_\infty$ pour l'atténuation des signaux exogènes.

Dans ce contexte, nous nous focalisons sur une nouvelle approche basée sur une sortie auxiliaire contenant la sortie du système et ses dérivées successives. Cette approche est utilisée pour le diagnostic des fautes des actionneurs et des capteurs, y compris la détection, l'estimation et l'isolation. Il est illustré que dans certains cas, les fautes peuvent être estimées exactement alors que les perturbations sont complètement découplées des signaux résiduels. Cependant, si la convergence exacte n'est pas assurée, certaines conditions relaxantes sont fournies pour maintenir une estimation asymptotique des défauts. Enfin, l'approche $\mathcal{H}_-/\mathcal{H}_\infty$ qui est améliorée en utilisant la sortie auxiliaire est présenté comme le pire scénario. Une procédure de conception générale est fournie, puis appliquée en simulation à un modèle de quadrotor pour démontrer que ce dispositif mis en place couvre les hypothèses identifiées.

En analysant les résultats obtenus par l'unité FDD de l'actionneur, une loi de contrôle active tolérante aux pannes est conçue. Après l'évaluation de la faute, le FDD fournit les données nécessaires qui aide le contrôleur à la prise de décision pour savoir si le dommage de l'actionneur peut être traité ou non. Dans ce cas, une loi de contrôle est définie afin de réduire les fautes et d'assurer un suivi précis de la trajectoire dans le système de commande.

université PARIS-SACLAY

ÉCOLE DOCTORALE
Sciences et technologies de l'information et de la communication (STIC)

Titre : Planification et Contrôle tolérants aux Défauts de Systèmes Quasi-LPV : Application sur un Quadrotor

Mots clés : Observateurs robustes - Drone - Commande $\mathcal{H}_\infty$ - Systèmes LPV

Résumé : Depuis plusieurs années, les systèmes autonomes sont largement déployés dans plusieurs domaines de notre vie quotidienne. C'est pourquoi, contrôle tolérant aux fautes (FTC) des systèmes autonomes a suscité un réel intérêt. En effet, si le système est doté d'une unité FTC, il sera capable dès la détection d'un défaut d'alerter les parties impactées tout en préservant une performance acceptable pour accomplir la tâche requise. Évidemment, Les drones sont des systèmes autonomes qui ont besoin de tels algorithmes FTC, car tout défaut du système peut toucher la sécurité des vols, en causant des dommages non seulement pour le véhicule mais aussi pour l'environnement. Ainsi, Dans cette thèse, nous soulignons l'importance de concevoir un algorithme FTC robuste pour un quadrotor qui peut être abordé à travers quelques étapes fondamentales en commençant par l'établissement d'un modèle fiable pour le système dans le cadre LPV représentant la dynamique physique avec précision. Ensuite, un contrôleur robuste basé sur la norme $\mathcal{H}_\infty$ est proposé pour stabiliser le quadrotor et garantir un suivi de trajectoire précis lorsque le système est soumis à des perturbations exogènes. Puis, pour fournir au quadrotor un schéma FTC efficace, une unité de détection et de diagnostic des défauts (FDD) est proposée pour identifier le type, la quantité et l'emplacement du défaut existant. L'unité FDD contient un observateur basé sur un modèle dont les gains sont assignés de telle sorte qu'il génère des signaux résiduels indiquant précisément l'occurrence du défaut. Sur la base des résultats obtenus par l'unité FDD, une loi de commande active tolérante aux défauts est conçue pour compenser les défauts et suivre une trajectoire précise en présence d'un dysfonctionnement du système.

Title : Fault tolerant control and path planning for quasi-LPV systems : application to quadrotor

Keywords : Robust observers - Quadrotor - $\mathcal{H}_\infty$ control - LPV systems

Abstract : Recently, autonomous systems are getting increasingly popular and are widely deployed in several applications in our daily life. That's why a great concern has been dedicated to the problem of autonomous systems fault-tolerant control (FTC). As if the system is provided with an FTC unit, it will be able to create an alert in case of system malfunction while preserving an acceptable performance to complete the required task. Evidently, the UAVs are among the systems that are in need of such FTC algorithms because any system malfunction can cause severe damage not just for the vehicle itself but for the surrounding environment as well. So in this work, we investigate the problem of designing an FTC algorithm for a quadrotor which can be tackled through some fundamental steps beginning with establishing a trustful model for the system in LPV framework representing the physical dynamics accurately. After that, a robust controller based on $\mathcal{H}_\infty$ norm is proposed to stabilize the quadrotor and guarantee precise trajectory tracking while the system is subjected to exogenous disturbances. Then, to provide the quadrotor with an efficient FTC scheme, first, a fault detection and diagnosis (FDD) unit is proposed to identify the type, amount, and location of the existent fault. The FDD unit contains a model-based observer whose gains are assigned such that it generates some residual signals indicating the fault occurrence precisely. Upon the obtained results from the FDD unit, an active fault-tolerant control law is designed aiming at fault compensation and precise trajectory tracking in the presence of system malfunction.